AD-A153 223 OVERLOAD EFFECTS ON SUSTAINED LOAD CRACK GROWTH AT ELEVATED TEMPERATURE(U) AIR FORCE INST OF TECH WRIGHT-PATTERSON AFB OH SCHOOL OF ENGINEERING 1/2

UNCLASSIFIED K E HARMS DEC 84 AFIT/GAE/AA/84D-8 F/G 11/6 NL

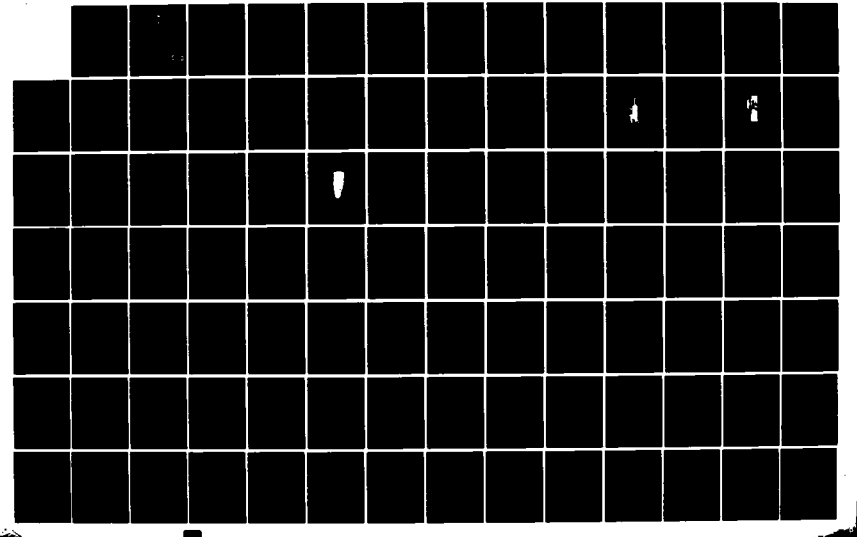

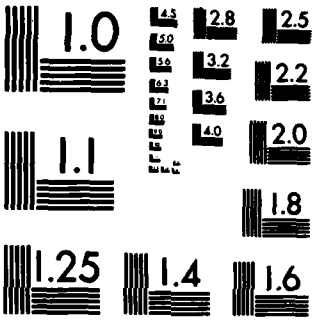

MICROCOPY RESOLUTION TEST CHART
NATIONAL BUREAU OF STANDARDS-1963-A

OVERLOAD EFFECTS ON SUSTAINED LOAD CRACK GROWTH AT ELEVATED TEMPERATURE

THESIS

Kevin E. Harms
Captain, USAF

AFIT/GAE/AA/84D-8

DEPARTMENT OF THE AIR FORCE
AIR UNIVERSITY
AIR FORCE INSTITUTE OF TECHNOLOGY

Wright-Patterson Air Force Base, Ohio

AFIT/GAE/AA/84D-8

OVERLOAD EFFECTS ON SUSTAINED LOAD CRACK GROWTH AT ELEVATED TEMPERATURE

THESIS

Kevin E. Harms
Captain, USAF

AFIT/GAE/AA/84D-8

Approved for public release; distribution unlimited

AFIT/GAE/AA/84D-8

OVERLOAD EFFECTS ON SUSTAINED LOAD CRACK GROWTH AT ELEVATED TEMPERATURE

THESIS

Presented to the Faculty of the School of Engineering
of the Air Force Institute of Technology
Air University
In Partial Fulfillment of the
Requirements for the Degree of
Master of Science in Aeronautical Engineering

Kevin E. Harms
Captain, USAF

December 1984

Preface

The purpose of this study was to support the Retirement for Cause maintenance program. RFC has been initiated by the USAF to conserve valuable resources in the jet engine inventory and to curtail overall life cycle costs. This effort represents an ongoing evolution in the field of engineering. Today's technology must not only provide designs that work, it must must also provide designs that are more durable, efficient and excel in performance. I personally found it very rewarding to be a part of this experience.

This study, however, would not have been possible without all the help and support that I have received. I am deeply indebted to Dr. T. Nicholas, AFWAL/MLLN, and his department for use of their facilities and their time and effort in assisting me. I would also like to thank Mr. G. Ahrens, UDRI, for his help in setting up the test apparatus and maintaining instrument calibrations. I also greatly appreciated the overall guidance of Major G. K. Haritos, AFIT/ENY, which was instrumental in directing this study to a successful conclusion.

Table of Contents

List of Figures

List of Tables

Abstract

This study investigates the crack growth behavior of Inconel 718 effected by overloads at elevated temperature. A cumulative damage model was developed to predict the total time-to-failure. Predictions were noted to improve at higer values of stress intensities.

All tests were conducted under sustained loading with insothermal conditions of 650°C. Precracked compact tension specimens were used to establish a data base for baseline and overload conditions. The delay time associated with crack growth retardation was determined by comparing the baseline behavior with the results of the overload specimens. The effects of 20-and 50-percent overloads of 1 minute or 1 hour duration were investigated. The shape of the crack tip plastic zone and, hence, the retardation effect was found to be independent of overload duration.

The retardation delay time was found to be dependent upon the overload magnitude and the value of K at which the overload was removed. It was also found that a sudden crack advancement occurred when the overload was applied. The above factors were accounted for in the model development. The model was generally capable of predicting the time-to-failure within about 10 percent of the actual material behavior.

OVERLOAD EFFECTS ON SUSTAINED LOAD CRACK GROWTH AT ELEVATED TEMPERATURE

I. Introduction

Background

Modern day jet engines are sophisticated devices with very demanding performance requirements. The components of the engine are subjected to severe operating conditions which limits their useful design life. Although much progress has been made to improve engine durability, critical components still must be periodically replaced to avoid catastrophic failure. Until recently, the method used by the USAF to predict the useful service life of engine components was very conservative. Life cycle predictions were based on statistical models which define a safe service life. In the case of turbine disks, this means a complete change-out when it's expected that 1 in 1,000 disks has developed a 0.03 inch fatigue-induced crack. Although the forced retirement of the entire population precludes catastrophic failure, the remaining 999 disks could still have considerable residual life left. It has been estimated that the useful life remaining could be significant with over 80-percent of the disks having at least 10 more lifetimes (1).

In order to take advantage of the potential life-cycle cost savings, the USAF initiated a "Retirement-for-Cause" (RFC) program to safely utilize the full life capability of jet-engine components. The RFC program requires critical engine components to be inspected after a specified period of time and Returned to Service (RTS) if no cracks are found. The RTS interval is determined by fracture mechanics calculations. The results indicate the amount of time it will take for a small crack, undetected by the first inspection, to grow to a critical size.

Success of the RFC program depends upon technical capability in two essential areas. The first is a Nondestructive Evaluation (NDE) procedure to realiably detect cracks that are larger than a predetermined rejection size. The second is the capability to accurately predict additional crack propagation in the engine environment. This second area requires a demonstrated understanding of the fracture mechanisms involved along with the development of reliable predictive models.

Objective

This study addresses a facet of the crack-growth-rate prediction problem. Specifically, the retardation effects of intermittent overloads on the sustained load crack-growth rate in the Inconel 718 is investigated. All

experiments are conducted at elevated temperature and results are used to develop a predictive model. The model's accuracy is verified by comparing predictions to experimental results obtained from a proof test.

Scope

A number of studies have been conducted in the past to investigate fatigue crack-growth-rate behavior in metals at elevated temperature. This includes studies under both cyclic and sustained loads. However, little has been found in the literature that describes the effects of overloads on crack-growth rates at elevated temperature. Macha et al. (2) studied the behavior of IN 100 and noted that the retardation benefit from single peak overloads decreases as temperatures increases. Others have also observed (for sustained and cyclic loadings) a strong temperature influence on crack-growth behavior (see e.g. (3), (4), (5), (6)). These occurrences are usually attributed to thermally activated micromechanisms. A further review of the literature also indicates that a number of other factors such as laboratory air vs inert gas environments, cyclic frequencies, hold times, and specimen geometry can influence the crack-growth behavior. With several variables affecting crack-growth rate, Sandananda and Shahinian (7) present a number of different correlating parameters to characterize a

material's behavior. The linear elastic stress intensity factor K, the J-integral, the C^* energy rate integral or the reference stress σ_r are a few of many to be considered.

In this study, experiments are performed with a compact tension geometry only. The material studied is Inconel 718 and all tests are conducted in a laboratory air environment under isothermal conditions of 650°C. Specimens are subjected to a constant sustained load except for infrequent overloads of variable duration. Under these conditions the crack-growth behavior is governed by a time-dependent process which includes both creep and environmental effects. However, Larsen and Nicholas (8) note that the environmental effects dominate when Inconel 718 is tested in laboratory air. The environmentally-enhanced growth rate is then sufficient enough to limit the plastic stress field at the crack tip. This condition allows the use of the linear elastic stress intensity factor K as a correlating parameter for the study. Additionally, Sandananda and Shahinian (7) indicate that fracture mechanics techniques are appropriate within a temperature range of 0.4 to 0.7 of the material's melting point. This study does not attempt to investigate the micromechanisms of crack initiation or propagation.

Approach

A total of 14 compact tension specimens were used during the course of this study to establish a data base for the model development. The history of each specimen was carefully controlled since time-dependent crack-growth can be very sensitive to changes in microstructure. Widely diverse behavior has even been observed for different batches of material with the same heat treatment (7). To eliminate this source of possible data scatter, all of the specimens used in this study were cut from the same plate and heat treated simultaneously. The machining was done such that the crack would grow in a direction parallel to the rolling direction (T-L orientation).

Fatigue precracking of all test specimens was performed at room temperature with an MTS hydraulic servo-controlled testing machine. A sine wave form was used to cyclically load each specimen until they were precracked to approximately 2.16 mm. Two of the specimens were selected for baseline testing. The baseline tests provided data to determine the sustained-load crack-growth-rate of Inconel 718 as a function of the stress intensity factor, K. The stress intensity threshold value was found to be approximately 24 MPA $\sqrt{m}$. The remaining specimens were subjected to 20-and 50-percent overloads for 1 minute or 1 hour hold times. The effects of the overload magnitude and hold time on the

subsequent sustained load crack-growth-rate was then determined by comparing overload and baseline data. The results were used to develop a model that accounted for crack-growth retardation effects generated by the overloads. The study was concluded with a proof test to verify the model's accuracy.

II. Description of Test Apparatus

Data were gathered for this study with a semi-automated creep test system. All testing was conducted at the Air Force Wright Aeronautical Laboratories, Materials Laboratory, Wright-Patterson Air Force Base, OH. A schematic of the test system is shown in Fig. 1. The system consisted of the following components:

1.) A Tektronix 4051 microcomputer

2.) A Daytronic 9000 signal conditioner

3.) A Swedish Creep test frame

4.) A clamshell-type resistance furnace

5.) Two Gaertner traveling microscopes

6.) An extensometer system with two Linear Variable Differential Transducers (LVDT)

7.) A link-type load cell transducer

The Tektronix 4051 microcomputer provided the software interface for the system and acted as the main recording and control device. The Tektronix could be preprogramed to take and record compliance measurements and other test parameters at regularly spaced time intervals. The data were recorded on magnetic tape and later transferred to the PDP host computer for further reduction.

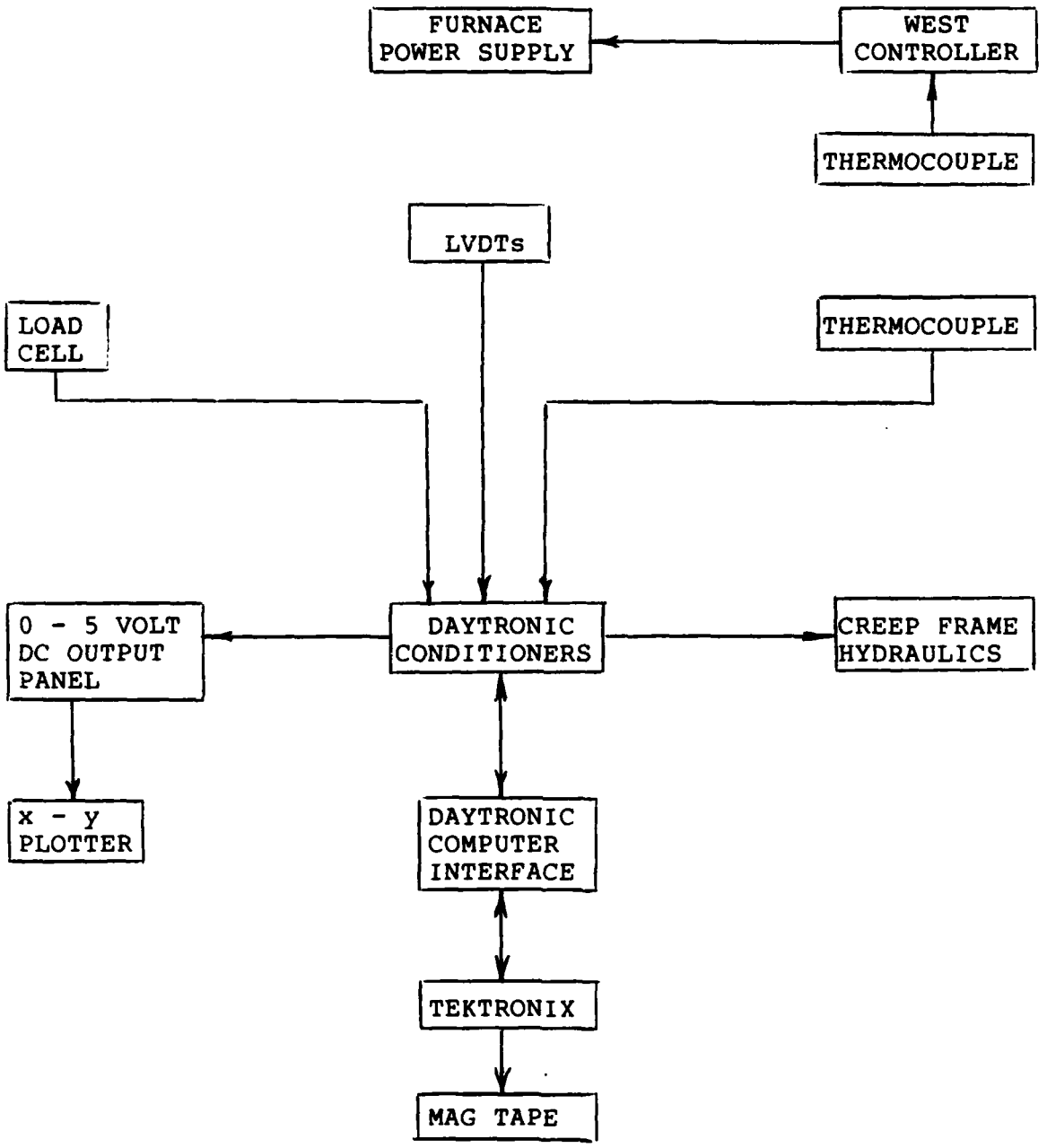

Figure 1 Test System Schematic

The Daytronics 9000 signal conditioner was also a key element for automated test control and data collection. It essentially provided the computer interface between the Tektronix and the measuring instruments. The Daytronics would continuously scan all data channels at a rate of 15,000 channels per second until queued by the Tektronix's programming to sample a specific channel. The Daytronics would then process the raw instrument data so that a smooth, stable analog output was attained. Appropriate conversion factors were applied to the conditioned signals to scale the data in physical terms. The following instrument calibrations were used:

LVDT	1 V = 0.020 inch
load cell	1 V = 250 lb
thermocouple	2.17mV = 1 °F

Analog signals were then converted to digital and forwarded to the Tektronix to be recorded. The Daytronics unit also provided a 5-volt digital output signal to the creep frame's servohydraulic mechanism. This enabled the computer to load and unload the frame at programed intervals.

For the tests, a 12,000 lb capacity Swedish creep frame was used to load the specimen. The frame has a 20 to 1 lever arm loading ratio and loading/unloading was accomplished through hydraulic ram displacement. Measured

weights were suspended at one end of the loading arm and a pull bar, specimen, and pull bar with a load cell were held in tension at the other end. An upward movement in the hydraulic ram would then buoy a fraction or all of the suspended weight and consequently unload the specimen. Loading was done in a converse manner.

The compact tension specimen was mounted between the two pull bars with Inconel clevises and secured with Inconel 718 holding pins. The specimen's configuration and nominal dimensions are shown in Fig. 2. A complete listing of all the specimens is given in Table I.

The specimen's load-line displacement was measured with an extensometer system. Two E-shaped plates, made of Inconel 718, were mounted directly on the top and the bottom of the specimen and supported two stainless steel rod-in-sleeve extension arms as shown in Fig. 3. The extension arms were suspended on opposite sides of the specimen and their length extended down through the bottom of the oven. The LVDT's were attached at the end of the extension arms which was adequately removed from the oven's heat. Previous work has demonstrated that this rigid fixture technique accurately measures the load-line displacement (9).

A clam shell-type oven was mounted on the creep frame and closed around the specimen, clevises, and a small portion of the pull bar and LVDT extension arms. The

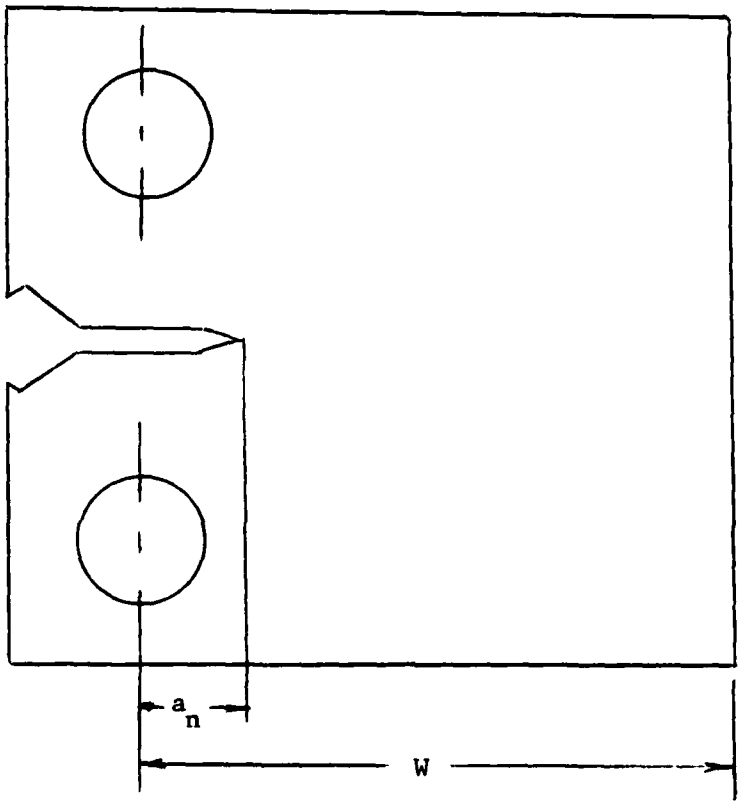

a_n = 7.0 mm

W = 40.0 mm

thickness (B) = 10.0 mm

Figure 2 Compact Tension Specimen

Table I

Exact Specimen Dimensions

All Measurements are in Millimeters

Specimen No.	Width (W)	Thickness (B)	Notch Length (a_n)
84-490,DD1	39.226	9.982	7.051
84-491-DD2	39.903	9.982	7.061
84-492-DD3	39.954	9.992	7.038
84-493,DD4	39.954	10.005	7.006
84-494,DD5	39.949	9.989	7.074
84-495,DD6	39.931	9.972	7.056
84-496,DD7	39.956	9.985	7.092
84-497,DD8	39.990	10.005	7.046
84-499,DD10	39.936	9.980	7.099
84-505,EE6	39.873	10.008	6.965
84-506,EE7	39.933	9.989	7.079
84-507,EE8	39.934	9.990	6.896
84-508,EE9	39.908	10.008	7.087
84-509,EE10	39.936	9.957	7.005

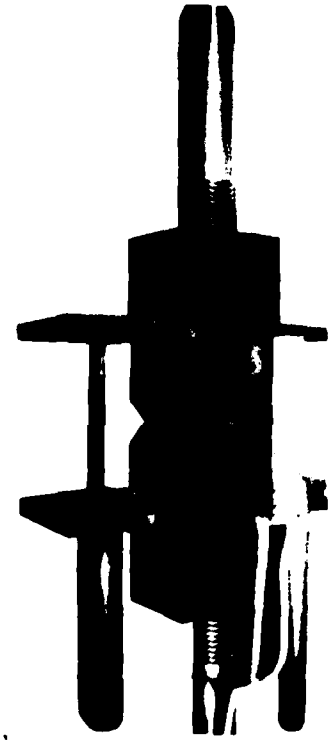

Figure 3 Test Configuration for CT Specimen

furnace was resistance wire wound with four independently controlled power zones. The power was supplied by a time proportioning West temperature controller. Typically, the power supply was limited to about 2 amperes per zone at 130 volts rms ac. The oven's temperature was controlled through a thermostat feedback loop in the West controller. A K-type, chromel-alumel, thermocouple was welded to the specimen and provided the necessary input to the controller. A second thermocouple on the specimen was monitored on the Daytronics digital display.

The internal dimensions of the furnace were approximately 7" X 7" X 5". The furnace had a viewing port on each side. Two Gaertner traveling microscopes were mounted along side of the viewing ports for optical crack length measurements. The configuration is shown in Fig. 4. The microscope displacement was monitored with a digital readout device which displayed measurements to the nearest tenth of a mil. In practice, however, measurements were reproducible to an accurracy on the order of a mil.

Figure 4 Test Apparatus

III. Test Procedures

The Inconel 718 compact tension specimens were mounted in the creep frame after being machined, polished, and precracked. The creep frame was capable of loading the specimen hydraulically (with or without computer control) or mechanically with a gear system. Initially, the specimens were partially loaded at room temperature by mechanical means. The LVDT and load cell response was recorded on an x-y plotter in the form of a compliance measurement. The result was checked for linearity and compared to an initial target value based on precrack length using a standard stress intensity solution (see below). Adjustments were made, as necessary, to assure that the instruments were well calibrated and aligned.

The furnace was then heated for approximately an hour until a stable temperature of 650°C was reached. The four separately powered zones of the furnace assured uniform heating of the specimen. The test was then put under computer control and the specimen was loaded.

Two specimens were used to establish baseline crack-growth-rate for the material under sustained load. The remaining specimens were subjected to sustained load interrupted by a series of overloads applied for various hold times. The overloads were either 20-or 50-percent

above the original loading which corresponded to an initial value of K of 25 MPA$\sqrt{m}$. The overload hold times were either 1 minute or 1 hour in duration. As shown in Table II the overload magnitudes, hold times and K levels at which they were applied were randomly distributed through the majority of specimens. The overload applications were targeted at specific values of K during the test. The values of K = 27.5, 30, 35, 40, 50 MPA $\sqrt{m}$ were chosen because the crack-growth interval between each of them was deemed sufficient enough to avoid any interaction effects from previous overloads. This range of K values also provided a wide data base for the development of the model. In general, the mixing of overload magnitudes, hold times and targeted K levels among the specimens was an attempt to foster measurements that were independent of each other.

A number of steps were taken to reliably determine when the targeted K values occurred. First, the following seven degree polynomial was solved for the crack length at the K value of interest:

$$K = \frac{P}{B\sqrt{w}} \quad \frac{(2+a/w)}{(1-a/w)^{3/2}} \cdot (0.886+4.64(a/w)-13.32(a/w)^2 + 14.72(a/w)^3 - 5.6(a/w)^4) \qquad (1)$$

where:

K = Stress Intensity Factor

P = Applied Load

Table II

Test Matrix

Specimen No.	TARGET K ($MPA\sqrt{m}$)				
	27.5	30	35	40	50
84-490,DD1	20% OL 1 min	20% OL 1 min	20% OL 1 min	20% OL 1 hr	20% OL 1 hr
84-491,DD2	Baseline---------->				
84-492,DD3	20% OL 1 hr	20% OL 1 hr	20% OL 1 hr	50% OL 1 hr	
84-493,DD4	Baseline---------->				
84-494,DD5	20% OL 1 min			20% OL 1 min	20% OL 1 min
84-495,DD6		20% OL 1 min	20% OL 1 min	20% OL 1 hr	20% OL 1 min
84-496,DD7	20% OL 1 min	50% OL 1 hr			
84-497,DD8			50% OL 1 min	20% OL 1 min	50% OL 40 min
84-498,DD10	50% OL 1 min	20% OL 1 hr	50% OL 1 hr		20% OL 1 hr
84-505,EE6	50% OL 1 hr	50% OL 1 min			
84-506,EE7	50% OL 1 min	20% OL 1 min	20% OL 1 min	50% OL 1 min	50% OL 1 min
84-507,EE8	50% OL 1 hr				
84-508,EE9	20% OL 1 hr		20%OL 1 hr	50%OL 1 min	50% OL 1 min
84-509,EE10	50% OL 1 min	50% OL 1 min	50% OL 1 min		
84-507,EE8		Proof Test---------->			

B = Specimen Thickness

a = Crack Length

w = Specimen width

This is a standard relationship for the compact tension specimen described in Fig. 2 as recommended in ASTM E647 (9). A Fortran program, referenced in the standard's appendix, was used to solve for crack length, a. The calculated crack length was used as a guide during the test to estimate when an overload should be applied. The calculated crack length, a, was compared with the average of the two optical measurements.

Throughout the test, the optical measurements had to be adjusted for the effects of crack tip tunneling (see Fig. 5). A correction factor was determined by using a method similar to the one recommended in ASTM E872 (9). The fracture surfaces of the previously ruptured baseline specimens were inspected, and a 5-point through-the-thickness measurement of the initial crack tip profiles was made. An average tunneling of 0.64 mm was found to exist and this increment was used to adjust optical readings for the remainder of the study.

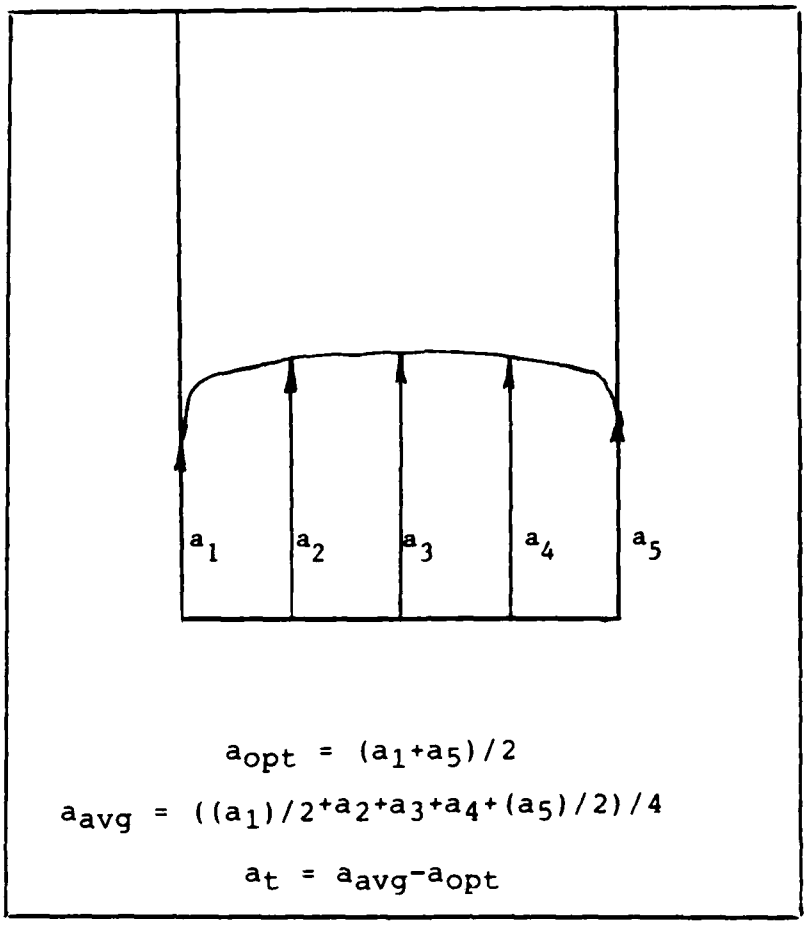

Figure 5 Crack Tip Tunneling Correction Term (a_t)

Fig. 5 demonstrates how a weighted average was used to correct for the significantly biasing effects of the surface measurements.

After each test, the initial profile on the fracture surface was measured since the heat tinting between the precracked and creep regions provided a clear line of demarcation. Unlike IN 100, which Donath (9) observed to have variable tunneling profiles, the precracked

profile of Inconel 718 was found to remain relatively constant. This observation was based on compliance data and was later verified with fracture surface measurements of another specimen. This is shown in Fig. 6. In this particular case, the specimen was precracked to A-A, and then subjected to time-dependent growth until B-B. At that point the specimen experienced a 50-percent overload and the crack was arrested. The specimen was then reprecracked again to C-C and the crack was nearly arrested again with an overload at D-D. Time-dependent crack growth resumed until rapid fracture occurred at E-E. Throughout the entire crack-growth history it can be seen that the crack tip profile did not change appreciably.

Although the optical measurements were important for predicting overload events, they were supplemental to compliance measurements in monitoring the overall crack growth behavior. During the compliance measurement, the computer would acquire up to 200 data points in the unloading/loading cycle. Initially, compliance was taken by unloading only 40-percent of the sustained load and using 50-percent of the data above and below the mean value to calculate the slope. However, this window of data proved to be too narrow and resulted in considerable scatter in crack length determination when the data were reduced. In order to eliminate this effect, the

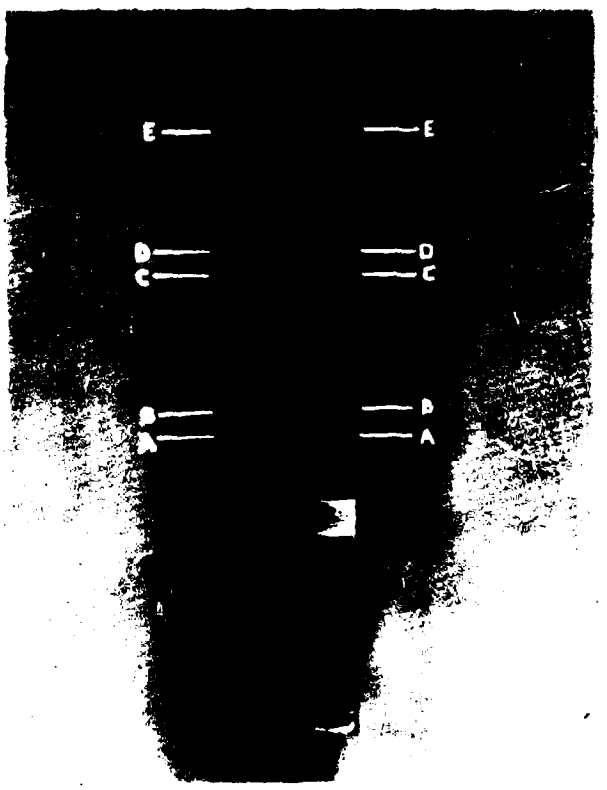

Figure 6 Load History on Fracture Surface EE6

window was expanded by unloading 90-percent of the total load and using 50-percent of the data above and below the mean to calculate the compliance. As can be seen in Fig. 7 this allowed a greater portion of the load-displacement line to be surveyed and greatly reduced this form of experimental scatter.

The necessity of taking compliance measurements, of course, subjected the specimen to periodic loading and unloading. This seemed to introduce a fatigue component into the crack growth behavior. However, Larsen and Nicholas (8) have shown that for sustained-load crack growth interrupted by fatigue cycles in Inconel 718, at 649 °C, the sustained-load crack-growth rate is not appreciably influenced by fatigue when the hold times are approximately greater than 10 seconds. Since compliance measurements were generally taken every 5 to 15 minutes the cyclic frequency effect was considered negligible. Under these conditions, it was concluded that the crack-growth behavior investigated in this study was purely time-dependent.

During the test, the specimen was subjected to overloads at predetermined intervals. When an overload was applied, the test was removed from computer control and the specimen hydraulically unloaded. The hydraulic system prevented the specimen from experiencing any sudden shocks or load spikes while additional weight was being

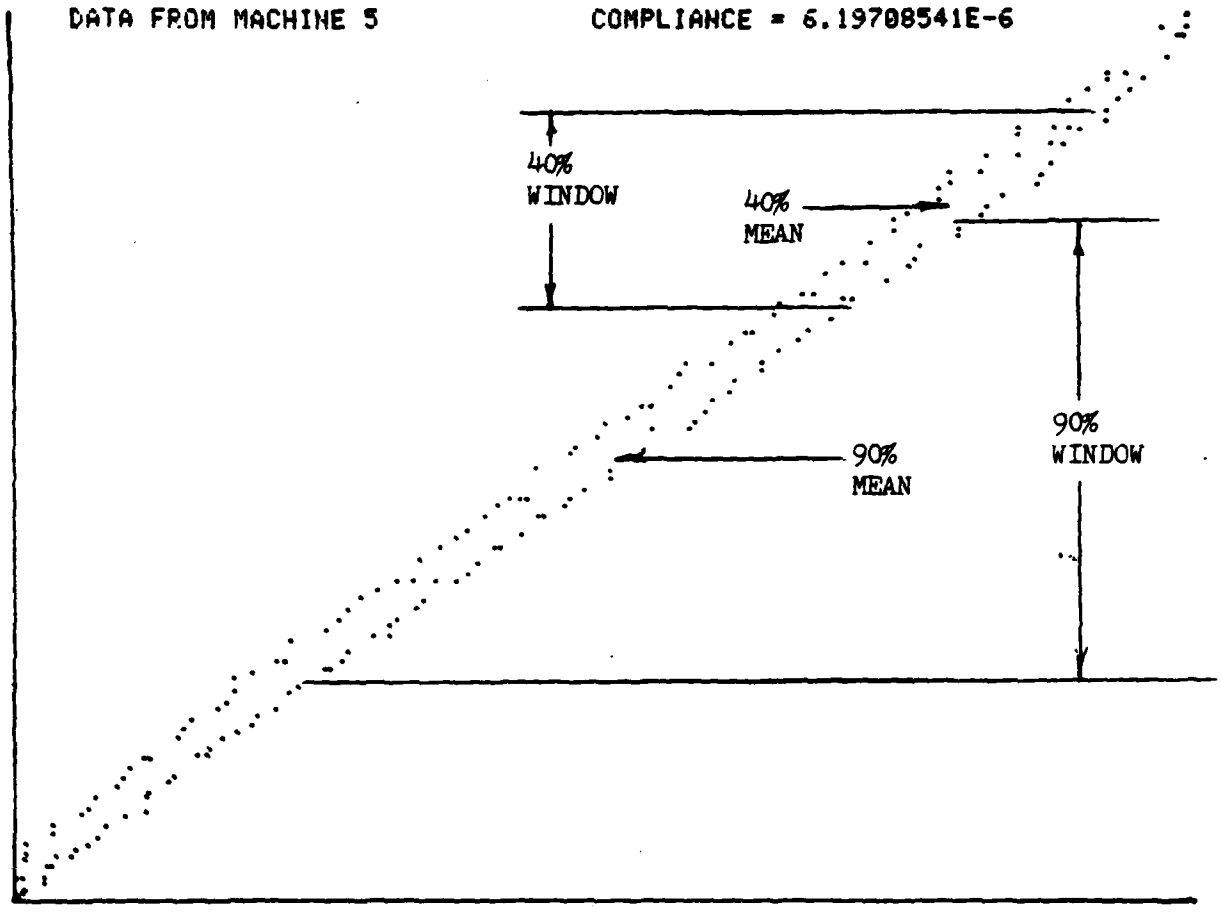

Figure 7 Compliance Window

added. The specimen was then reloaded for the duration of the overload.

Since continuous monitoring of the specimen to determine when another overload should be applied was impractical, occassional overnight shutdowns were required. To prevent any additional crack growth, the specimen was unloaded to 10-percent of its original value and allowed to remain at test temperature. The time associated with this shutdown was later edited from the data tape. Since the specimen experienced thermal soaking during the shutdown, precautions were taken to re-establish the previous growth rate. This was accomplished by reloading the specimen for a least an hour before the next overload was applied. The test then proceeded as before.

IV. Data Reduction

At the completion of each test the data, recorded on magnetic tape by the Tektronix, were transferred to the PDP host computer system. The format of the raw data was changed and all data were reduced. Load, time, and compliance measurements, along with the specimen's configuration and material properties at 650°C, were used as inputs to determine crack length (a), stress intensity factor (K), and the crack growth rate (da/dt).

The crack length was calculated directly from the compliance which is defined as the relative load-line displacement between specimen's top and bottom per unit load. The relationship used for calculating the crack length from this compliance was derived by Ashbaugh (10) from a finite element analysis of a CT specimen. His polynomial fit to the data yields the following equation:

$$a = W*(-.1683106*U*U+1.017563*U-.6948032) \qquad (2)$$

where:

U = log (E*B* compliance)

E = material modulus at 650°C

B = specimen thickness

W = specimen width

a = crack length

Because of experimental scatter, the input data would often cause point to point irregularities in the crack length calculation. This effect was smoothed by using a sliding seven-point least squares polynomial fit on the crack length results. The method used was similar to the one recommended in ASTM E647 (9) with the following second-order polynomial equation:

$$a_i = b_o + b_1(N_i - C_1)/C_2 + b_2((N_i - C_1)/C_2)^2 \qquad (3)$$

with

$$-1 \leq (N_i - C_1)/C_2 \leq 1 \qquad (4)$$

where

a_i = the fitted crack length value at N_i

b_o, b_1, b_2 = regression parameters determined by the least squares method

N_i = current cycle or time

$C_1 = 1/2(N_i - n + N_i + n)$

$C_2 = 1/2(N_i + n - N_i - n)$

n = 3 for a 7-point fit

The crack-growth-rate could then be calculated by differentiating the above polynomial to give:

$$(da/dN)_{ai} = b_1/c_2 + 2b_2(N_i - C_1)/C_2^2 \qquad (5)$$

The stress intensity factor was calculated by using the fitted crack length value and the stress intensity solution previously presented in Section III.

Although the above polynomial technique helped in smoothing results, at times the scatter in the raw data was so severe that gross irregularities still persisted. Point to point differences in crack length up to 2 mm introduced an intolerable degree of bias in the overall crack growth trend. The most extreme scatter was usually encountered during periods of slow crack growth and short crack length (low compliance). A portion of the problem can be stated mathematically as:

$$\frac{da}{dt} = \frac{\Delta a}{\Delta t} + \frac{\Delta ae}{\Delta t} \qquad (6)$$

where:

$\frac{\Delta a}{\Delta t}$ = the crack growth per increment of time

$\frac{\Delta ae}{\Delta t}$ = the error term associated with the measurement

It is evident that during periods of very slow growth the $\Delta a/\Delta t$ term can become very small. As a result, the calculated growth rate, da/dt, can be largely influenced by the remaining error term.

Although this is a reasonable explanation for the higher experimental scatter at low growth rates, it was also noted that there was significantly less scatter at longer crack lengths, even during periods of retardation. A possible reason for this behavior could be attributed to limitations in the LVDT extensometry. Since a portion of

the push rods are exposed to high temperatures, it's conceivable that an oxide layer buildup on the stainless steel rods would cause sticking during compliance measurements. Because of the high degree of sensitivity involved, small frictional effects could introduce a significant error during periods of limited displacement. At longer crack lengths, however, a small amount of sticking could be dislodged by the larger displacements. Fig. 8 shows the effects of friction on a typical compliance measurement.

It is reasonable to assume that the experimental scatter was caused by a combination of factors such as the two just mentioned; but unfortunately little could be done to eliminate them. In order to more accurately ascertain the crack-growth-rate behavior, it became necessary to eliminate highly spurious points which unreasonably biased the remaining data. A systematic approach involving the comparison of optical measurements and calculated crack lengths was developed for this purpose.

Basically, an iterative process was used by first plotting the a vs t behavior of the reduced data and comparing it with the optical measurements made during the test. In most cases the optical readings agreed remarkably well with an assumed mean crack length vs time curve. A reasonable envelope was then established around the mean curve and points outside of it were deleted. If

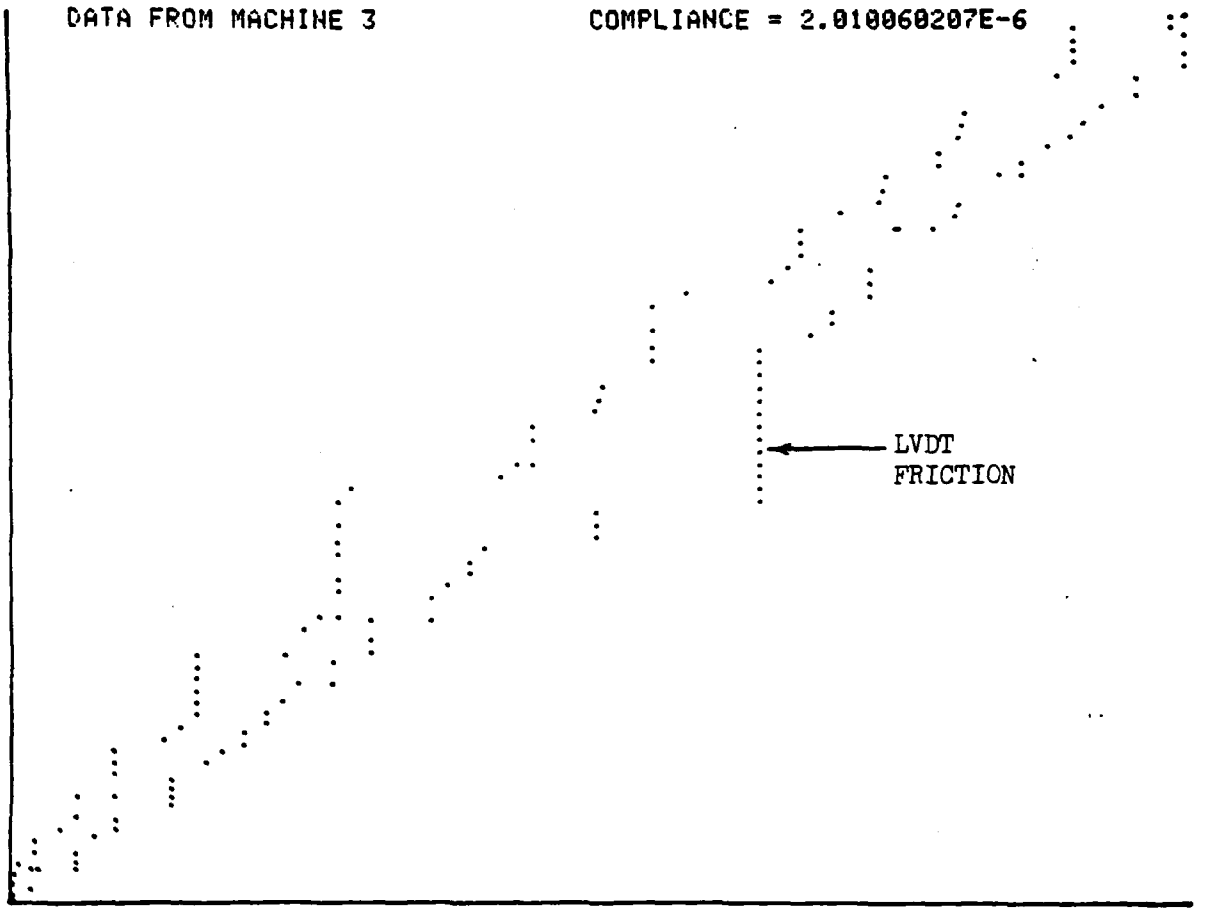

Figure 8 Frictional Effects on Compliance Measurements

more iterations were required, the process was repeated by shrinking the envelope on each successive iteration. Typically, though, most points were within 0.5 mm of the mean after the second iteration. An example of a case that required only one iteration is shown in Fig. 9.

It can also be seen in Fig. 10 that similar results could be attained by using a larger number of points for the least squares polynomial fit. However, to fit the initial and final points the polynomial method requires an extrapolation at the beginning and end of each data set. Therefore, reducing the data with a seven point fit creates an uncertainty in the value of the first 3 and last 3 points. In general, a 2n-1 point fit makes the first n and last n points questionable.

Since the objective of this study required individual analysis of each overload event, independent of the others, the raw data were divided into a number of separate segments. Since the number of data points within each segment was limited, it was desirable to maintain the integrity of as much of the reduced data as possible. For this reason, all data reduction was limited to a seven-point fit.

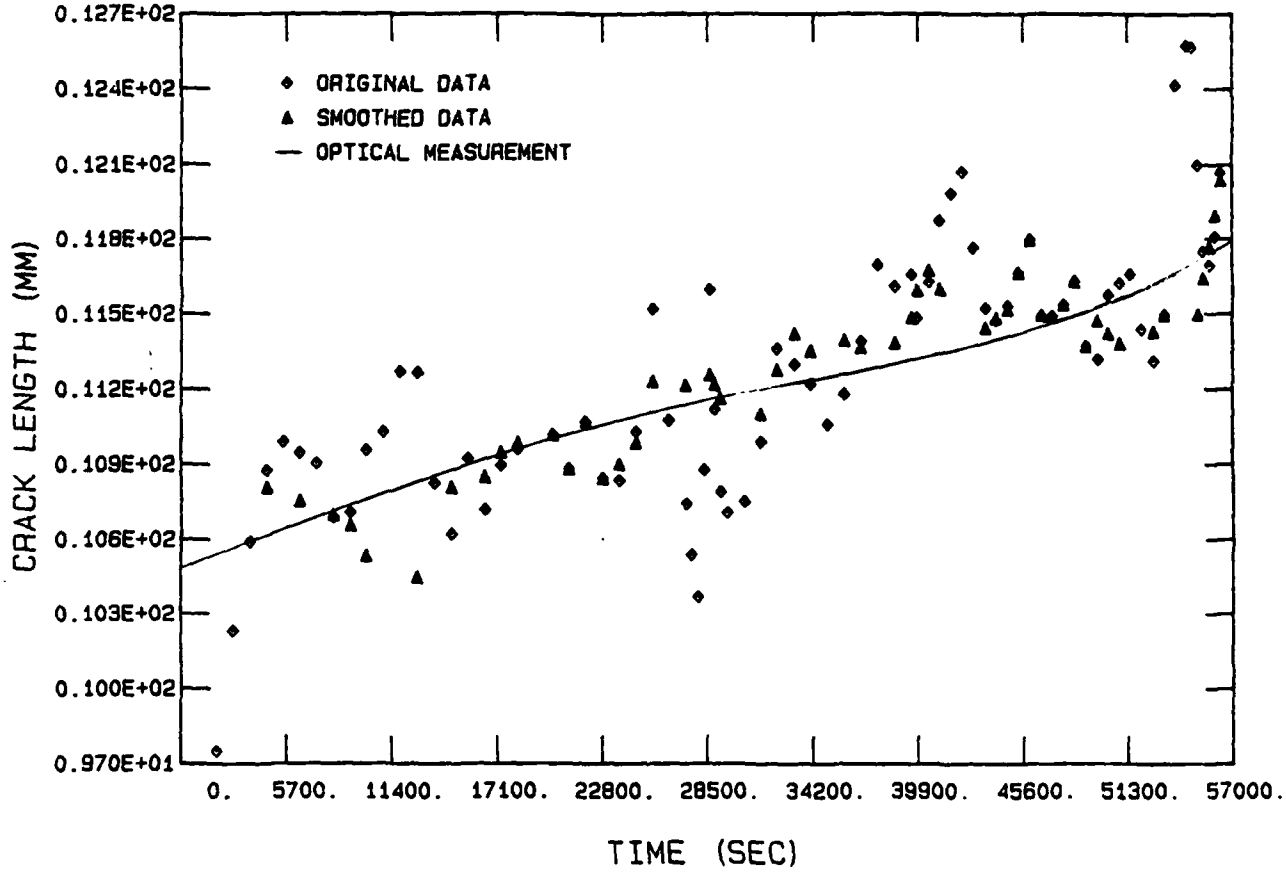

Figure 9 Experimental Scatter reduced by Eliminating Spurious Points

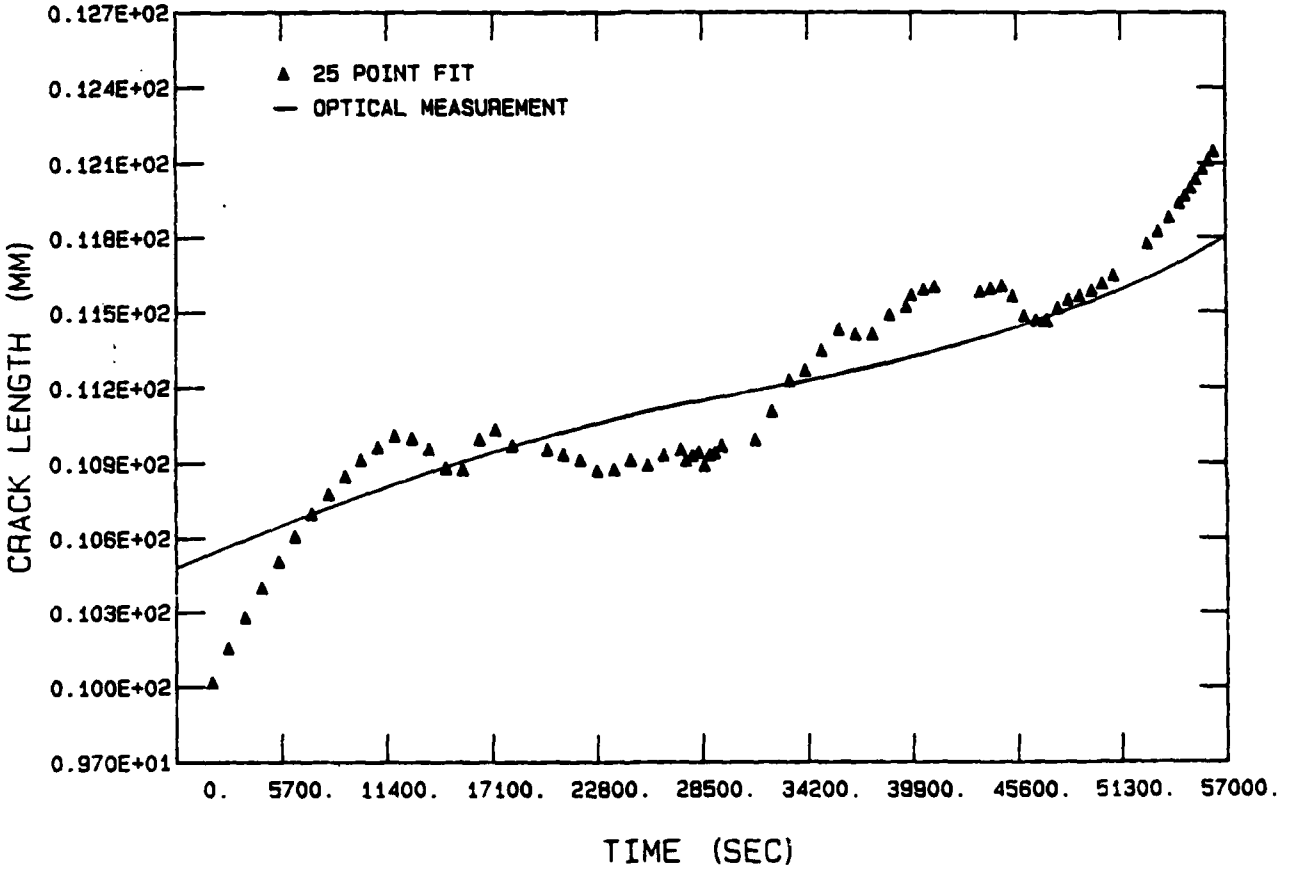

Figure 10 Experimental Scatter reduced by a 25 point Polynomial Fit

V. Model Development

The sustained-load retardation model is developed in this section. Experimental results are also presented, when necessary, to support the model development. Table III presents the overload magnitudes, the values of K when the overload was removed, and the resulting delay times. From this summary of data the overall trends are examined and used to develop the sustained-load retardation model. The model will be limited to isothermal conditions and overloads of 20-and 50-percent. A small correction factor was added to the model to account for observed transient effects of overloading. However, a detailed discussion of this last point is deferred to the next section.

To begin the model development, data was needed to characterize the material's behavior. As previously mentioned, this was done with two constant, sustained-load baseline tests. The data from these tests provided a continuous crack-growth rate (da/dt) vs K relationship. A sigmoidal-shaped curve was then fitted to the data as shown in Fig. 11. The equation of the sigmoidal curve is given by the Modified Sigmoidal Equation (MSE) model developed by the General Electric Company (12). For a sustained-load test the MSE model yields:

$$da/dt = \exp (B)(K/K^*)^P (\ln(K/K^*))^Q (\ln(K_c/K))^D \qquad (7)$$

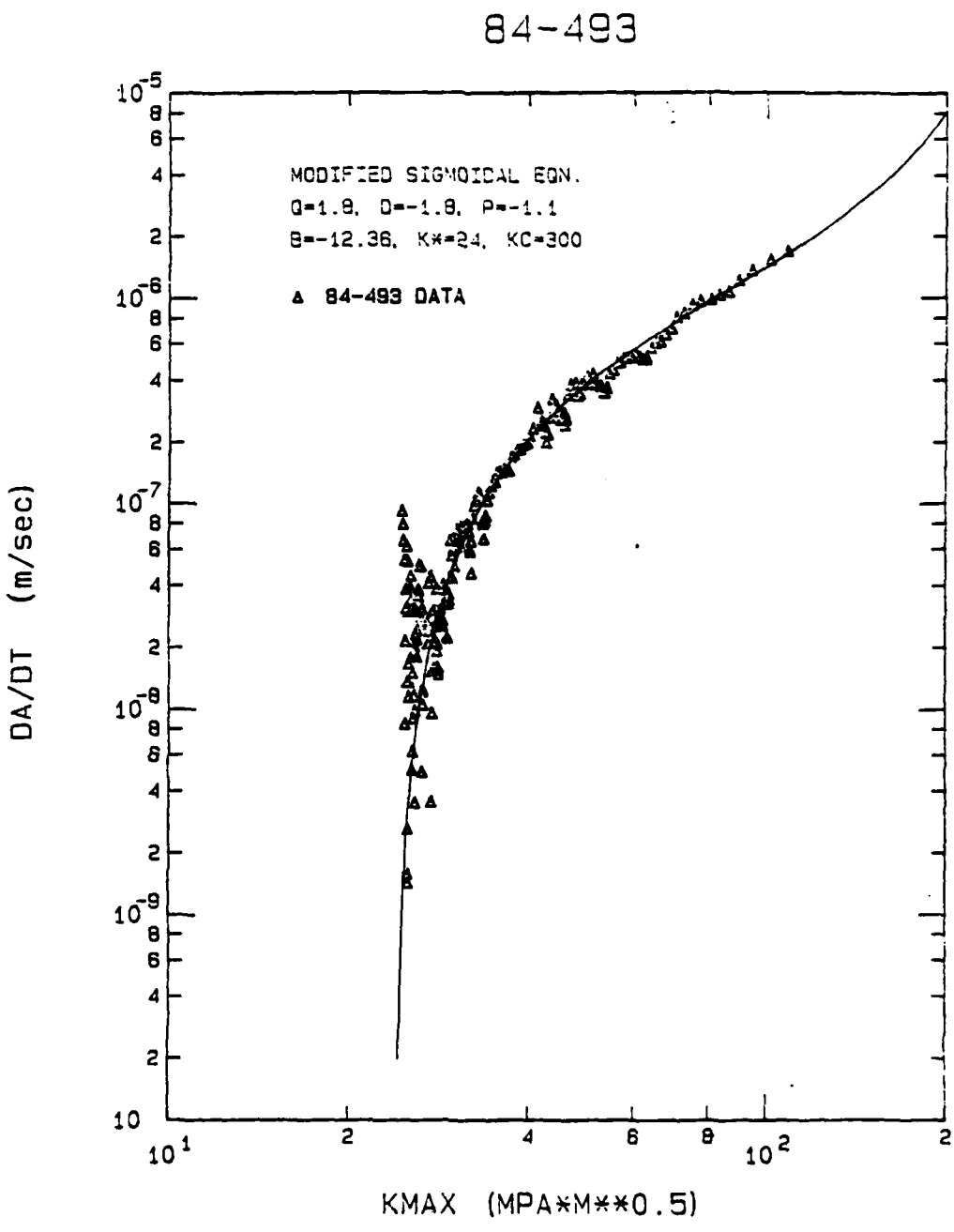

Figure 11 MSE Model Fitted to Baseline Behavior

where

da/dt = the crack growth rate

K = the current value of stress intensity

K_C = the critical value of stress intensity

K^* = the threshold value of stress intensity

B,P,Q,D = parameters that shift the curve to fit the data

The parameter values that gave an acceptable fit to the baseline data are shown in Fig. 11. It should be noted that the true material value of K_C is obviously much smaller than 300 MPA $\sqrt{m}$. The 300 MPA $\sqrt{m}$ value simply provided a good fit to the top end of the da/dt vs K curve. Since the model development was generally limited to the lower portions of the curve, the actual value of K_C was of little consequence.

Having an expression for da/dt as a function of K provided a means to theoretically generate crack length vs time behavior. The time it takes to grow from an initial crack length, a_o, to a larger crack length, a, is determined from:

$$\Delta t = \int_{a_o}^{a} \frac{da}{da/dt} \qquad (8)$$

where da/dt can be obtained from the MSE equation (7) for a specific value of K. K, in turn can be obtained from the compact tension geometry solution, given in equation

(1), for a specific value of a. The integral was evaluated numerically by using a Simpson's rule technique. The theoretical curves were compared with the baseline data in Figures 12 and 13 and showed reasonably good agreement. It was noted, however, that predicting the total time-to-failure was very sensitive to the value selected for K^*. Both baseline tests were started with an initial K of 25 MPA $\sqrt{m}$, but specimen DD4 took 2.5 days to fail whereas DD2 required 4.5 days. Respective values of 22.89 and 24.86 MPA $\sqrt{m}$ were used for K^* to model this behavior with the MSE equation. This large difference in behavior can be attributed to the dramatic change in da/dt for small shifts of K^* on a log-log plot.

For consistency, an average value of 23.1 MPA $\sqrt{m}$ was selected for K^* and used to analyze all of the data in this study. Unlike the arbitrary value for K_C, however, the influence of K^* was found to be very strong until the crack-growth rate was well above the threshold regime ($K > 30$ MPA$\sqrt{m}$). Since the threshold crack-growth-behavior varies widely from specimen to specimen, it was realized that a general model couldn't accurately predict behavior for all specimens in the slow growth region. For this reason, much of the data gathered was for stress intensity factors thought to be above the threshold influences.

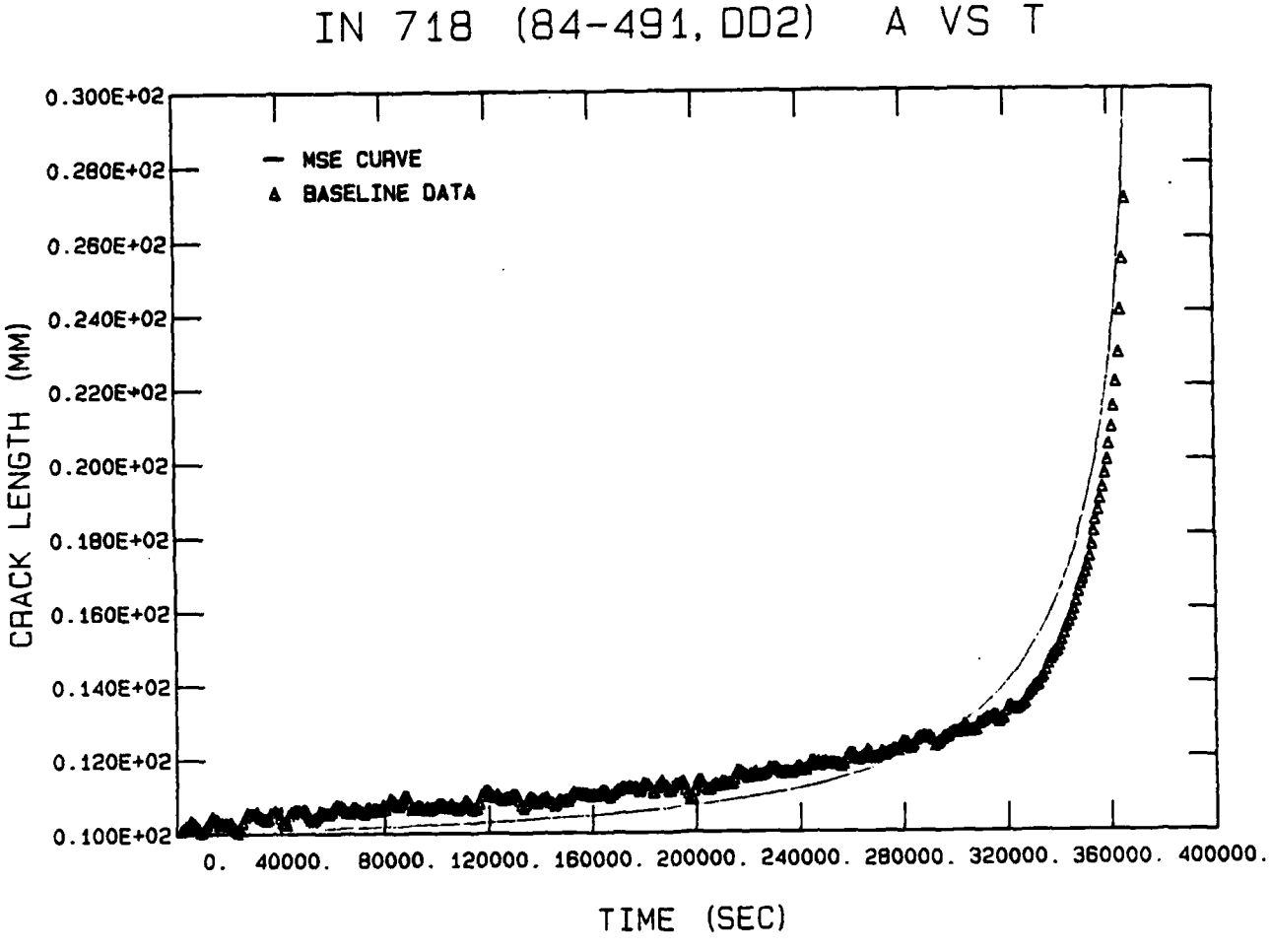

Figure 12 Theoretical and Actual Crack Growth Behavior for Specimen DD2

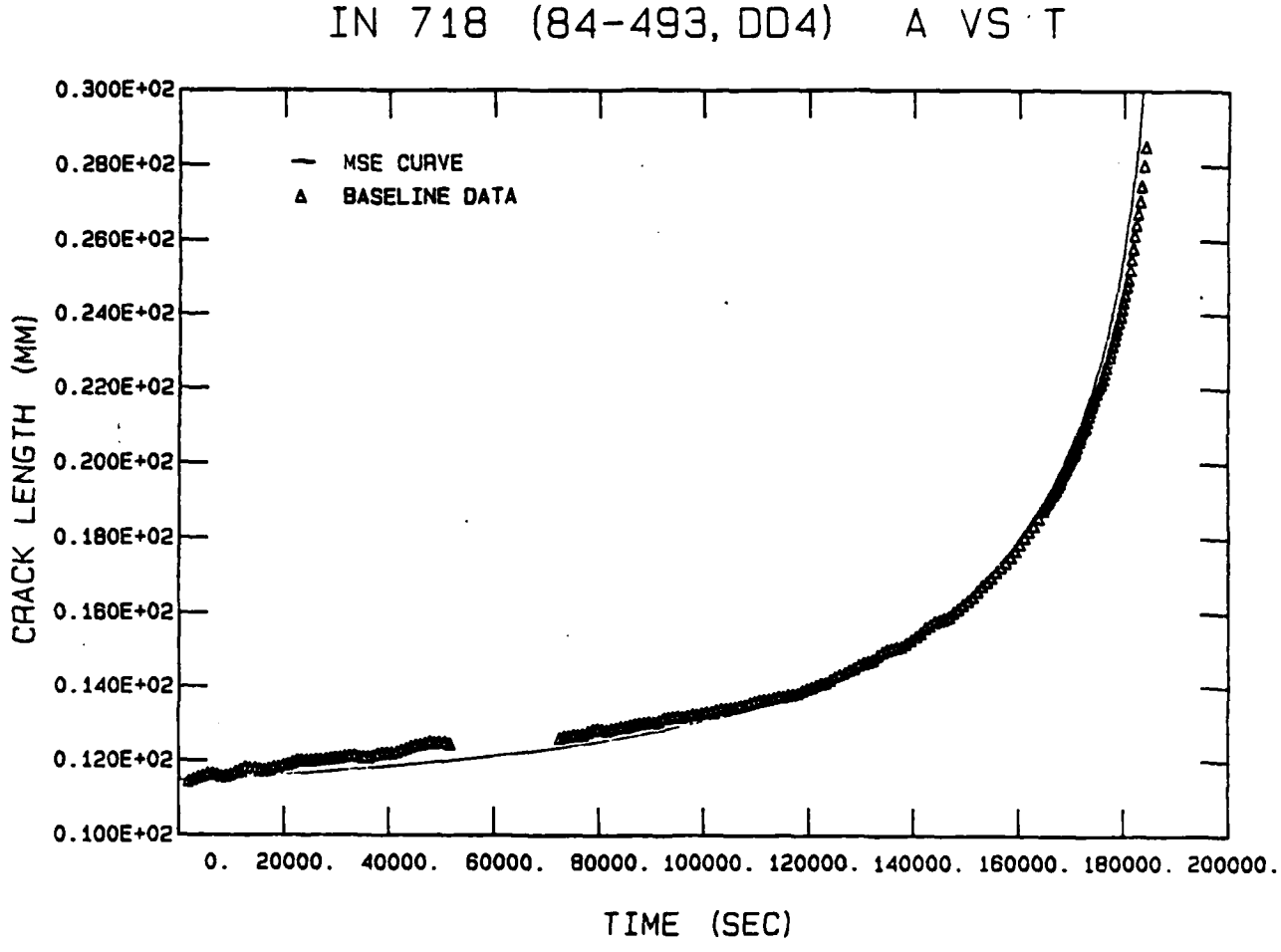

Figure 13 Theoretical and Actual Crack Growth Behavior for Specimen DD4

After establishing a method to reasonably model the baseline behavior, the remaining specimens were subjected to a series of periodic overloads during sustained load testing. The details of the overloads and crack-growth history are shown for all the specimens in Figures 14 through 28. The crack length data for the specimen's overall crack growth history were segmented at each overload point to investigate the resulting crack growth after each overload application. The crack length data were segmented prior to data reduction to avoid any influence between overload regions, due to the seven-point polynomial fit. The delay time (Δt_r) for each segment was then found by comparing the actual data with a baseline curve generated with the integrated MSE equation. The delay time was defined as the difference between the time it took to grow to a new crack length after overloads and the time it took to grow to this new crack length during steady state behavior without overloads (baseline). The new crack length was chosen at the point where the next overload was applied and corresponded to a value where steady state growth had been established. The values for the delay time are presented in Table III.

As can be seen from Table III the values of Δt_r diverge rapidly for overloads applied closer to the threshold region. The trend was exaggerated even further

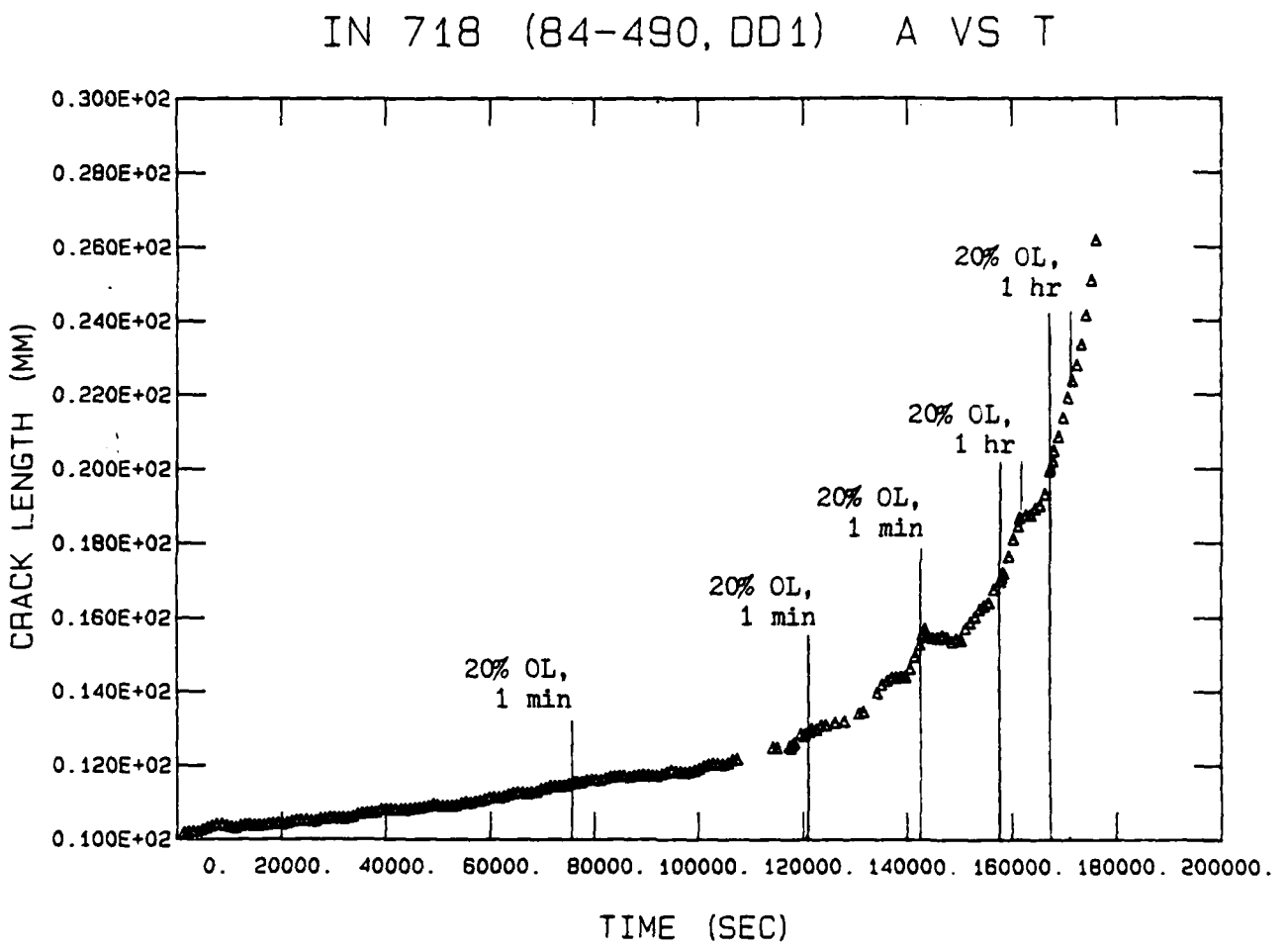

Figure 14 Time-Load History of Specimen DD1

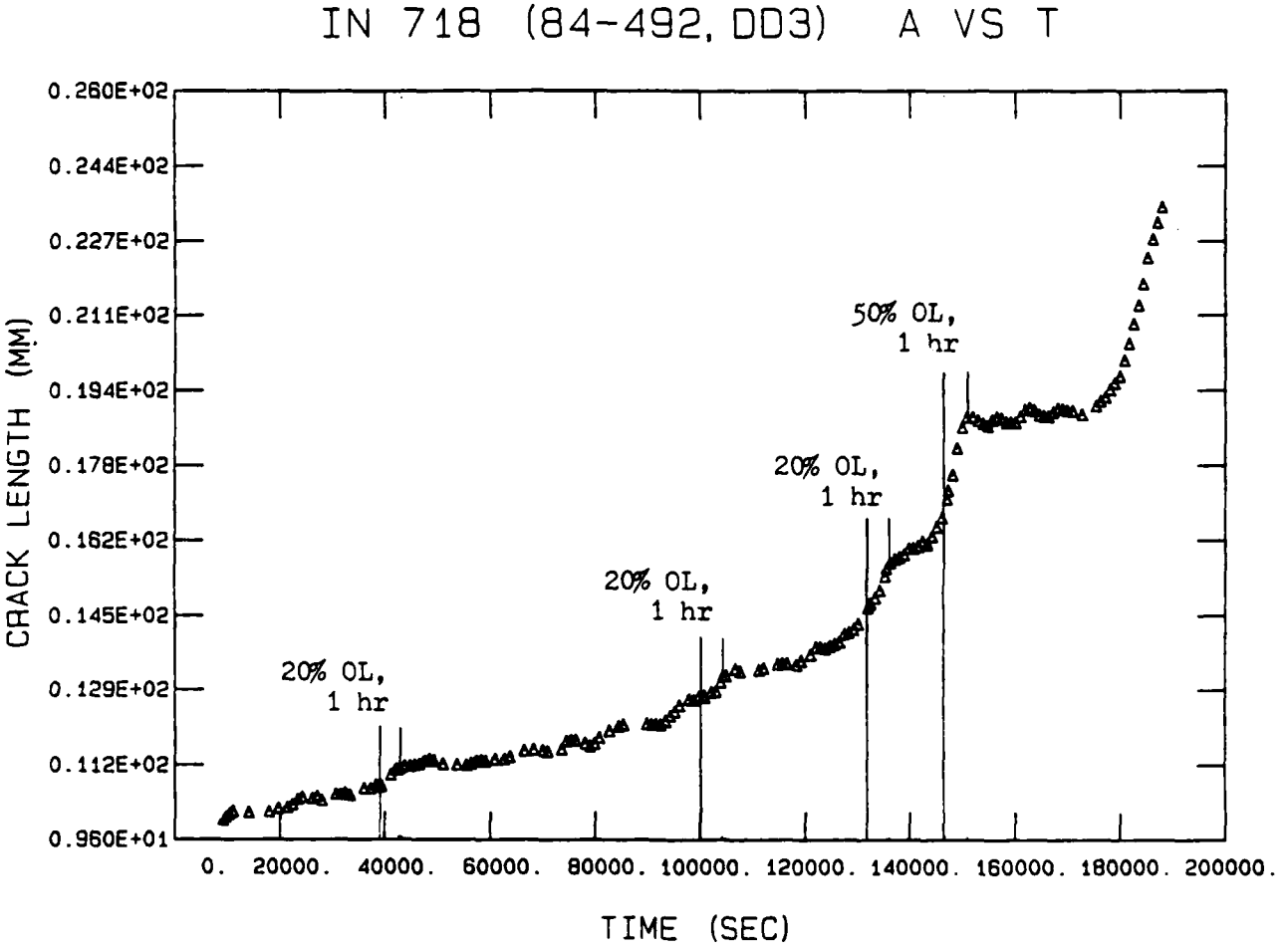

Figure 15 Time-Load History of Specimen DD3

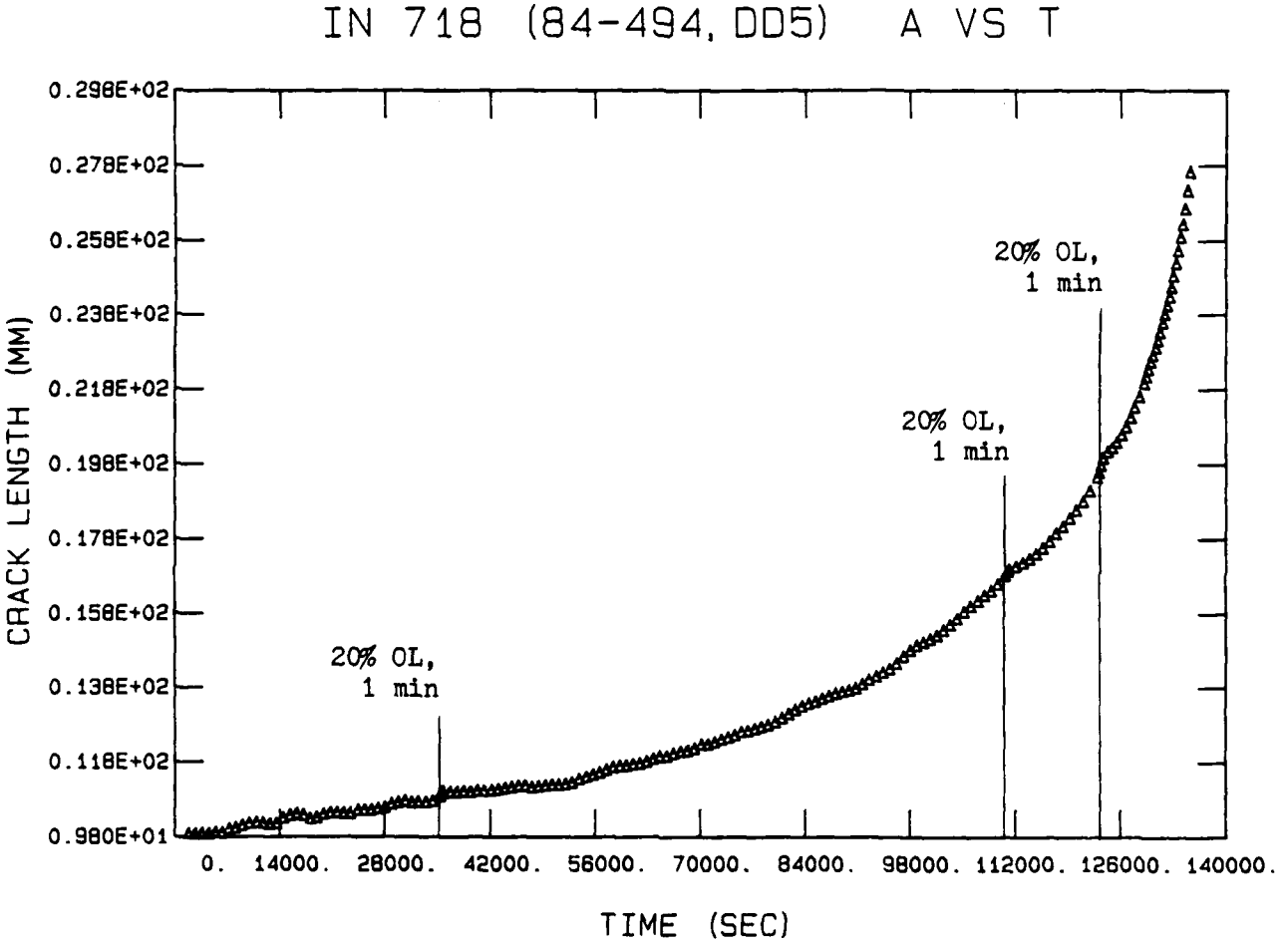

Figure 16 Time-Load History of Specimen DD5

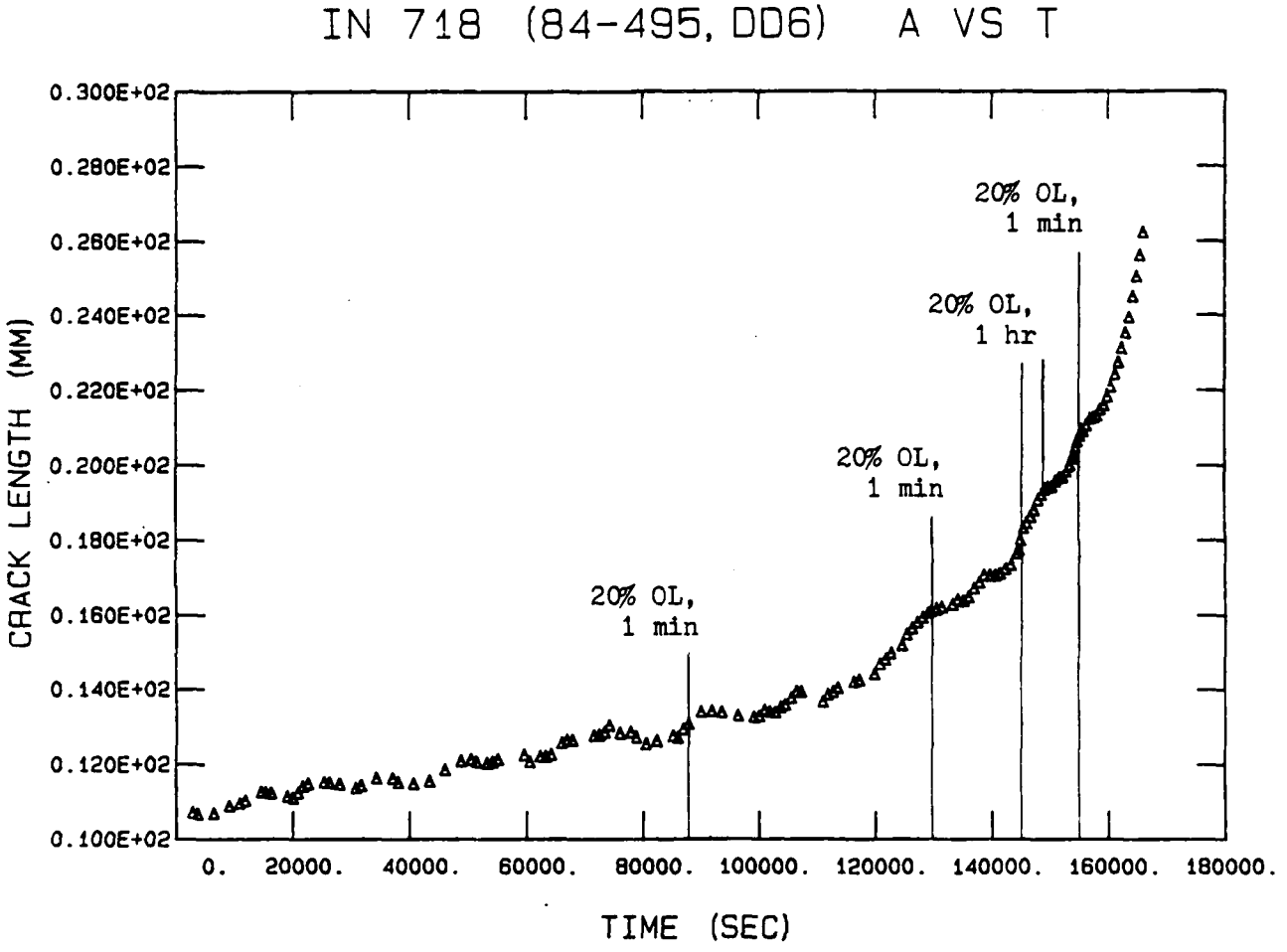

Figure 17 Time-Load History of Specimen DD6

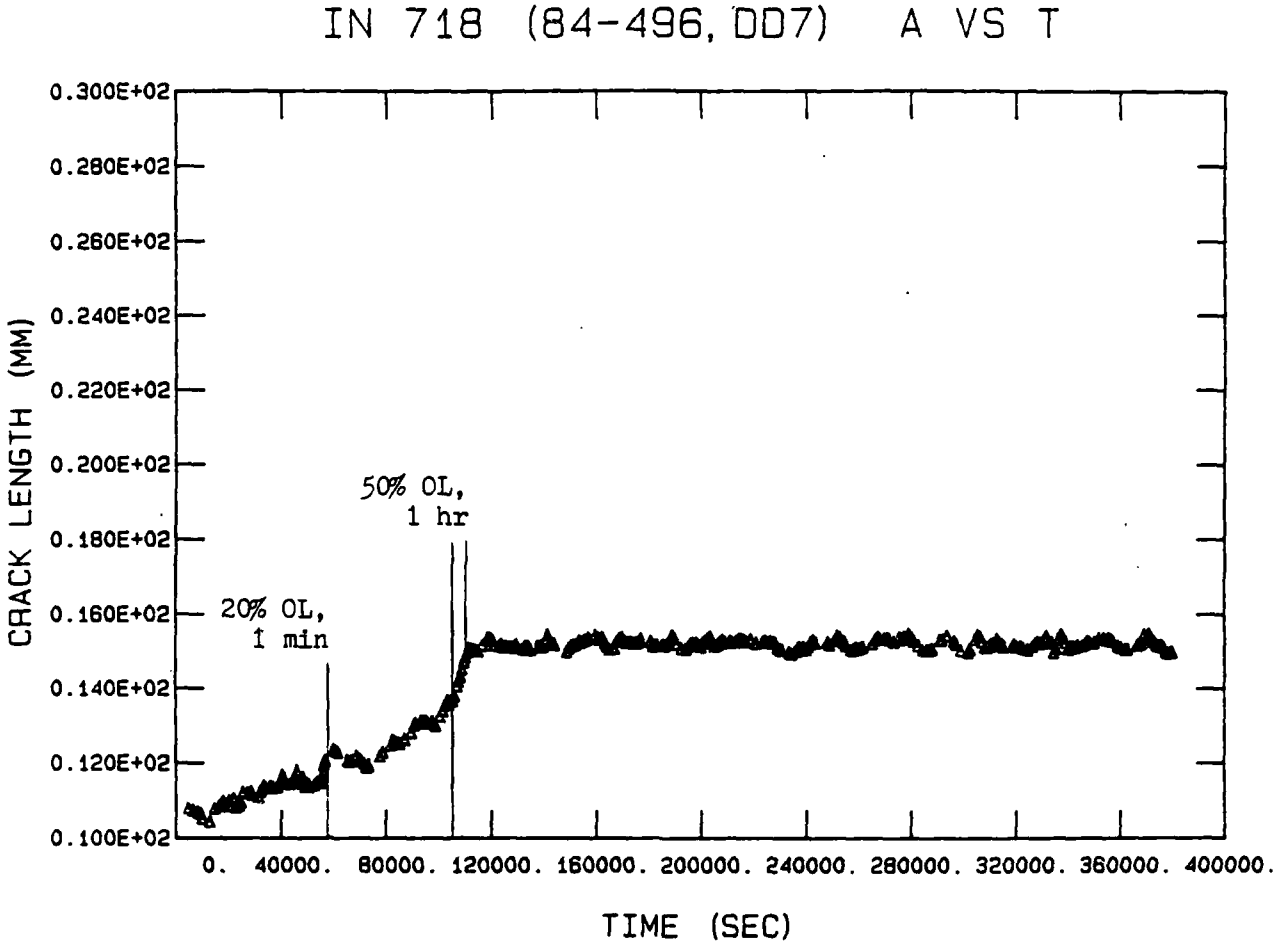

Figure 18 Time-Load History of Specimen DD7

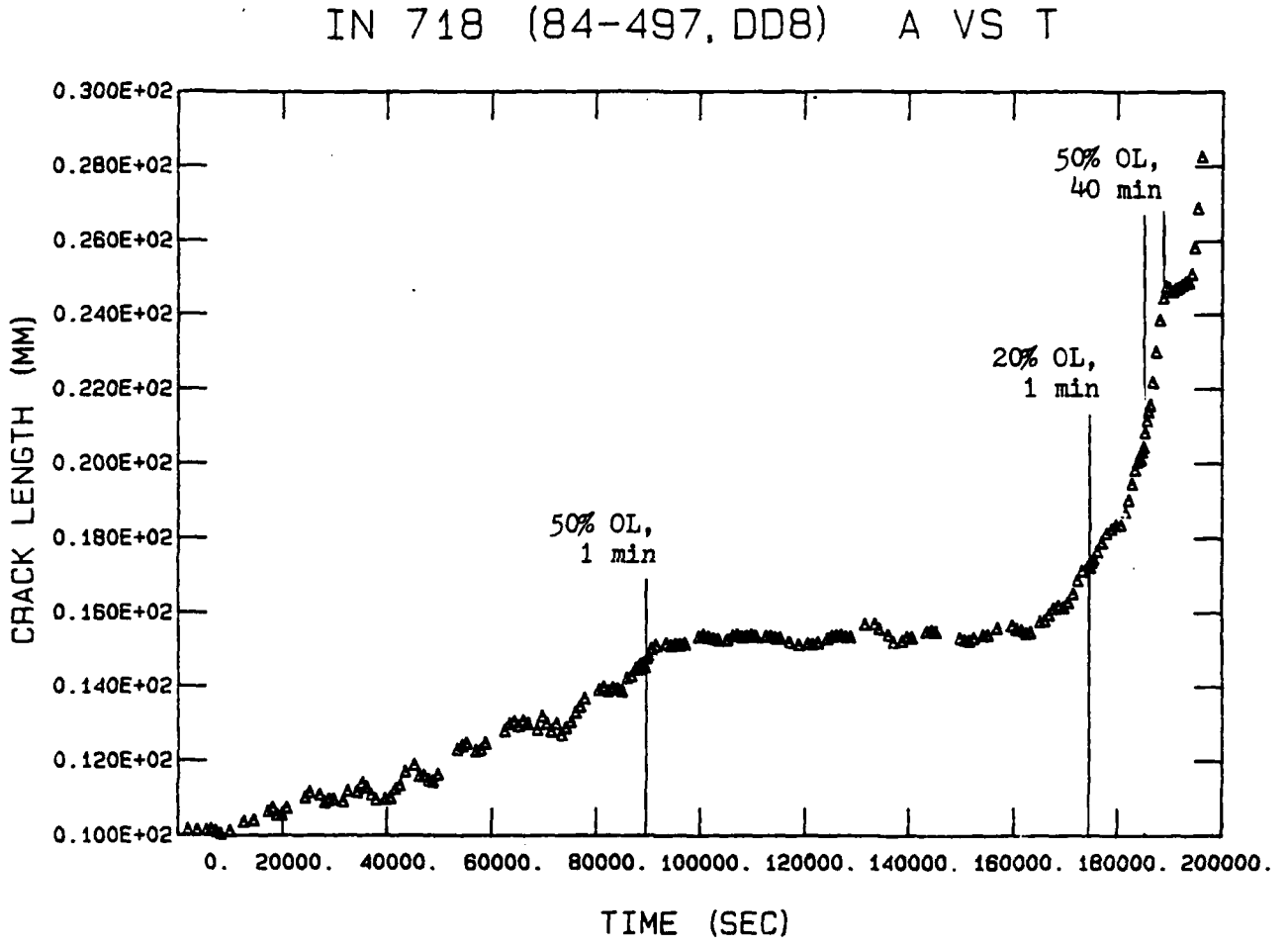

Figure 19 Time-Load History of Specimen DD8

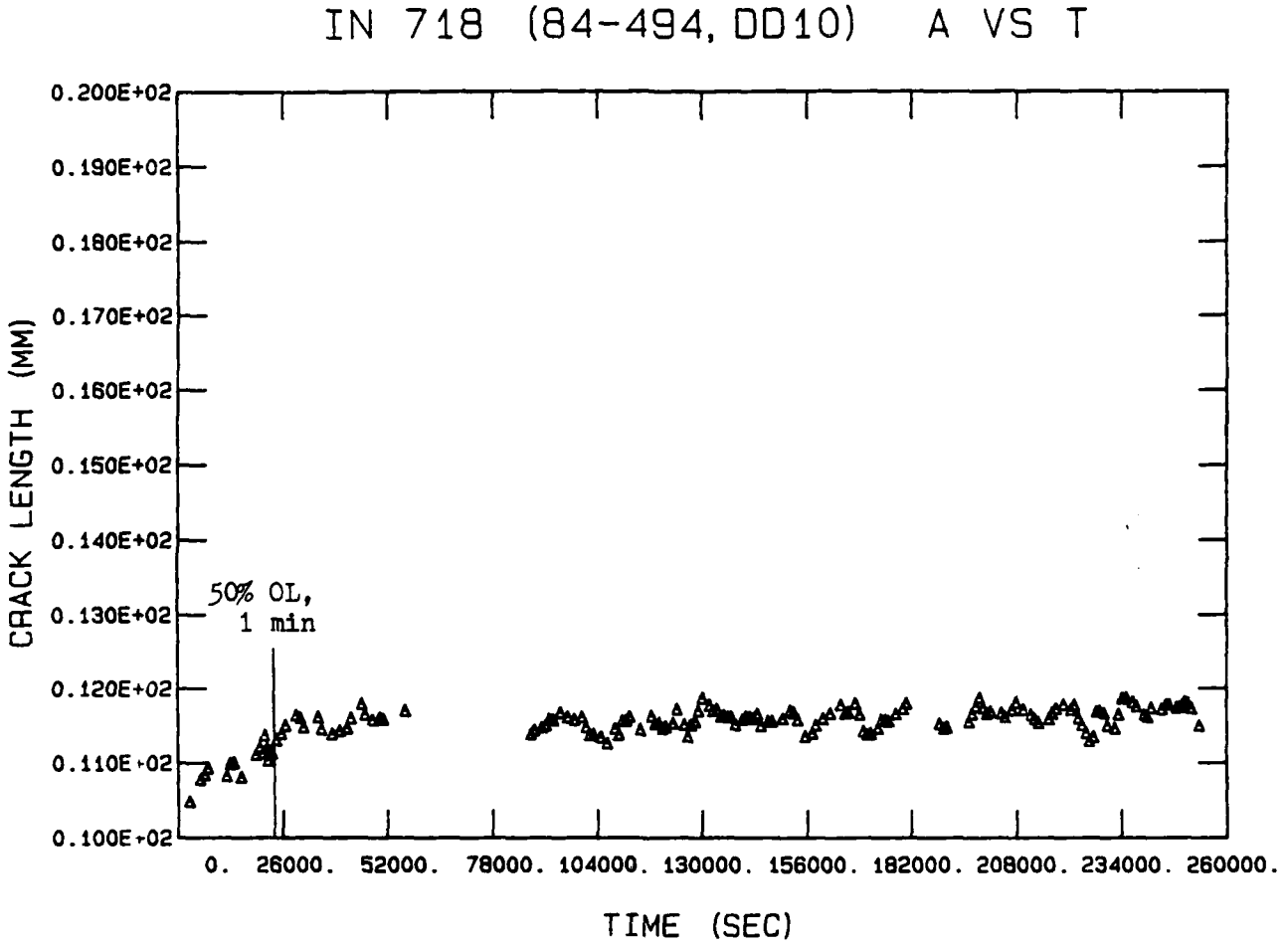

Figure 20 Time-Load History of Specimen DD10 (Part A)

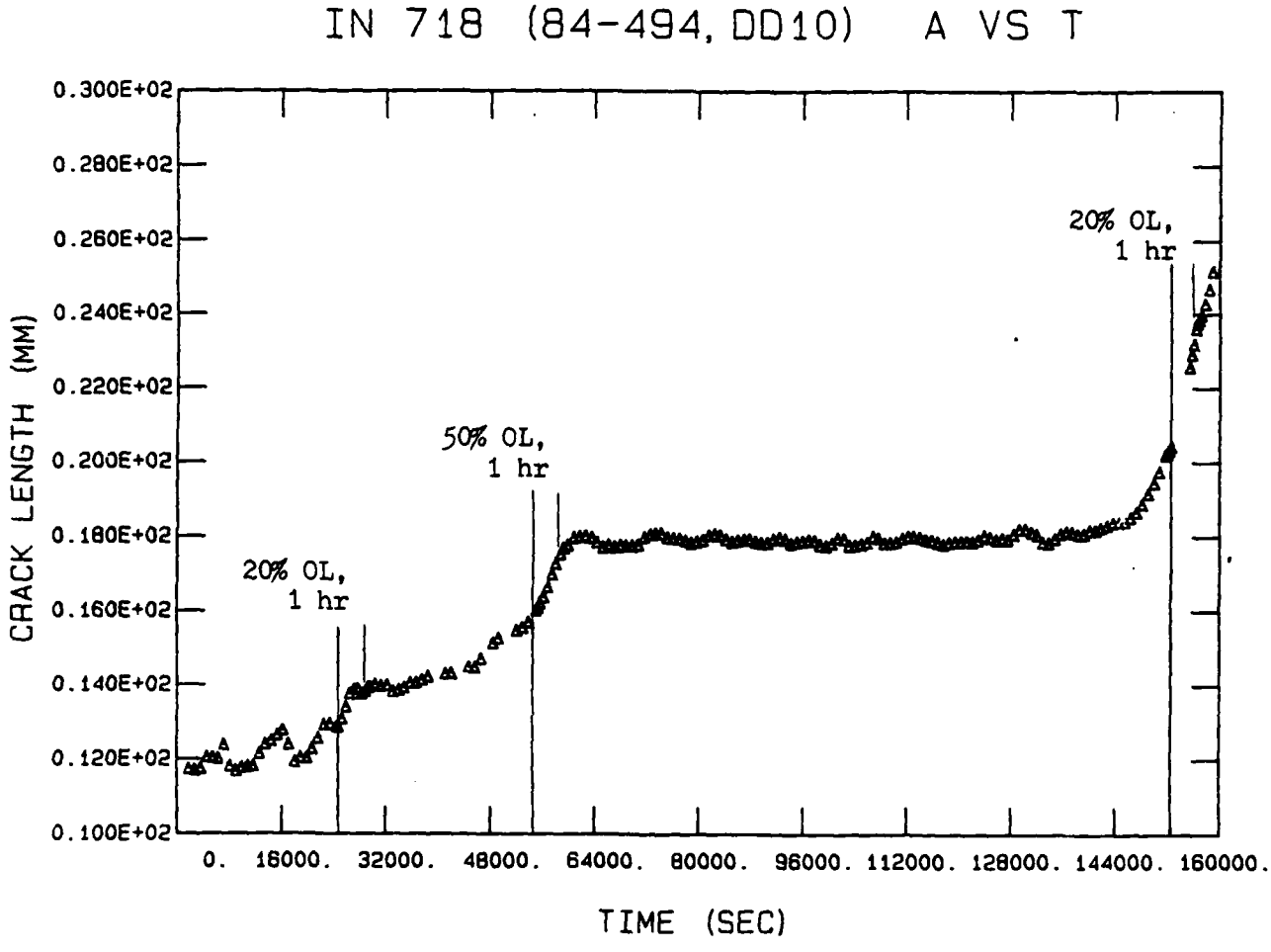

Figure 21 Time-Load History of Specimen DD10 (Part B)

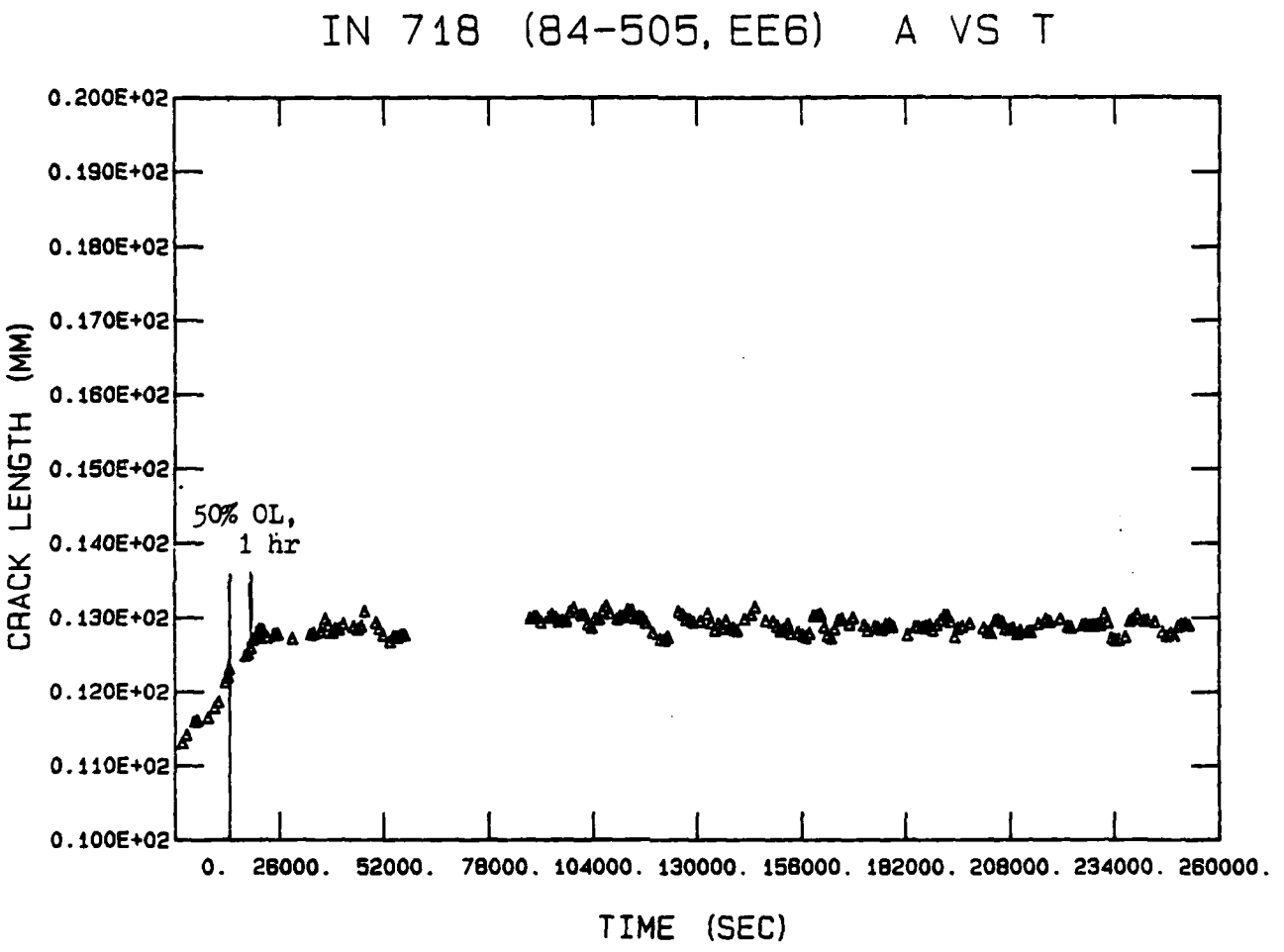

Figure 22 Time-Load History of Specimen EE6 (Part A)

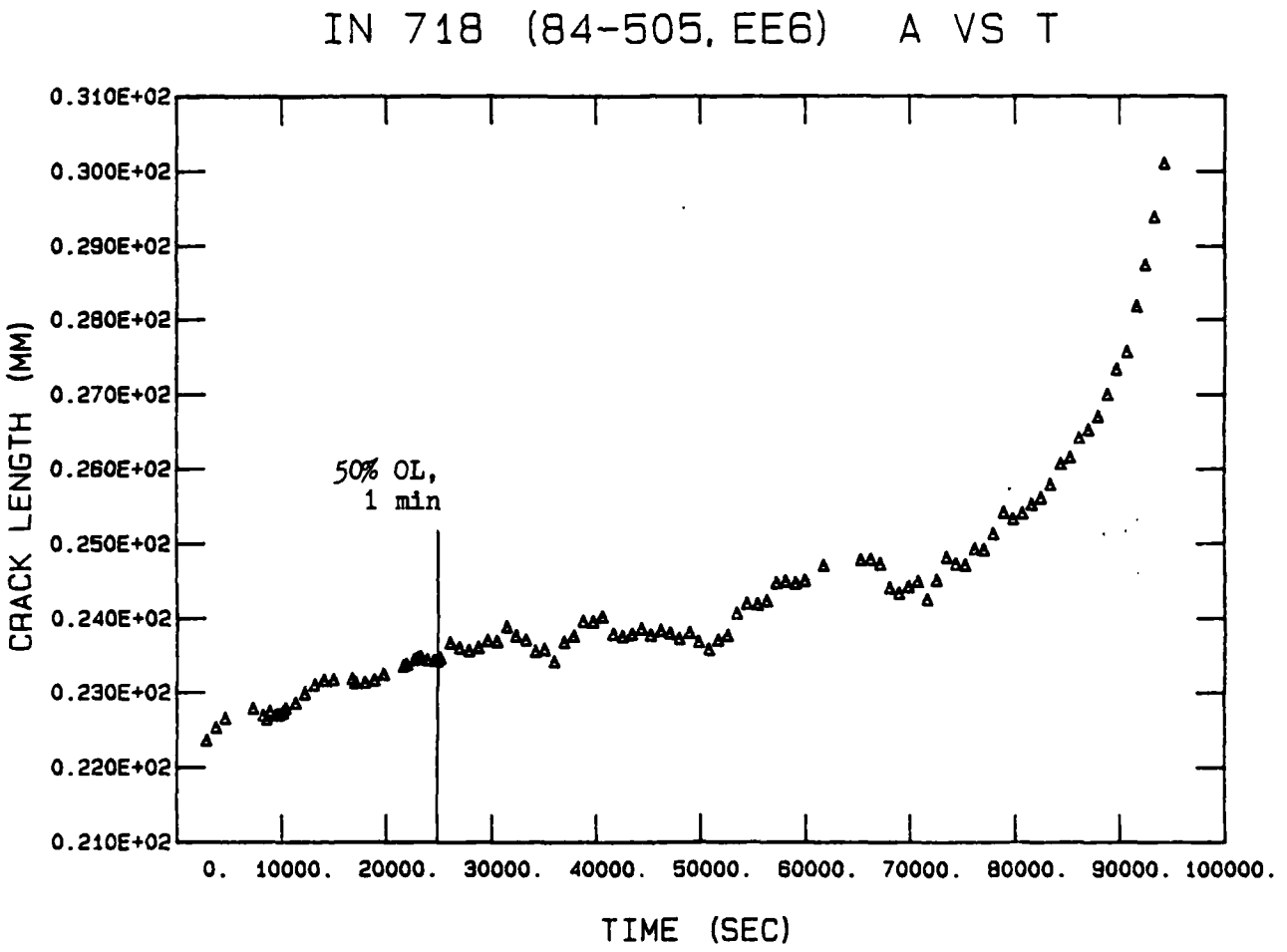

Figure 23 Time-Load History of Specimen EE6 (Part B)

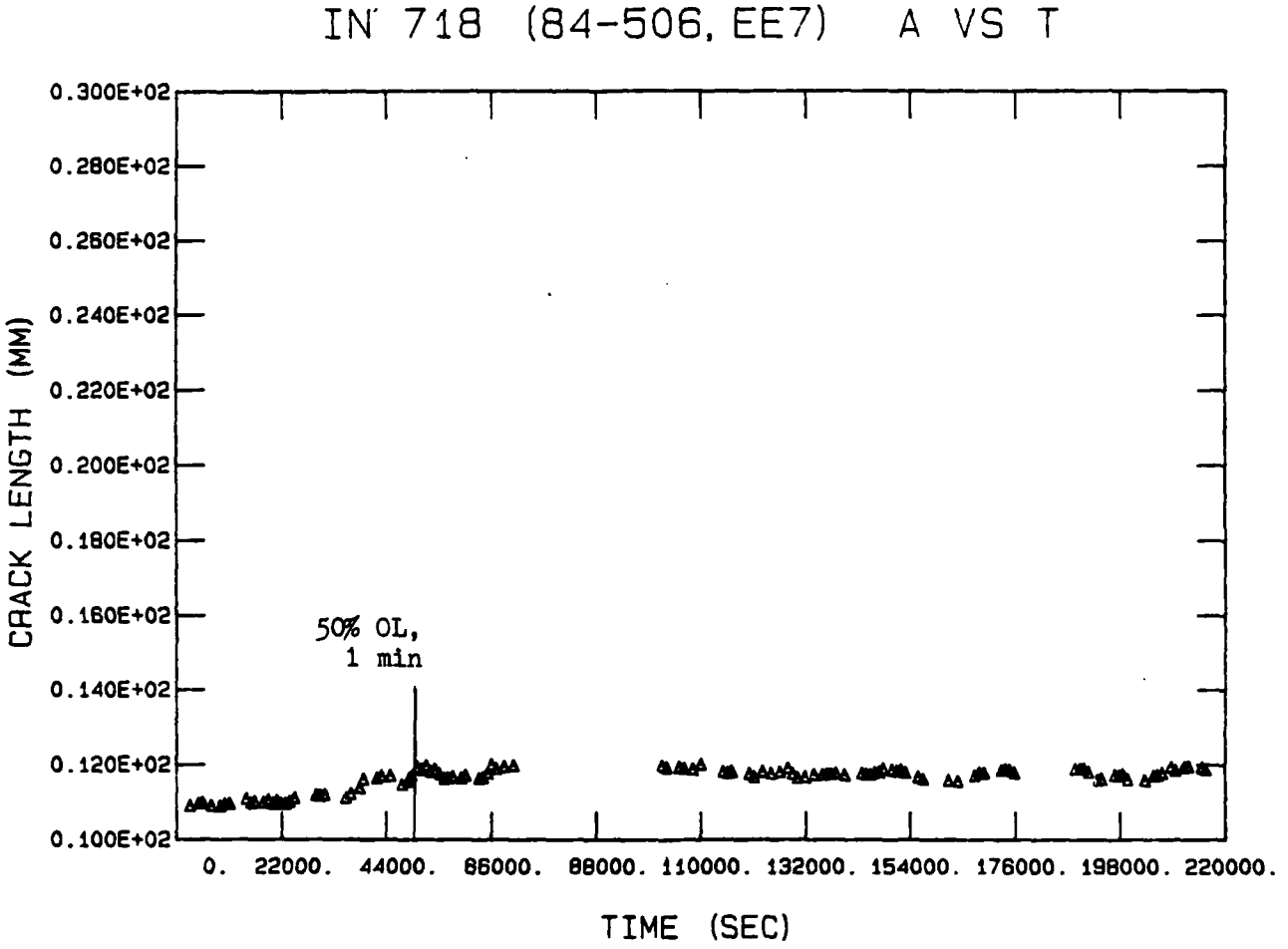

Figure 24 Time-Load History of Specimen EE7 (Part A)

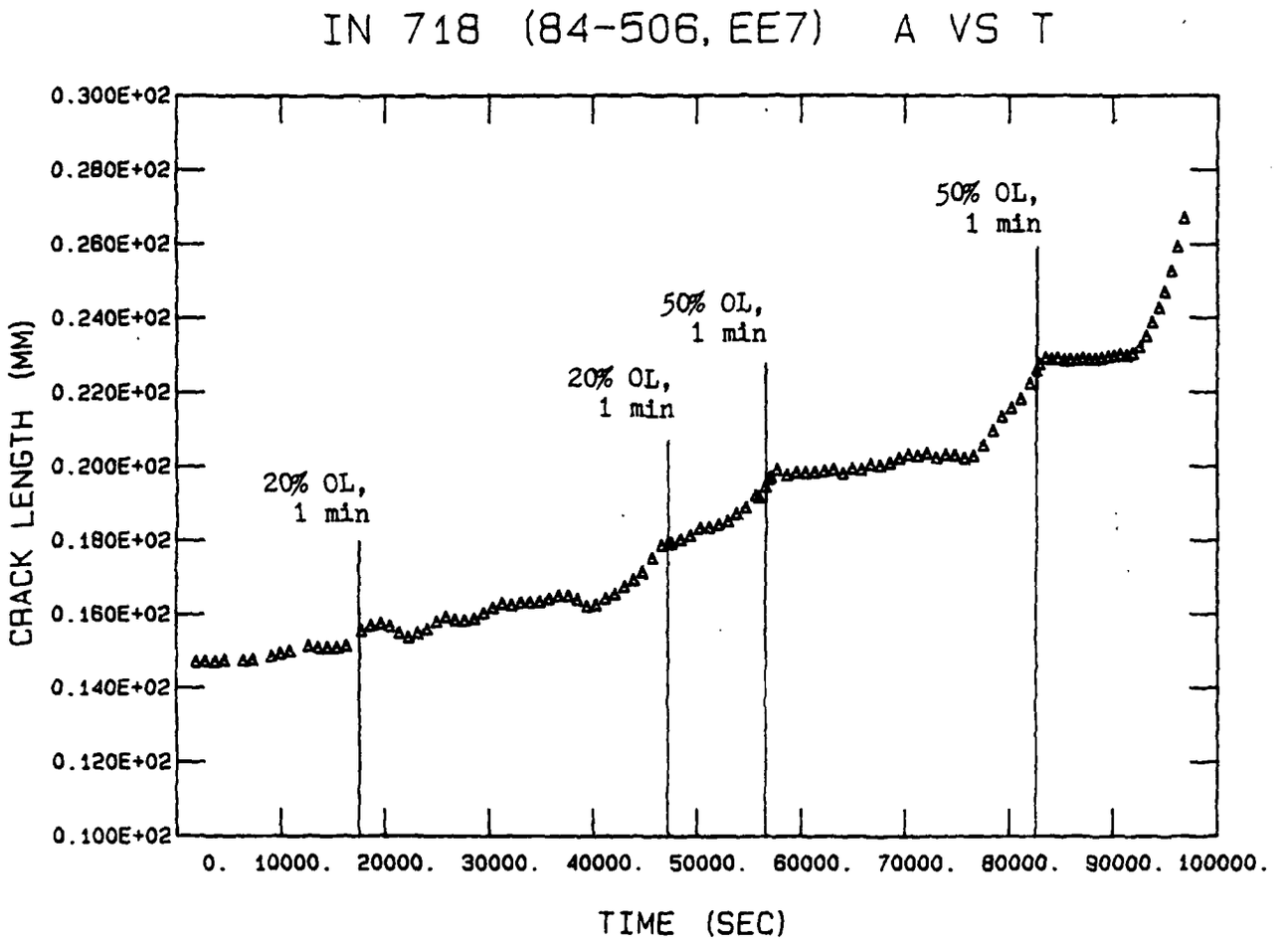

Figure 25 Time-Load History of Specimen EE7 (Part B)

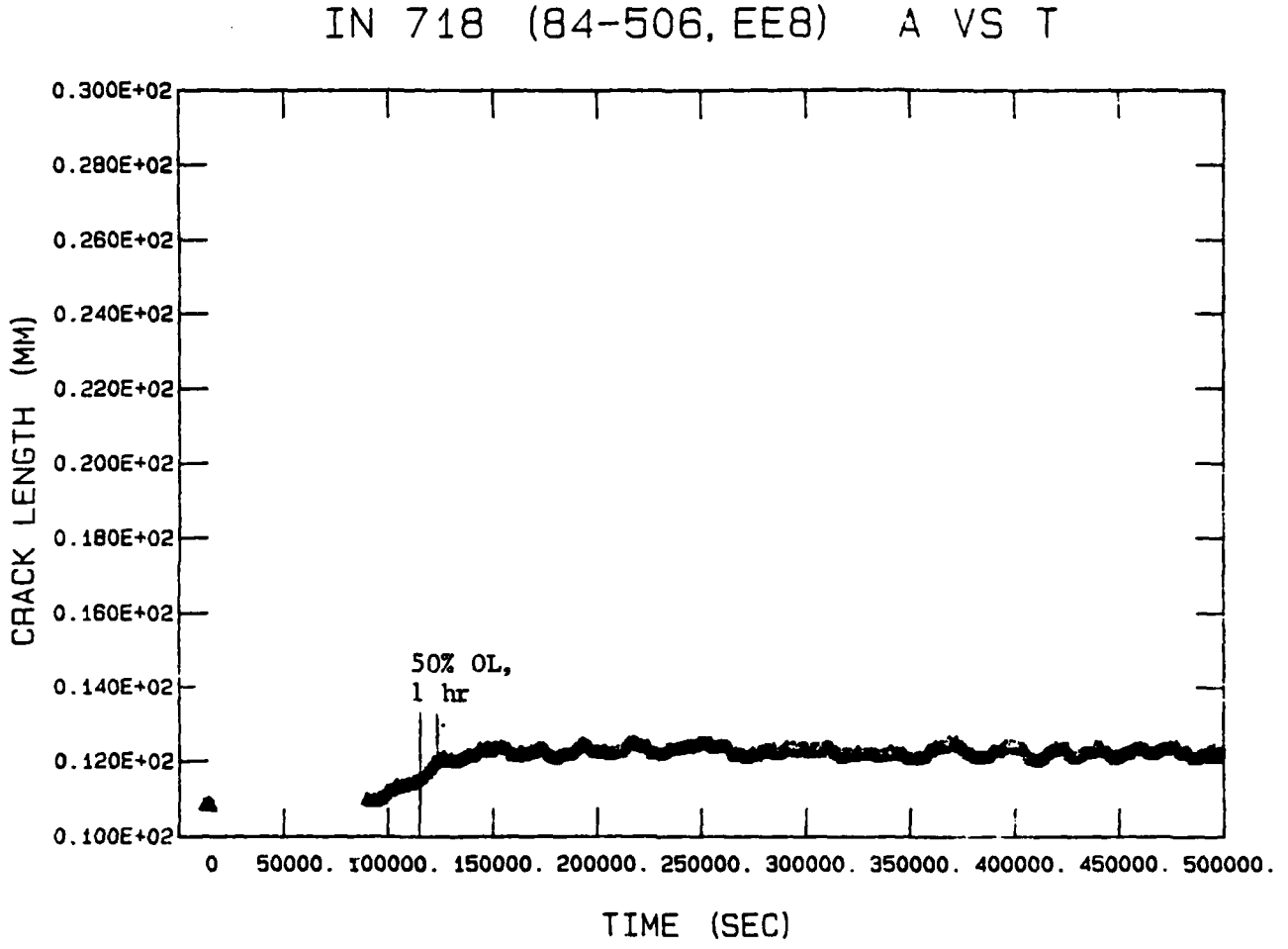

Figure 26 Time-Load History of Specimen EE8

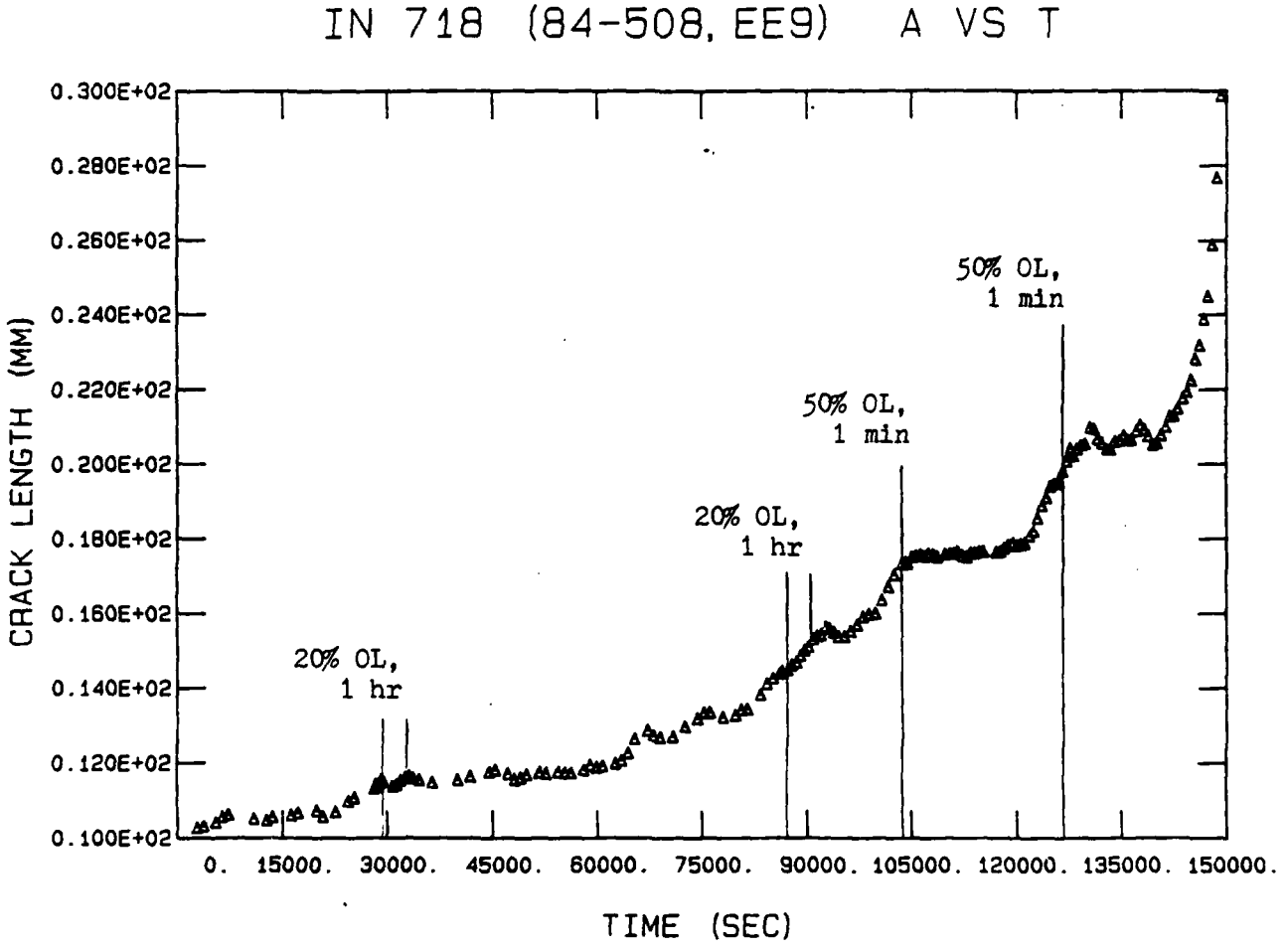

Figure 27 Time-Load History of Specimen EE9

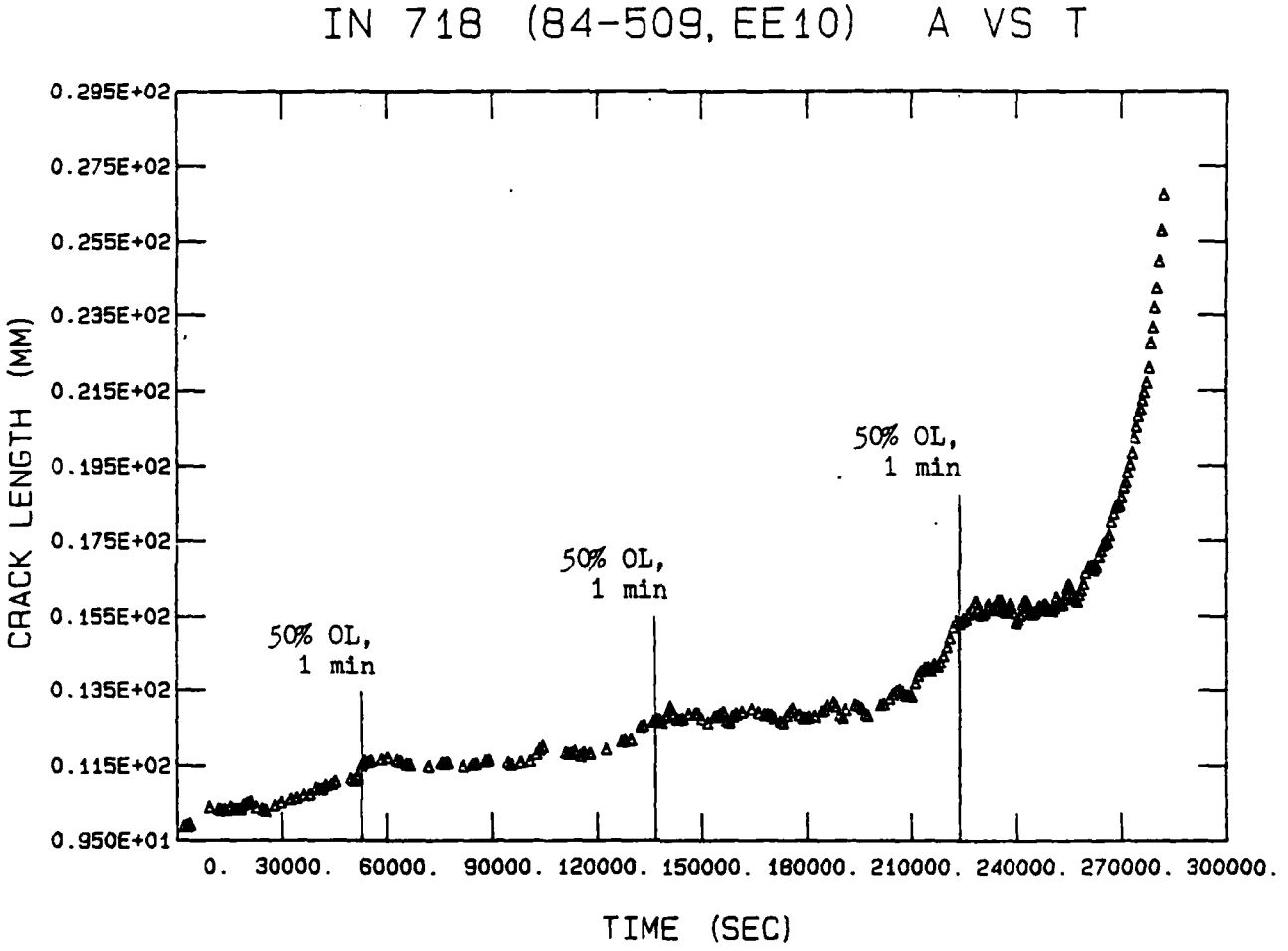

Figure 28 Time-Load History of Specimen EE10

Table III

Test Results for Overload Delay Time

K (MPA $\sqrt{m}$)	Delay Time (Δt_r)	Specimen ID
20% OL	(sec)	
27.31	9000	DD5
27.56	26600	DD3
28.19	20000	DD1
28.20	17000	EE9
30.45	7700	EE7
30.46	16500	DD6
31.06	0	DD1
31.42	13800	DD3
31.63	9000	DD10
35.88	3600	EE9
36.06	1400	EE7
36.83	7500	DD1
36.83	4100	DD3
36.91	8300	DD6
40.24	3200	DD5
45.91	1800	DD8
45.67	2400	DD1
45.71	3000	DD6
50.29	2000	DD5
53.05	2700	DD6
61.01	400	DD1
66.36	600	DD10

Table III

Test Results for Overload Delay Time Continued

K (MPA $\sqrt{m}$)	Delay Time (Δt_r)	Specimen ID
50% OL	(sec)	
27.09	ARREST	DD10
27.37	ARREST	EE6
27.52	ARREST	EE7
28.13	65220	EE10
28.20	ARREST	EE8
29.00	33400	EE6
30.30	60000	EE10
40.85	14900	EE9
41.41	85800	DD10
41.43	18200	EE7
45.60	26500	DD3
50.46	12000	EE9
53.22	8900	EE7
71.61	4500	DD8

by the 50-percent overload case with the possibility of total crack arrest. As noted earlier, the application of a predictive model should be limited to stress intensities above these regions of uncertainty.

Previous work by a number of investigators attempts to model the retardation behavior associated with single peak overloads during fatigue cycling (13, 14). The predictive models that have been developed generally fall into one of the three following categories:

a.) crack-tip blunting models

b.) crack-closure models

c.) residual-stress models

A residual-stress model was developed in this study with an approach similar to the one used by Wheeler (15). From Fig. 29 it can be seen that an overload will cause an increase in the size of the plastic zone ahead of the crack tip, from r_p under baseline loading to $\tilde{r}_p$ under the overload. After the overload is removed, a region of plastically deformed material remains. This results in a compressive state of stress in the enlarged plastic zone. Consequently, crack-growth retardation will remain in effect until the crack grows through the compressive plastic zone ($a_1=a_2$).

Wheeler introduced a retardation parameter, C_{pi}, to account for the delay time associated with the size of the compressive plastic zone (15). The parameter modifies the

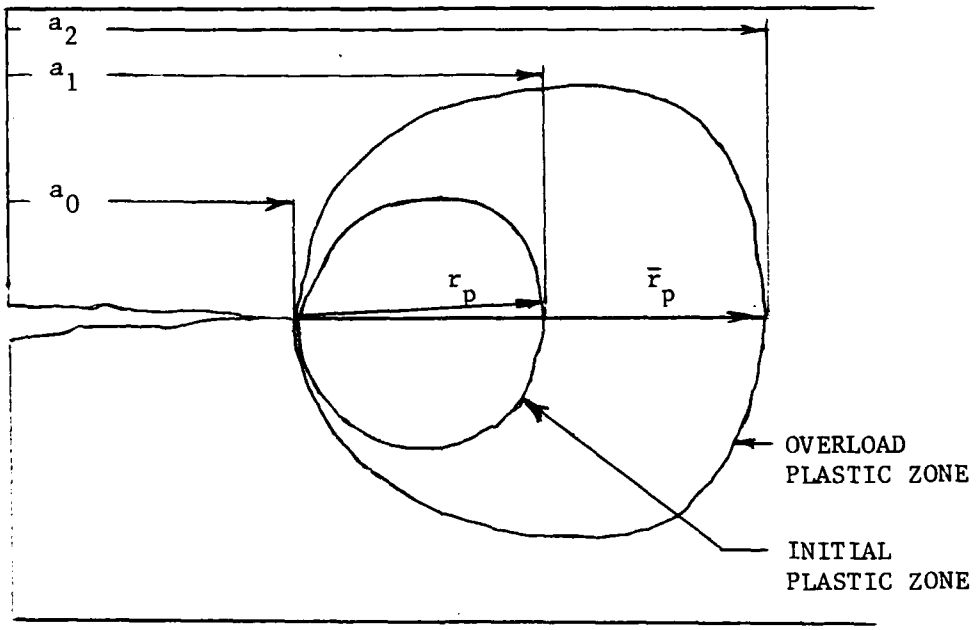

Figure 29 Crack Tip Plastic Zones

crack-growth-rate such that:

$$\left(\frac{da}{dt}\right)_{retarded} = C_{pi}\left(\frac{da}{dt}\right)_{linear} \qquad (9)$$

Wheeler proposed that C_{pi} be a power-law function of the form:

$$C_{pi} = [(r_p/(a_2-a_o)]^m \quad \text{for } a_1 < a_2 \qquad (10)$$

and

$$C_{pi} = 1 \quad \text{for} \quad a_1 \geq a_2 \qquad (11)$$

where a_2, a_1, a_o , r_p are defined in Fig. 29 and m is a material-dependent shaping exponent. Thus according to the Wheeler model the crack resumed its normal growth behavior after it had grown through the overload plastic zone. For this study a model was developed in which two controlling parameters, α and β, were introduced. The relationship which was proposed was of the following form:

$$K_{eff} = K(1-\alpha\exp(-\beta\Delta a)) \qquad (12)$$

where

K = the current value of stress intensity

$\Delta a = a_2-a_1$

$\alpha = f_1(K)$

$\beta = f_2(K,\sigma_y,\gamma)$

$\gamma = K_{ol}/K$ (overload ratio)

In contrast to the Wheeler model, which contains one parameter, this model provides additional flexibility by introducing two parameters. It can independently model the growth rate initially after overload removal through the parameter α, as well as control the distance over which the retardation occurs through the parameter β.

The above relation is formulated in terms of an effective value of K and can be applied to typical results as shown in Fig. 30. The overload effects result in an initial decrease in crack-growth rate below the steady state values shown by the MSE baseline curve. The initial growth rate is approximately 10^{-8} m/s at a K of 35 MPA$\sqrt{m}$ as shown in Fig. 30. This corresponds to a baseline growth rate at a K value given by K_{eff} in the figure. This effective K is determined by the parameter α in the model. The growth rate eventually matches the steady state value after some amount of crack extension. The parameter β controls the amount of extension before K_{eff} approaches K, ie. the retardation effect vanishes. This amount of crack extension is related to the size of the overload plastic zone and the baseline plastic zone. Therefore the parameters α and β have to be optimized to model the initial growth rate, the distance over which retardation occurs, and the resulting delay time. For numerical computations, since K_{eff} is defined on the MSE curve, its value can be directly substituted into the MSE

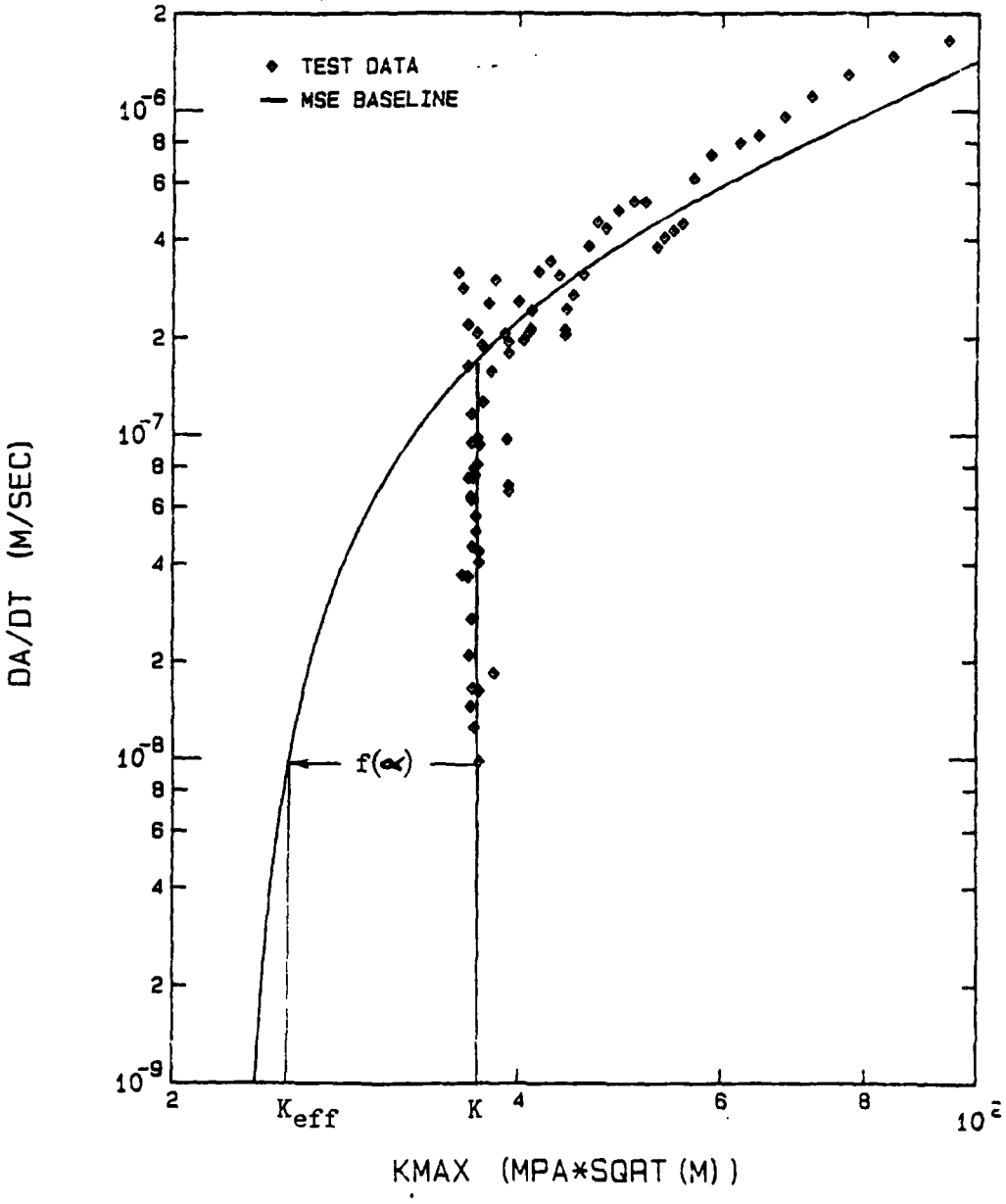

Figure 30 Retardation Behavior Compared with the MSE Baseline

equation. The equation could then be integrated to attain a crack length vs time prediction. The prediction would model the retardation behavior by accounting for the appropriate delay time.

Before retardation predictions could be made, however, a consistent method for evaluating α and β had to be developed. It was desirable to define these parameters in terms of the physical constraints of the problems. A general comparison between the Wheeler model and the model put forth in this work was made on a non-dimensional plot shown in Fig. 31.

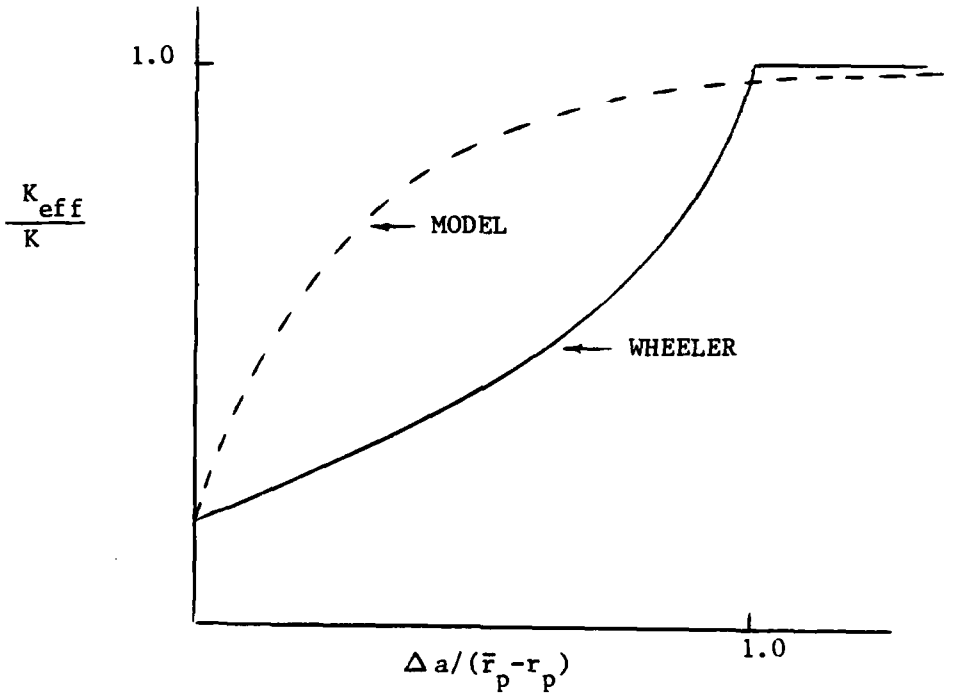

Figure 31 Sustained Load Retardation Model and Wheeler Model

As can be seen in Fig. 31, and noted before, the Wheeler model predicts a complete return to steady state crack-growth behavior ($K_{eff}/K = 1$) when the overload plastic zone is traversed ($\Delta a/(\bar{r}_p - r_p) = 1$). The exponential model, on the other hand, approaches the normal growth rate asympotically. Ideally, the model should express no retarded growth beyond the overload plastic zone. Therefore, the exponential term in the proposed model must approach a small finite value when the overload boundary is reached. The following relationship was postulated:

$$\beta(a_2 - a_1) = \beta(\bar{r}_p - r_p) = \pi \qquad (13)$$

The plastic zone radius for the initial and overload conditions were originally defined in terms of plane strain. This seemed reasonable since the specimen's thickness was adequate to produce a plane strain profile at the crack tip. However, when the above relation was solved for β, very large numbers resulted. Consequently, the exponential term in the function decayed too rapidly for reasonable increments of Δa. This in turn caused numerical difficulties for integration with the Simpson's rule technique.

Rather than change the postulate, β was redefined in terms of a plane stress plastic zone. This resulted in the following:

$$\bar{r}_p = 1/\sqrt{2}\pi(K_{ol}/\sigma_y)2 \qquad (14)$$

$$r_p = 1/\sqrt{2}\pi(K/\sigma_y)^2 \qquad (15)$$

and

$$\beta = (\sqrt{2}\pi^2\sigma_y^2)/(K^2(\gamma^2-1)) \text{ (units of 1/length)} \qquad (16)$$

where

γ = the overload ratio (K_{ol}/K)

Defining β in terms of the plane stress plastic zone reduced its magnitude by a factor of 4 and eliminated the numerical problems. More importantly, however, the relation predicted a size for the overload plastic zone that agreed very well with experimental data. It's also interesting to note that others, such as Macha (4) and Hertzberg (16), have shown a significant correlation between retarded crack-growth behavior and the plane stress region at the specimen's surface. Thus defining β in terms of a plane stress plastic zone was deemed appropriate.

A further study was made to see if an adjustment for β was needed to account for overload-hold-time effects. After examining the data, it appeared that hold time had a greater influence at higher stress intensity factors. Upon closer inspection, though, this trend was attributed to respective differences in crack-growth

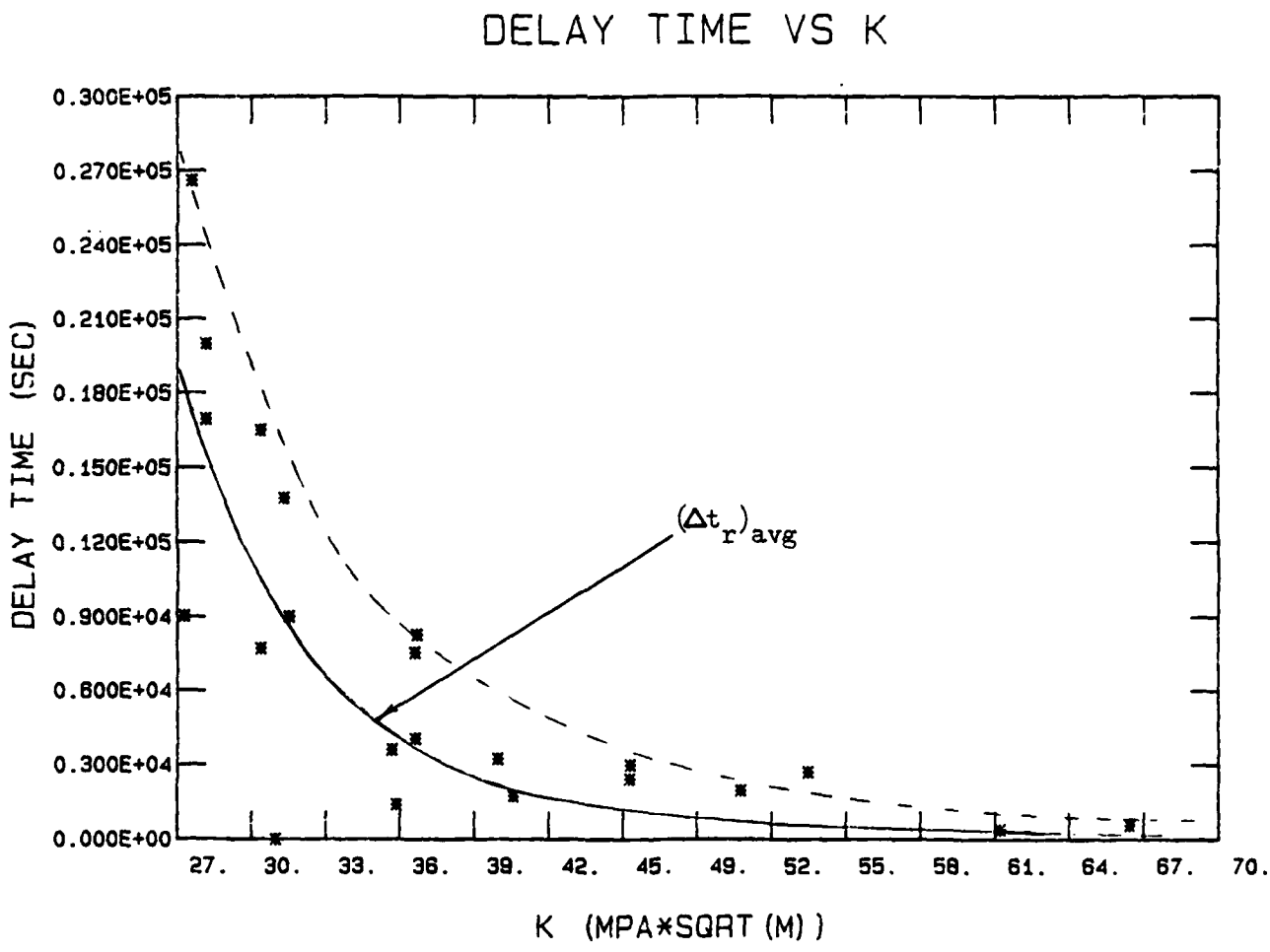

Figure 32 Delay Times Resulting from 20 Percent Overloads at Various Stress Intensities

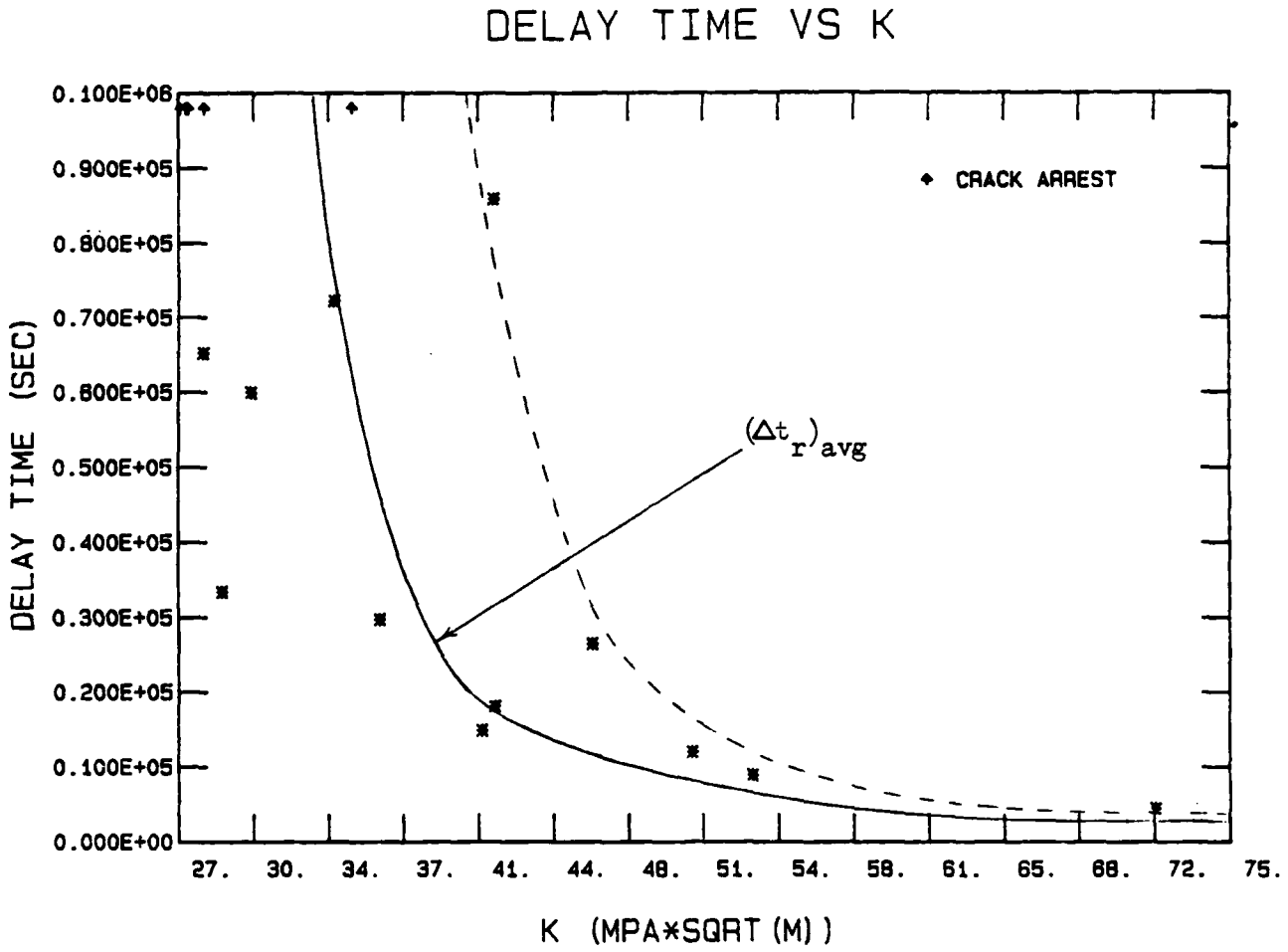

Figure 33 Delay Times Resulting from 50 Percent Overloads at Various Stress Intensities

rate. In other words, when a crack was at a high K, and subjected to an hour overload, it experienced a more dramatic growth rate acceleration than a crack at a low K. Additionally, when the overloads were removed, both types of cracks exhibited behavior similar to one minute overloads at comparable stress intensities. Therefore it was assumed that the plastic zone size did not change as a result of overload hold time; but merely grew along with the crack. The same observation was noted by Keck et al. (16) based on numerical computations of sustained load crack-growth in a superalloy at elevated temperature. Consequently, no adjustment was made for hold time duration on β and all the data was treated without regard to hold time.

Having defined β, an analytical expression was sought for α. It was noted that the delay times and, hence, the value of K_{eff} appeared to change systematically with K. Since α is primarily responsible for modeling the magnitude of K_{eff}, a function of the form $\alpha = f(K)$ was investigated. Figures 32 and 33 show the relationship between Δt_r and K for the 20-and 50-percent overload cases. The high and low values of Δt_r were used to generate a delay time envelope for the range of stress intensities. As noted earlier, this envelope diverges as K approaches threshold. The boundaries of the envelope were used to approximate an average delay time, $\Delta(t_r)_{avg}$,

curve. Specific values of $\Delta(t_r)_{avg}$ were then used as a guide to determine α. This required an iterative process. A value of α was chosen and used with a specified value of K in the model to generate a Δt_r. This was compared with the $\Delta(t_r)_{avg}$ value at the same K. Adjustments in were then made for successive iterations until Δt_r and $\Delta(t_r)_{avg}$ agreed reasonably well. By repeating the process for the full range of stress intensities, a functional relationship for Δt_r, K and α was established.

For ease of expression, non-dimensional relationships for α and K were introduced and referenced to threshold conditions. Since the threshold value for stress intensity, K^*, was previously established, the threshold parameter α^* was determined from Equation (12) by setting $\Delta a = 0$, $K_{eff} = K^*$, and $\alpha = \alpha^*$. Solving the equation for α^* resulted in $\alpha^* = 1-(K^*/K)$ and the following limiting values:

$$\frac{\alpha}{\alpha^*} = 1 \quad \text{total crack arrest} \tag{17}$$

$$\frac{\alpha}{\alpha^*} = 0 \quad \text{no retardation} \tag{18}$$

A plot of α/α^* vs K/K^* is shown in Fig. 34 for the 20-and 50-percent overload cases. Fitting a polynomial equation to each of these curves yielded the following α functions:

$$\alpha = \alpha^{*}[(-.0730791E-01)(K/K^{*})^{3} + (0.303086)(K/K^{*})^{2} - (0.422108)(K/K^{*}) + (0.117517E-01)] \quad (19)$$

for a 20 % overload and

$$\alpha = \alpha^{*}[(-.121127E-01)(K/K^{*})^{2} + (0.239231E-01)(K/K^{*}) + (0.987133)] \quad (20)$$

for a 50 % overload.

With all the parameters defined, the sustained load retardation model was capable of predicting retarded crack growth behavior. A flowchart for the principal equations is shown in Fig. 35 and was incorporated into a numerical routine. The results of a typical specimen analysis, comparing the theoretical baseline, actual and modeled behavior, are shown in Figures 36 through 41. Although the model developed above gave reasonable results, there were small crack-growth discontinuities that were not accounted for. These discontinuities were a transient product of overloading and appeared in the data as sudden "crack jumps". This phenomenon was also observed by Larsen and Nicholas (18) in their study of crack-growth transients at elevated temperature. This model does not directly account for the transient effects since it was developed by analyzing individual overload segments. Therefore, no attempt was made to provide perfect continuity between segments. Although the discontinuities are small, their

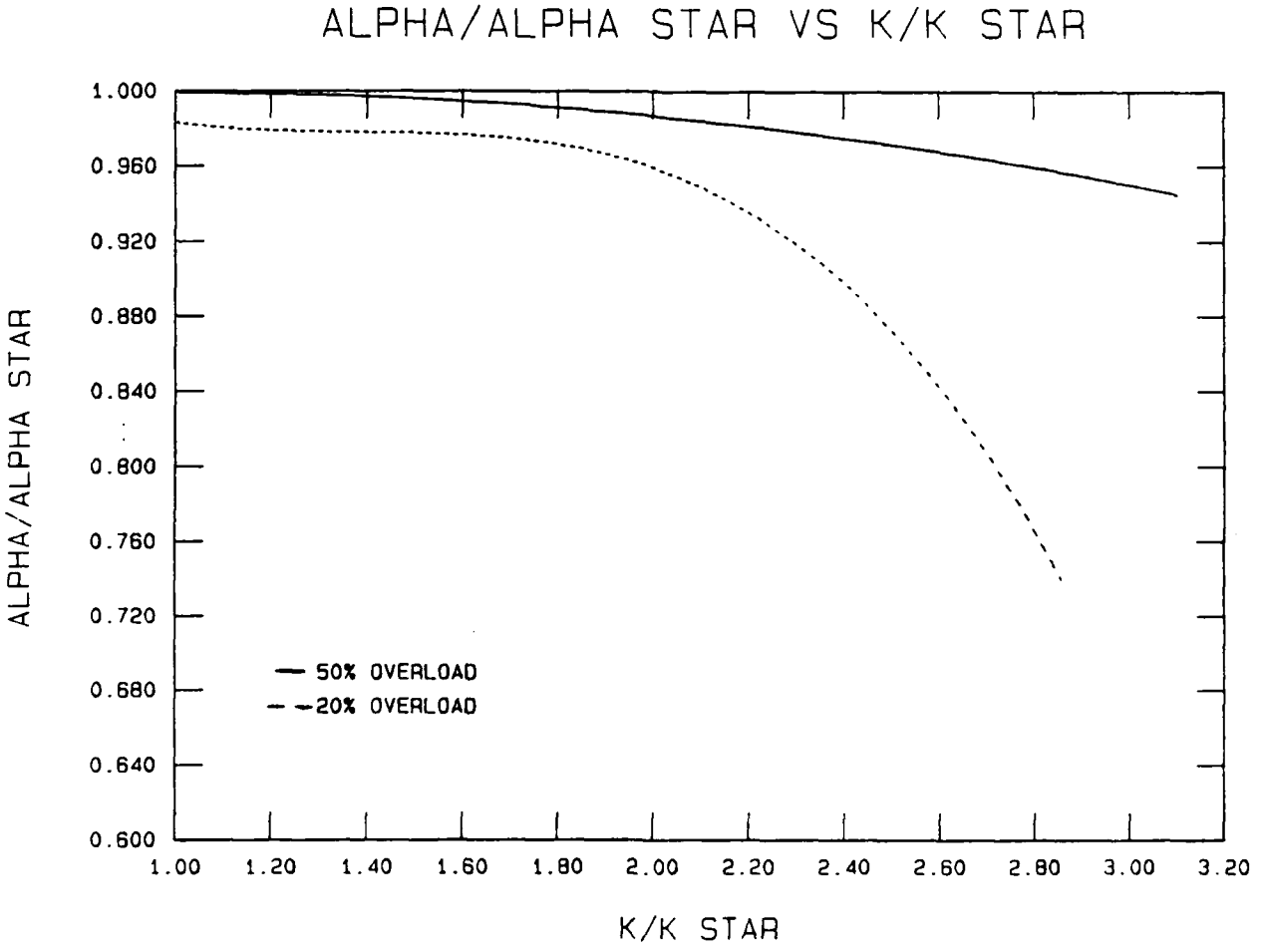

Figure 34 α Functions

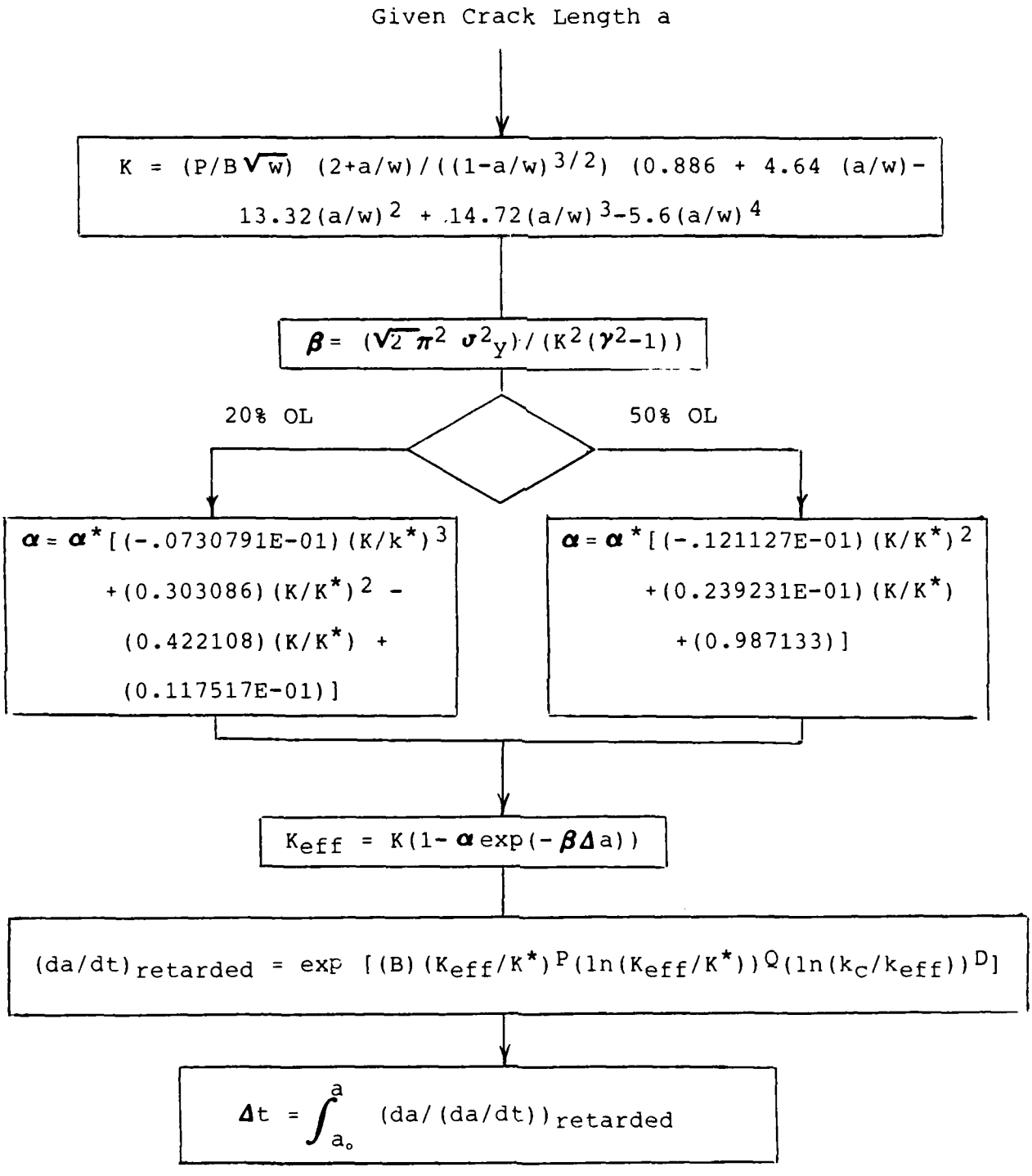

NOTE: $\Delta t_r = \int_{a_o}^{a} (da/(da/dt))_{retarded} - \int_{a_o}^{a} (da/(da/dt))_{baseline}$

Figure 35 Sustained Load Retardation Model

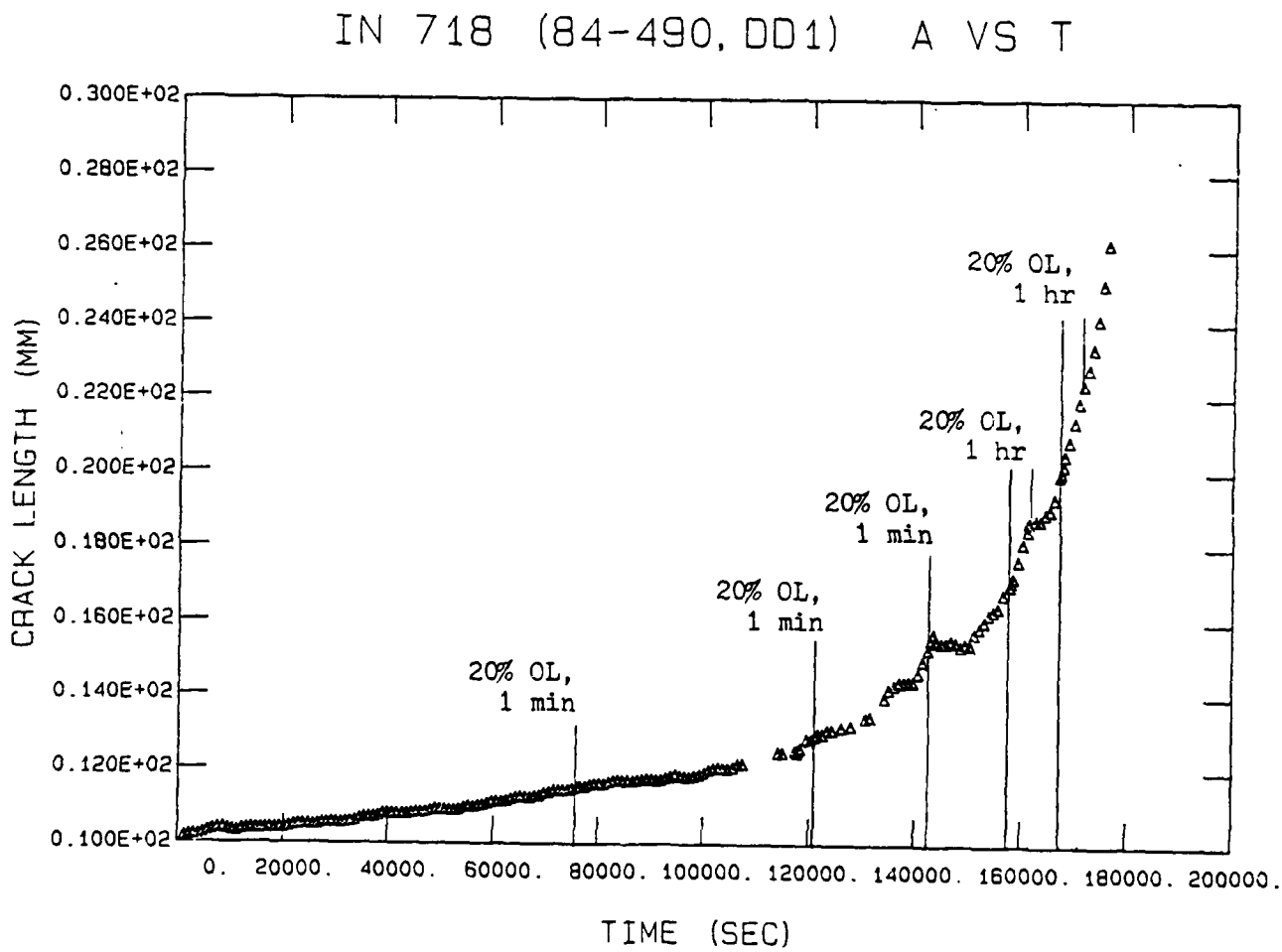

Figure 36 Time-Load History of Specimen DD1

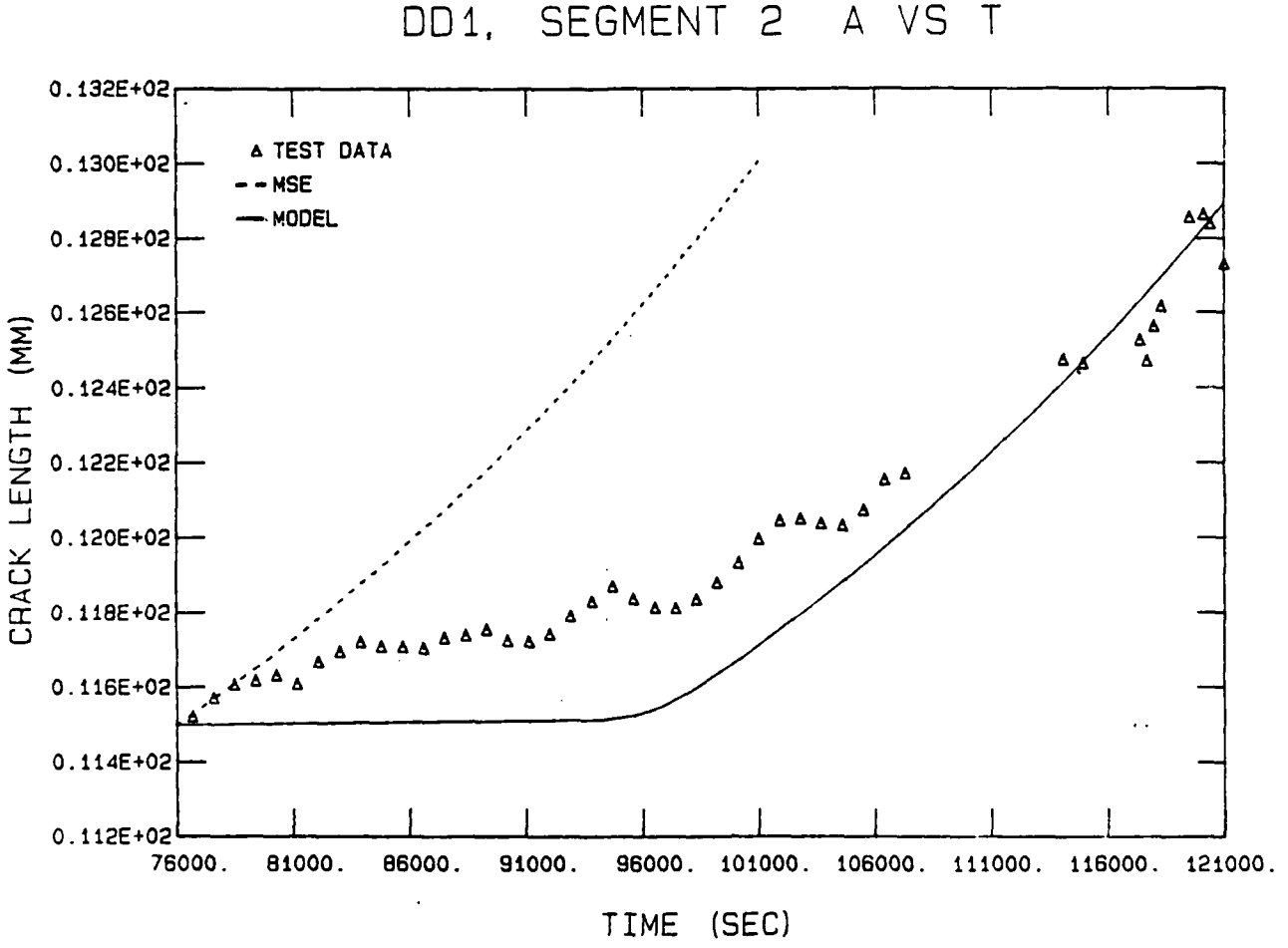

Figure 37 Crack-Growth Behavior of First Overload Segment

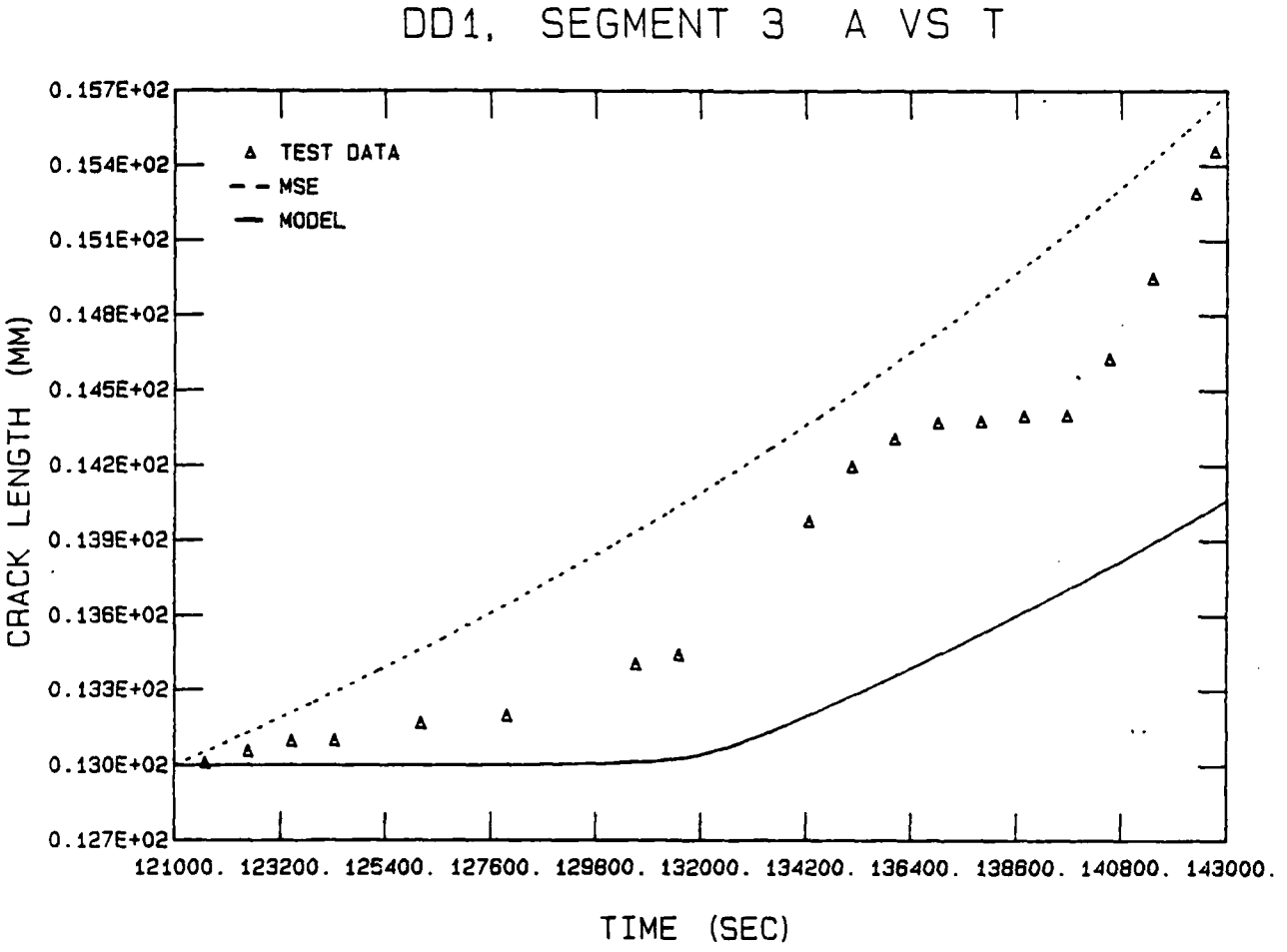

Figure 38 Crack-Growth Behavior of Second Overload Segment

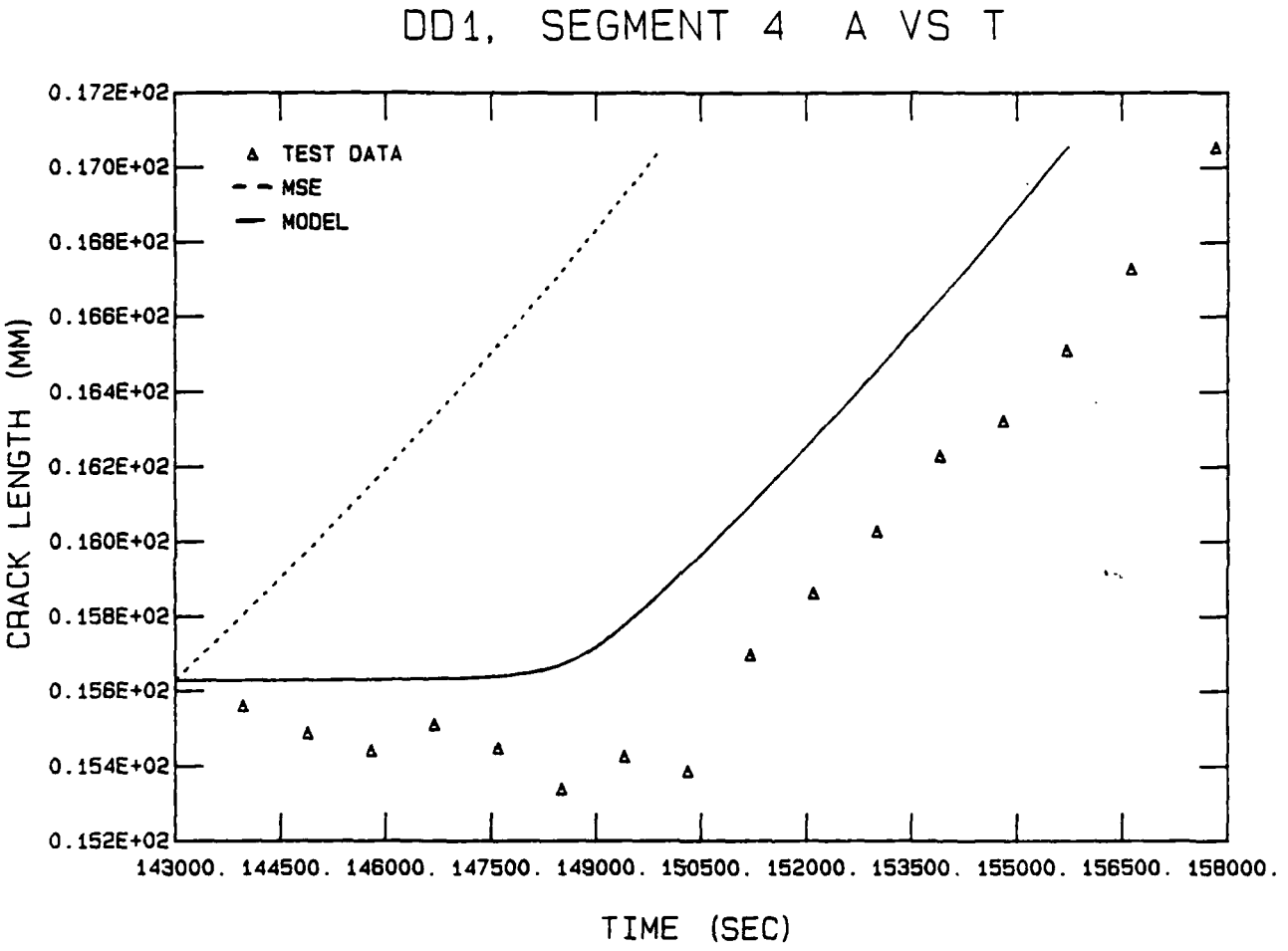

Figure 39 Crack-Growth Behavior of Third Overload Segment

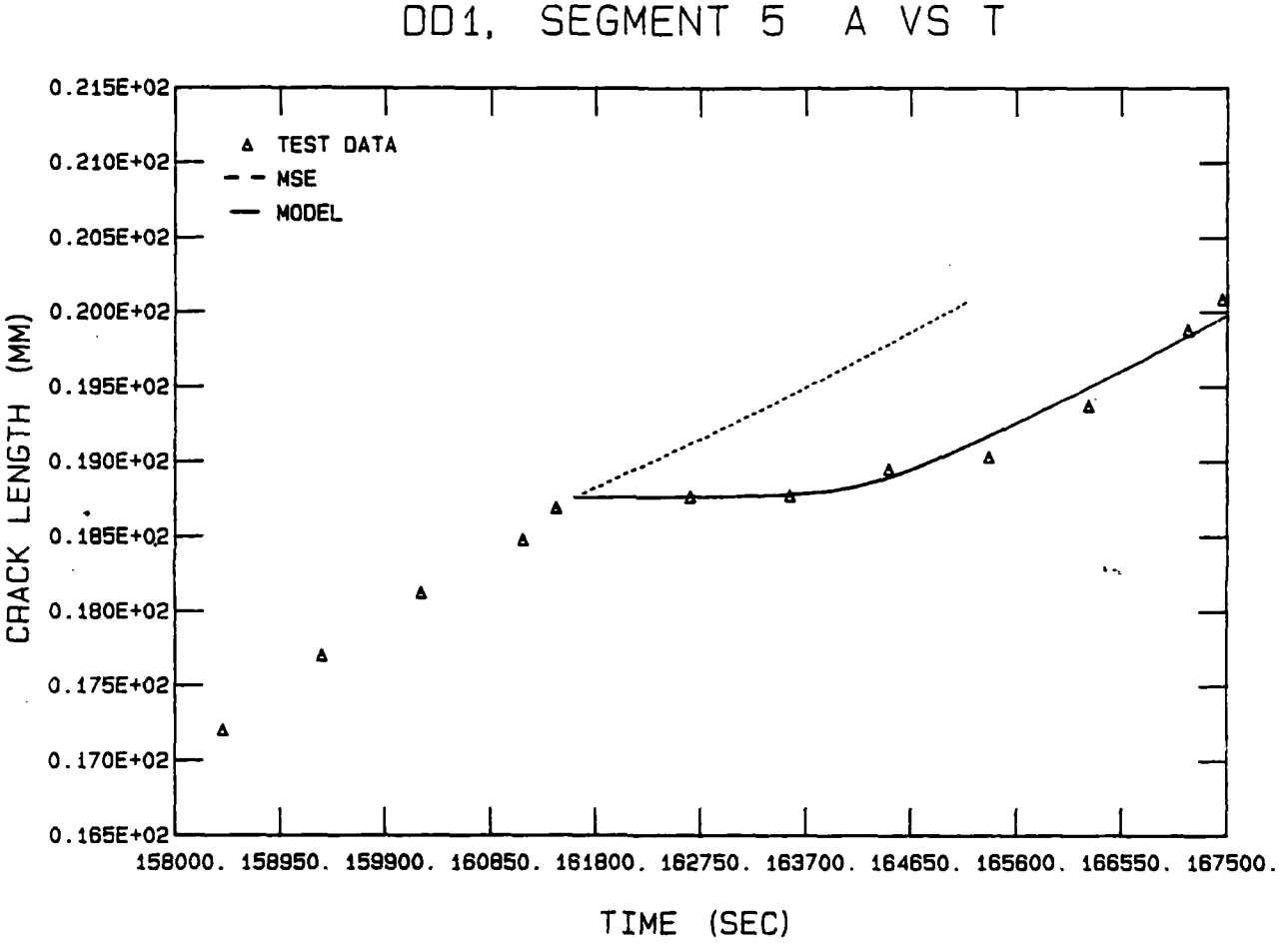

Figure 40 Crack-Growth Behavior of Fourth Overload Segment

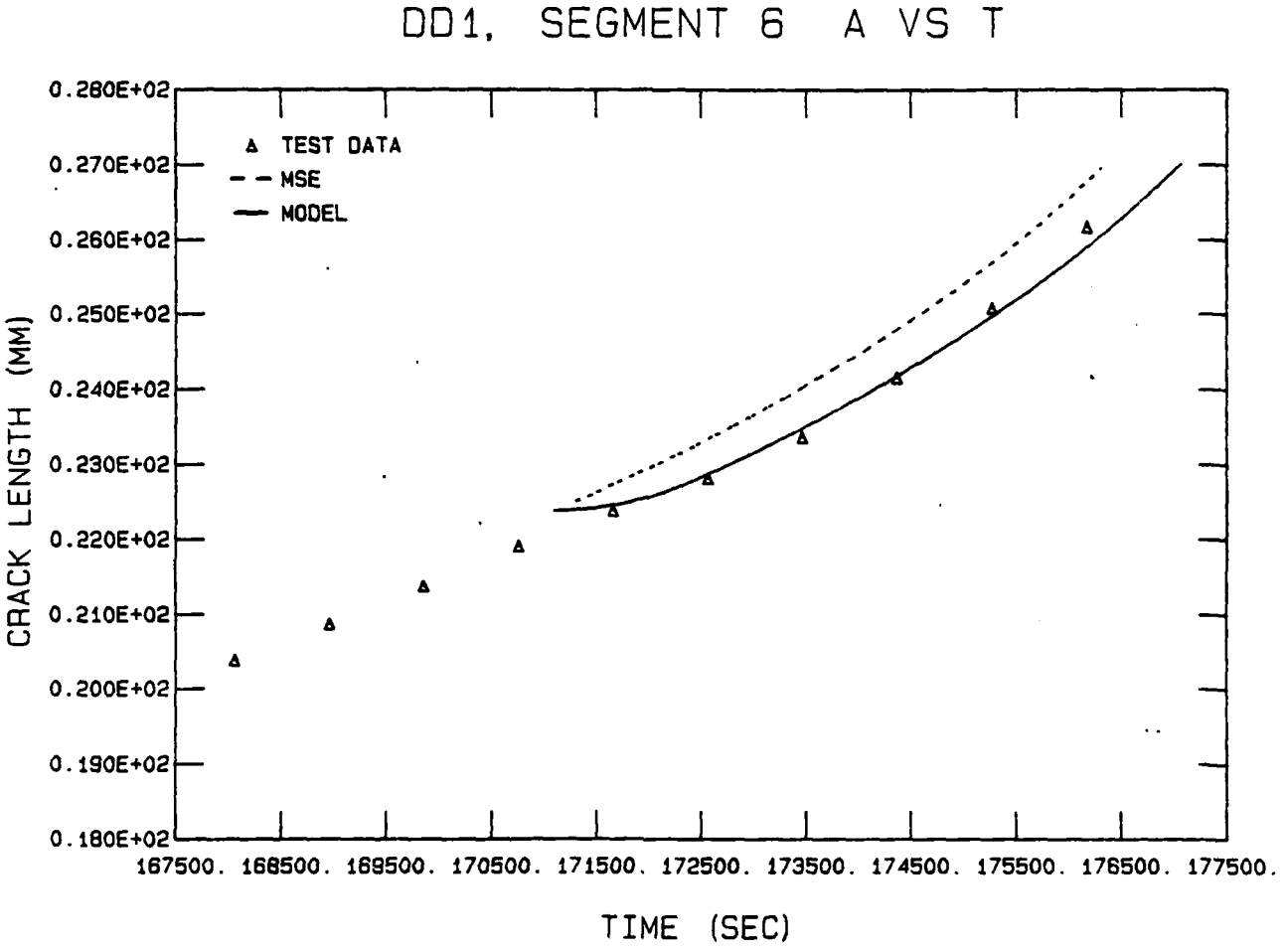

Figure 41 Crack-Growth Behavior of Fifth Overload Segment

importance was clearly demonstrated in the proof test. For this reason, the development of an adjustment factor was considered and is presented in the next section.

VI. Experimental Results and Discussion

Most of the experimental results in this study were used to develop the sustained load retardation model. The parameters for the MSE equation, B, P, W, D, K^*, and K_C, and those for the model, α and β, were essentially defined by the experimental data alone. In its entirety, the model would employ both the original and a modified form of the MSE equation to predict crack-growth behavior. The original form of the MSE equation was used to model the initial baseline behavior and the rate of crack propagation during hour long overloads. The modified form of the MSE equation was used to model the retardation behavior resulting from 20-and 50-percent overloads. The main element in the modified equation was a K_{eff} function which was developed in the previous section and supported extensively with experimental data. The accuracy of the sustained load retardation model was verified with a final proof test.

The proof test procedures and conditions were the same as those outlined in Section III with the exception of frequently applied overloads. Overloading was initiated when K was about 30 MPA $\sqrt{m}$ and repeated approximately every hour. All overloads were 20-percent in magnitude and 1 minute in duration. Fig. 42 shows that a total of

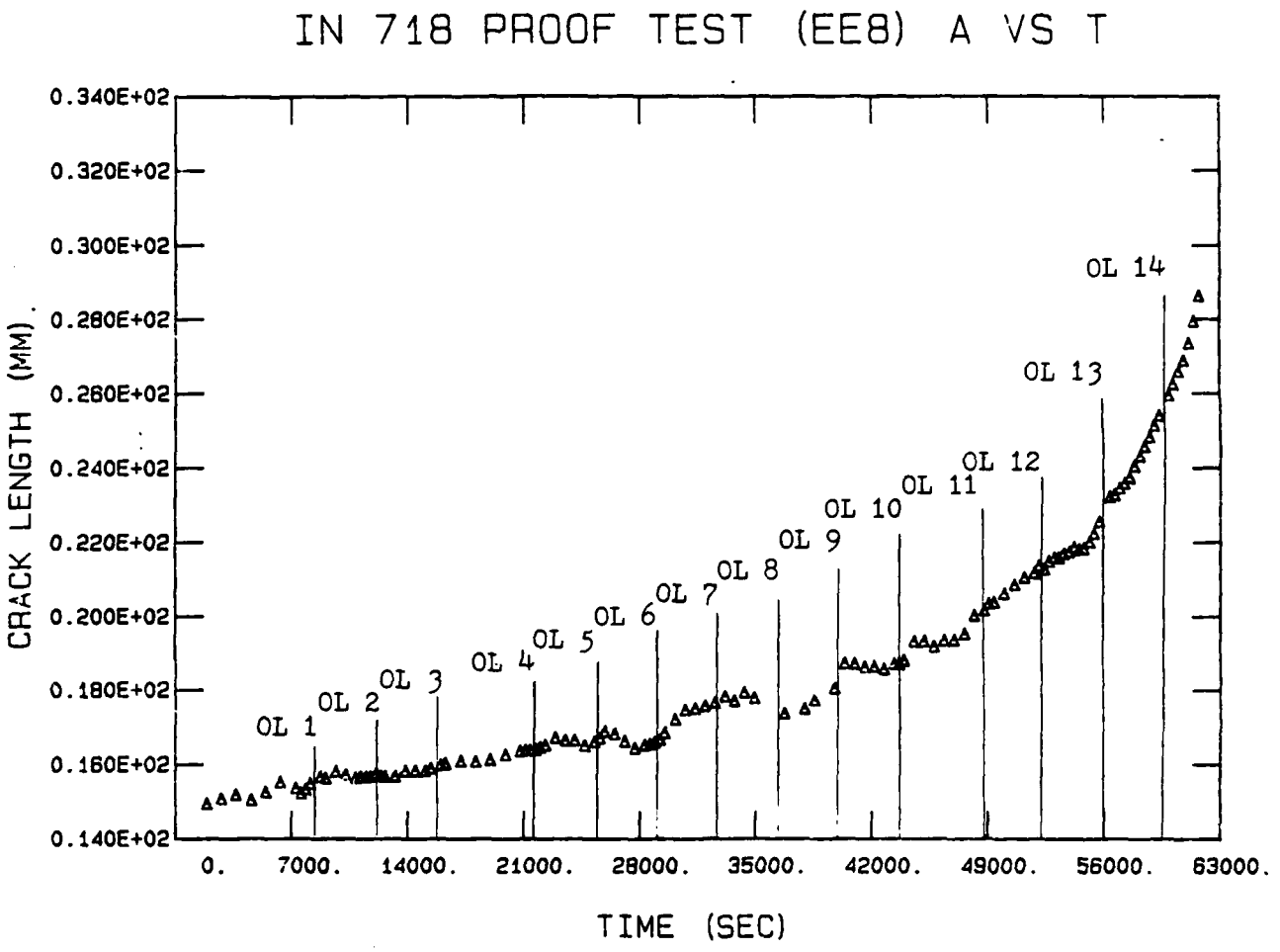

Figure 42 Time-Load History for Proof Test (Specimen EE8)

14 overloads were applied for stress intensities ranging from 30 MPA $\sqrt{m}$ to 75 MPA $\sqrt{m}$. The test was shut down overnight between overloads 3 and 4 and restarted according to the procedure outlined in Section III. During restart time, the crack was allowed to grow a visible amount before overloading was resumed. Except for the deletion of the shutdown time, the proof test data were not segmented prior to reduction.

Unlike previous tests, the overload intervals were so closely spaced that their retardation effects interacted with each other. Interaction was noted for overloads 1 through 3, and 4 through 9. During these periods of time no crack-growth was observed except for sudden apparent jumps in displacement when overloads were applied. Larsen and Nicholas (8) have noted that strong interaction effects can result for frequently occurring overloads. In fact, the overloads themselves can be the primary source of crack propagation. This appeared to be the case for the proof test since no crack extension was observed between overloads through much of the first half of the test. However, small increments of crack extension appeared to occur right at the time of overload application. The model developed in the previous section, however, did not account for this "jump" phenomenon. Consequently, when the model was used to evaluate the proof test, it predicted a state of complete crack

retardation or arrest. Therefore, it was necessary to adjust the model with some form of "crack-jump" increment to match the experimental data.

Optical measurements from previous tests also showed a sudden crack extension as a result of overloading. The crack length increments typically ranged from 0.25 mm to 0.5 mm with the larger crack extensions occurring generally at high values of K. In the proof test, the last two overloads were applied when K was very large (60 to 75 MPA$\sqrt{m}$) and crack extensions of the order of 0.65 mm to 1.0 mm were noticed. Fig. 43 shows that there is an apparent trend for these crack length increments to increase with K. However, considering the scatter, the amount of data was insufficient to develop a functional relationship. Instead a constant value of 0.38 mm was chosen for an overload crack increment and incorporated into the model. This adjustment gave dramatically improved results with the model predicting the actual time-to-failure within 5-percent. The baseline, actual and model crack-growth behaviors are compared in Fig. 44.

A closer inspection of Fig. 44 also suggests that a variable crack increment would further enhance the model. However, despite the small offset errors in crack length, the model predicted the retardation pattern for each overload segment reasonably well. Therefore, for the purpose of this study, adding a constant crack increment

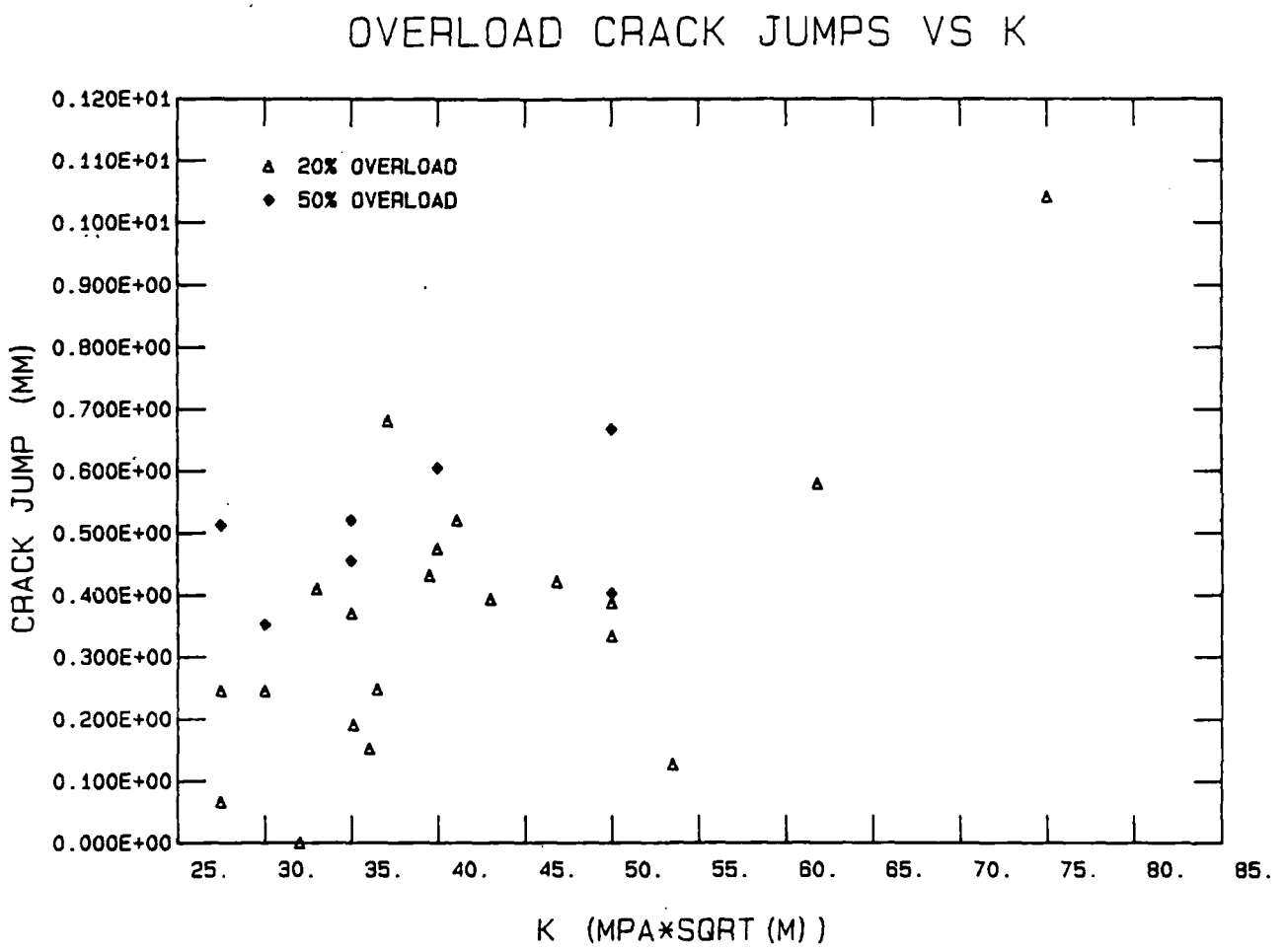

Figure 43 Crack Jumps from Overloading (Optical Measurements)

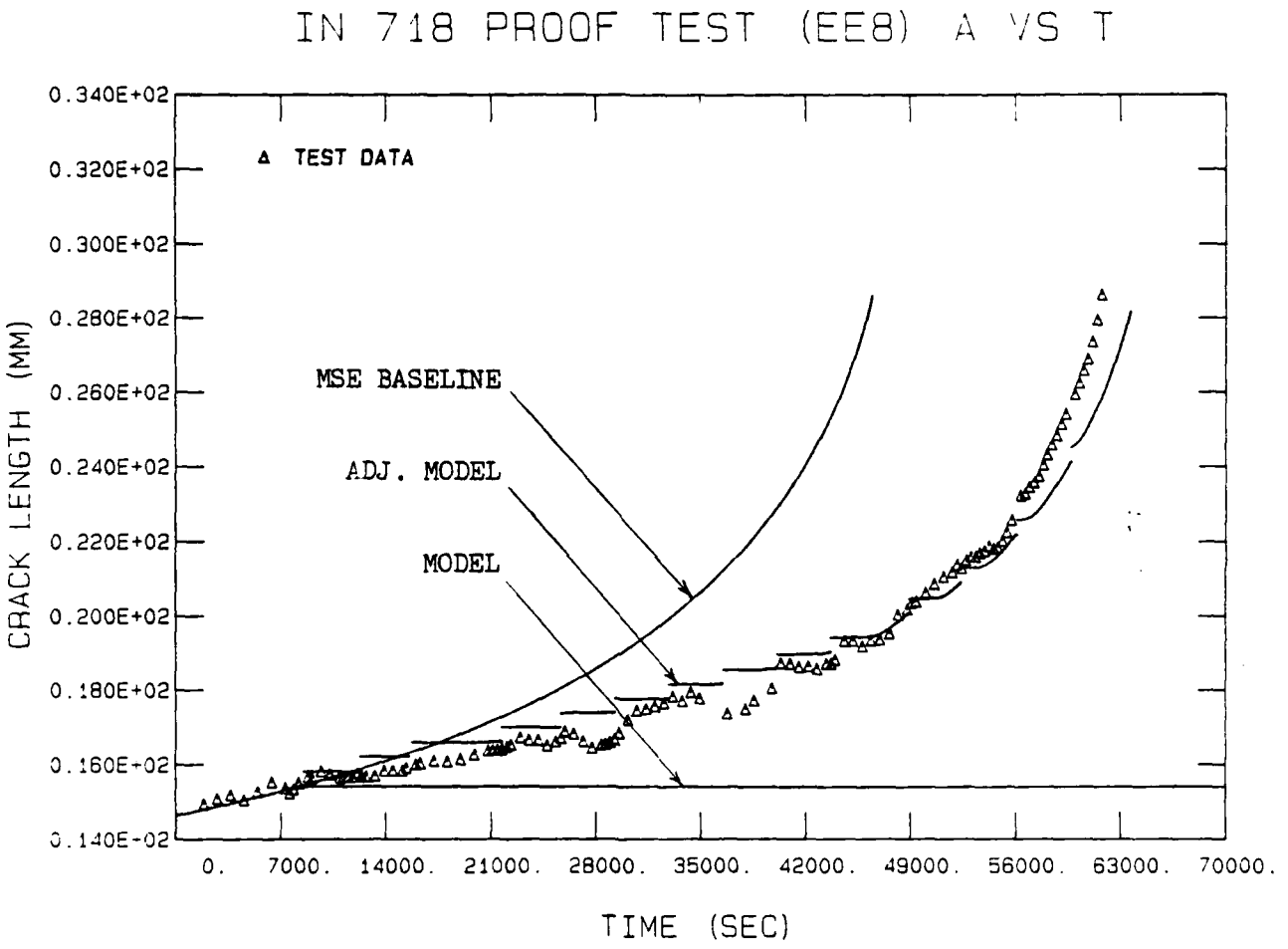

Figure 44 Proof Test Predictions Compared with Actual and MSE Baseline Behavior

of 0.38 mm for each overloading was deemed adequate and no further adjustments were made.

As an additional verification of accuracy, the model was also applied to the data of previous tests to predict total time-to-failure. Both the original and increment adjusted model were used. For the sake of comparison, only the results of the retardation behavior are shown in the following figures. No baseline results for the overload durations are shown and no attempt was made to model the initial baseline behavior up to the first overload, since it was near threshold and very specimen dependent. The modeling began at the application of the first overload and the baseline MSE equation was used to model all of the hour overloads that were applied. Since these particular specimens did not experience overload interactions, the adjusted model was not expected to produce drastically different results form the original. As expected, the adjusted model yielded more conservative results. However, as can be seen in Figures 45 through 59, the adjusted model also generally provided better predictions. Overall accuracy of time-to-failure predictions, for the adjusted model, was on the order of 10-percent. Results are presented in Tables IV. Two notable exceptions, however, were specimens EE10 and EE6. In those particular cases, the model predicted total crack arrest while in the experiment the cracks propagated to

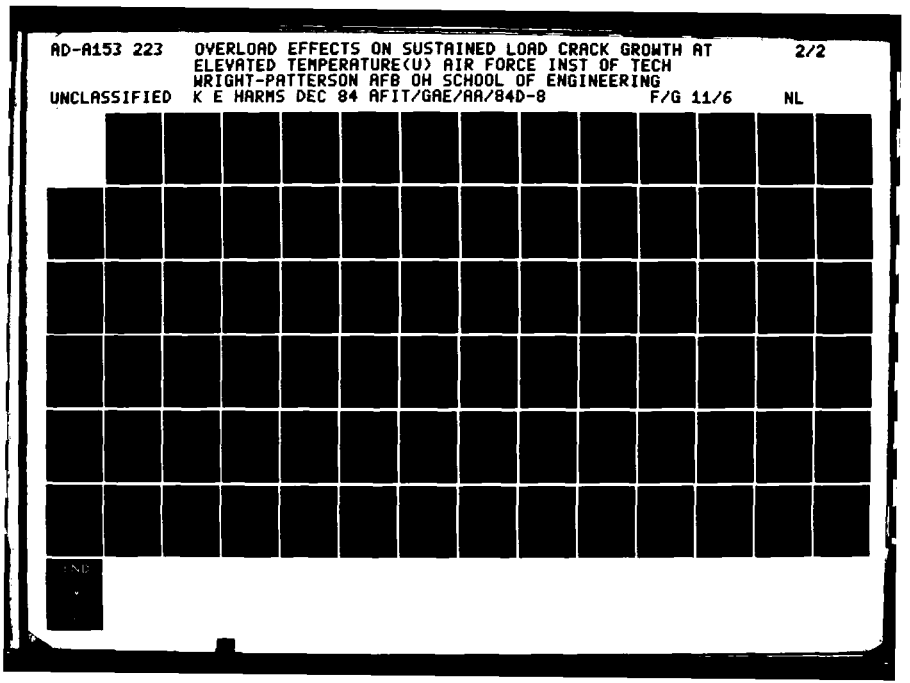
AD-A153 223 OVERLOAD EFFECTS ON SUSTAINED LOAD CRACK GROWTH AT ELEVATED TEMPERATURE(U) AIR FORCE INST OF TECH WRIGHT-PATTERSON AFB OH SCHOOL OF ENGINEERING
2/2
UNCLASSIFIED K E HARMS DEC 84 AFIT/GAE/AA/84D-8
F/G 11/6
NL

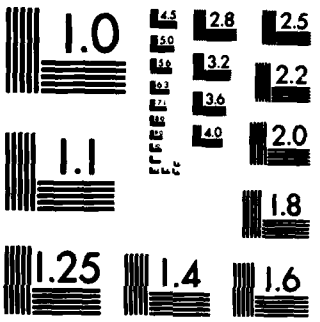

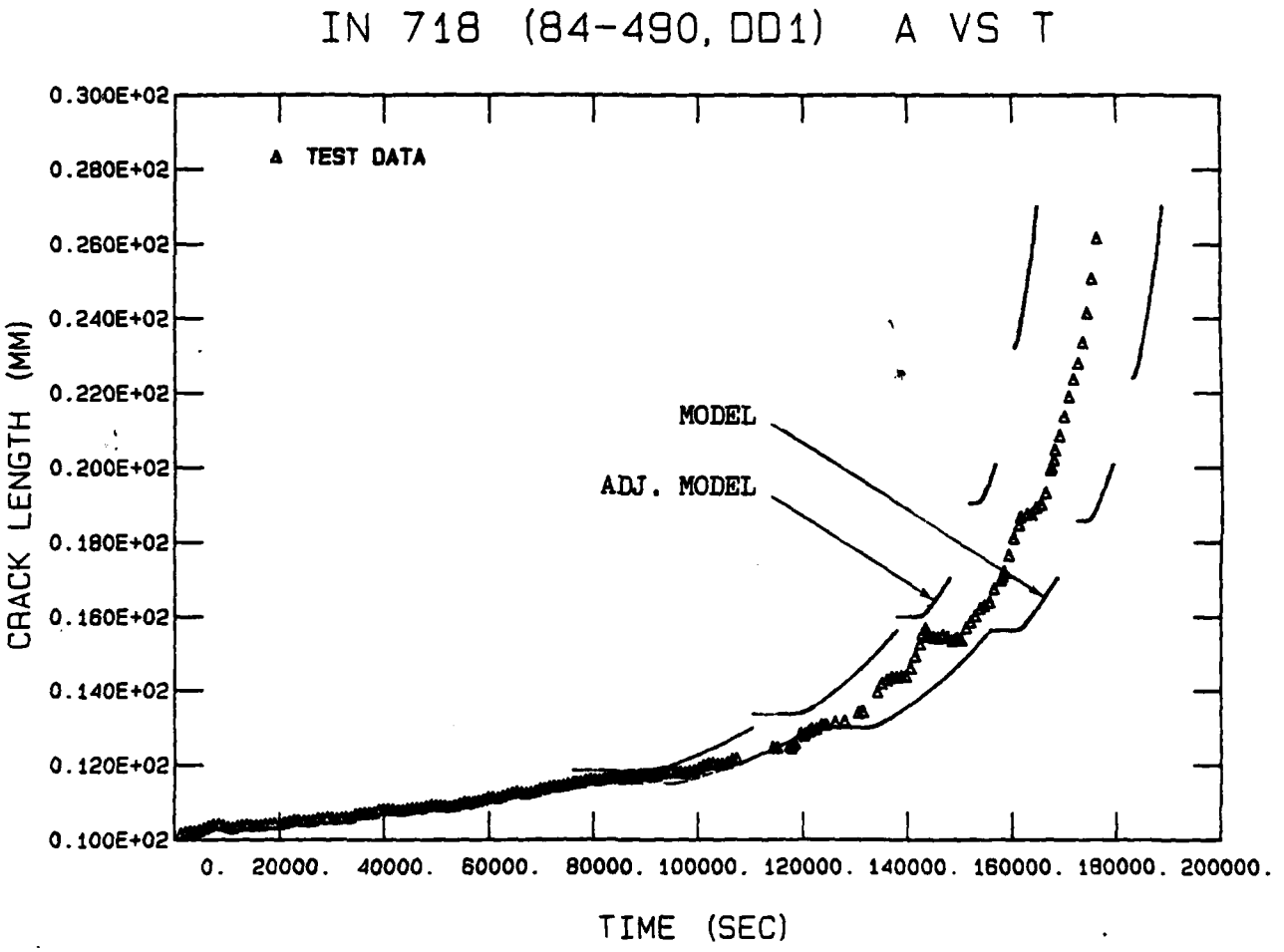

Figure 45 Model Prediction for Specimen DD1

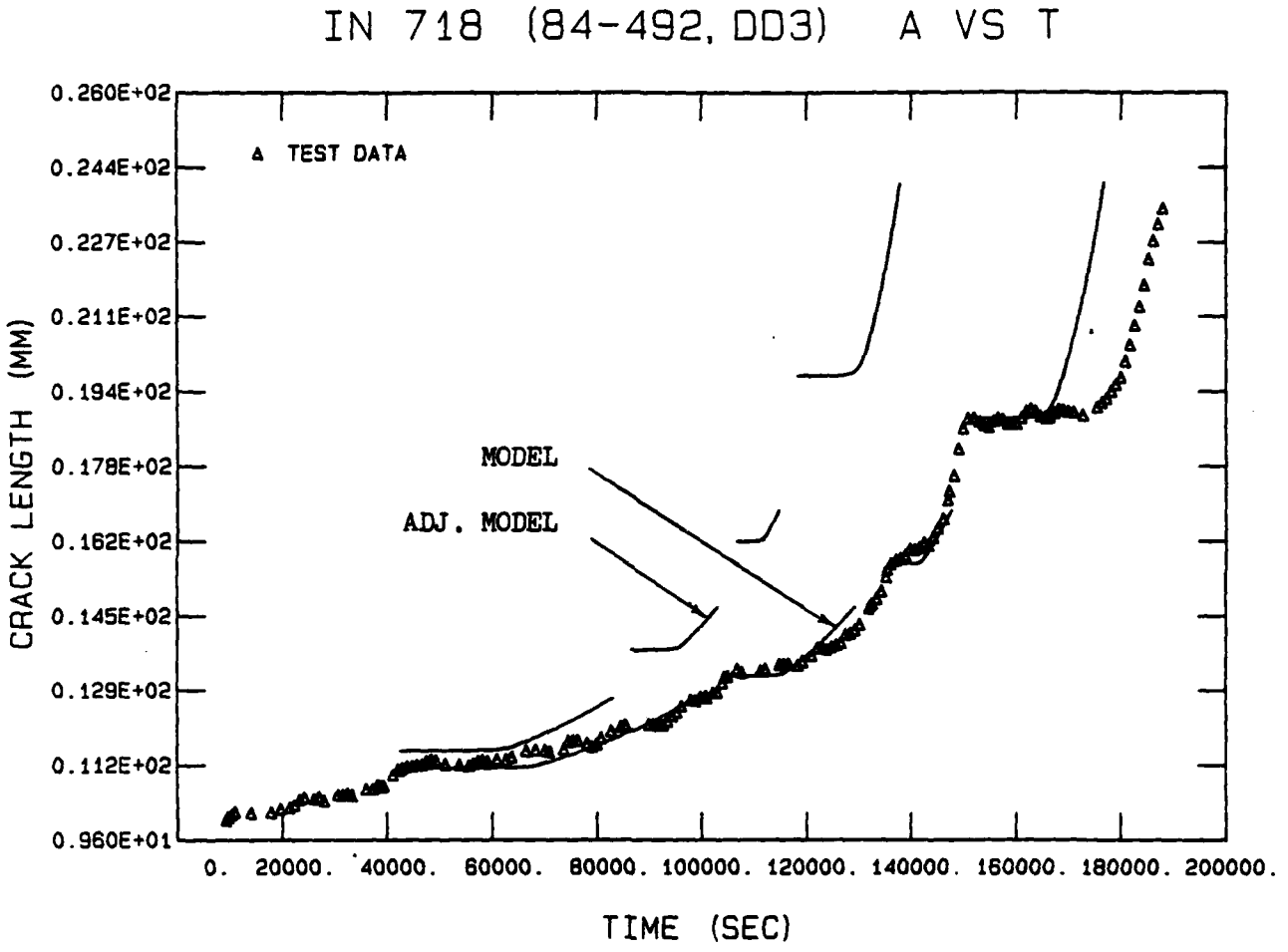

Figure 46 Model Prediction for Specimen DD3

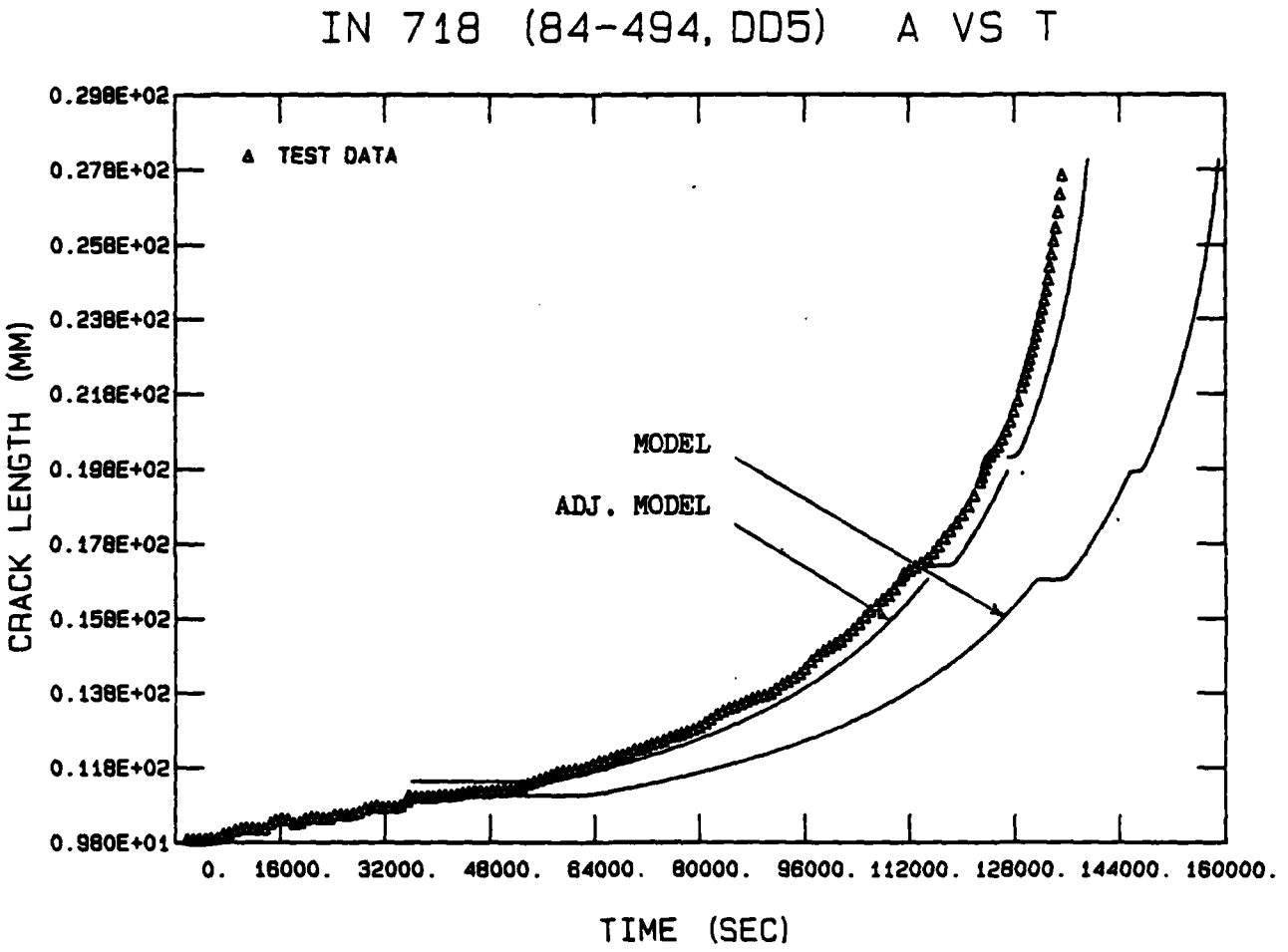

Figure 47 Model Prediction for Specimen DD5

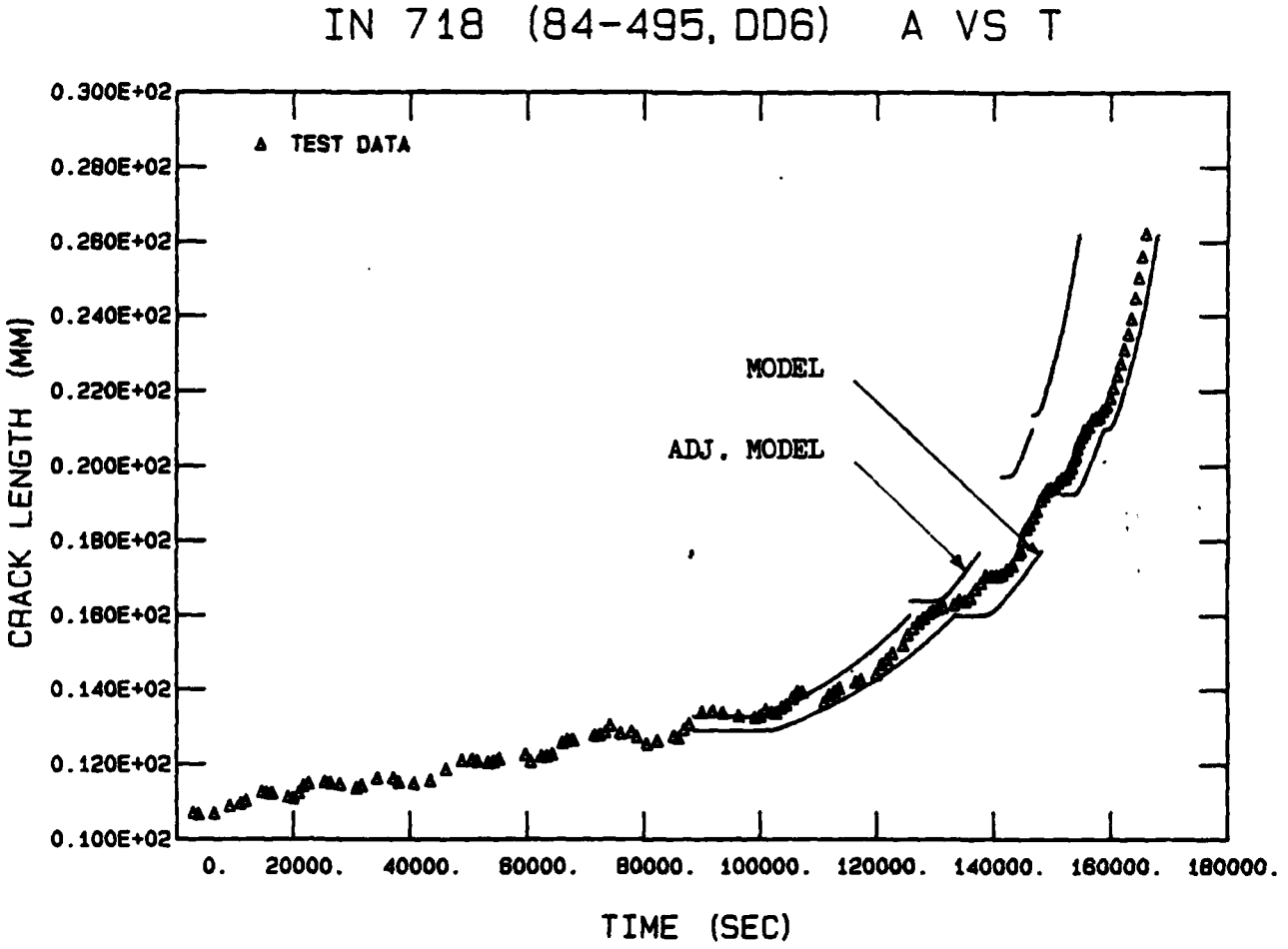

Figure 48 Model Prediction for Specimen DD6

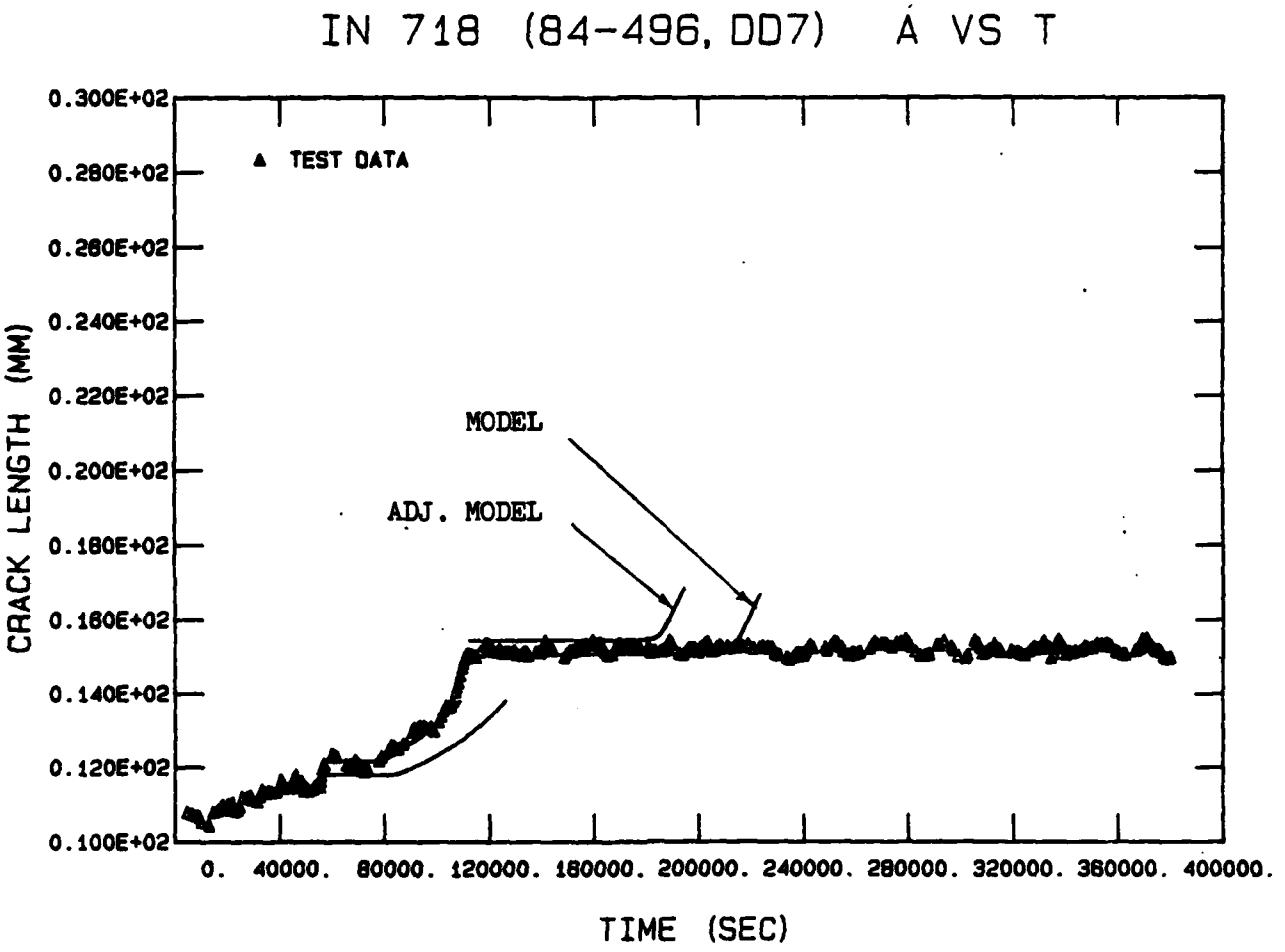

Figure 49 Model Prediction for Specimen DD7

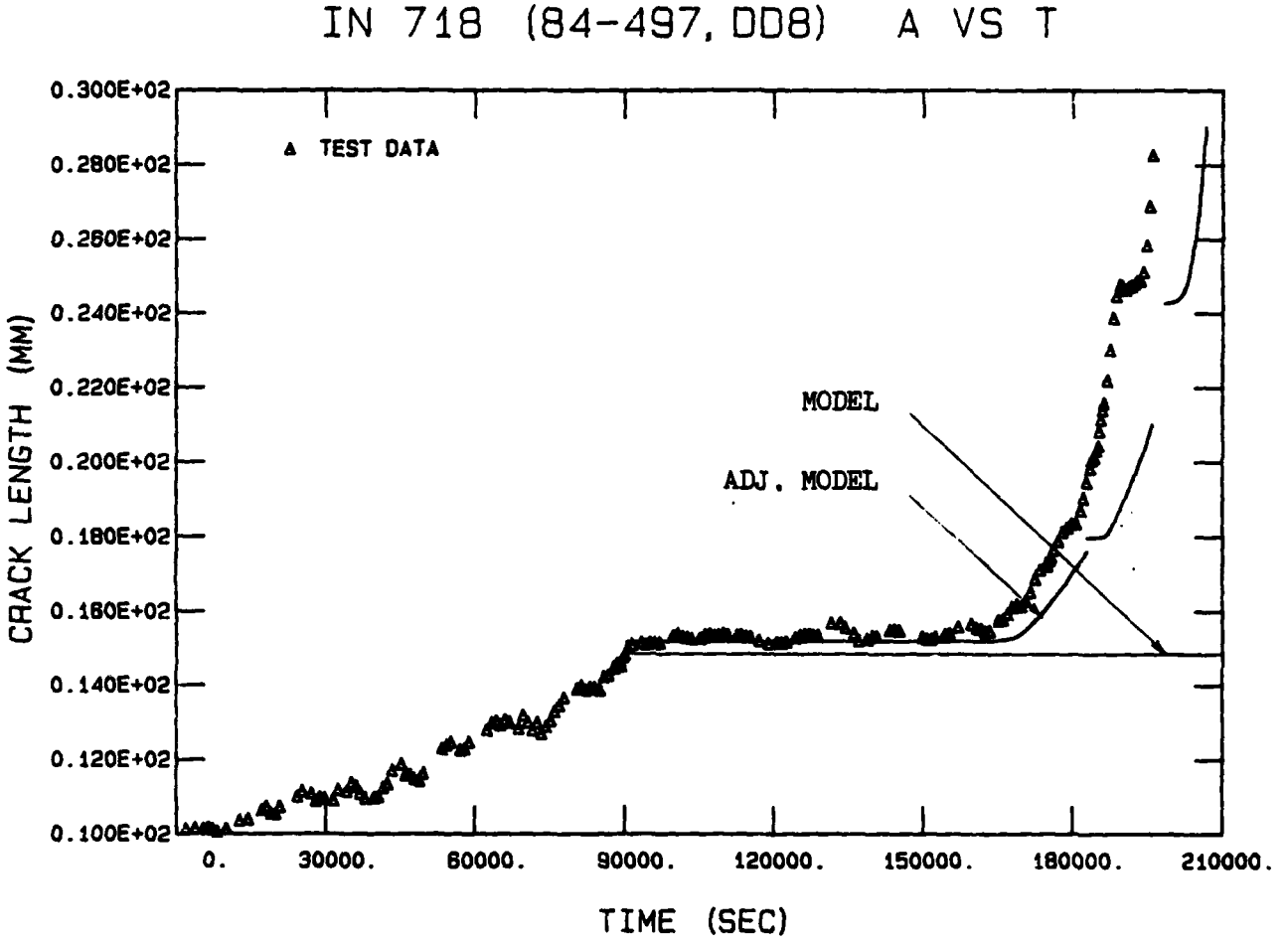

Figure 50 Model Prediction for Specimen DD8

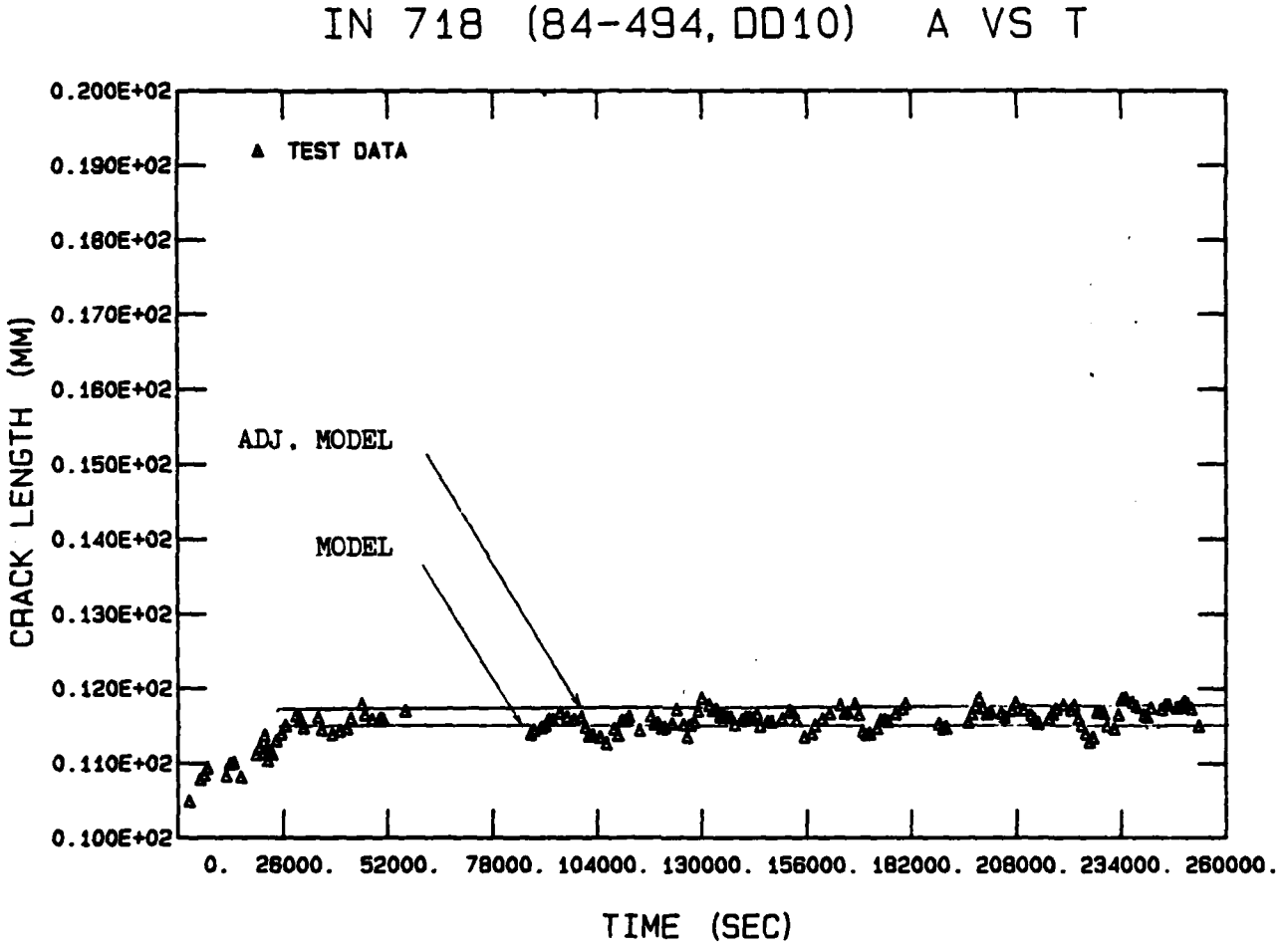

Figure 51 Model Prediction for Specimen DD10 (Part A)

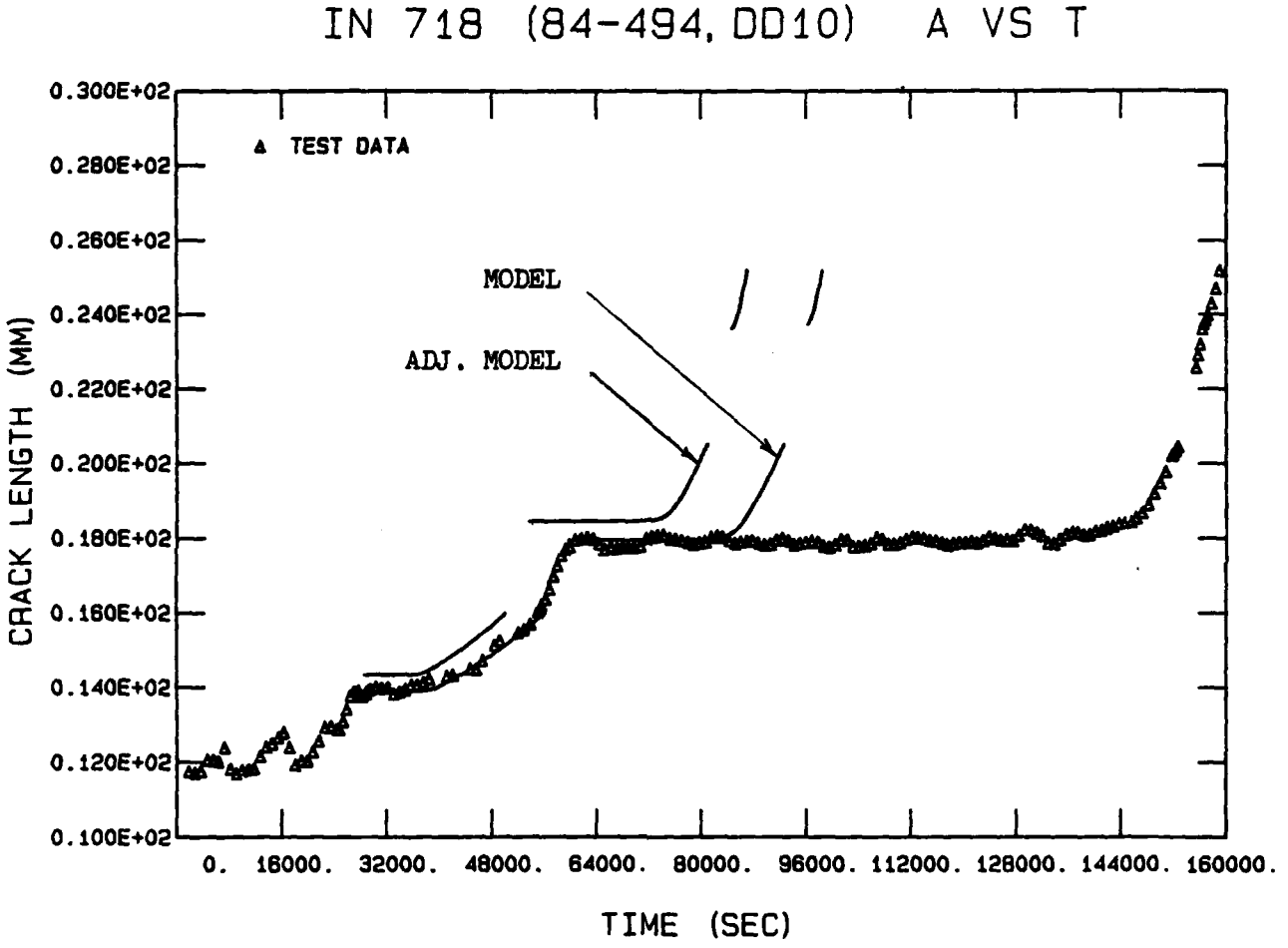

Figure 52 Model Prediction for Specimen DD10 (Part B)

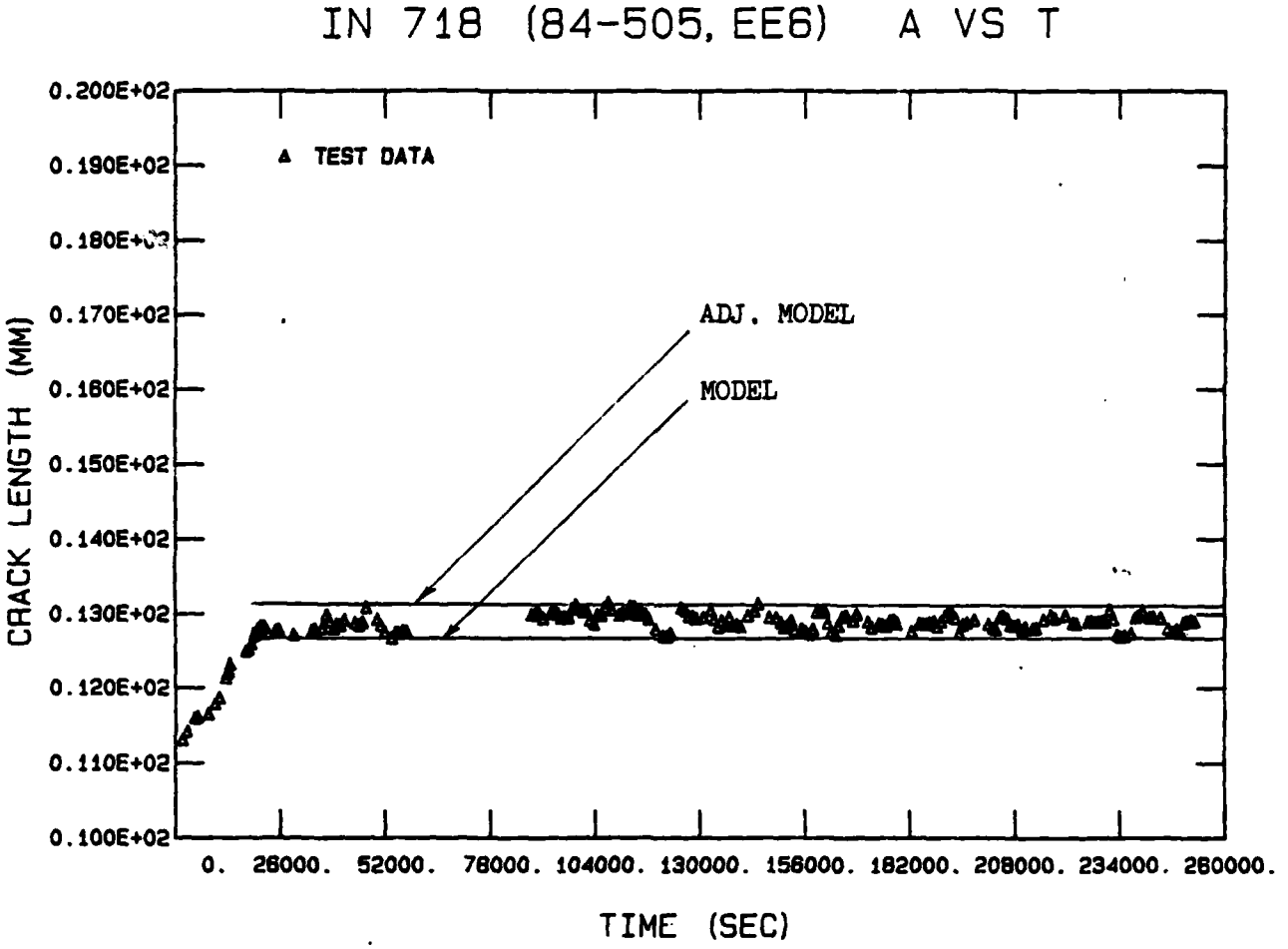

Figure 53 Model Prediction for Specimen EE6 (Part A)

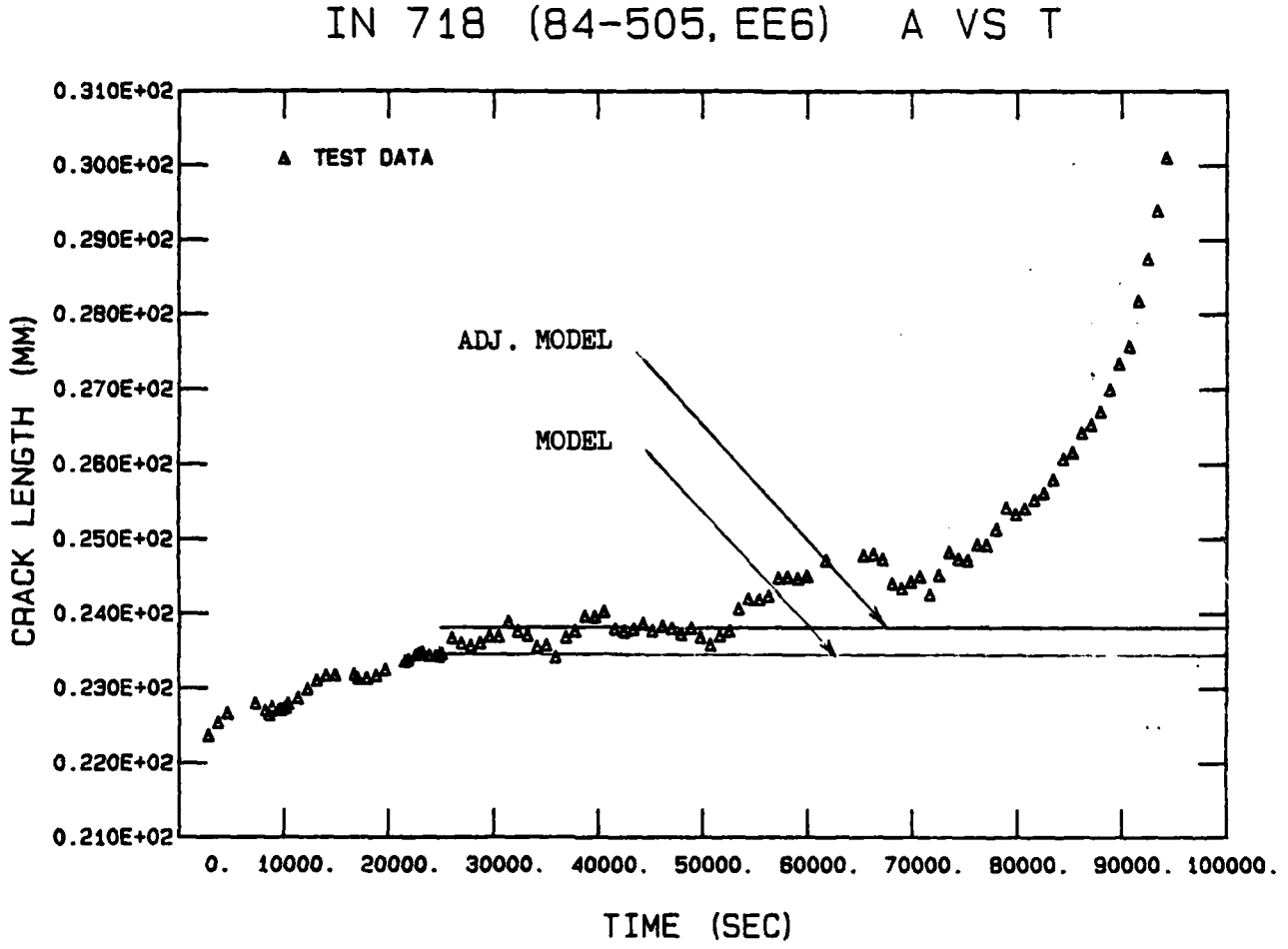

Figure 54 Model Prediction for Specimen EE6 (Part B)

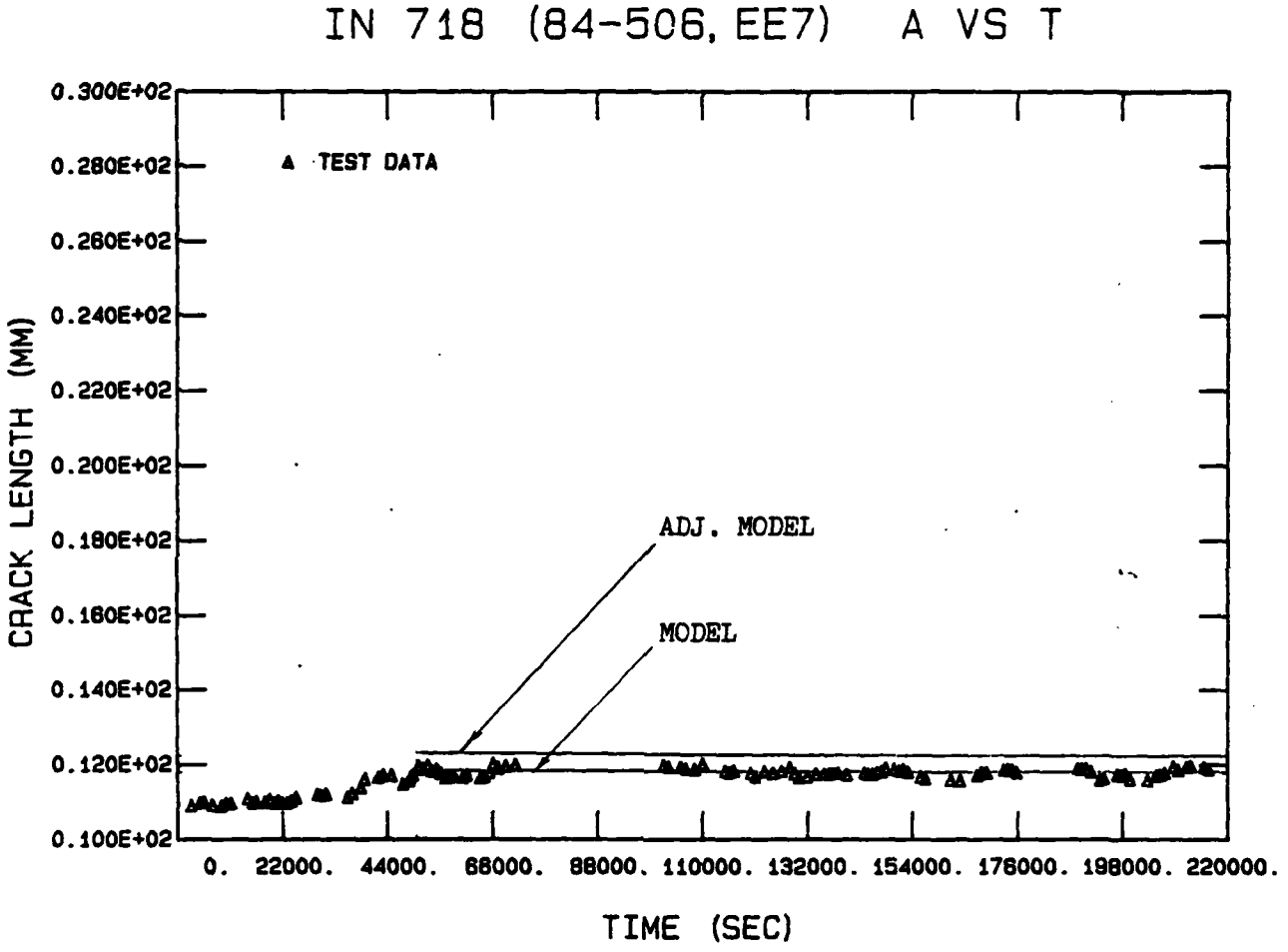

Figure 55 Model Prediction for Specimen EE7 (Part A)

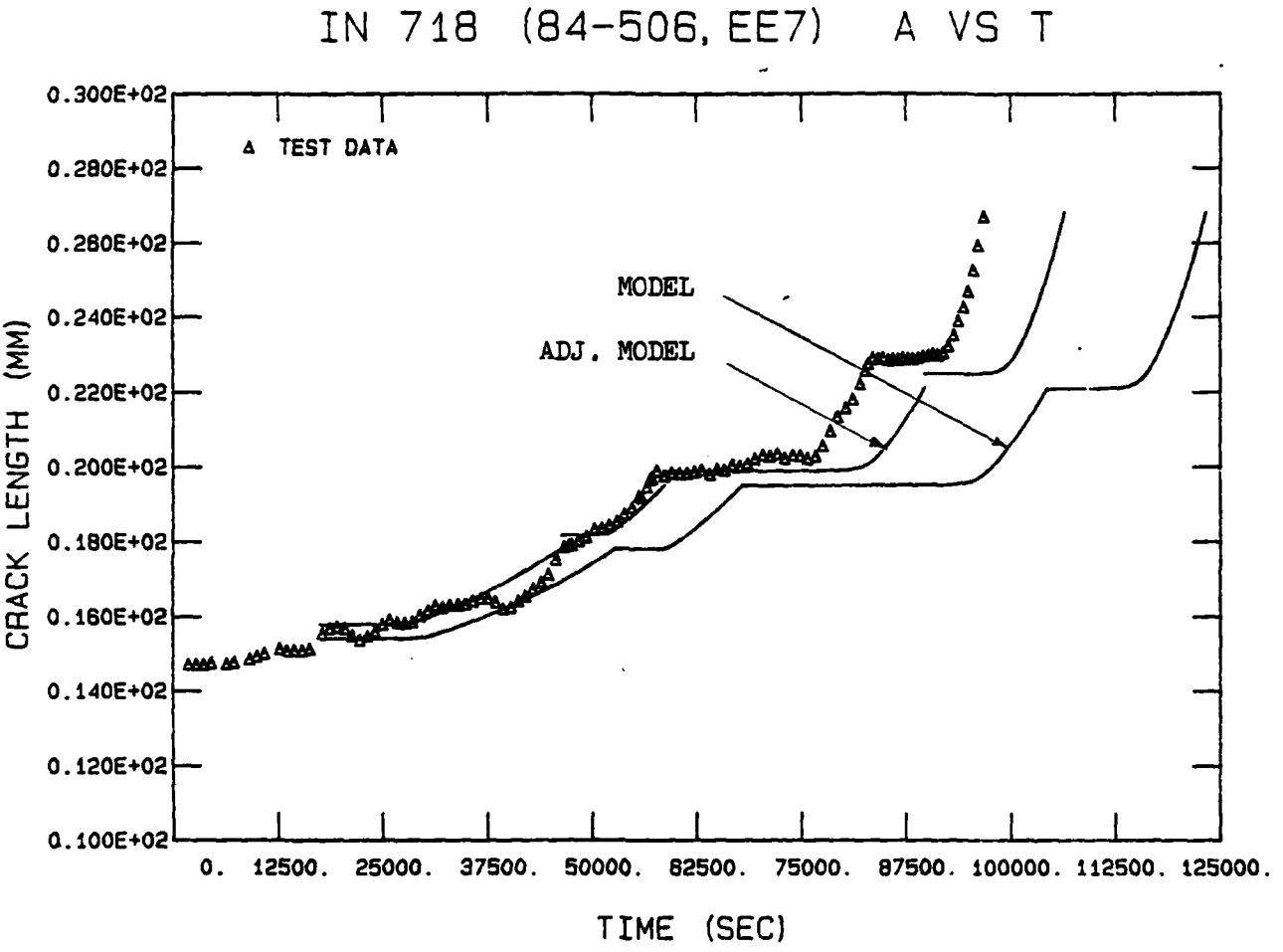

Figure 56 Model Prediction for Specimen EE7 (Part B)

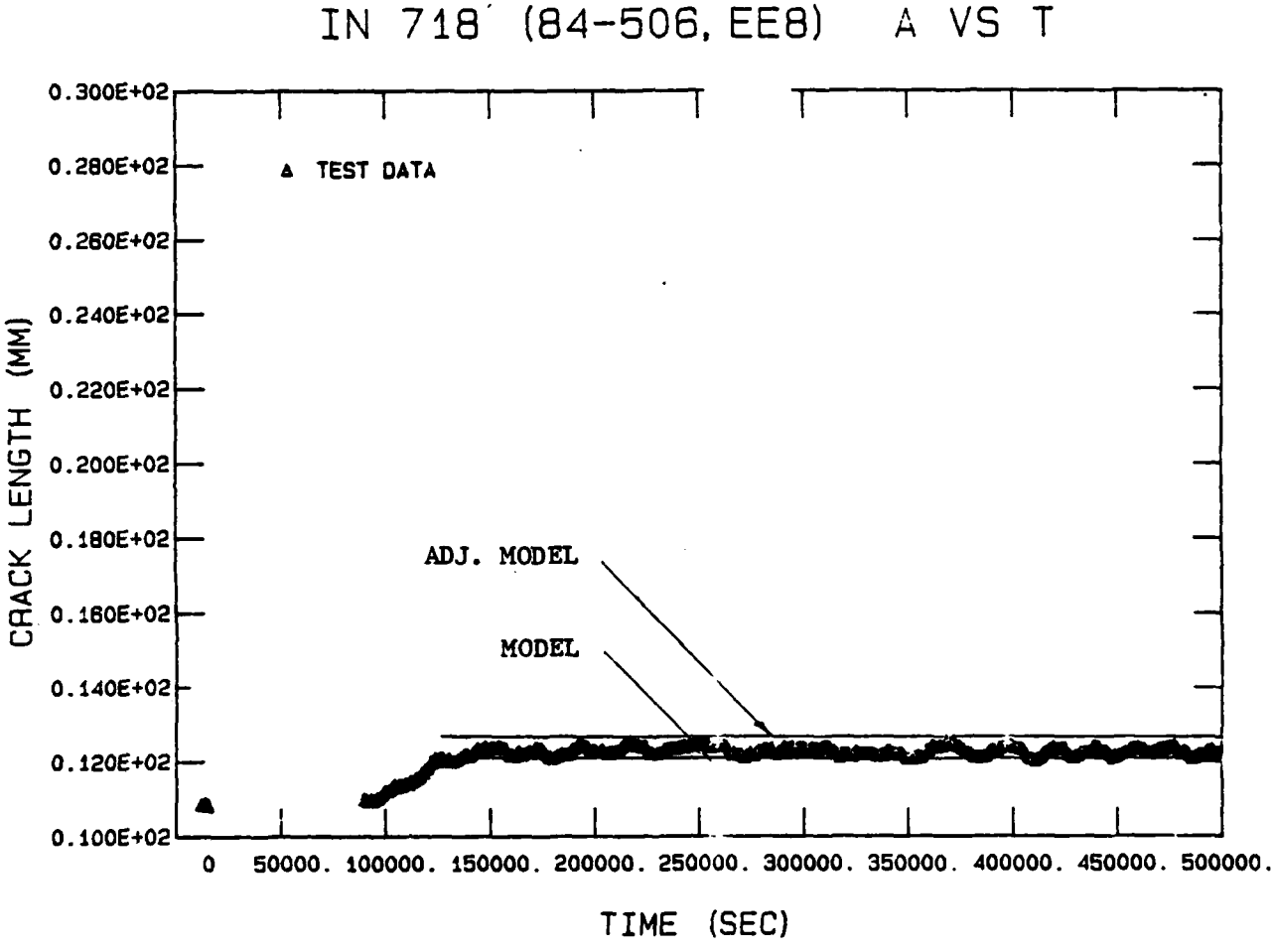

Figure 57 Model Prediction for Specimen EE8

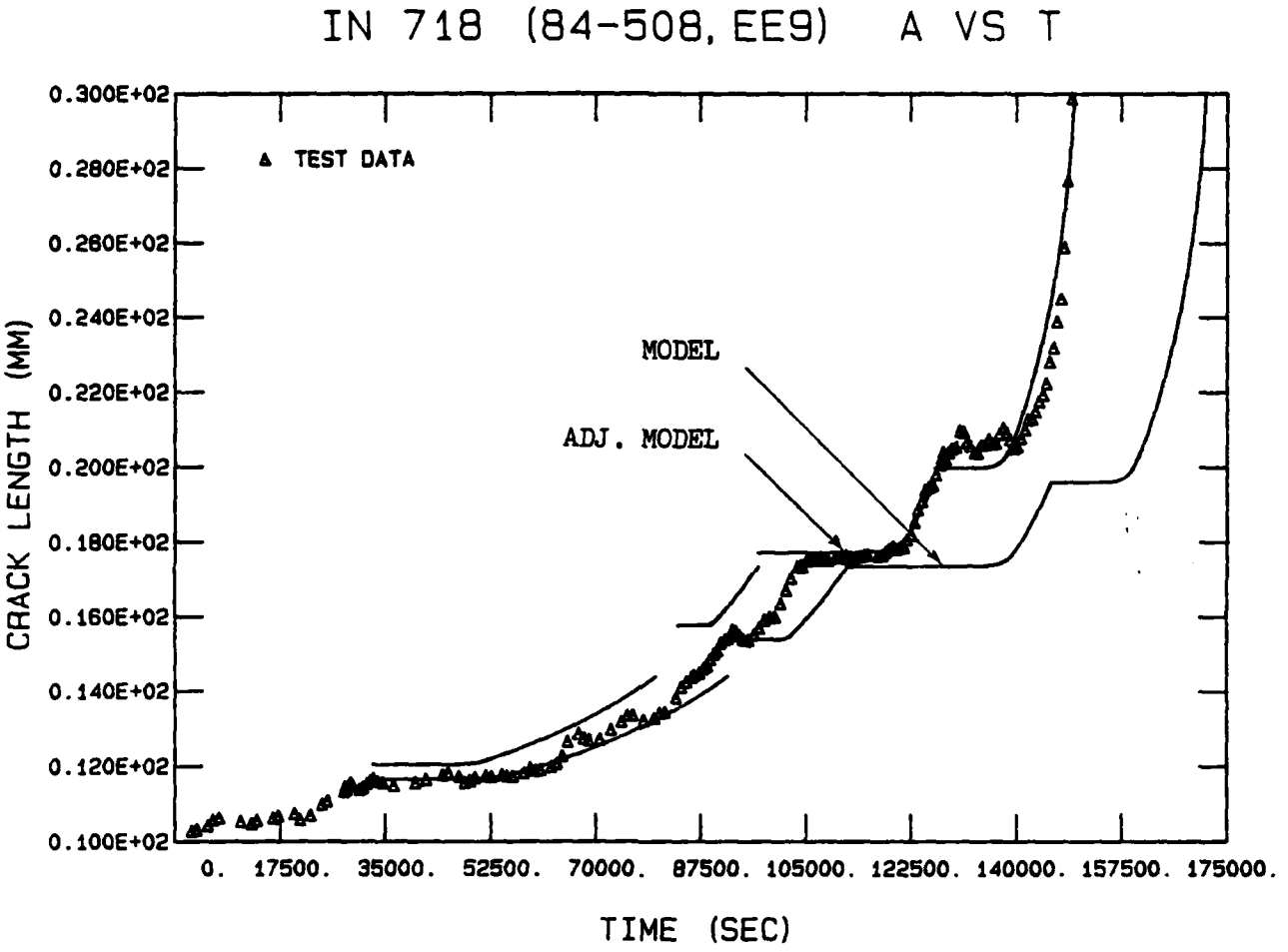

Figure 58 Model Prediction for Specimen EE9

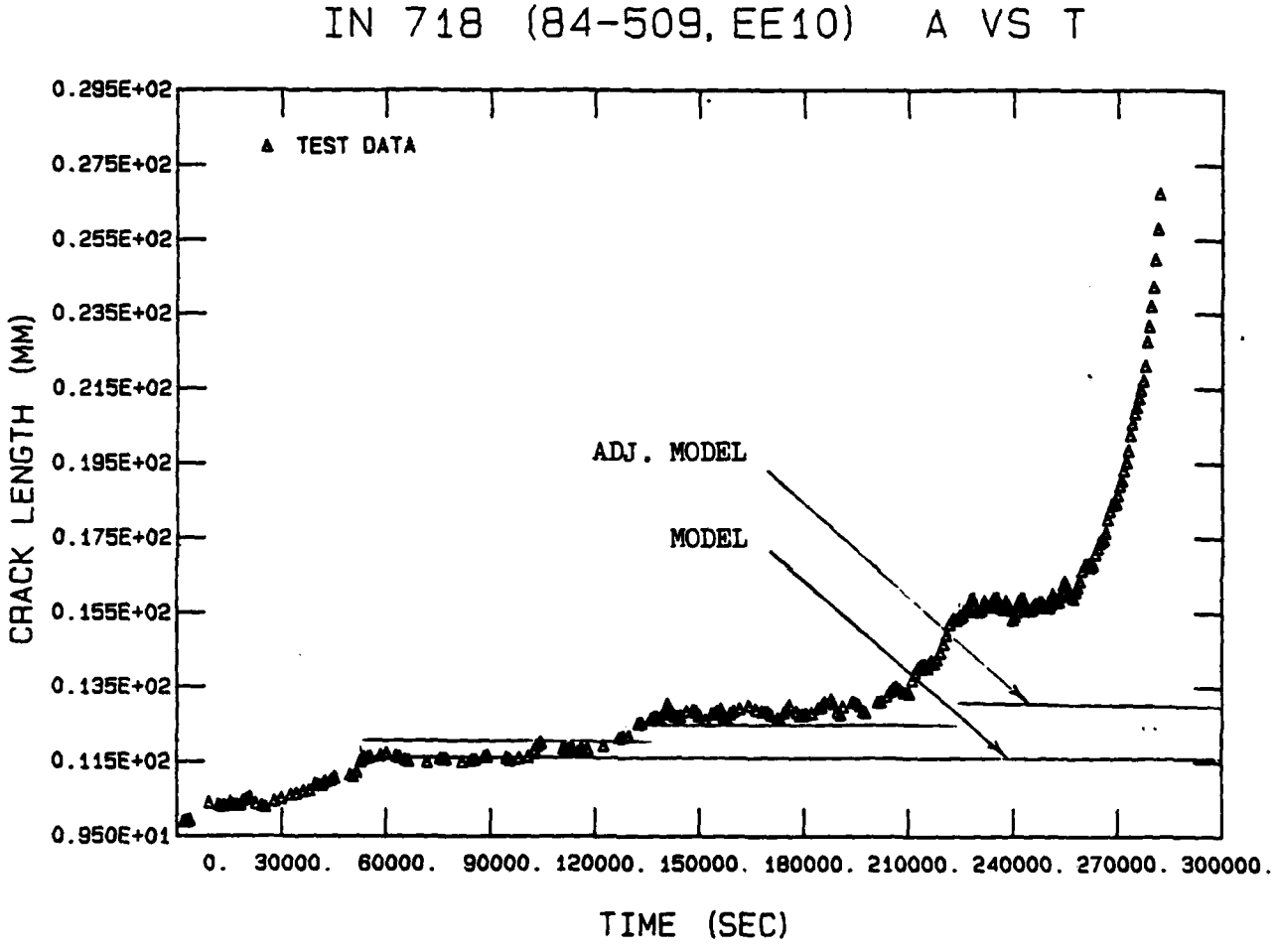

Figure 59 Model Prediction for Specimen EE10

Table IV

Accuracy of Time-to-Failure Predictions

Specimen ID	Model Error	Adjusted Model Error
DD1	-11.9%	+10.9%
DD3	+7.5%	+33.3%
DD5	-23.2%	-3.2%
DD6	-2.3%	13.9%
DD7	+ARREST	+ARREST
DD8	-ARREST	-10.1%
DD10 (a)	ARREST	ARREST
DD10 (b)	+45.4%	+54.0%
EE6 (a)	ARREST	ARREST
EE6 (b)	-ARREST	-ARREST
EE7 (a)	ARREST	ARREST
EE7 (b)	-31.8%	-11.6%
EE8 (a)	ARREST	ARREST
EE8 (Proof Test)	-ARREST	-1.4%
EE9	-18.6%	-0.7%
EE10	-ARREST	-ARREST

+ indicates a conservative error

- indicates a unconservative error

failure. This difference can be largely attributed to the variability in each specimen's threshold behavior. As was shown earlier, the threshold can dramatically effect crack-growth behavior. Since specimens EE10 and EE6 were also subjected to 50-percent overloads they were especially sensitive to threshold influences. In fact, many of the 50-percent overload predictions are somewhat crude because of the wide range of delay times encountered. The overly conservative predictions for specimens DD3, DD7, and DD10 are due in part to the use of 50-percent overload segments that could not be accurately modeled. However, the accuracy for the 50-percent case does improve for stress intensities above 45 MPA $\sqrt{m}$. This is evidenced by specimens EE7, EE9, and DD8 which experienced 50-percent overloads at a large K and were modeled with reasonable accuracy.

VII. Conclusions and Recommendations

Conclusions

During the course of this study a substantial body of data was generated and used to develop a new sustained load retardation model. In the process of formulating the model, the following 3 observations were made:

a.) A plane stress profile reasonably described the plastic zone size for retardation behavior.

b.) The size of the plastic zone was strictly a function of K and overload ratio and was independent of overload durations.

c.) Overloads produce crack growth discontinuities (jumps) that must be accounted for.

The cumulative damage model produced reasonably accurate time-to-failure predictions. All predictions, except for specimens EE10, EE6, and DD7 were well within a factor of two of the actual behavior. Except for specimens DD10, DD7 and DD3, which because of their 50-percent overloads were overly conservative, most predictions were on the order of 10-percent. Generally, the model provided better predictions as stress intensity increased. Predictions became less accurate as the model was applied closer to the threshold levels.

For design purposes, the model should be limited to regions that are beyond threshold influences. This was

approximately 30 MPA $\sqrt{m}$ for the 20-percent overload case and 45 MPA $\sqrt{m}$ for the 50-percent case. Predictions for both cases could be made more conservative by adjusting the α functions, but this should be supported with additional experimental data.

Adding the "crack-jump" increment to the model produced results that were generally more conservative and more accurate. A constant increment of 0.38 mm was found to be adequate for a substantial range of crack-growth behavior. The data, however, appeared to suggest that a variable increment would offer an additional refinement in predictions.

Recommendations

In order to further enhance the model developed in this study, additional data should be gathered to verify if the overload "crack jump" increment is a function of K. It would also be important to confirm whether or not the increment is a function of γ.

The entire model should also be redeveloped for other values of γ. Additional tests for overload ratios of 1.3 and 1.4 should be conducted to see if their behavior is bounded by the two cases in the study. Furthermore, it would be important to see if some kind of relationship could be developed to interpolate between α functions of one case to another.

It was noted that all of the experiments in this study were conducted with one material, Inconel 718. Additional tests on other materials should be performed to see if the model is applicable to them. Another nickel-base superalloy such as Rene 95 is recommended.

For an additional measure of confidence, the model should also be subjected to a second proof test. In this test, the overload intervals should be adequately spaced so interactions don't occur. Overloads of different magnitudes could then be applied and their effects investigated.

Finally, the model developed in this study should be compared with other retardation models such as Wheeler's. This would illustrate the model's relative accuracy and flexibility.

Bibliography

1. Harris, J. A., Sims, D. L. and Annis, C. G., "Concept Definition: Retirement for Cause of F-100 Rotor Components", AFWAL-TR-80-4118. Wright-Patterson AFB, OH 1980.

2. Macha, D. E., Grandt, A. F., Wicks, B. J., "Effects of Gas Turbine Engine Load Spectrum Variable son Crack Propagation", ASTM STP714, American Society for Testing and Materials, 1980, pp 108-127.

3. Collinis, J. A., Failure of Materials in Mechanical Design, New York, John Wiley and Sons, 1976, Ch. 13.

4. Macha, D. E., "Fatigue Crack Growth Retardation Behavior of IN-100 at Elevated Temperature "Engineering Fracture Mechanics, 1979, Vol.12, pp 1-11.

5. Sandananda, K. and Shahinian, P., "Creep Crack Growth Behavior of Several Structural Alloys", Metallurgical Transactions, August 2, 1982, pp 1467-1479.

6. Sandananda, K. and Shahinian, P., "High Temperature Time-Dependent Crack Growth" Micro and Macro Mechanics of Crack Growth,1981, pp 119-130.

7. Sandananda, K. and Shahinian, P. "Application of Fracture Mechanics Techniques to High Temperatures Crack Growth." Fracture Mechanics, 1978, pp 685-703.

8. Larsen, J. M. and Nicholas, T. "Cumulative Damage Modeling of Fatique Crack Growth in Turbine Engine Materials," Engineering Fracture Mechanics (in press).

9. Annual Book of ASTM Standards, Part 10; Metals-Mechanical, Fracture, and Corrosion Testing; Erosion and Wear; Effect of Temperature,1981.

10. Donath, R. C. "Crack Growth Behavior of Alloy IN100 Under Sustained Load at 732 C", AFWAL-TR-80-4131, Wright-Patterson AFB, OH April 1981.

11. Ashbaugh, N. E. "Material Evaluation: Part I-Mechanical Property Testing and Materials Evaluation Modeling", AFML-TR-79-4127 Part I, September 1979, pp 62-65.

12. Utah, D. A. General Electric Co., "Crack Growth Modeling in an Advanced Powder Metallurgy Alloy", AFWAL-TR-80-4098, Wright-Patterson AFB, OH 1980.

13. Rolfe, S. T.,and Barsom, J. M. Fracture and Fatique Controlin Structures, Englewood Cliffs, Prentice-Hall Inc., 1977, pp 274-275.

14. Broek, D. Elementary Engineering Fracture Mechanics, Third Edition, London, Martinue Nijhoff Publishers, 1982, pp 266-271.

15. Wheeler, D.E. "Spectrum Loading and Crack Growth" Journal of Basic Engineering, March 1972, pp 181-186.

16. Hertzberg, R. W. Deformation and Fracture Mechanics of Engineering Materials, New York, John Wiley and Sons, 1976, pp 485-501.

17. Keck, J. E. Nicholas, T. and Palazotto, A. N. "High Temperature Viscoplastic Fatigue of a Compact Tension Specimen", Engineering Fracture Mechanics (in press).

18. Larsen J. M. and Nicholas, T. "Load Sequence Crack Grwoth Transients in a Superalloy at Elevated Temperature", Fracture Mechanics: Fourteenth Symposium Volune II: Testing and Applications, ASTM STP 791, J.C. Lewis and G. Siner Eds., American Society for Testing and Materials, 1983, pp II-536-II-552.

Appendix A

Heat Treatment History of Test Specimens

Anneal at 968 °C for 1 hour - air cool

Age harden at 718 °C for 8 hours-furnace cool to 621 °C

Age harden at 621 °C for a total of an additional 10 hours

Appendix B

Crack Growth Rate Curves for Overload Segments

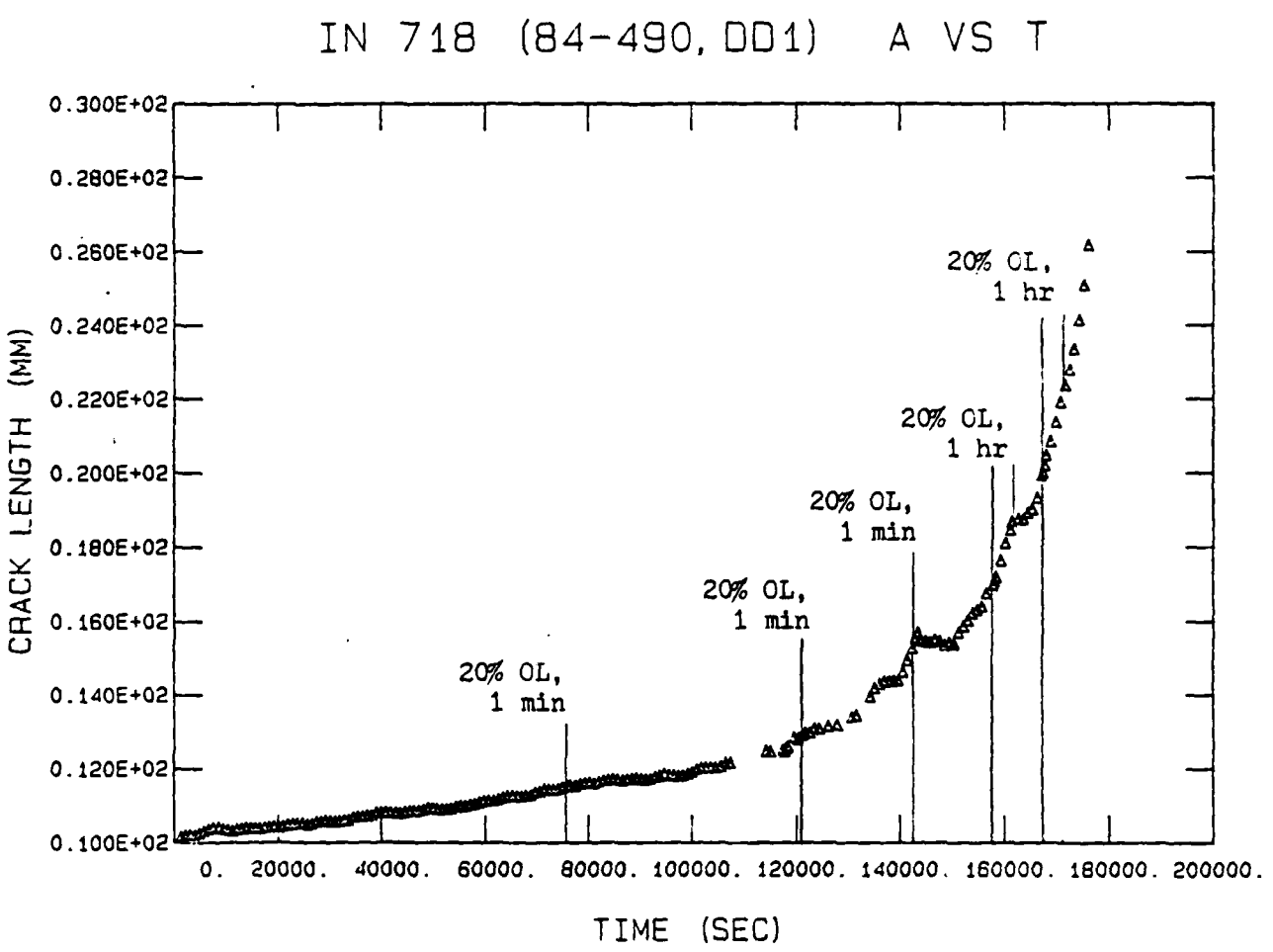
IN 718 (84-490, DD1) A VS T
CRACK LENGTH (MM)
0.300E+02
0.280E+02
0.260E+02
0.240E+02
0.220E+02
0.200E+02
0.180E+02
0.160E+02
0.140E+02
0.120E+02
0.100E+02
20% OL, 1 min
20% OL, 1 min
20% OL, 1 min
20% OL, 1 hr
20% OL, 1 hr
0. 20000. 40000. 60000. 80000. 100000. 120000. 140000. 160000. 180000. 200000.
TIME (SEC)

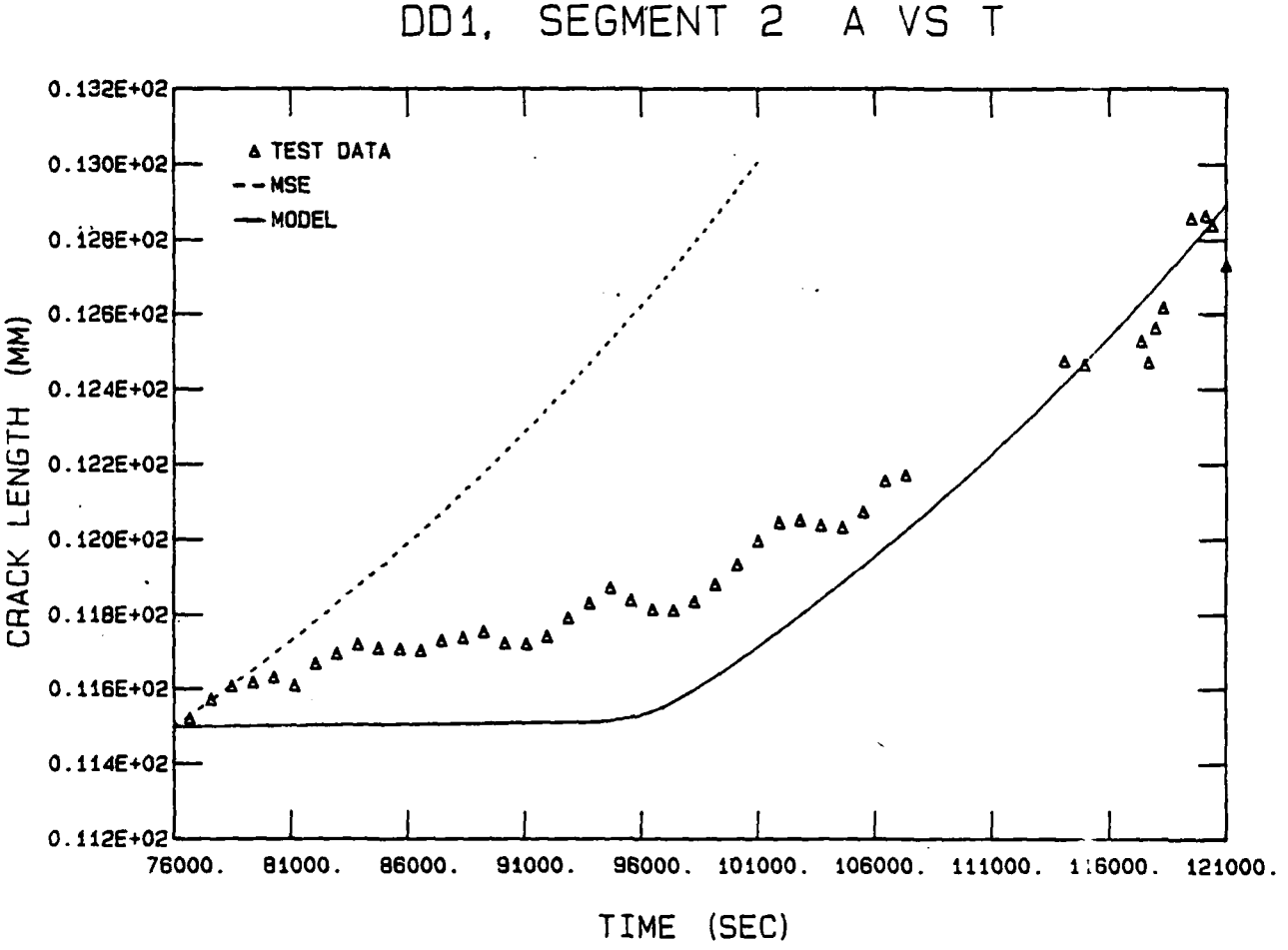
DD1, SEGMENT 2 A VS T
0.132E+02
0.130E+02
0.128E+02
0.126E+02
0.124E+02
0.122E+02
0.120E+02
0.118E+02
0.116E+02
0.114E+02
0.112E+02
CRACK LENGTH (MM)
TEST DATA
MSE
MODEL
76000.
81000.
86000.
91000.
96000.
101000.
106000.
111000.
116000.
121000.
TIME (SEC)

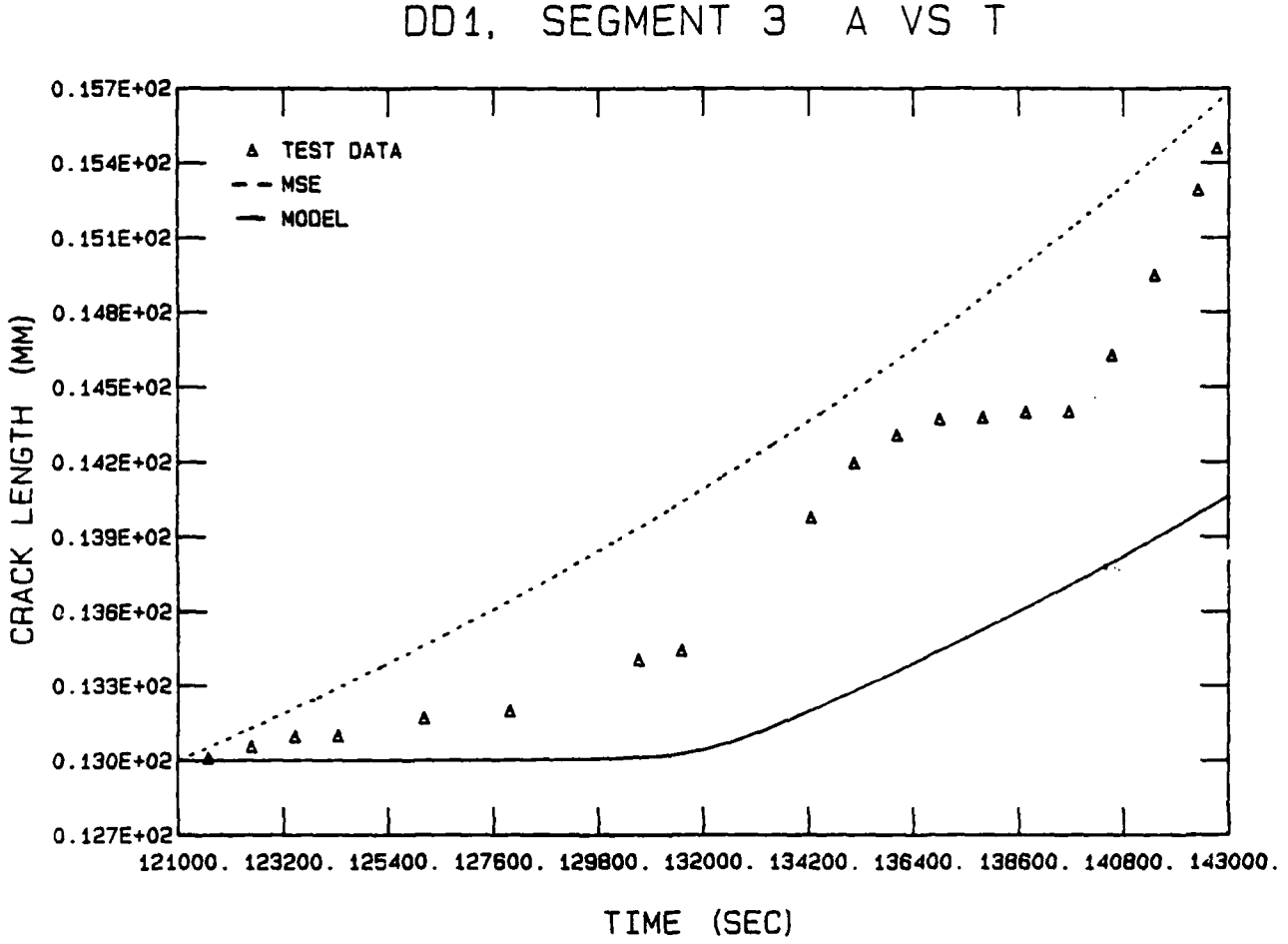
DD1, SEGMENT 3 A VS T
0.157E+02
0.154E+02
0.151E+02
0.148E+02
0.145E+02
0.142E+02
0.139E+02
0.136E+02
0.133E+02
0.130E+02
0.127E+02
CRACK LENGTH (MM)
TEST DATA
MSE
MODEL
121000. 123200. 125400. 127600. 129800. 132000. 134200. 136400. 138600. 140800. 143000.
TIME (SEC)

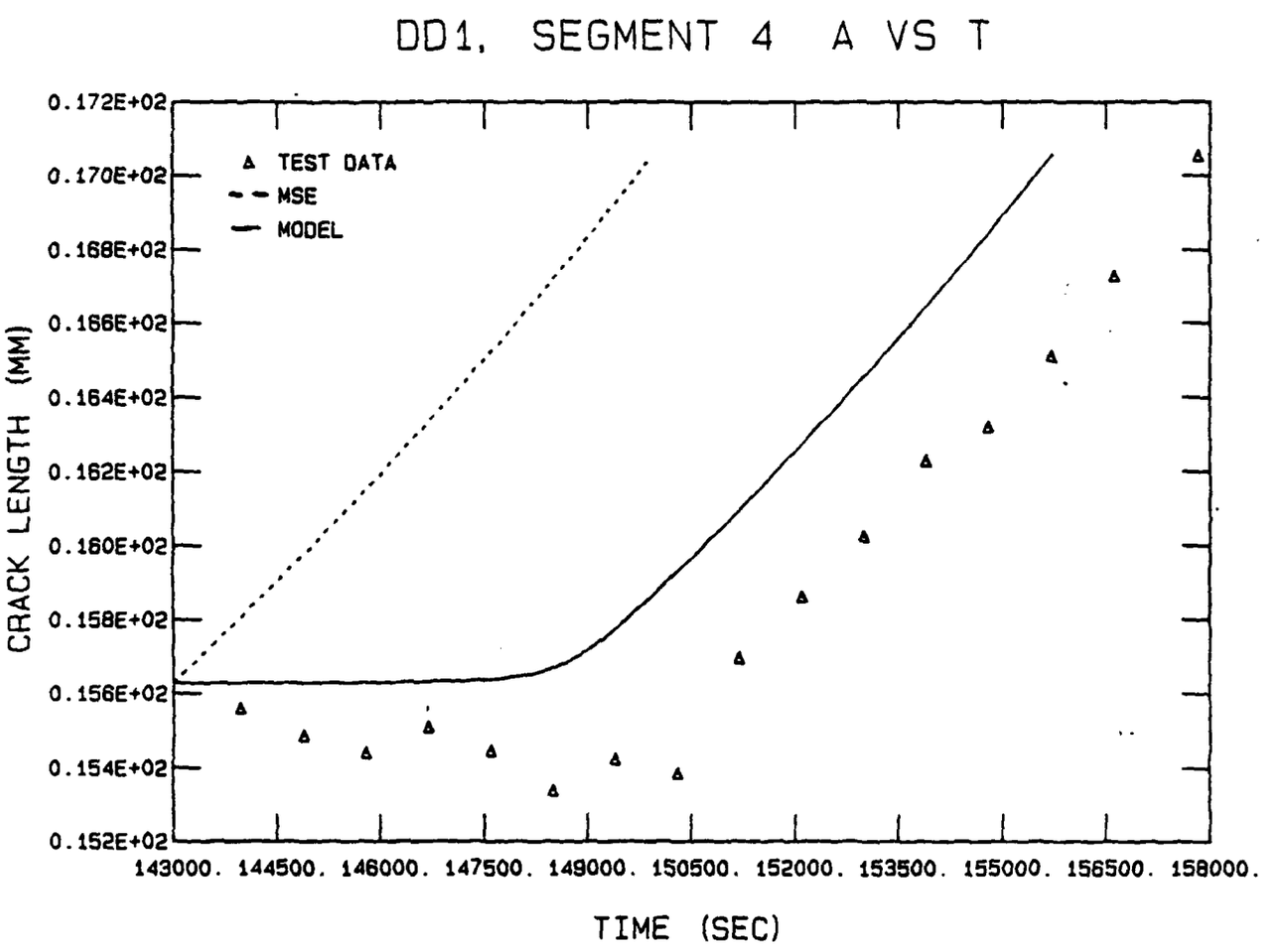
DD1, SEGMENT 4 A VS T
TEST DATA
MSE
MODEL
CRACK LENGTH (MM)
0.172E+02
0.170E+02
0.168E+02
0.166E+02
0.164E+02
0.162E+02
0.160E+02
0.158E+02
0.156E+02
0.154E+02
0.152E+02
143000. 144500. 146000. 147500. 149000. 150500. 152000. 153500. 155000. 156500. 158000.
TIME (SEC)

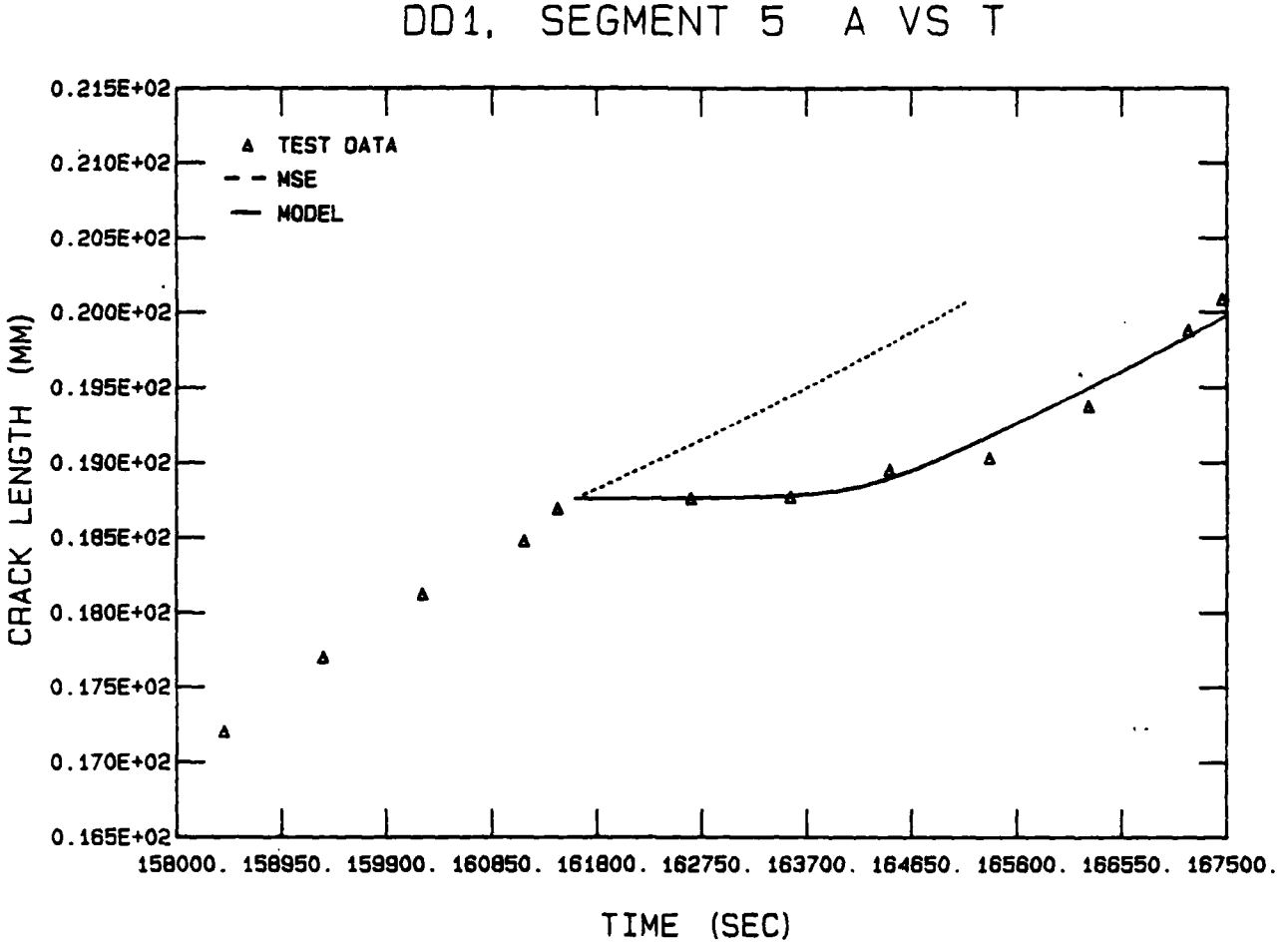
DD1, SEGMENT 5 A VS T
TEST DATA
MSE
MODEL
CRACK LENGTH (MM)
0.215E+02
0.210E+02
0.205E+02
0.200E+02
0.195E+02
0.190E+02
0.185E+02
0.180E+02
0.175E+02
0.170E+02
0.165E+02
158000. 158950. 159900. 160850. 161800. 162750. 163700. 164650. 165600. 166550. 167500.
TIME (SEC)

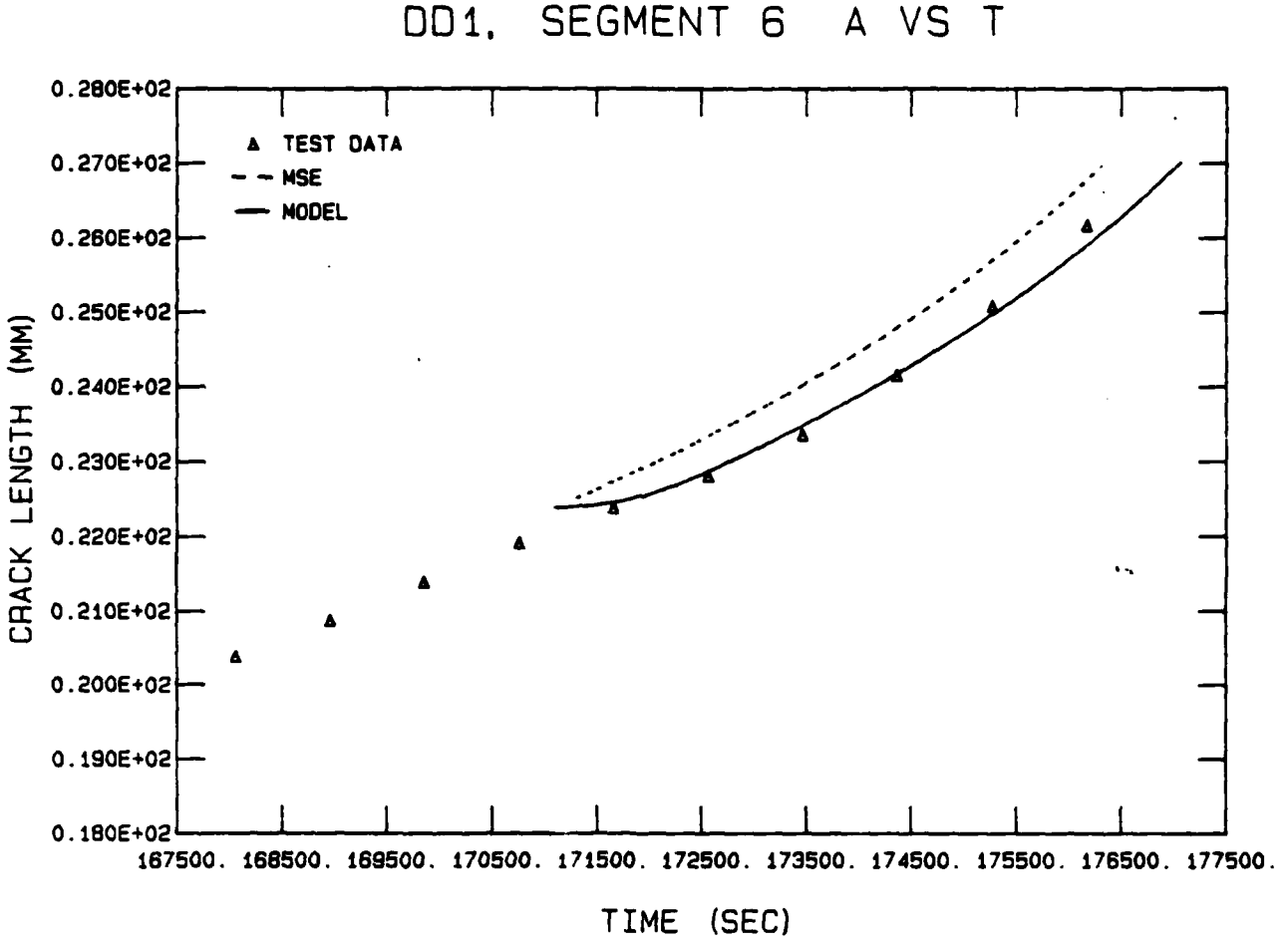
DD1, SEGMENT 6 A VS T
TEST DATA
MSE
MODEL
CRACK LENGTH (MM)
0.280E+02
0.270E+02
0.260E+02
0.250E+02
0.240E+02
0.230E+02
0.220E+02
0.210E+02
0.200E+02
0.190E+02
0.180E+02
167500. 168500. 169500. 170500. 171500. 172500. 173500. 174500. 175500. 176500. 177500.
TIME (SEC)

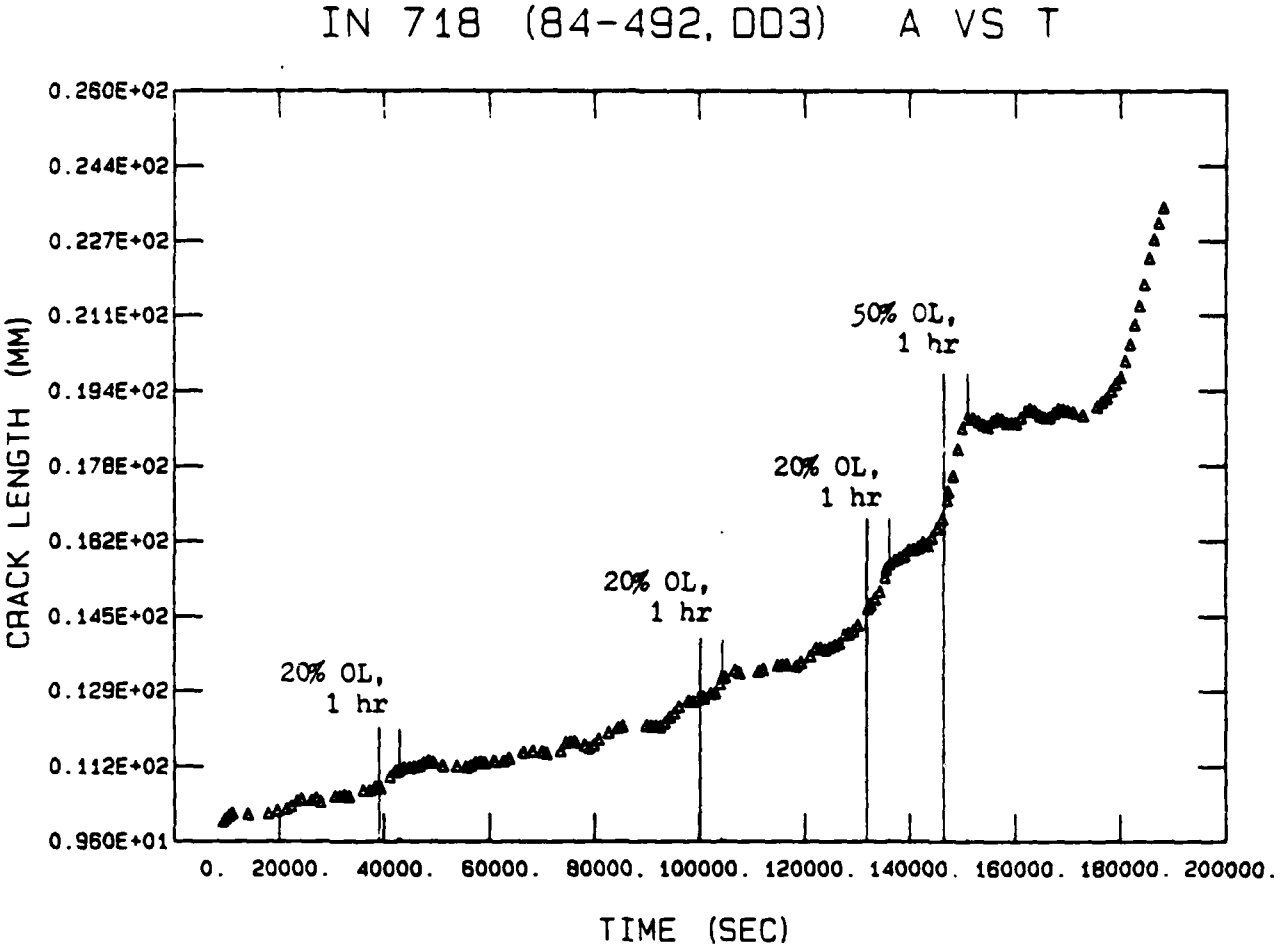
IN 718 (84-492, DD3) A VS T
0.260E+02
0.244E+02
0.227E+02
0.211E+02
0.194E+02
0.178E+02
0.162E+02
0.145E+02
0.129E+02
0.112E+02
0.960E+01
CRACK LENGTH (MM)
20% OL, 1 hr
20% OL, 1 hr
20% OL, 1 hr
50% OL, 1 hr
0. 20000. 40000. 60000. 80000. 100000. 120000. 140000. 160000. 180000. 200000.
TIME (SEC)

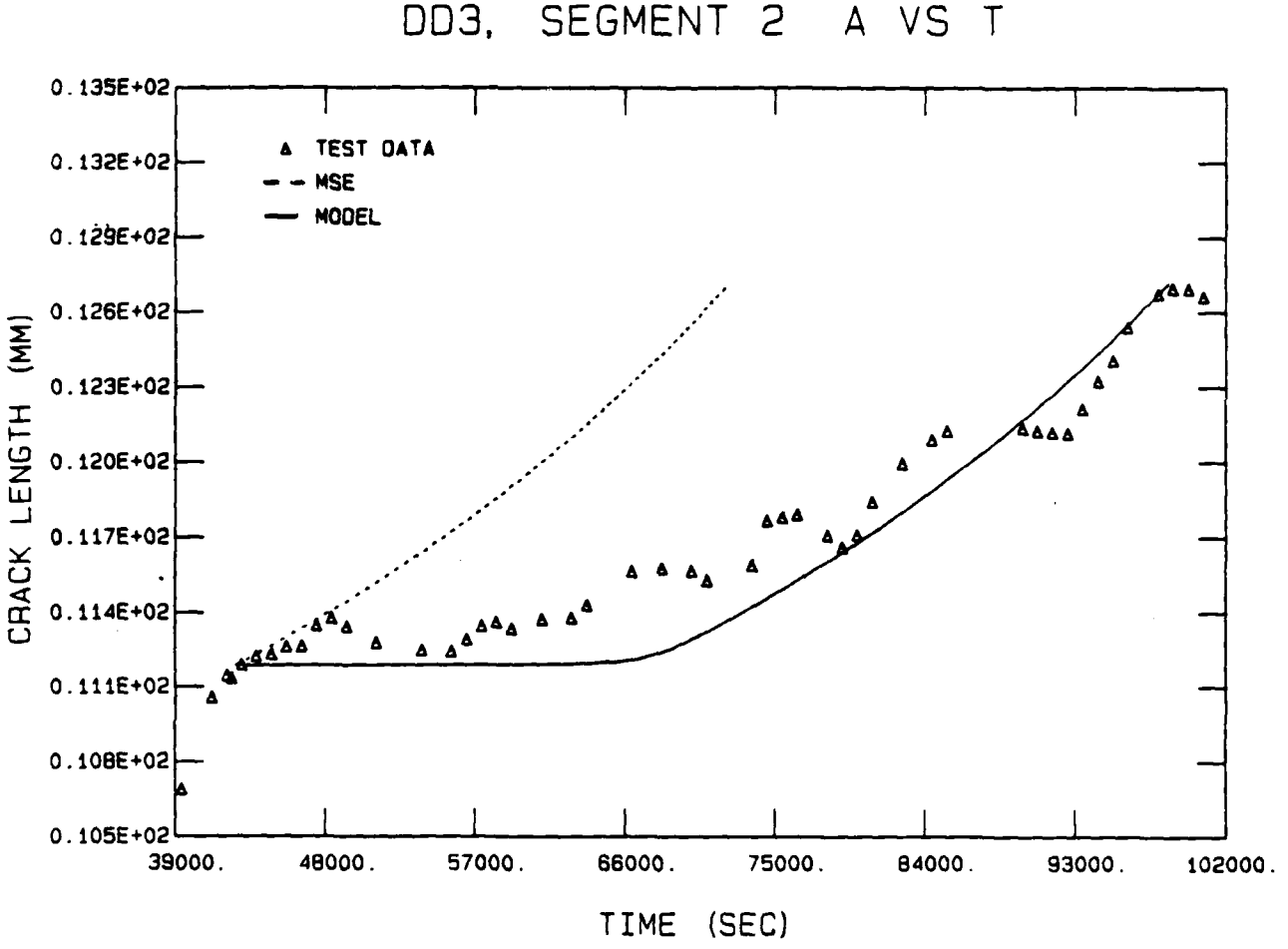
DD3, SEGMENT 2 A VS T
TEST DATA
MSE
MODEL
CRACK LENGTH (MM)
0.135E+02
0.132E+02
0.129E+02
0.126E+02
0.123E+02
0.120E+02
0.117E+02
0.114E+02
0.111E+02
0.108E+02
0.105E+02
39000.
48000.
57000.
66000.
75000.
84000.
93000.
102000.
TIME (SEC)

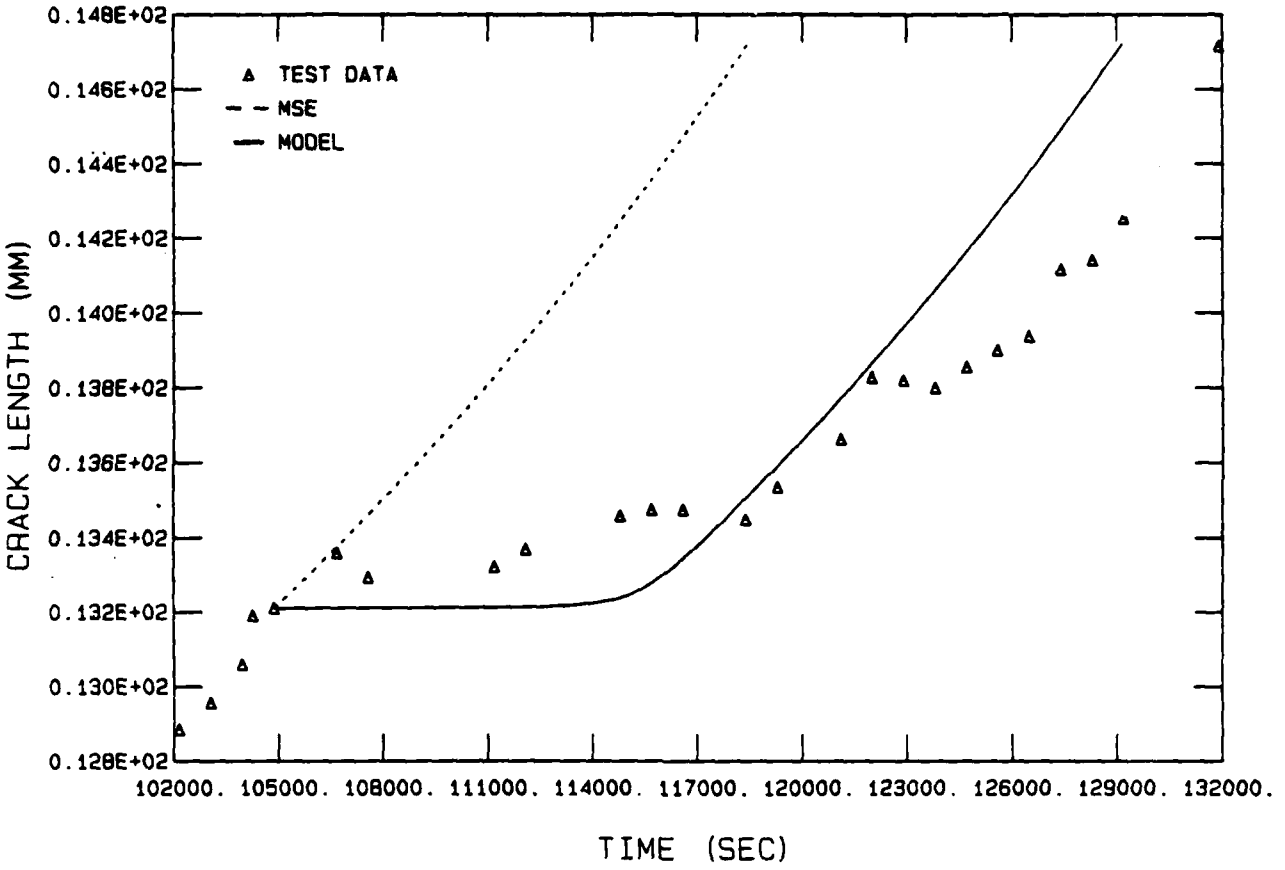
DD3, SEGMENT 3 A VS T
TEST DATA
MSE
MODEL
CRACK LENGTH (MM)
0.148E+02
0.146E+02
0.144E+02
0.142E+02
0.140E+02
0.138E+02
0.136E+02
0.134E+02
0.132E+02
0.130E+02
0.128E+02
102000. 105000. 108000. 111000. 114000. 117000. 120000. 123000. 126000. 129000. 132000.
TIME (SEC)

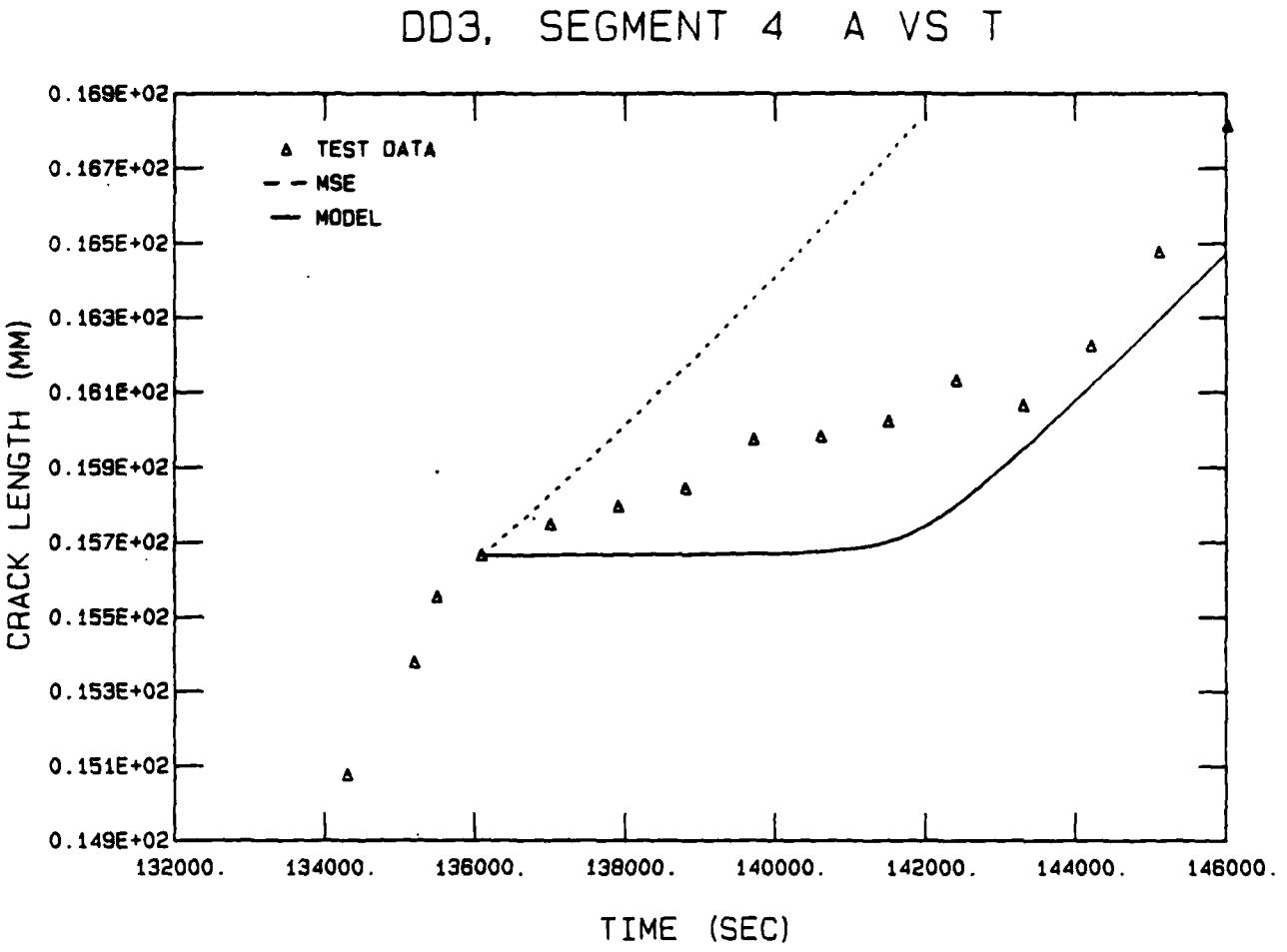
DD3, SEGMENT 4 A VS T
0.169E+02
0.167E+02
0.165E+02
0.163E+02
0.161E+02
0.159E+02
0.157E+02
0.155E+02
0.153E+02
0.151E+02
0.149E+02
CRACK LENGTH (MM)
TEST DATA
MSE
MODEL
132000.
134000.
136000.
138000.
140000.
142000.
144000.
146000.
TIME (SEC)

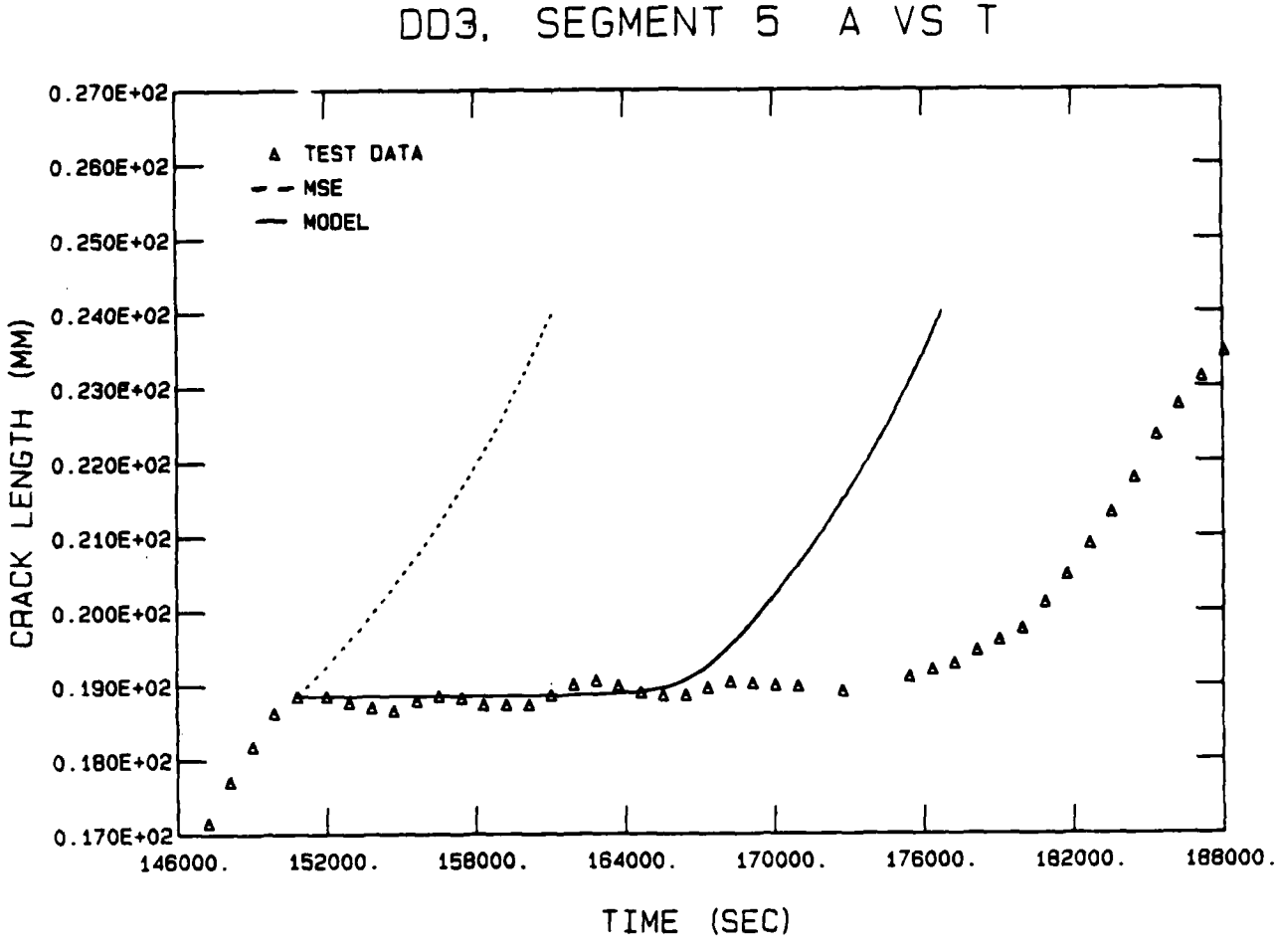
DD3, SEGMENT 5 A VS T
0.270E+02
0.260E+02
0.250E+02
0.240E+02
0.230E+02
0.220E+02
0.210E+02
0.200E+02
0.190E+02
0.180E+02
0.170E+02
CRACK LENGTH (MM)
TEST DATA
MSE
MODEL
146000.
152000.
158000.
164000.
170000.
176000.
182000.
188000.
TIME (SEC)

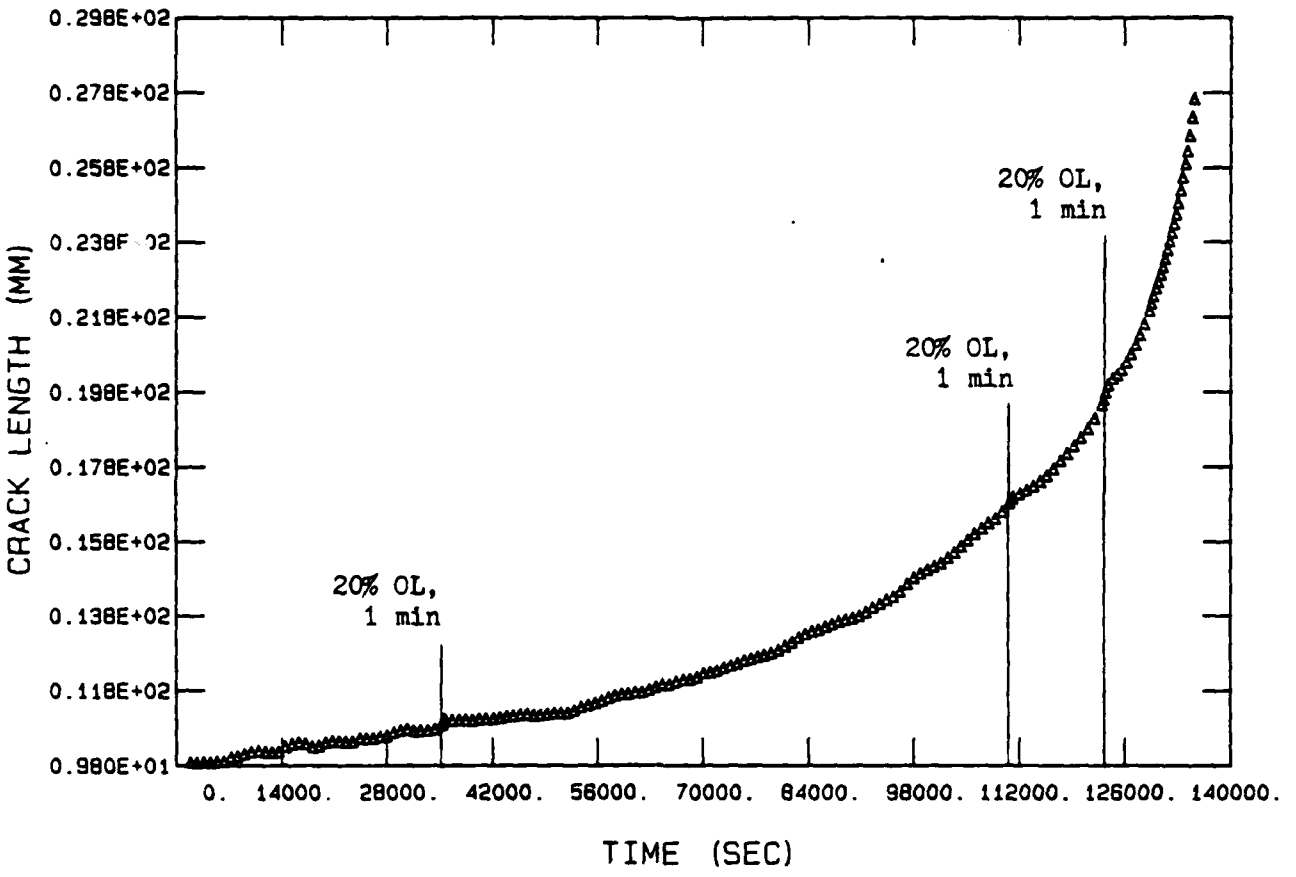
IN 718 (84-494, DD5) A VS T
CRACK LENGTH (MM)
0.298E+02
0.278E+02
0.258E+02
0.238E+02
0.218E+02
0.198E+02
0.178E+02
0.158E+02
0.138E+02
0.118E+02
0.980E+01
20% OL, 1 min
20% OL, 1 min
20% OL, 1 min
0. 14000. 28000. 42000. 56000. 70000. 84000. 98000. 112000. 126000. 140000.
TIME (SEC)

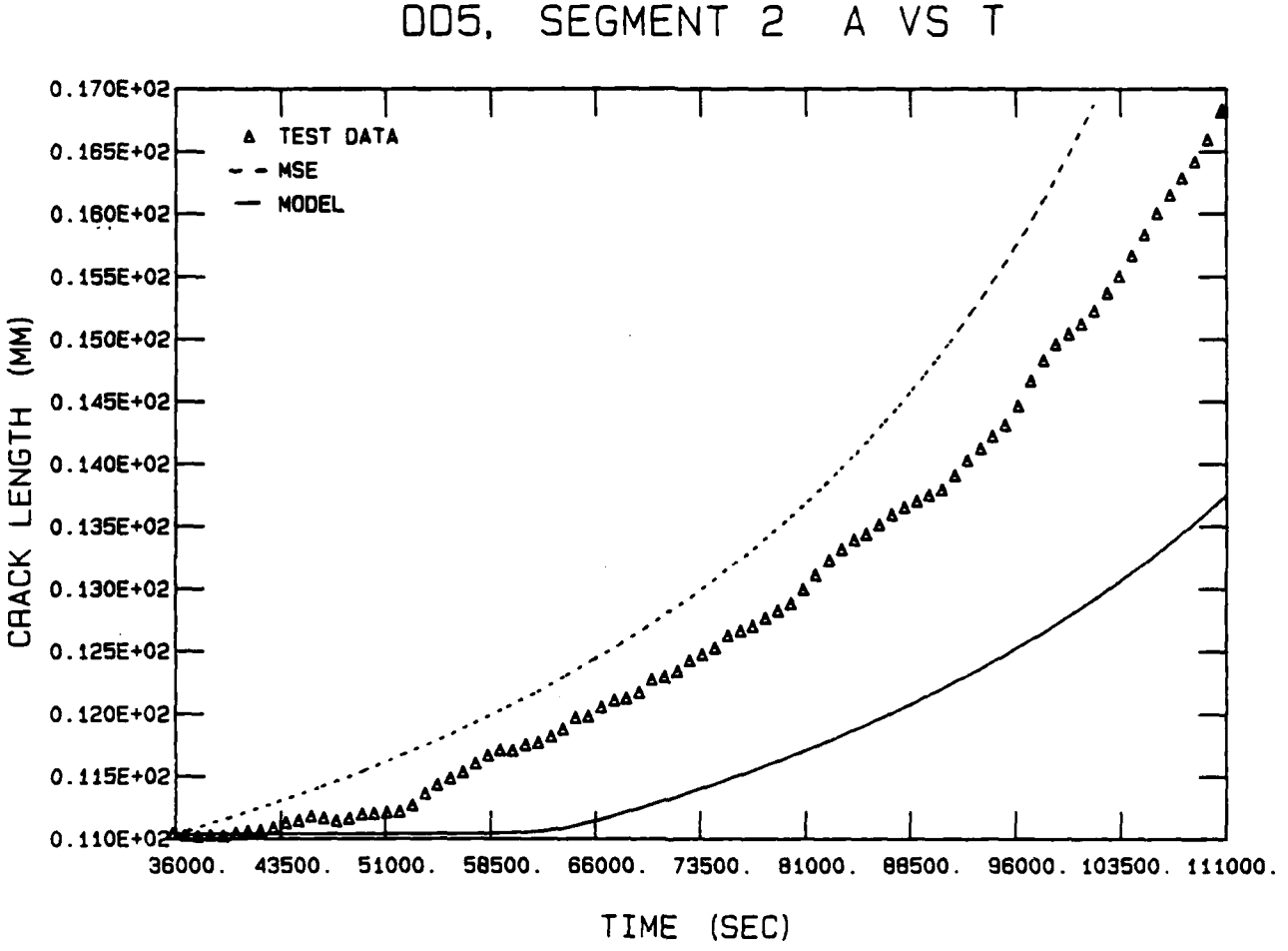
D05, SEGMENT 2 A VS T
TEST DATA
MSE
MODEL
CRACK LENGTH (MM)
0.170E+02
0.165E+02
0.160E+02
0.155E+02
0.150E+02
0.145E+02
0.140E+02
0.135E+02
0.130E+02
0.125E+02
0.120E+02
0.115E+02
0.110E+02
36000. 43500. 51000. 58500. 66000. 73500. 81000. 88500. 96000. 103500. 111000.
TIME (SEC)

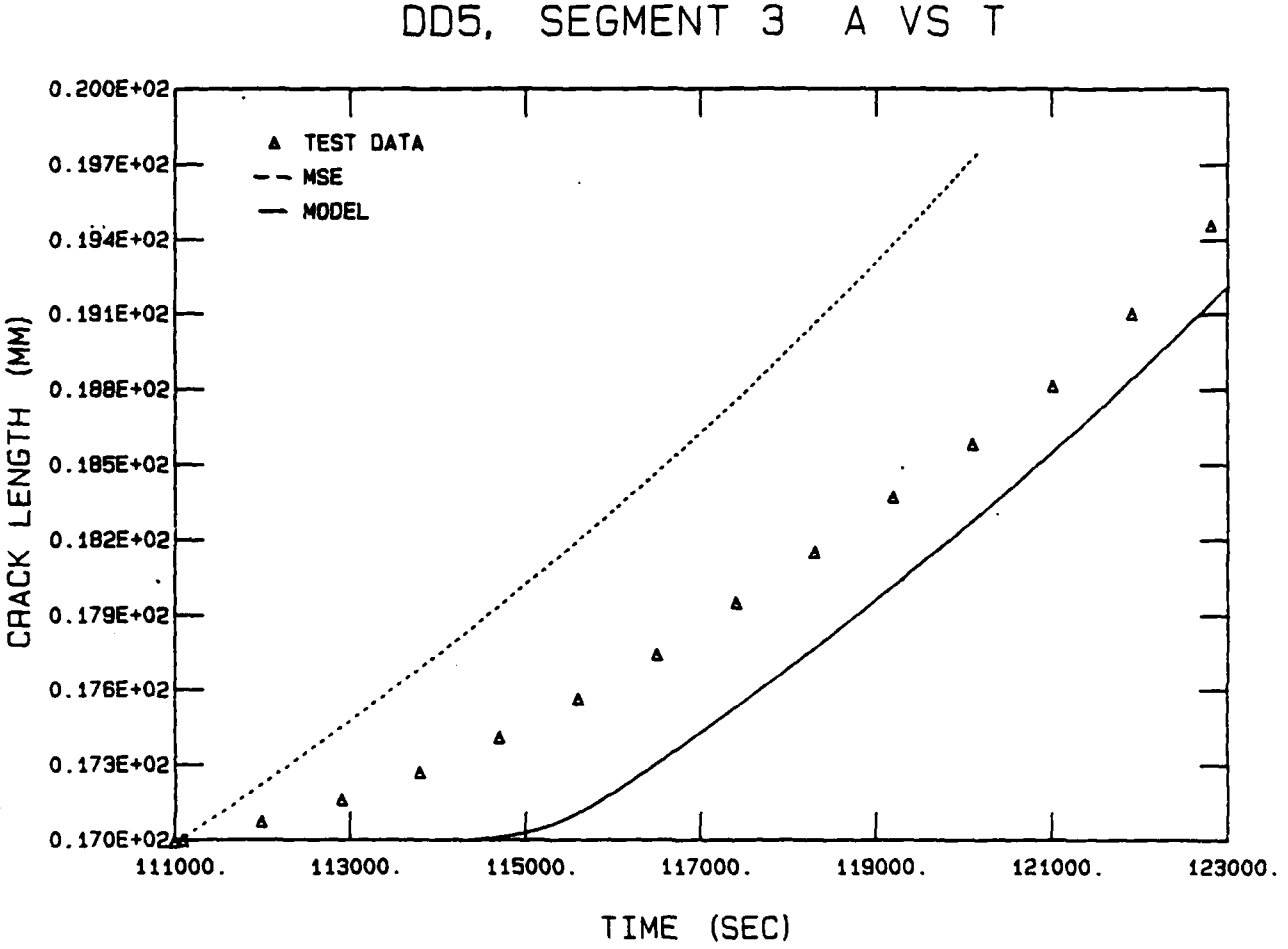
DD5, SEGMENT 3 A VS T
TEST DATA
MSE
MODEL
CRACK LENGTH (MM)
0.200E+02
0.197E+02
0.194E+02
0.191E+02
0.188E+02
0.185E+02
0.182E+02
0.179E+02
0.176E+02
0.173E+02
0.170E+02
111000.
113000.
115000.
117000.
119000.
121000.
123000.
TIME (SEC)

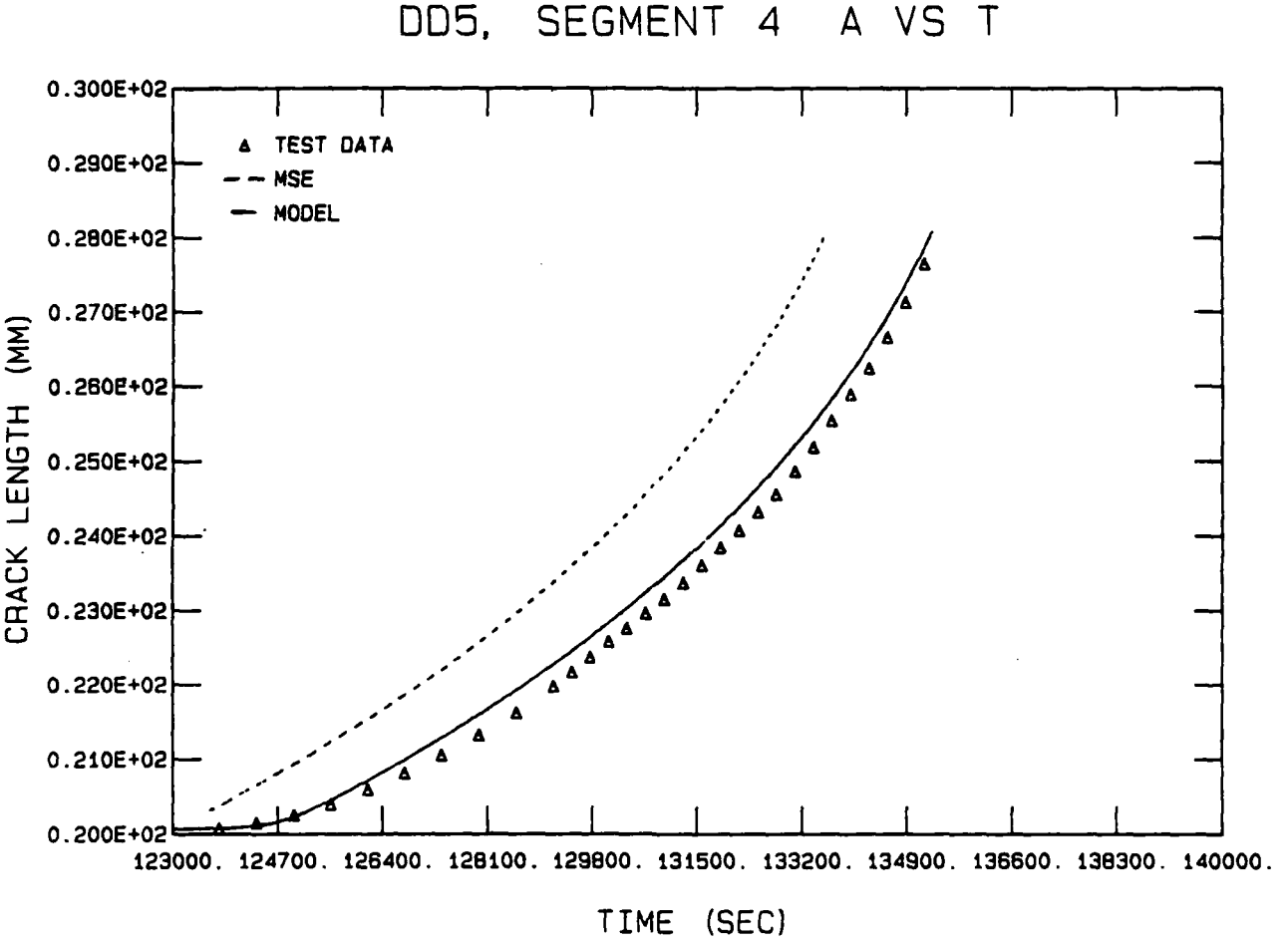
DD5, SEGMENT 4 A VS T
0.300E+02
0.290E+02
0.280E+02
0.270E+02
0.260E+02
0.250E+02
0.240E+02
0.230E+02
0.220E+02
0.210E+02
0.200E+02
CRACK LENGTH (MM)
TEST DATA
MSE
MODEL
123000. 124700. 126400. 128100. 129800. 131500. 133200. 134900. 136600. 138300. 140000.
TIME (SEC)

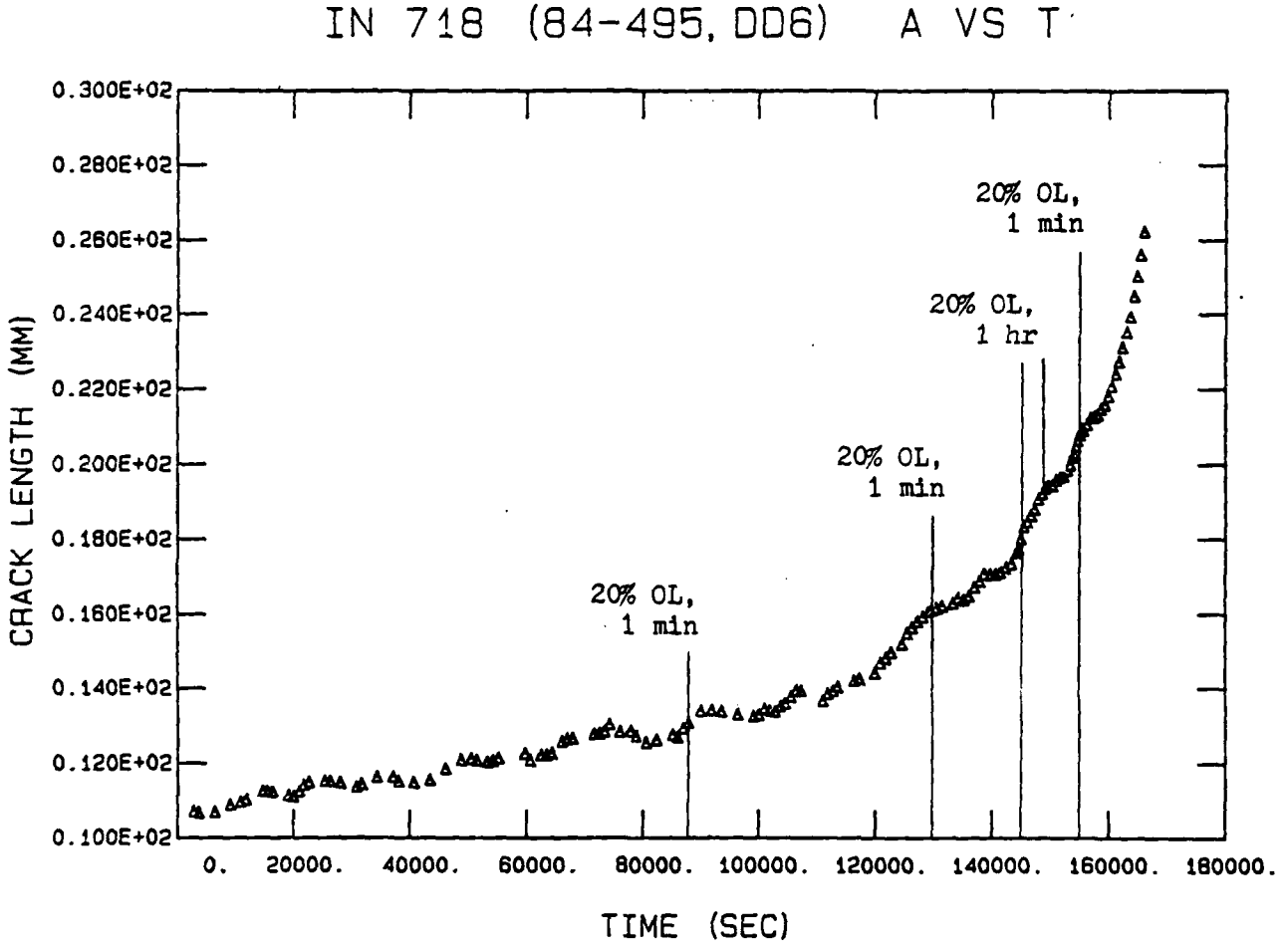
IN 718 (84-495, DD6) A VS T
0.300E+02
0.280E+02
0.260E+02
0.240E+02
0.220E+02
0.200E+02
0.180E+02
0.160E+02
0.140E+02
0.120E+02
0.100E+02
CRACK LENGTH (MM)
20% OL, 1 min
20% OL, 1 min
20% OL, 1 hr
20% OL, 1 min
0.
20000.
40000.
60000.
80000.
100000.
120000.
140000.
160000.
180000.
TIME (SEC)

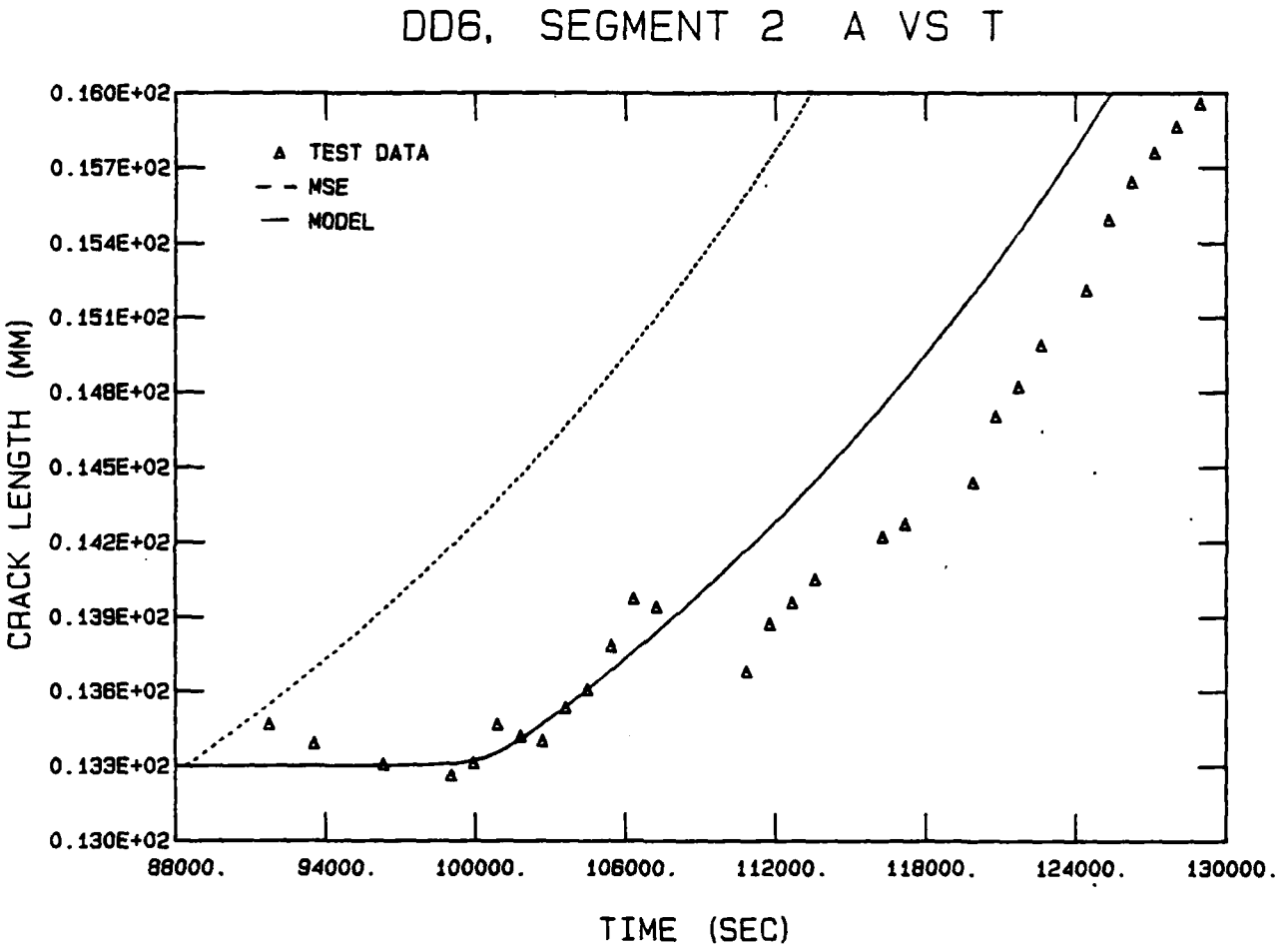
DD6, SEGMENT 2 A VS T
TEST DATA
MSE
MODEL
CRACK LENGTH (MM)
0.160E+02
0.157E+02
0.154E+02
0.151E+02
0.148E+02
0.145E+02
0.142E+02
0.139E+02
0.136E+02
0.133E+02
0.130E+02
88000.
94000.
100000.
106000.
112000.
118000.
124000.
130000.
TIME (SEC)

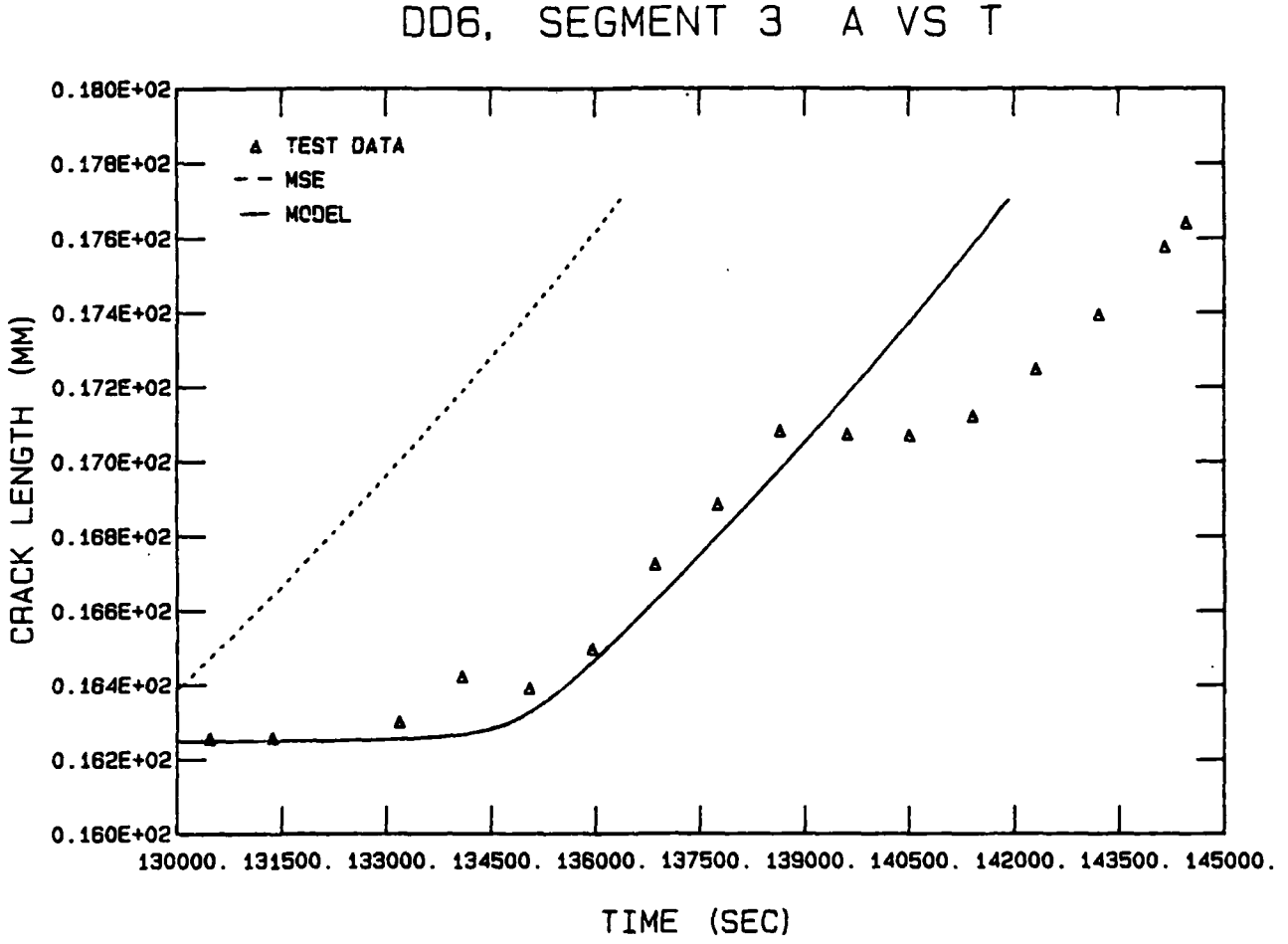
DD6, SEGMENT 3 A VS T
TEST DATA
MSE
MODEL
CRACK LENGTH (MM)
0.180E+02
0.178E+02
0.176E+02
0.174E+02
0.172E+02
0.170E+02
0.168E+02
0.166E+02
0.164E+02
0.162E+02
0.160E+02
130000. 131500. 133000. 134500. 136000. 137500. 139000. 140500. 142000. 143500. 145000.
TIME (SEC)

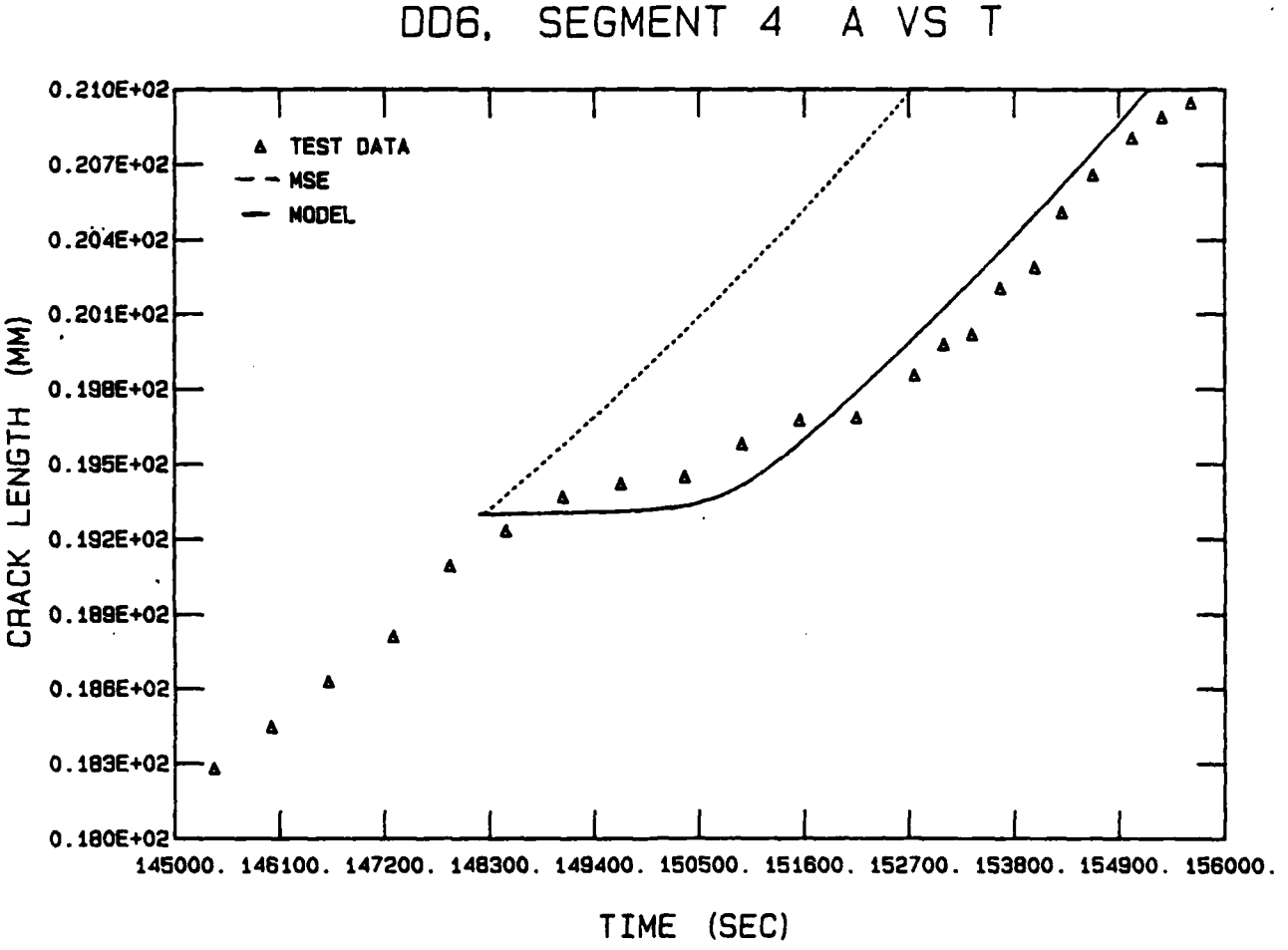
DD6, SEGMENT 4 A VS T
TEST DATA
MSE
MODEL
CRACK LENGTH (MM)
0.210E+02
0.207E+02
0.204E+02
0.201E+02
0.198E+02
0.195E+02
0.192E+02
0.189E+02
0.186E+02
0.183E+02
0.180E+02
145000. 146100. 147200. 148300. 149400. 150500. 151600. 152700. 153800. 154900. 156000.
TIME (SEC)

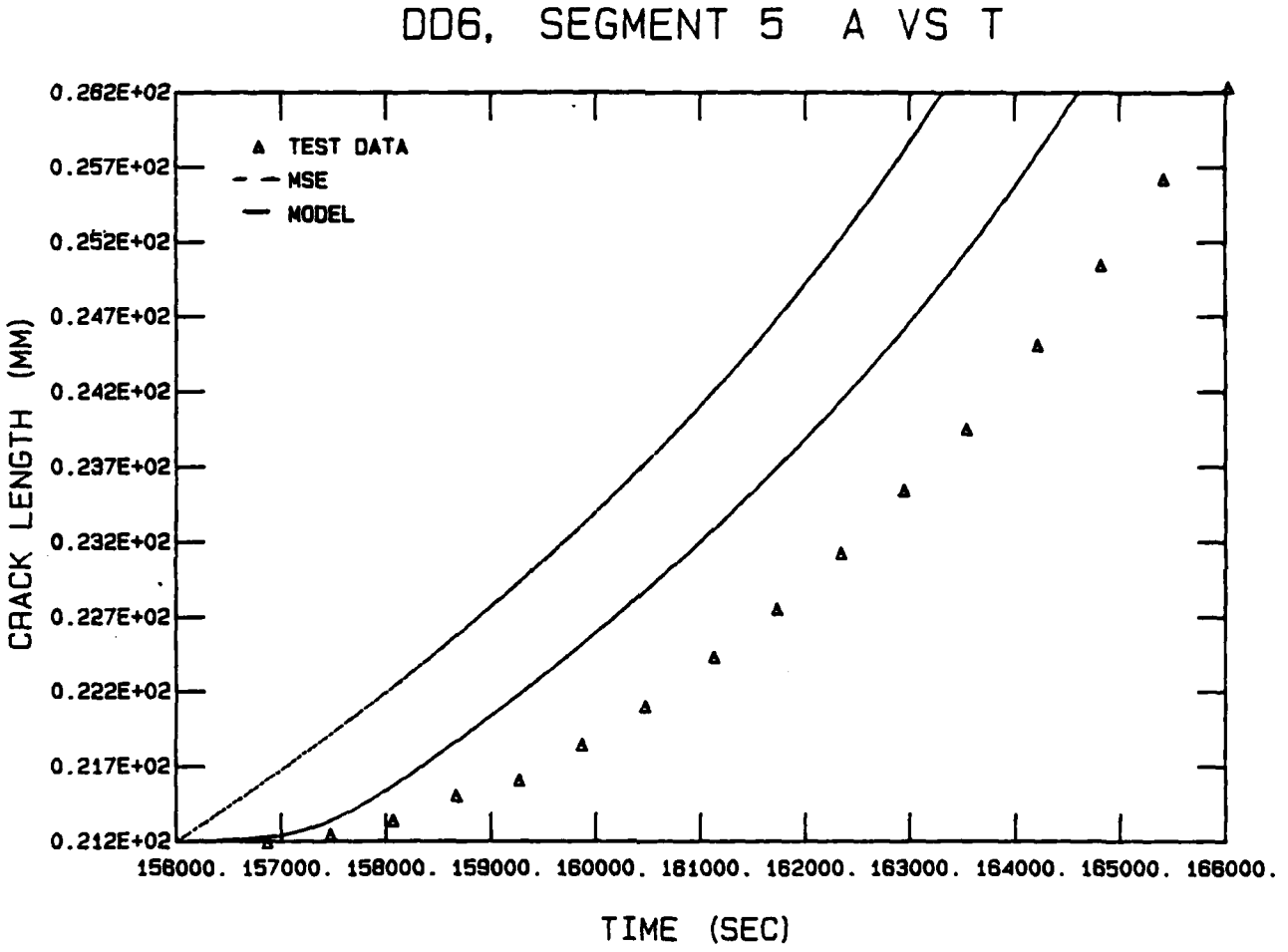
DD6, SEGMENT 5 A VS T
TEST DATA
MSE
MODEL
CRACK LENGTH (MM)
0.262E+02
0.257E+02
0.252E+02
0.247E+02
0.242E+02
0.237E+02
0.232E+02
0.227E+02
0.222E+02
0.217E+02
0.212E+02
156000. 157000. 158000. 159000. 160000. 161000. 162000. 163000. 164000. 165000. 166000.
TIME (SEC)

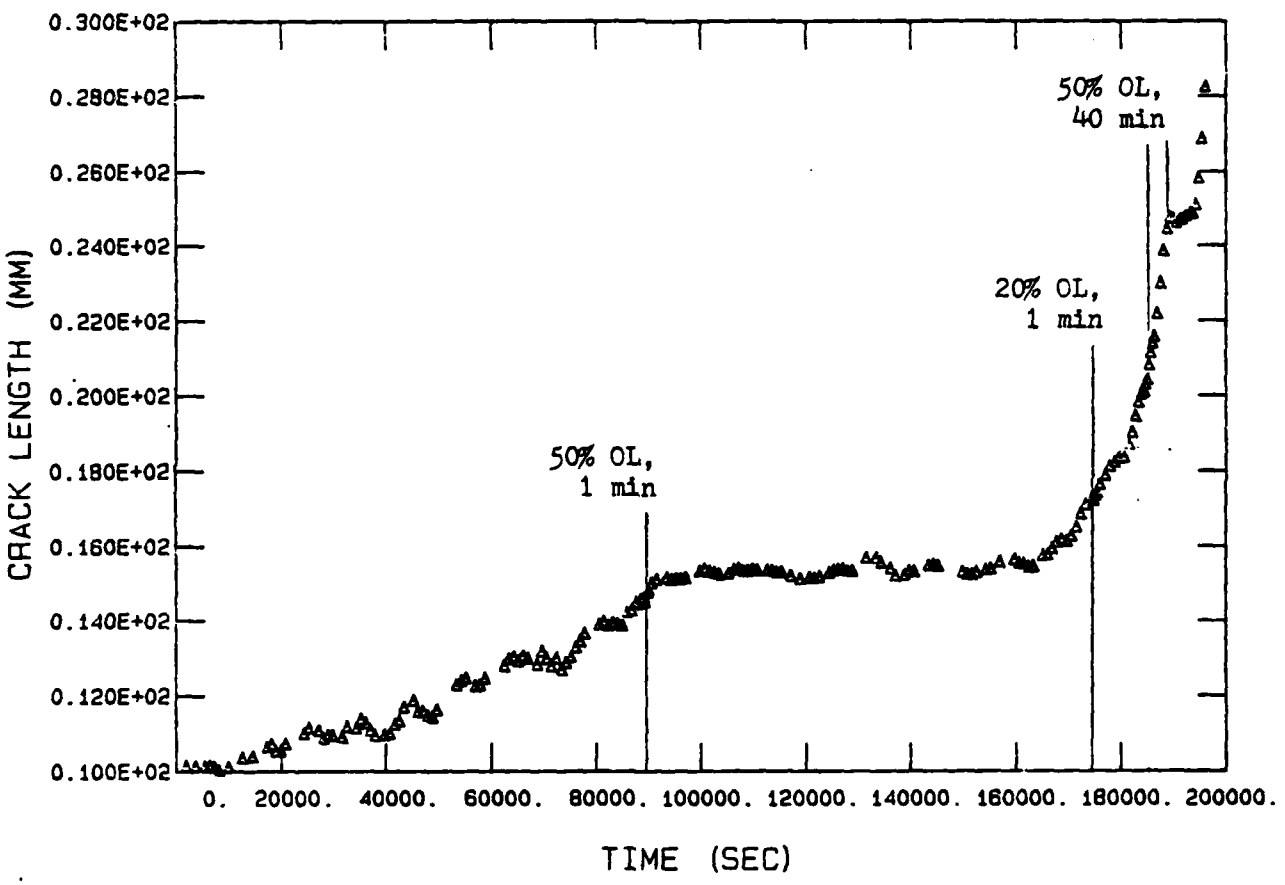
IN 718 (84-497, DD8) A VS T
CRACK LENGTH (MM)
0.300E+02
0.280E+02
0.260E+02
0.240E+02
0.220E+02
0.200E+02
0.180E+02
0.160E+02
0.140E+02
0.120E+02
0.100E+02
50% OL,
40 min
20% OL,
1 min
50% OL,
1 min
0. 20000. 40000. 60000. 80000. 100000. 120000. 140000. 160000. 180000. 200000.
TIME (SEC)

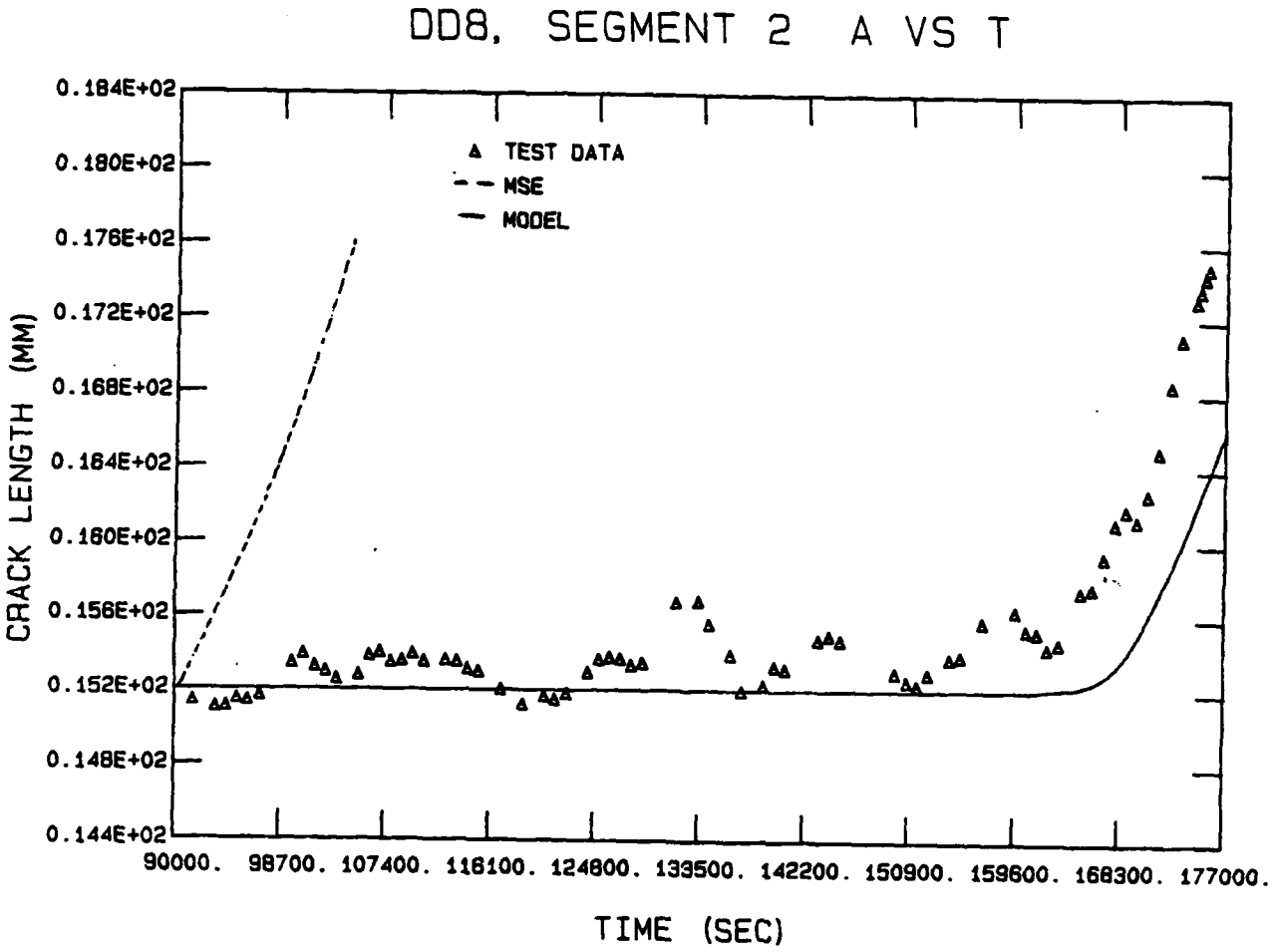
DD8, SEGMENT 2 A VS T
TEST DATA
MSE
MODEL
CRACK LENGTH (MM)
0.184E+02
0.180E+02
0.176E+02
0.172E+02
0.168E+02
0.164E+02
0.160E+02
0.156E+02
0.152E+02
0.148E+02
0.144E+02
90000. 98700. 107400. 116100. 124800. 133500. 142200. 150900. 159600. 168300. 177000.
TIME (SEC)

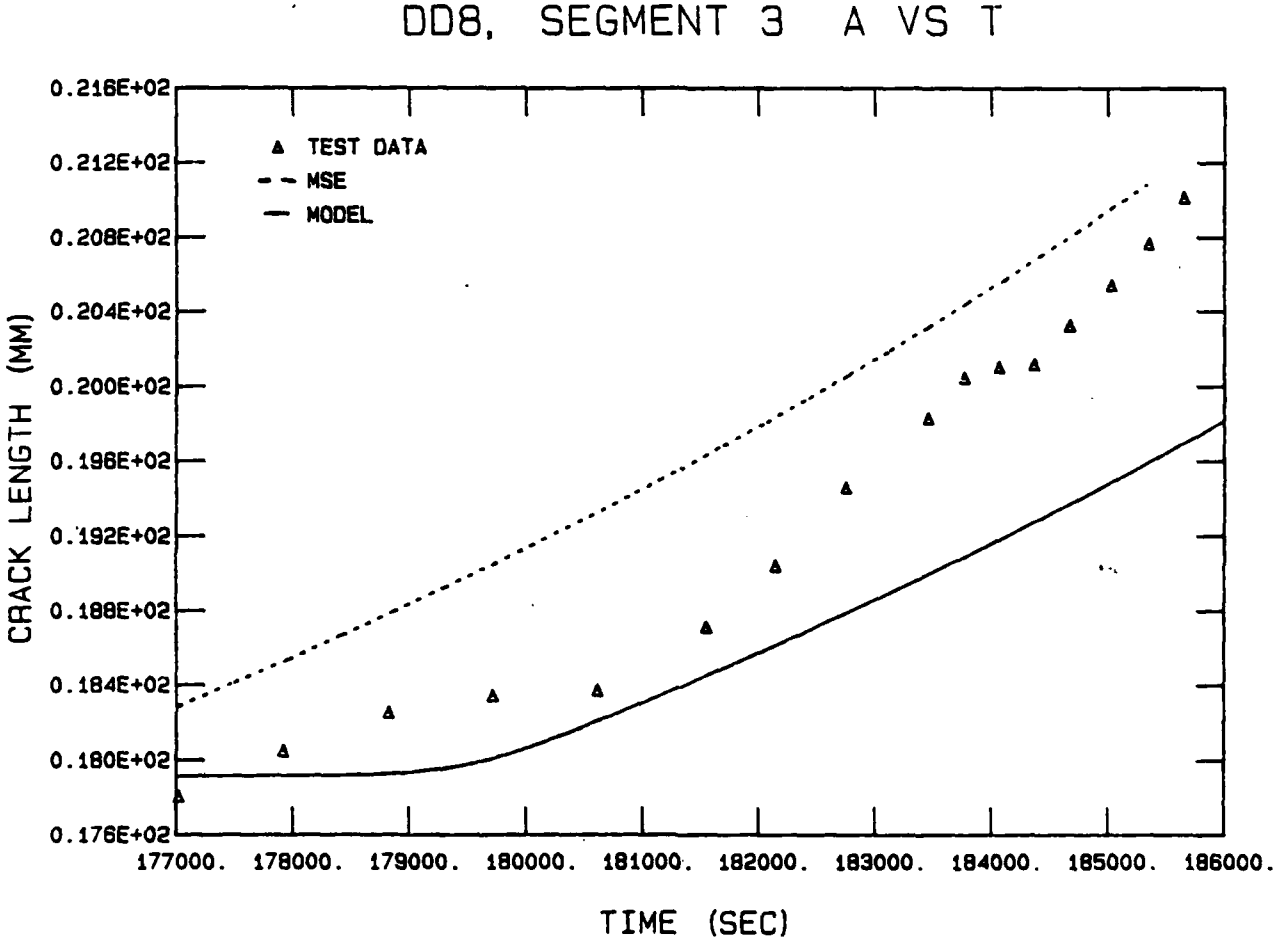
DD8, SEGMENT 3 A VS T
TEST DATA
MSE
MODEL
CRACK LENGTH (MM)
0.216E+02
0.212E+02
0.208E+02
0.204E+02
0.200E+02
0.196E+02
0.192E+02
0.188E+02
0.184E+02
0.180E+02
0.176E+02
177000.
178000.
179000.
180000.
181000.
182000.
183000.
184000.
185000.
186000.
TIME (SEC)

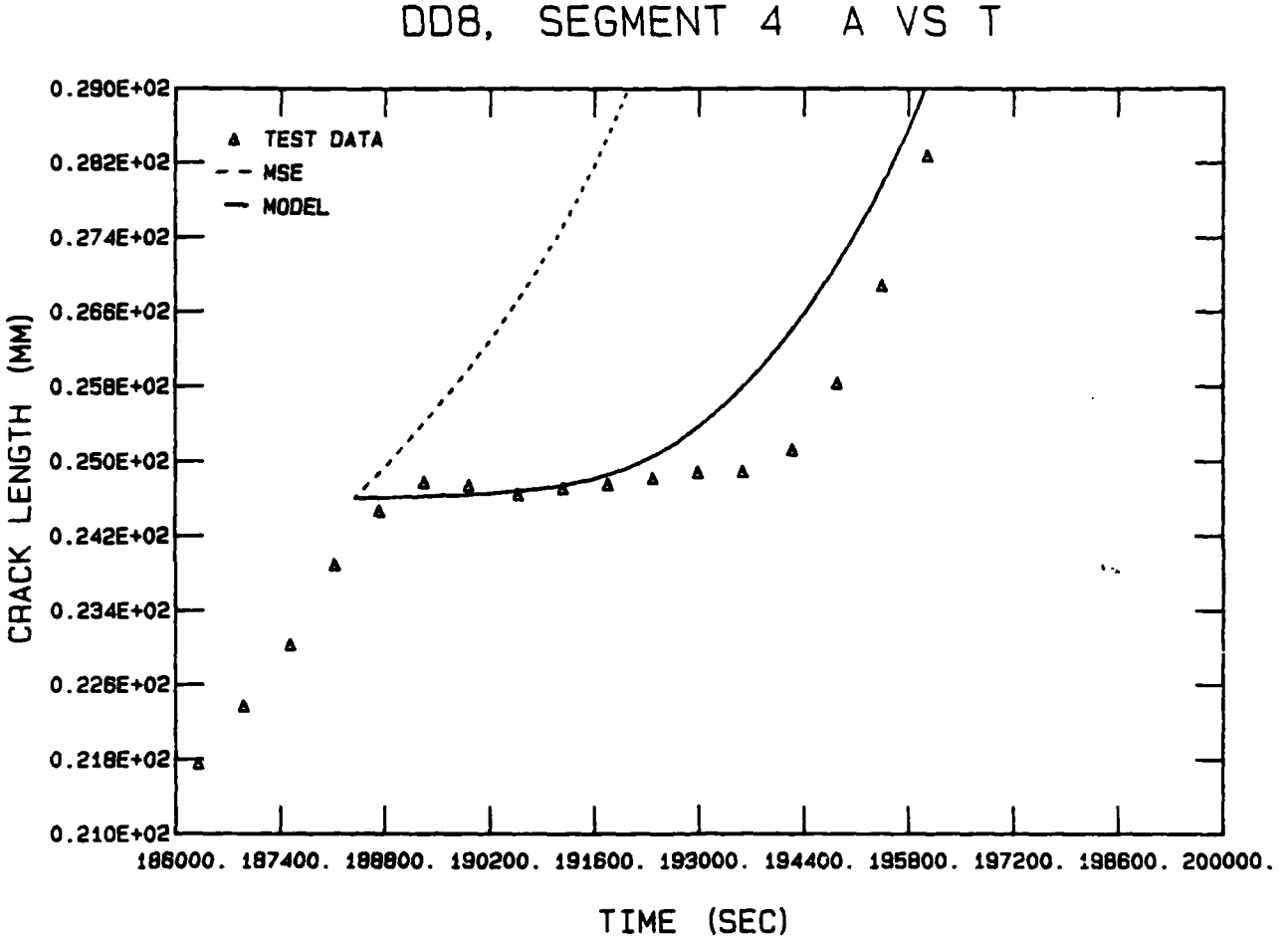
DD8, SEGMENT 4 A VS T
0.290E+02
0.282E+02
0.274E+02
0.266E+02
0.258E+02
0.250E+02
0.242E+02
0.234E+02
0.226E+02
0.218E+02
0.210E+02
TEST DATA
MSE
MODEL
CRACK LENGTH (MM)
186000. 187400. 188800. 190200. 191600. 193000. 194400. 195800. 197200. 198600. 200000.
TIME (SEC)

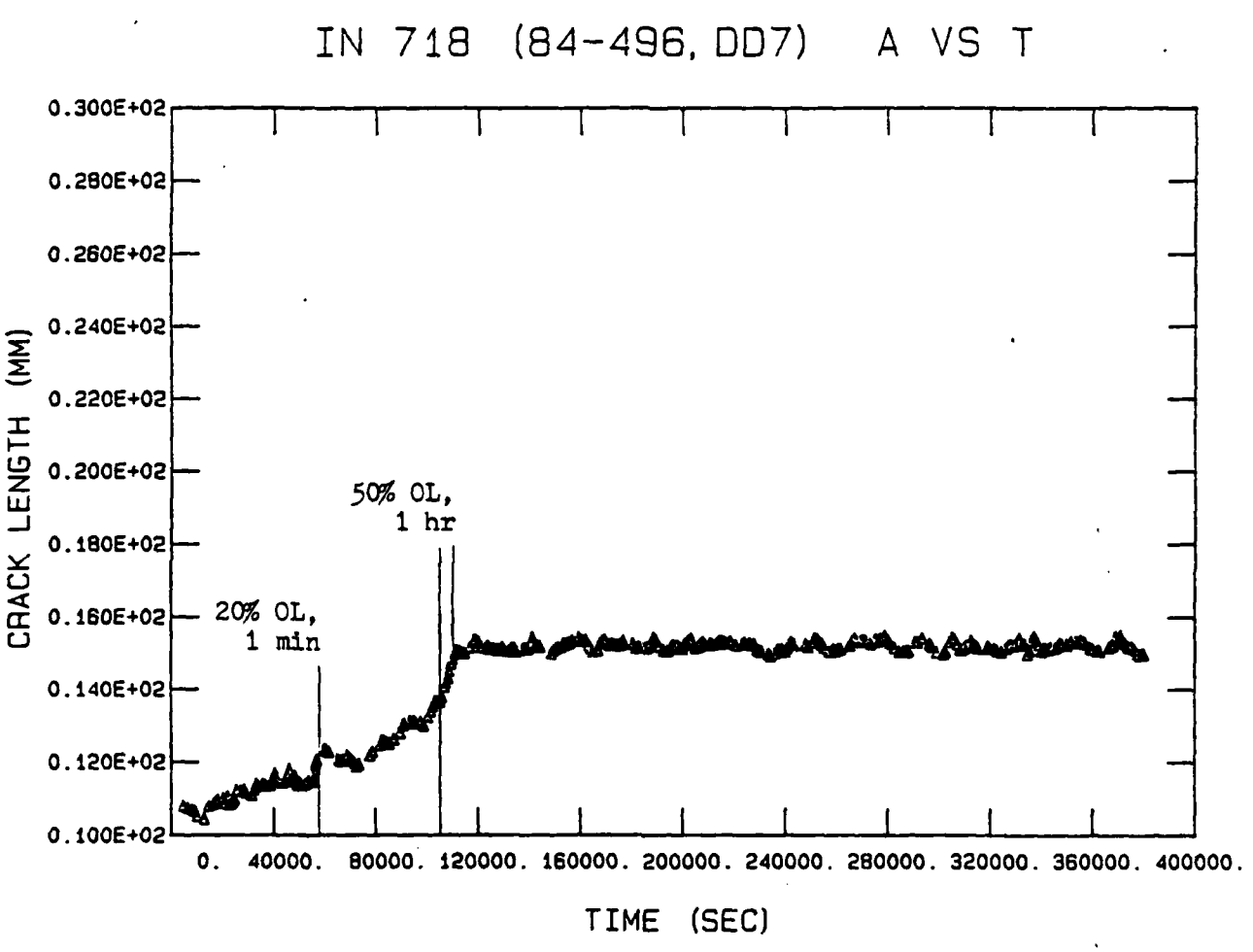
IN 718 (84-496, DD7) A VS T
CRACK LENGTH (MM)
0.300E+02
0.280E+02
0.260E+02
0.240E+02
0.220E+02
0.200E+02
0.180E+02
0.160E+02
0.140E+02
0.120E+02
0.100E+02
20% OL,
1 min
50% OL,
1 hr
0. 40000. 80000. 120000. 160000. 200000. 240000. 280000. 320000. 360000. 400000.
TIME (SEC)

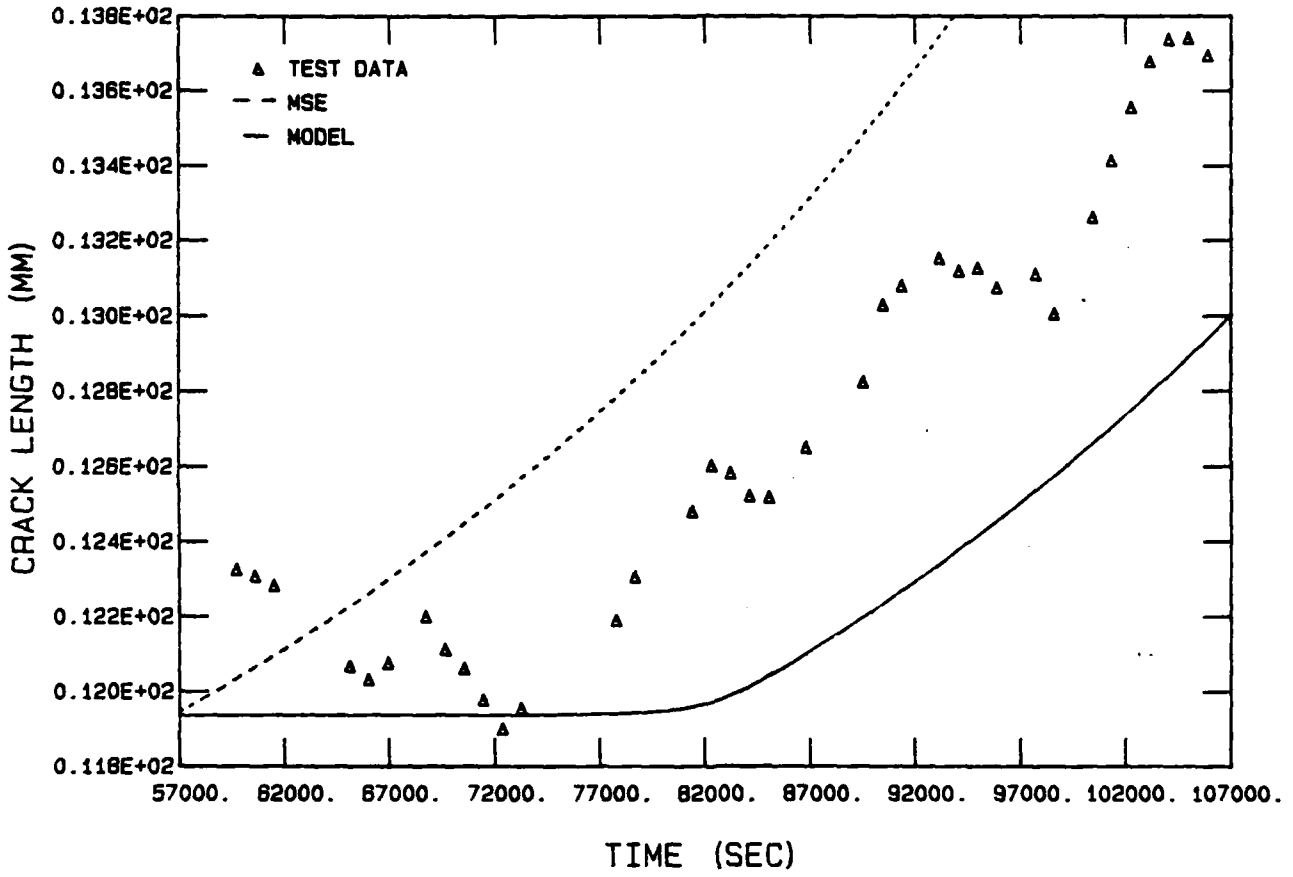
DD7, SEGMENT 2 A VS T
TEST DATA
MSE
MODEL
CRACK LENGTH (MM)
0.138E+02
0.136E+02
0.134E+02
0.132E+02
0.130E+02
0.128E+02
0.126E+02
0.124E+02
0.122E+02
0.120E+02
0.118E+02
57000. 62000. 67000. 72000. 77000. 82000. 87000. 92000. 97000. 102000. 107000.
TIME (SEC)

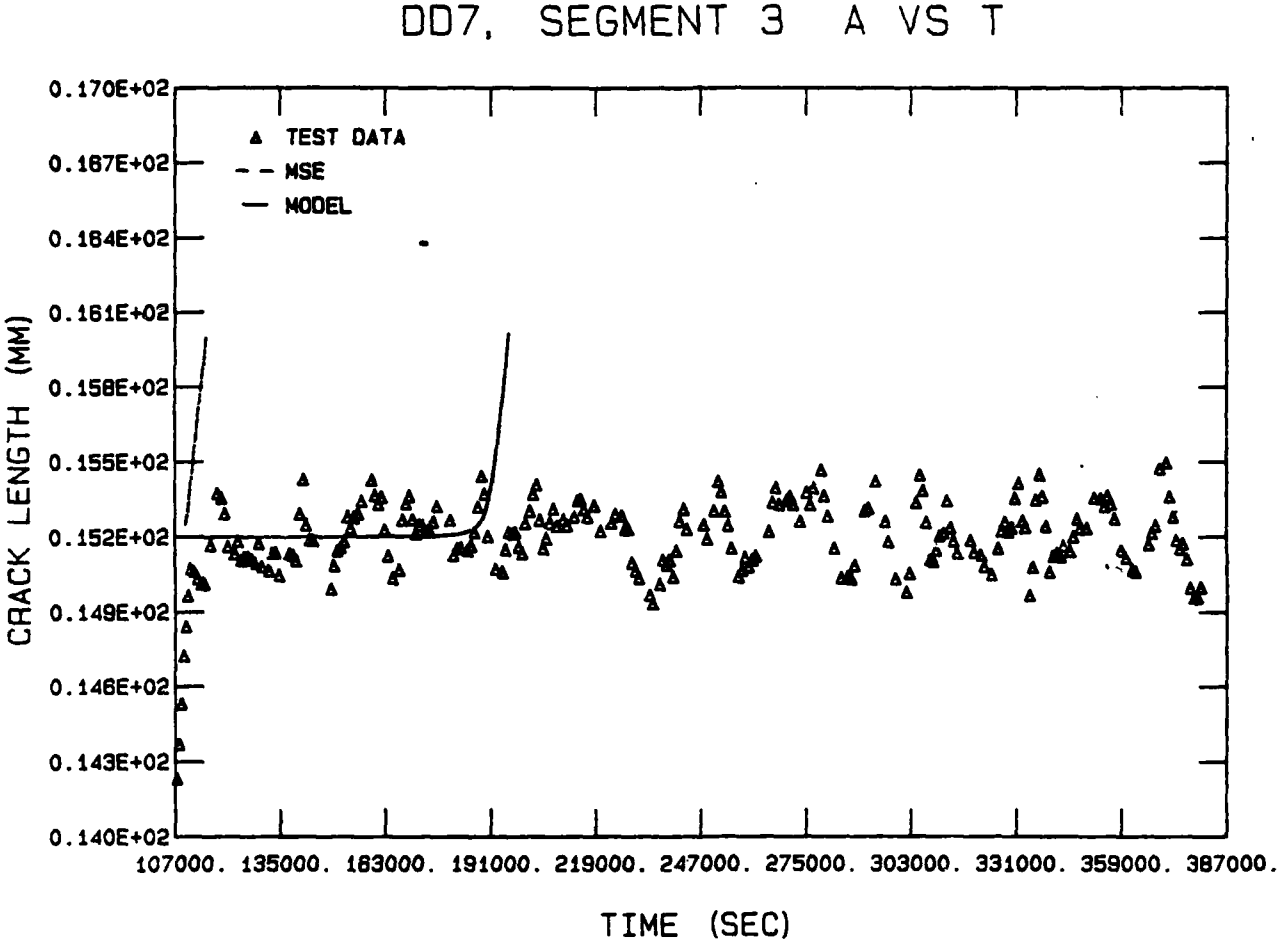
DD7, SEGMENT 3 A VS T
TEST DATA
MSE
MODEL
CRACK LENGTH (MM)
0.170E+02
0.167E+02
0.164E+02
0.161E+02
0.158E+02
0.155E+02
0.152E+02
0.149E+02
0.146E+02
0.143E+02
0.140E+02
107000. 135000. 163000. 191000. 219000. 247000. 275000. 303000. 331000. 359000. 387000.
TIME (SEC)

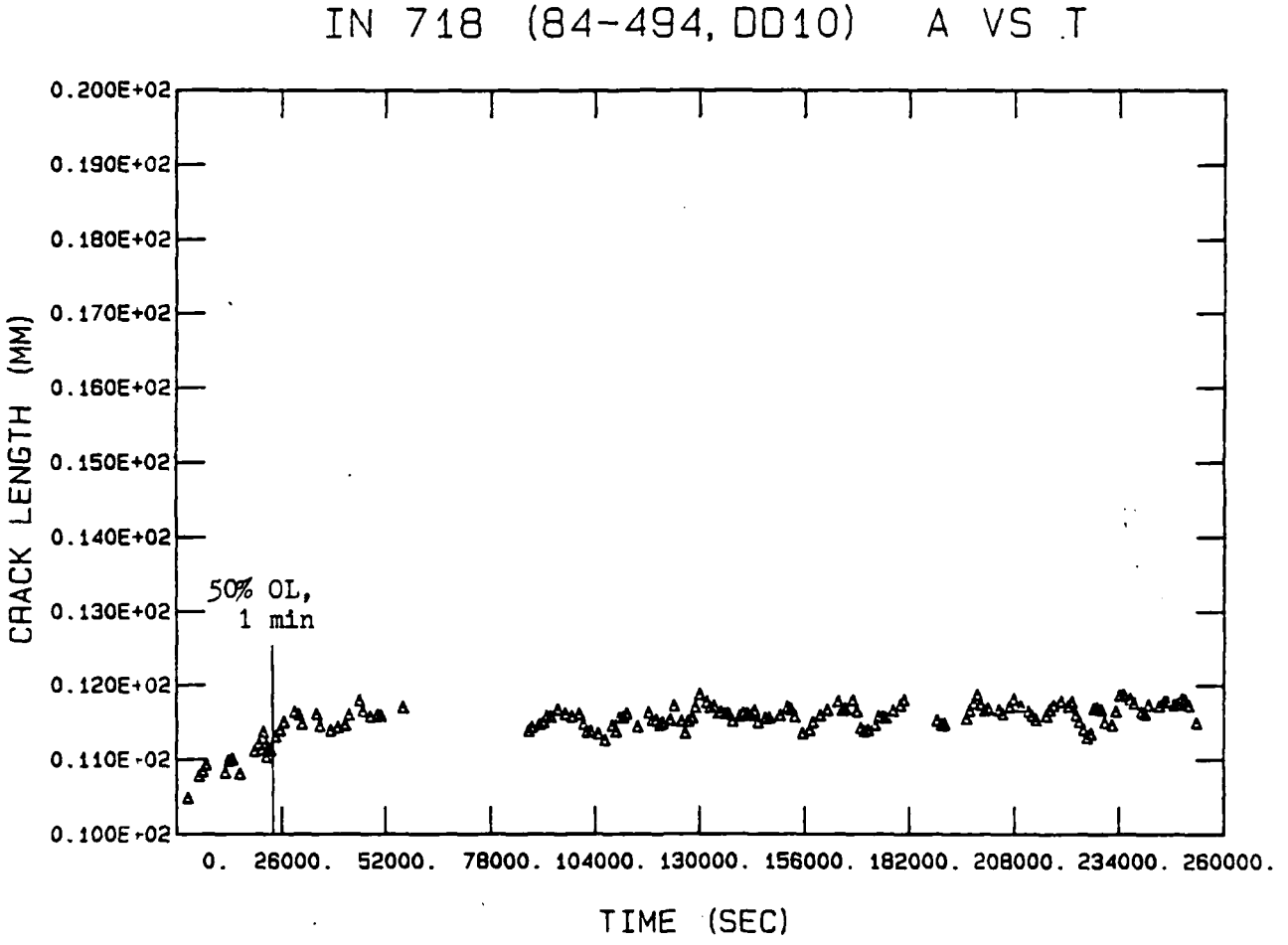
IN 718 (84-494, DD10) A VS T
0.200E+02
0.190E+02
0.180E+02
0.170E+02
0.160E+02
0.150E+02
0.140E+02
0.130E+02
0.120E+02
0.110E+02
0.100E+02
CRACK LENGTH (MM)
50% OL,
1 min
0. 26000. 52000. 78000. 104000. 130000. 156000. 182000. 208000. 234000. 260000.
TIME (SEC)

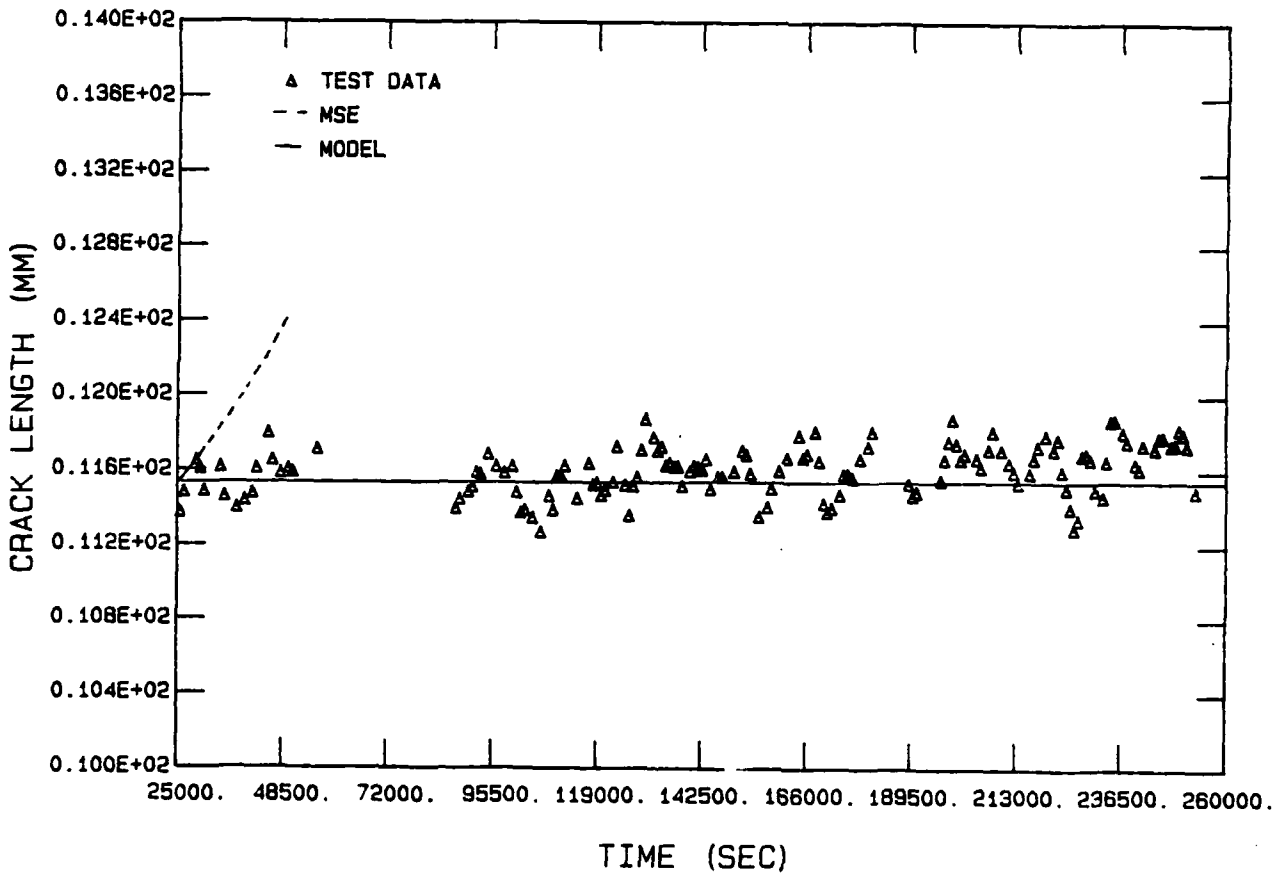
DD10, SEGMENT 2 A VS T
0.140E+02
0.136E+02
0.132E+02
0.128E+02
0.124E+02
0.120E+02
0.116E+02
0.112E+02
0.108E+02
0.104E+02
0.100E+02
CRACK LENGTH (MM)
TEST DATA
MSE
MODEL
25000. 48500. 72000. 95500. 119000. 142500. 166000. 189500. 213000. 236500. 260000.
TIME (SEC)

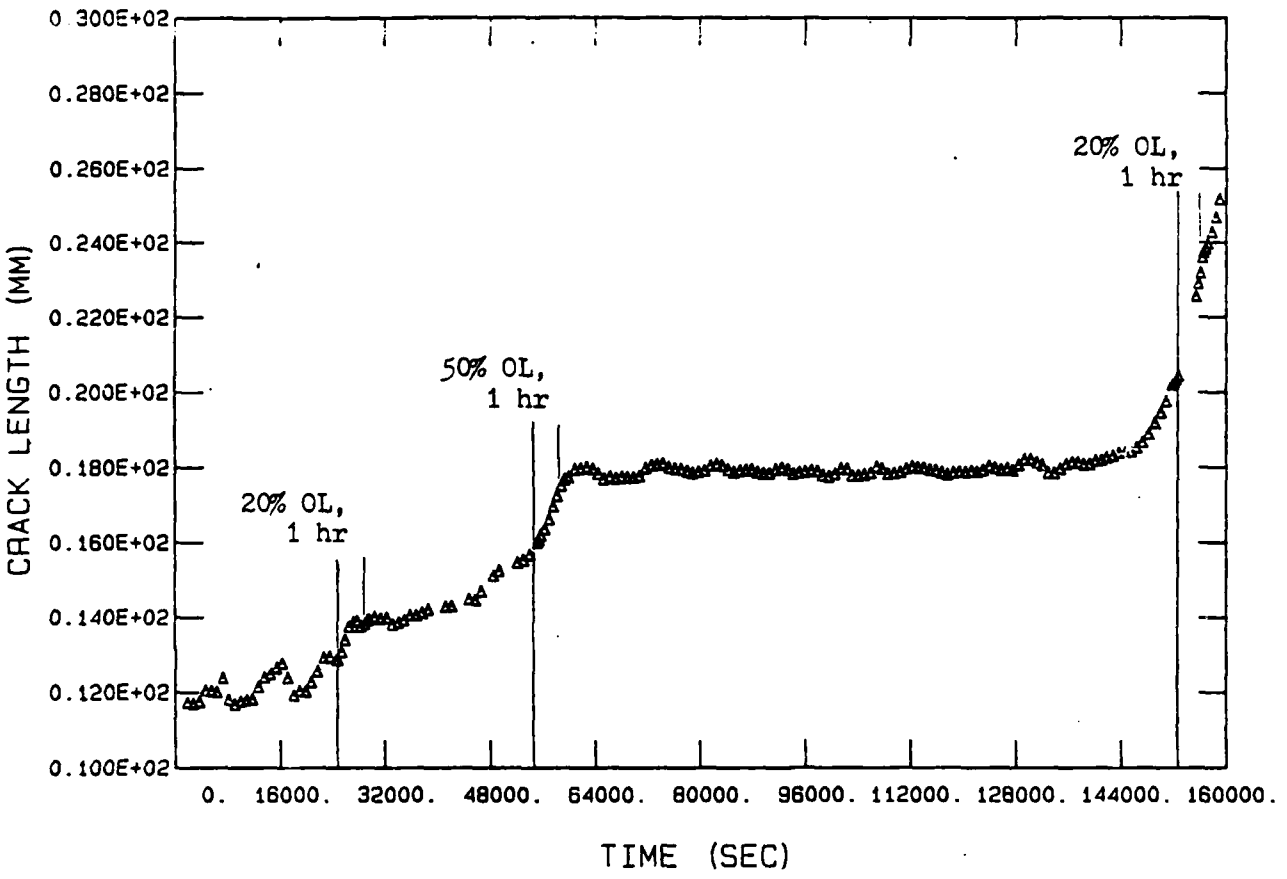
IN 718 (84-494, DD10) A VS T
0.300E+02
0.280E+02
0.260E+02
0.240E+02
0.220E+02
0.200E+02
0.180E+02
0.160E+02
0.140E+02
0.120E+02
0.100E+02
CRACK LENGTH (MM)
20% OL, 1 hr
50% OL, 1 hr
20% OL, 1 hr
0. 16000. 32000. 48000. 64000. 80000. 96000. 112000. 128000. 144000. 160000.
TIME (SEC)

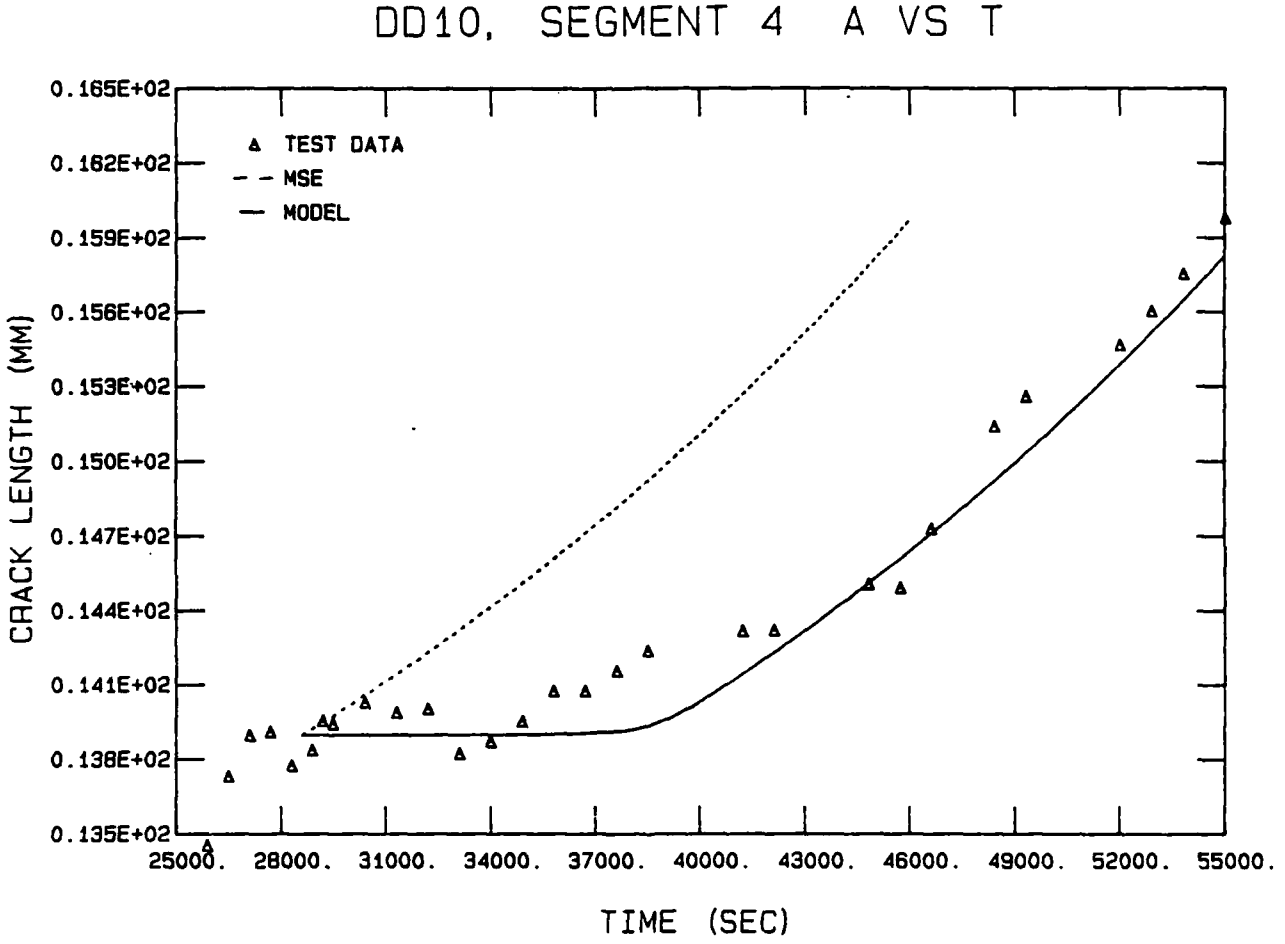
DD10, SEGMENT 4 A VS T
TEST DATA
MSE
MODEL
CRACK LENGTH (MM)
0.165E+02
0.162E+02
0.159E+02
0.156E+02
0.153E+02
0.150E+02
0.147E+02
0.144E+02
0.141E+02
0.138E+02
0.135E+02
25000.
28000.
31000.
34000.
37000.
40000.
43000.
46000.
49000.
52000.
55000.
TIME (SEC)

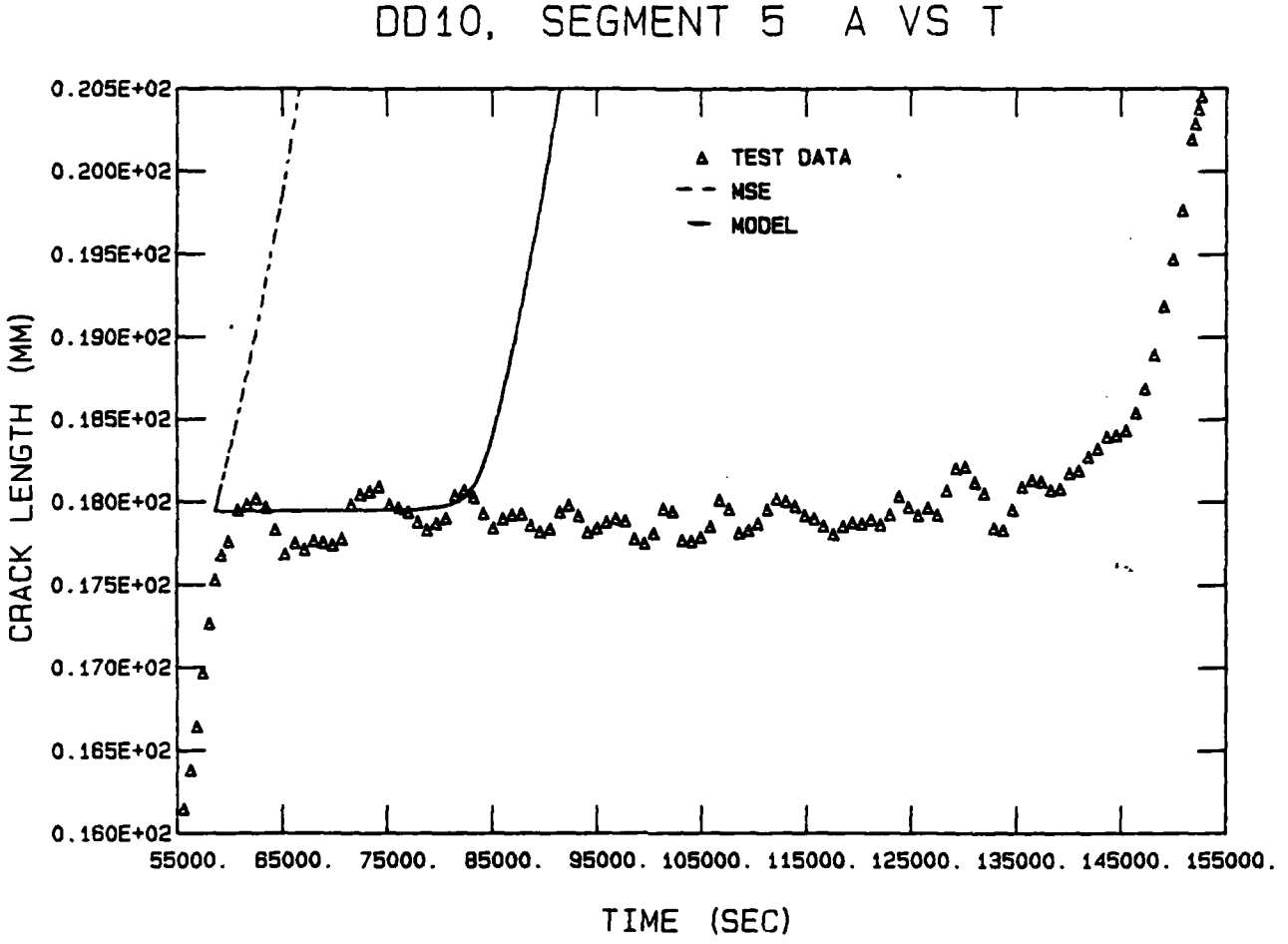
DD10, SEGMENT 5 A VS T
0.205E+02
0.200E+02
0.195E+02
0.190E+02
0.185E+02
0.180E+02
0.175E+02
0.170E+02
0.165E+02
0.160E+02
CRACK LENGTH (MM)
TEST DATA
MSE
MODEL
55000. 65000. 75000. 85000. 95000. 105000. 115000. 125000. 135000. 145000. 155000.
TIME (SEC)

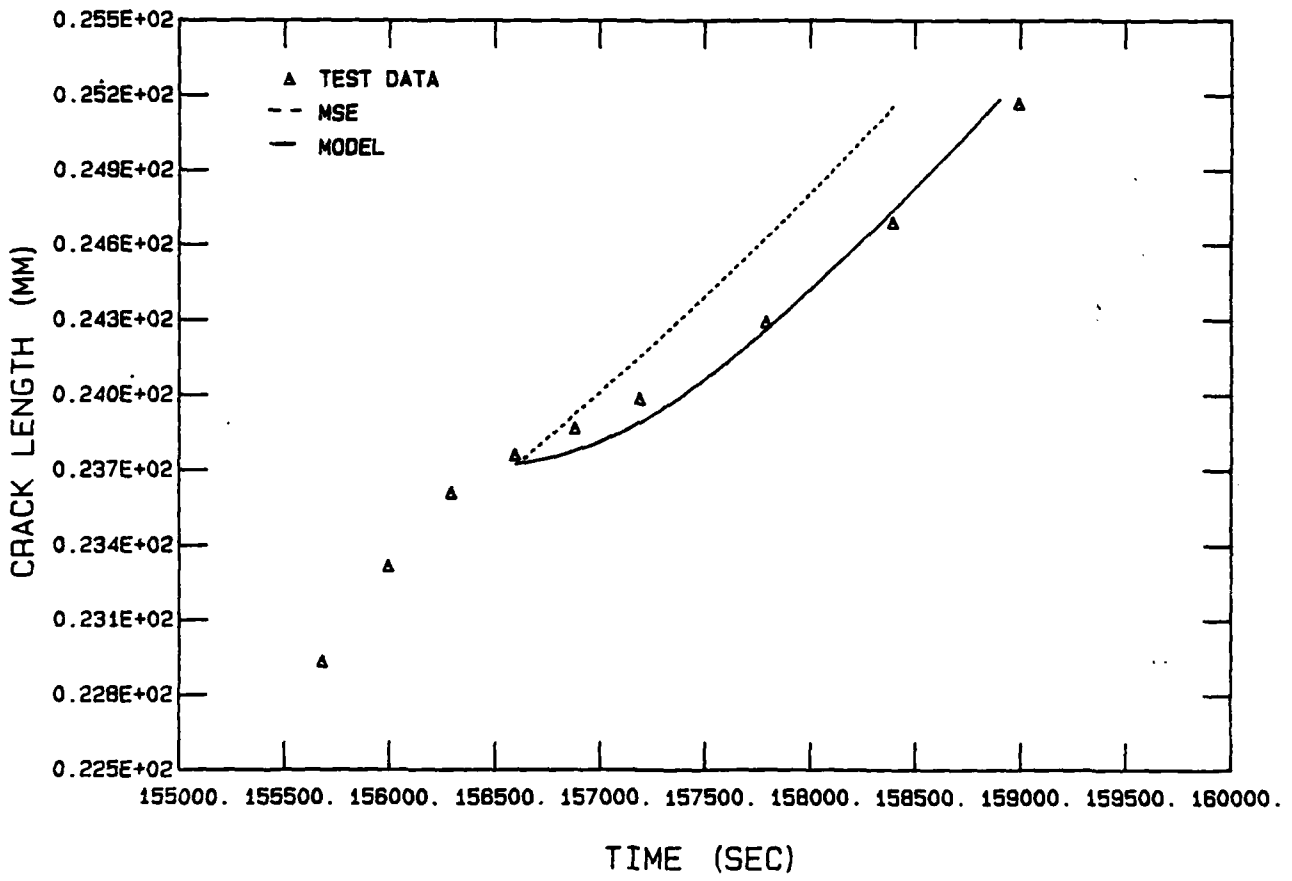
DD10, SEGMENT 6 A VS T
TEST DATA
MSE
MODEL
CRACK LENGTH (MM)
0.255E+02
0.252E+02
0.249E+02
0.246E+02
0.243E+02
0.240E+02
0.237E+02
0.234E+02
0.231E+02
0.228E+02
0.225E+02
155000. 155500. 156000. 156500. 157000. 157500. 158000. 158500. 159000. 159500. 160000.
TIME (SEC)

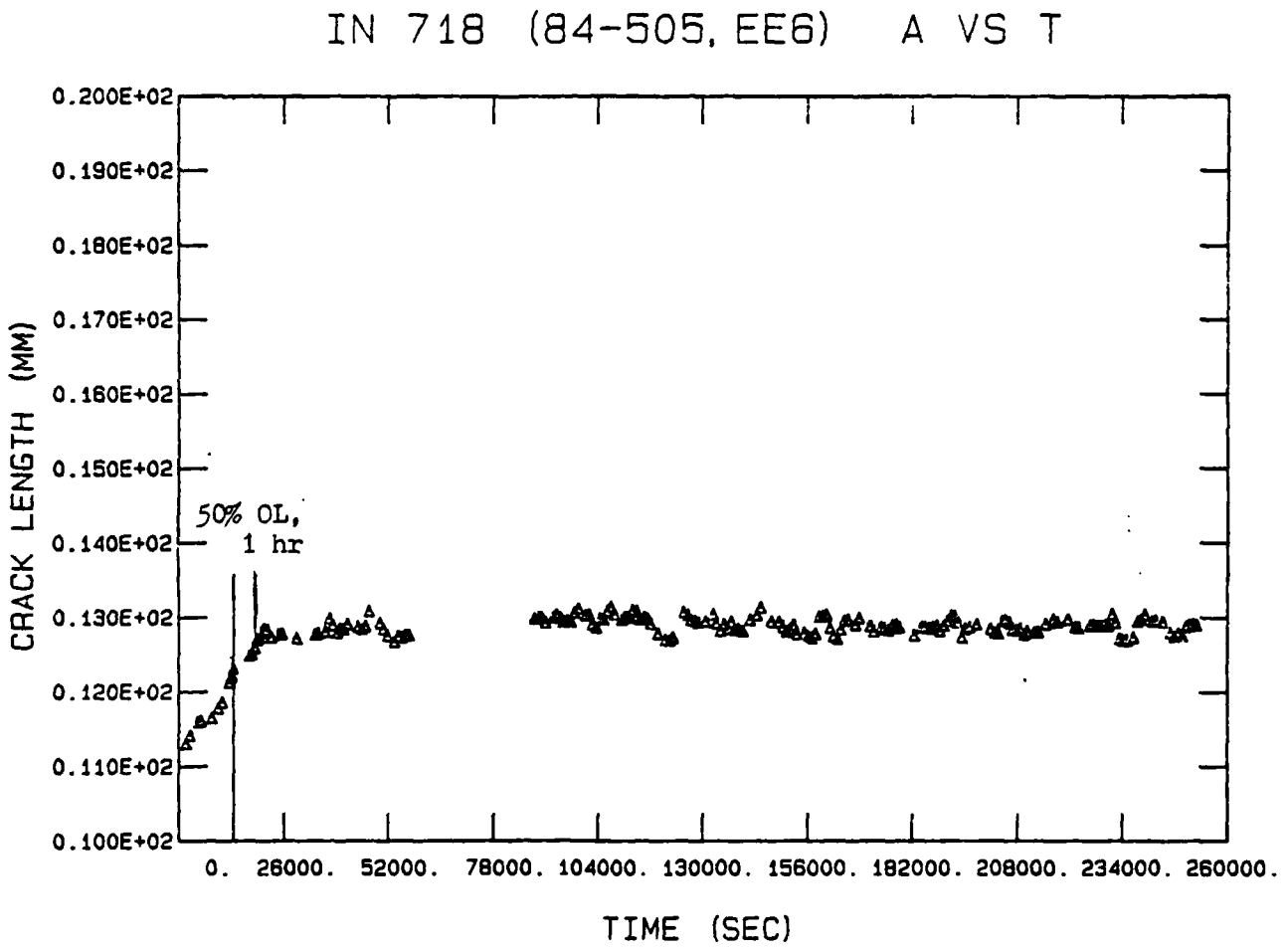
IN 718 (84-505, EE6) A VS T
0.200E+02
0.190E+02
0.180E+02
0.170E+02
0.160E+02
0.150E+02
0.140E+02
0.130E+02
0.120E+02
0.110E+02
0.100E+02
CRACK LENGTH (MM)
50% OL,
1 hr
0. 26000. 52000. 78000. 104000. 130000. 156000. 182000. 208000. 234000. 260000.
TIME (SEC)

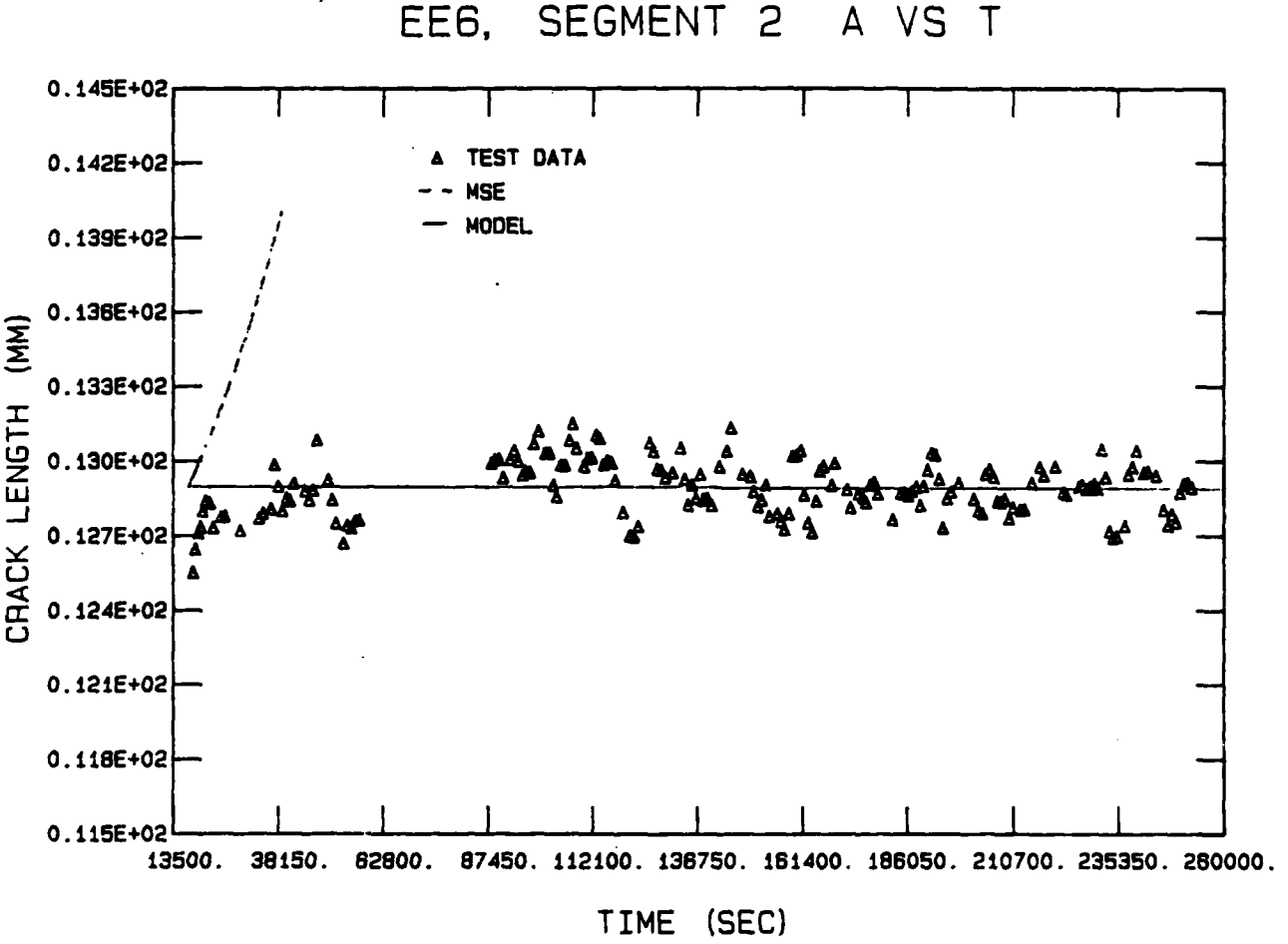
EE6, SEGMENT 2 A VS T
TEST DATA
MSE
MODEL
CRACK LENGTH (MM)
0.145E+02
0.142E+02
0.139E+02
0.136E+02
0.133E+02
0.130E+02
0.127E+02
0.124E+02
0.121E+02
0.118E+02
0.115E+02
13500. 38150. 62800. 87450. 112100. 136750. 161400. 186050. 210700. 235350. 260000.
TIME (SEC)

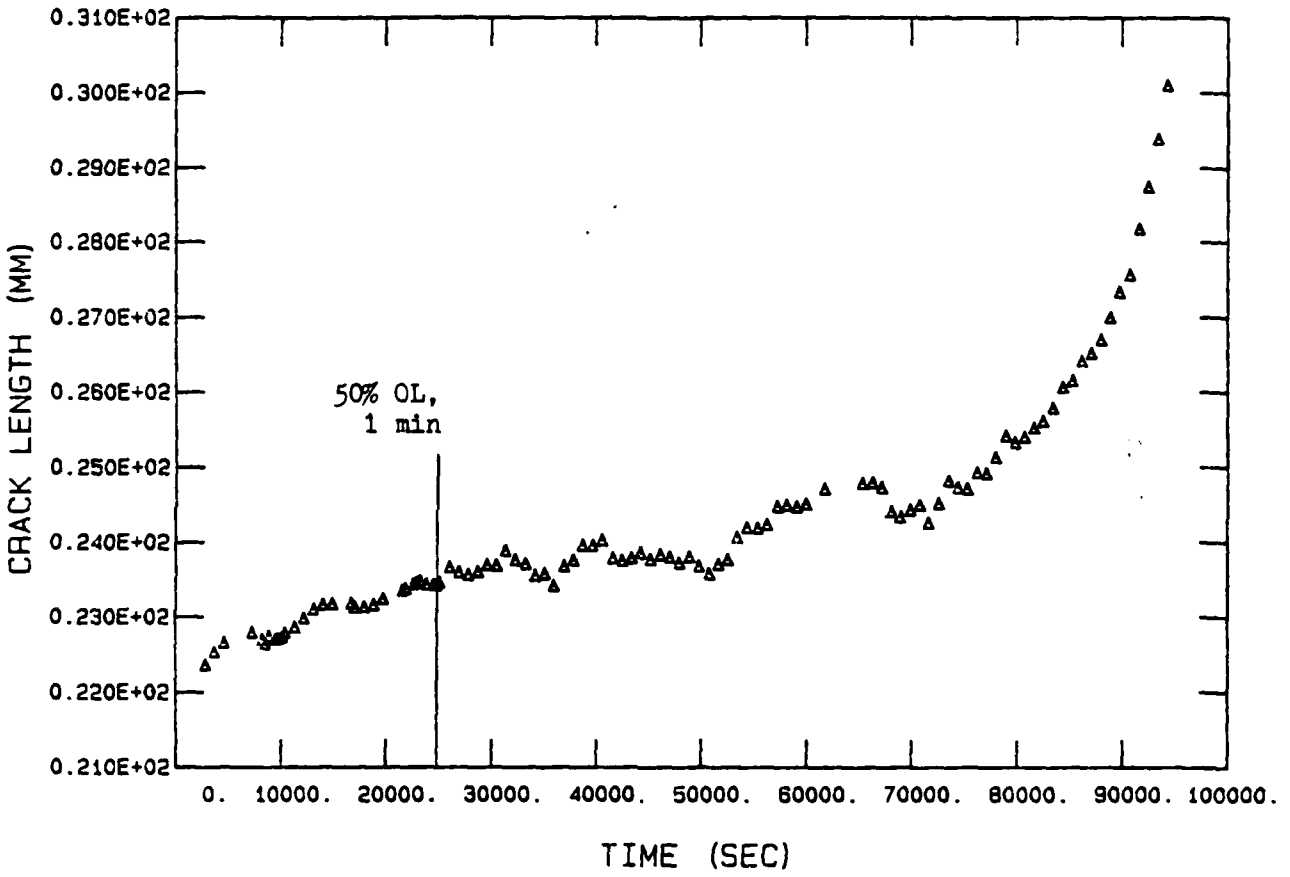
IN 718 (84-505, EE6) A VS T
0.310E+02
0.300E+02
0.290E+02
0.280E+02
0.270E+02
0.260E+02
0.250E+02
0.240E+02
0.230E+02
0.220E+02
0.210E+02
CRACK LENGTH (MM)
50% OL,
1 min
0. 10000. 20000. 30000. 40000. 50000. 60000. 70000. 80000. 90000. 100000.
TIME (SEC)

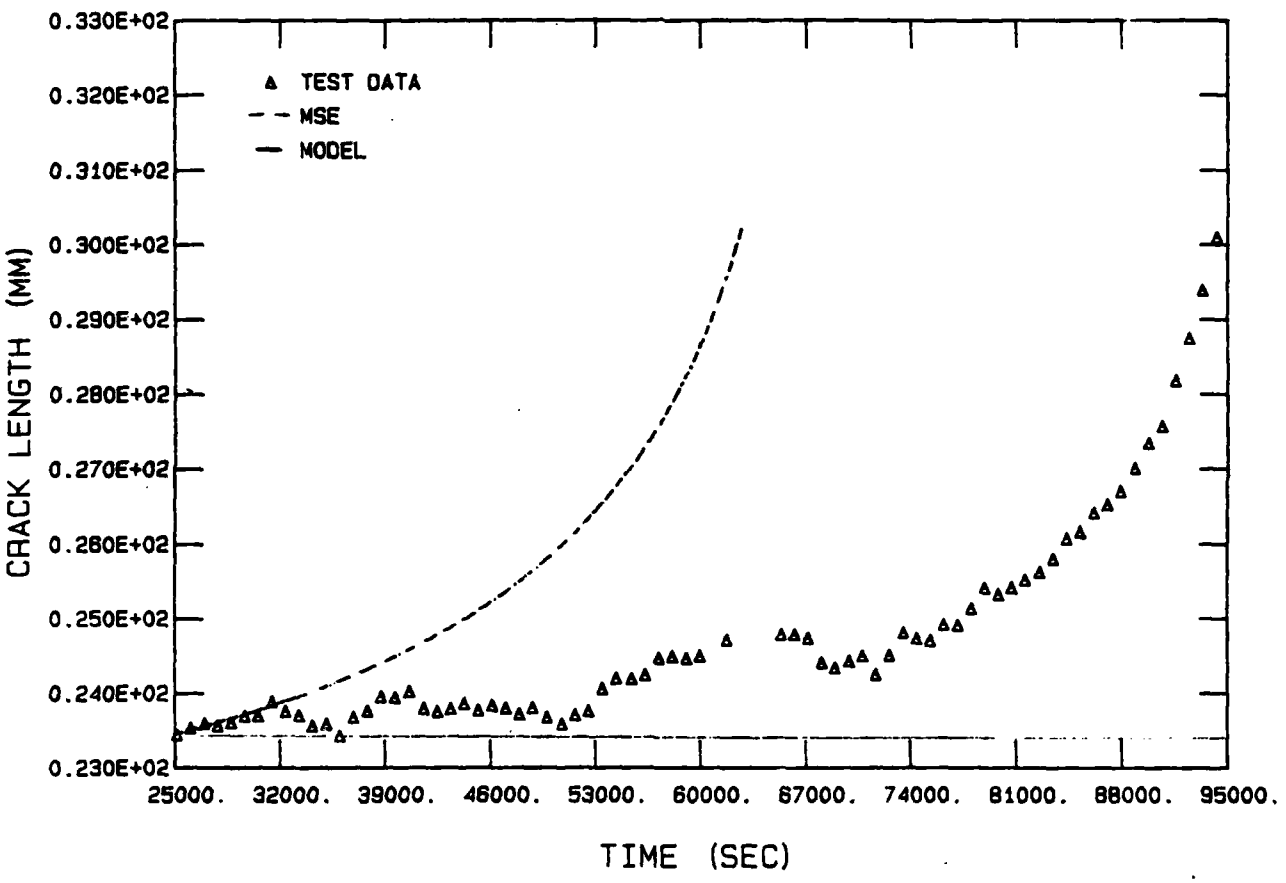
EE6, SEGMENT 4 A VS T
TEST DATA
MSE
MODEL
CRACK LENGTH (MM)
0.330E+02
0.320E+02
0.310E+02
0.300E+02
0.290E+02
0.280E+02
0.270E+02
0.260E+02
0.250E+02
0.240E+02
0.230E+02
25000.
32000.
39000.
46000.
53000.
60000.
67000.
74000.
81000.
88000.
95000.
TIME (SEC)

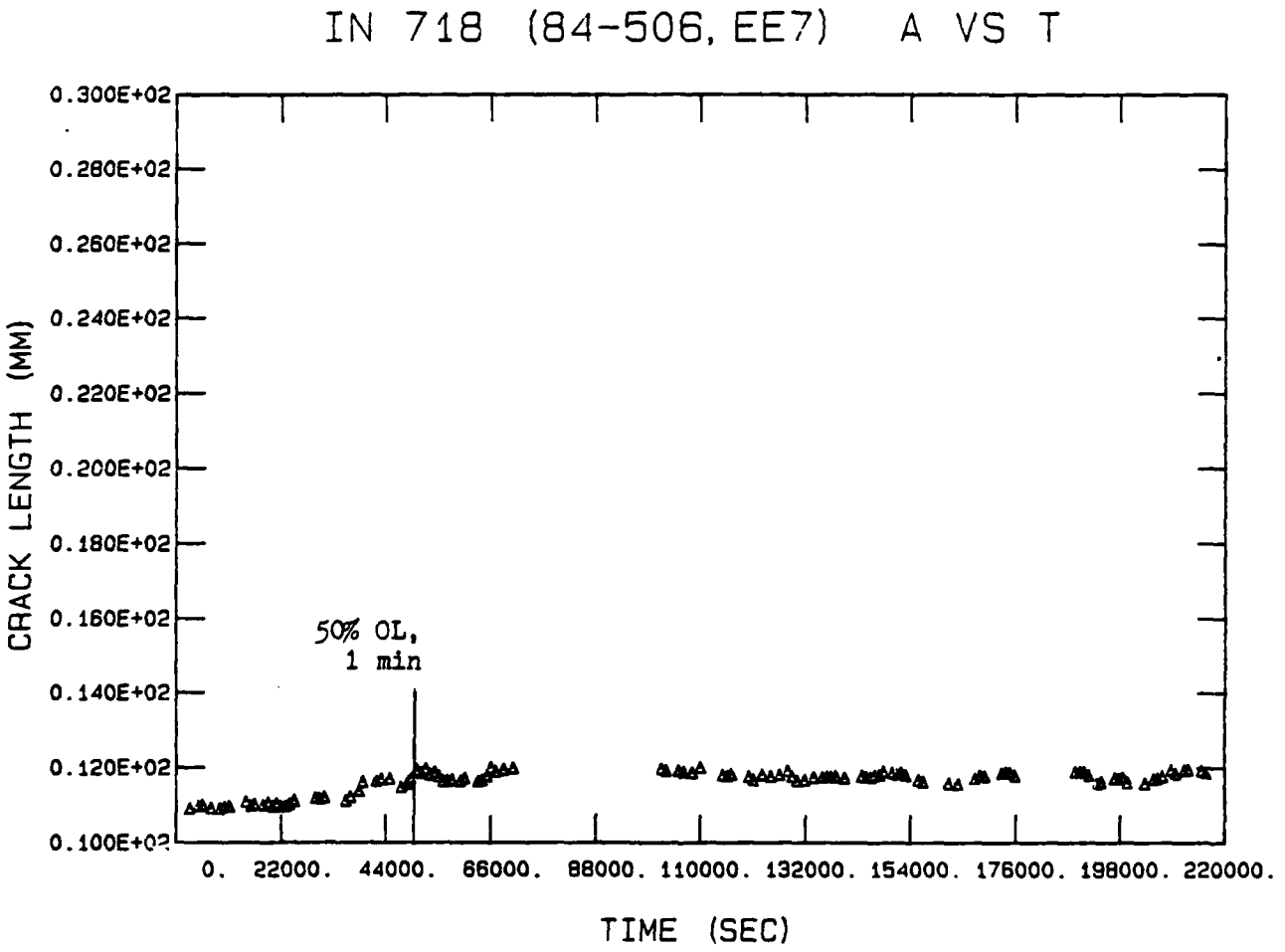
IN 718 (84-506, EE7) A VS T
0.300E+02
0.280E+02
0.260E+02
0.240E+02
0.220E+02
0.200E+02
0.180E+02
0.160E+02
0.140E+02
0.120E+02
0.100E+02
CRACK LENGTH (MM)
50% OL,
1 min
0. 22000. 44000. 66000. 88000. 110000. 132000. 154000. 176000. 198000. 220000.
TIME (SEC)

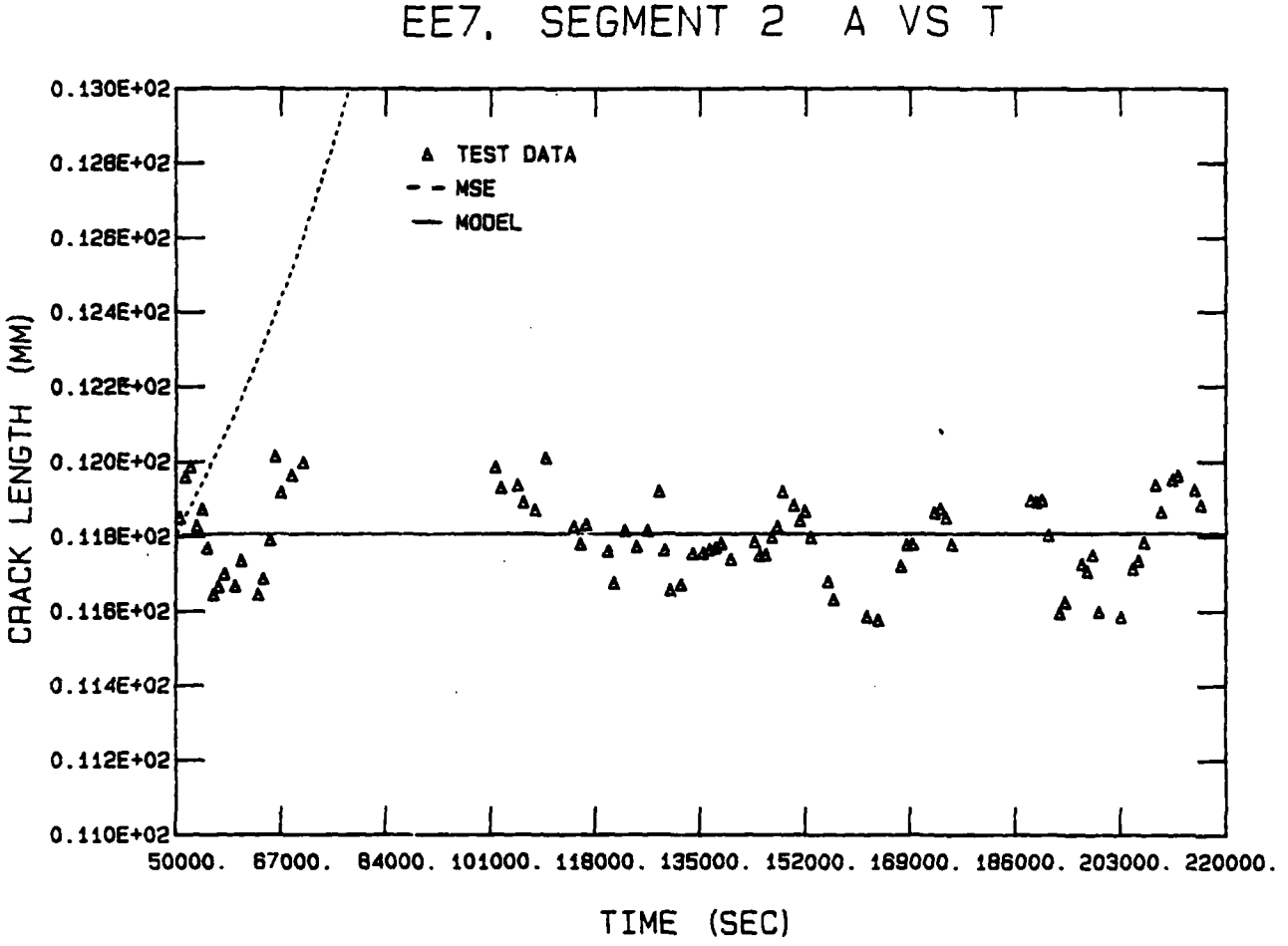
EE7, SEGMENT 2 A VS T
TEST DATA
MSE
MODEL
CRACK LENGTH (MM)
0.130E+02
0.128E+02
0.126E+02
0.124E+02
0.122E+02
0.120E+02
0.118E+02
0.116E+02
0.114E+02
0.112E+02
0.110E+02
50000. 67000. 84000. 101000. 118000. 135000. 152000. 169000. 186000. 203000. 220000.
TIME (SEC)

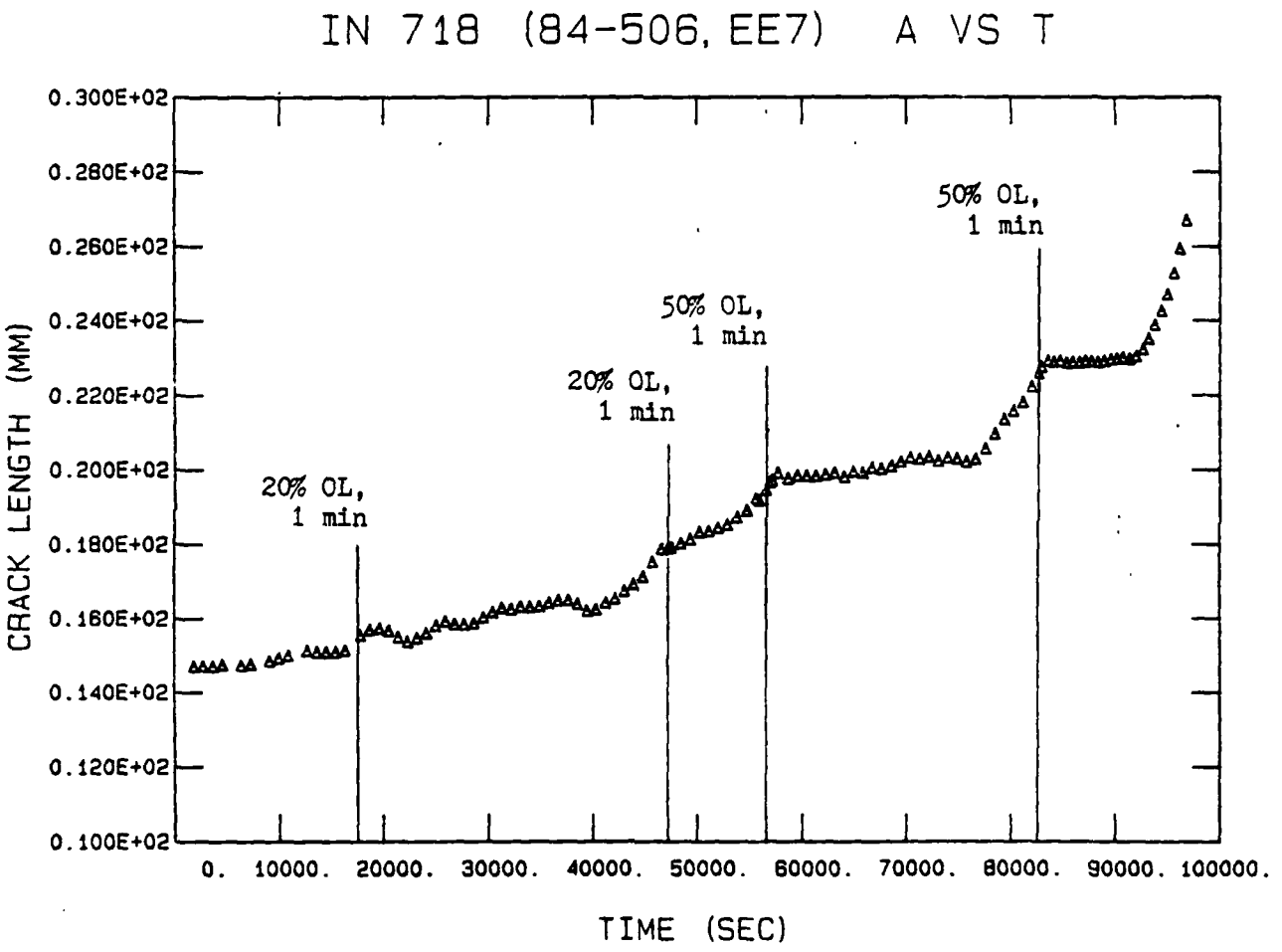
IN 718 (84-506, EE7) A VS T
0.300E+02
0.280E+02
0.260E+02
0.240E+02
0.220E+02
0.200E+02
0.180E+02
0.160E+02
0.140E+02
0.120E+02
0.100E+02
CRACK LENGTH (MM)
20% OL,
1 min
20% OL,
1 min
50% OL,
1 min
50% OL,
1 min
0. 10000. 20000. 30000. 40000. 50000. 60000. 70000. 80000. 90000. 100000.
TIME (SEC)

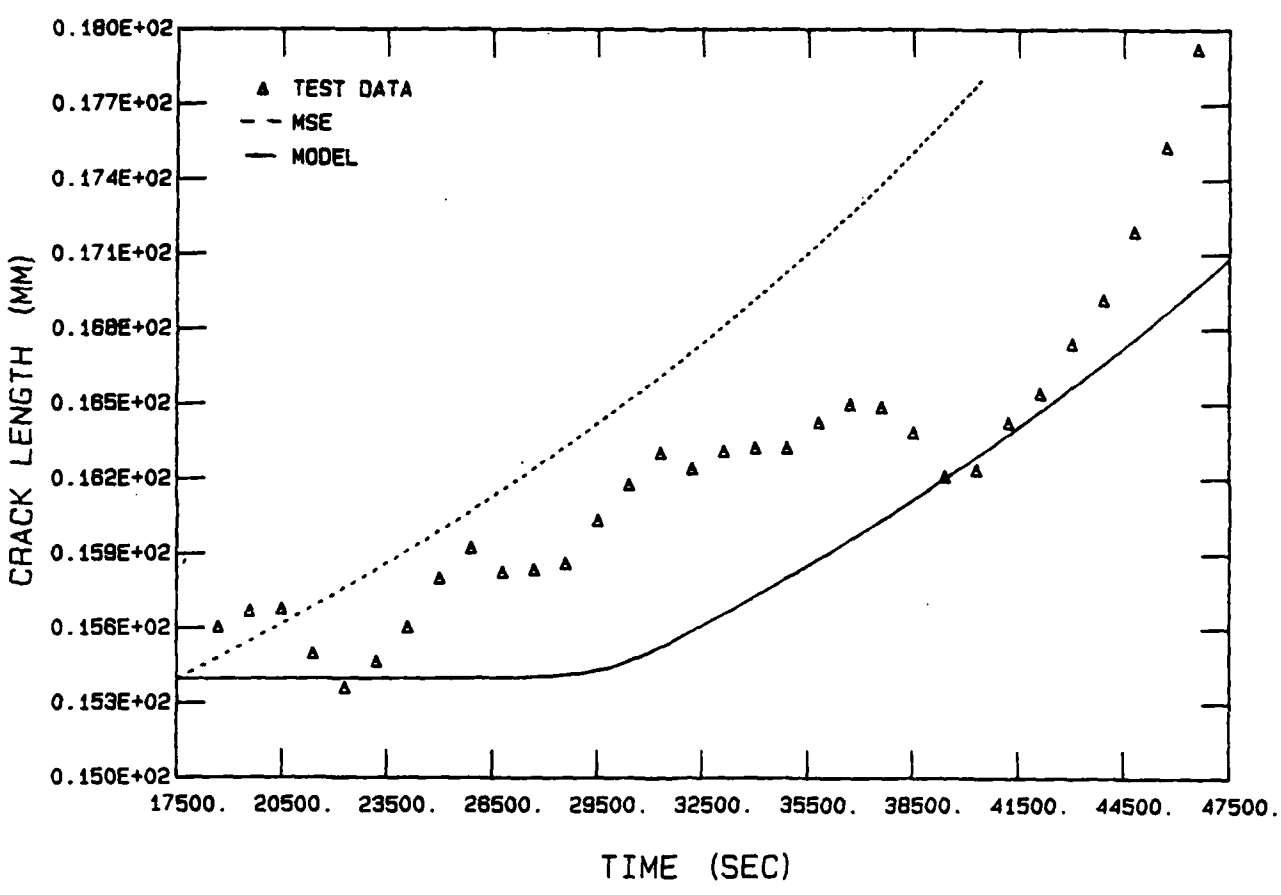
EE7, SEGMENT 4 A VS T
0.180E+02
0.177E+02
0.174E+02
0.171E+02
0.168E+02
0.165E+02
0.162E+02
0.159E+02
0.156E+02
0.153E+02
0.150E+02
CRACK LENGTH (MM)
TEST DATA
MSE
MODEL
17500.
20500.
23500.
26500.
29500.
32500.
35500.
38500.
41500.
44500.
47500.
TIME (SEC)

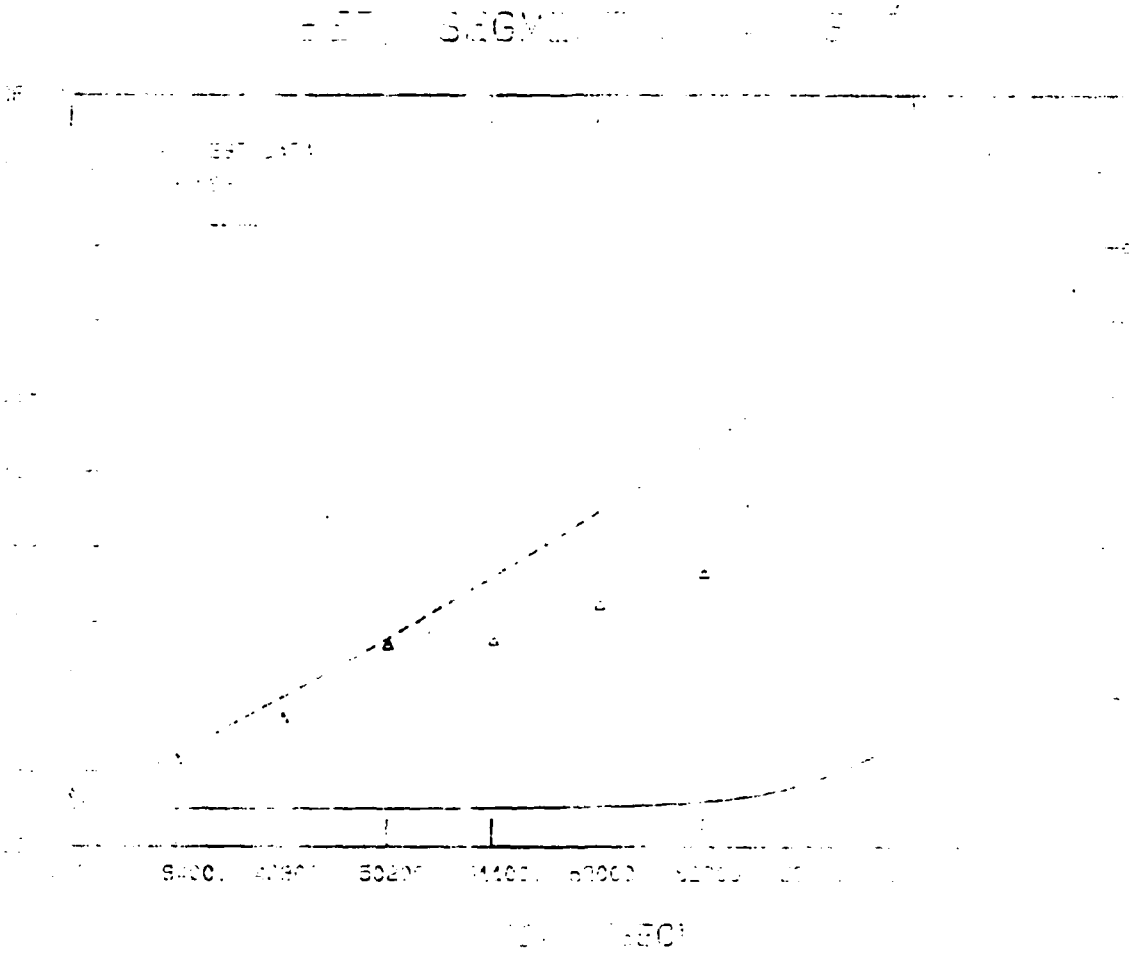

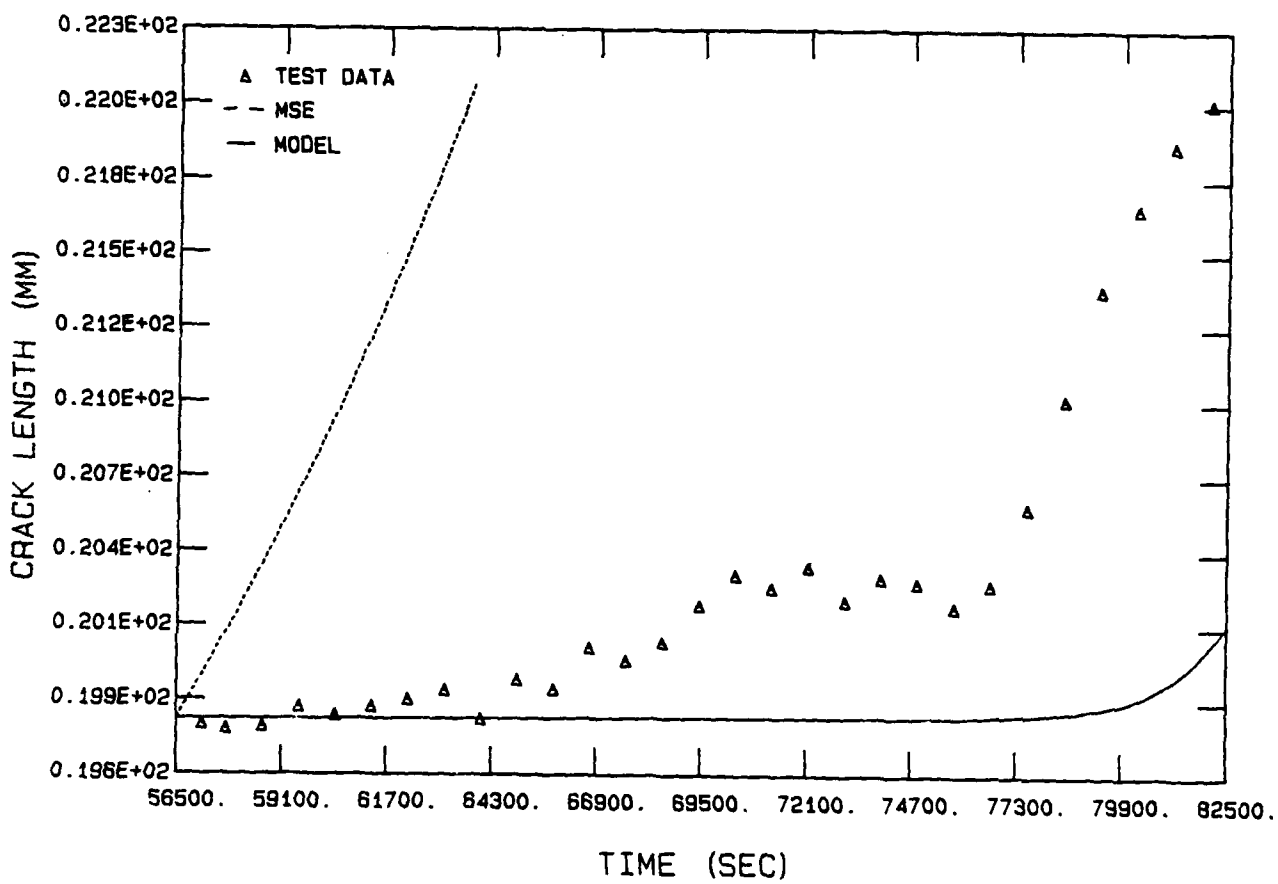
EE7, SEGMENT 6 A VS T
0.223E+02
0.220E+02
0.218E+02
0.215E+02
0.212E+02
0.210E+02
0.207E+02
0.204E+02
0.201E+02
0.199E+02
0.196E+02
CRACK LENGTH (MM)
TEST DATA
MSE
MODEL
56500.
59100.
61700.
64300.
66900.
69500.
72100.
74700.
77300.
79900.
82500.
TIME (SEC)

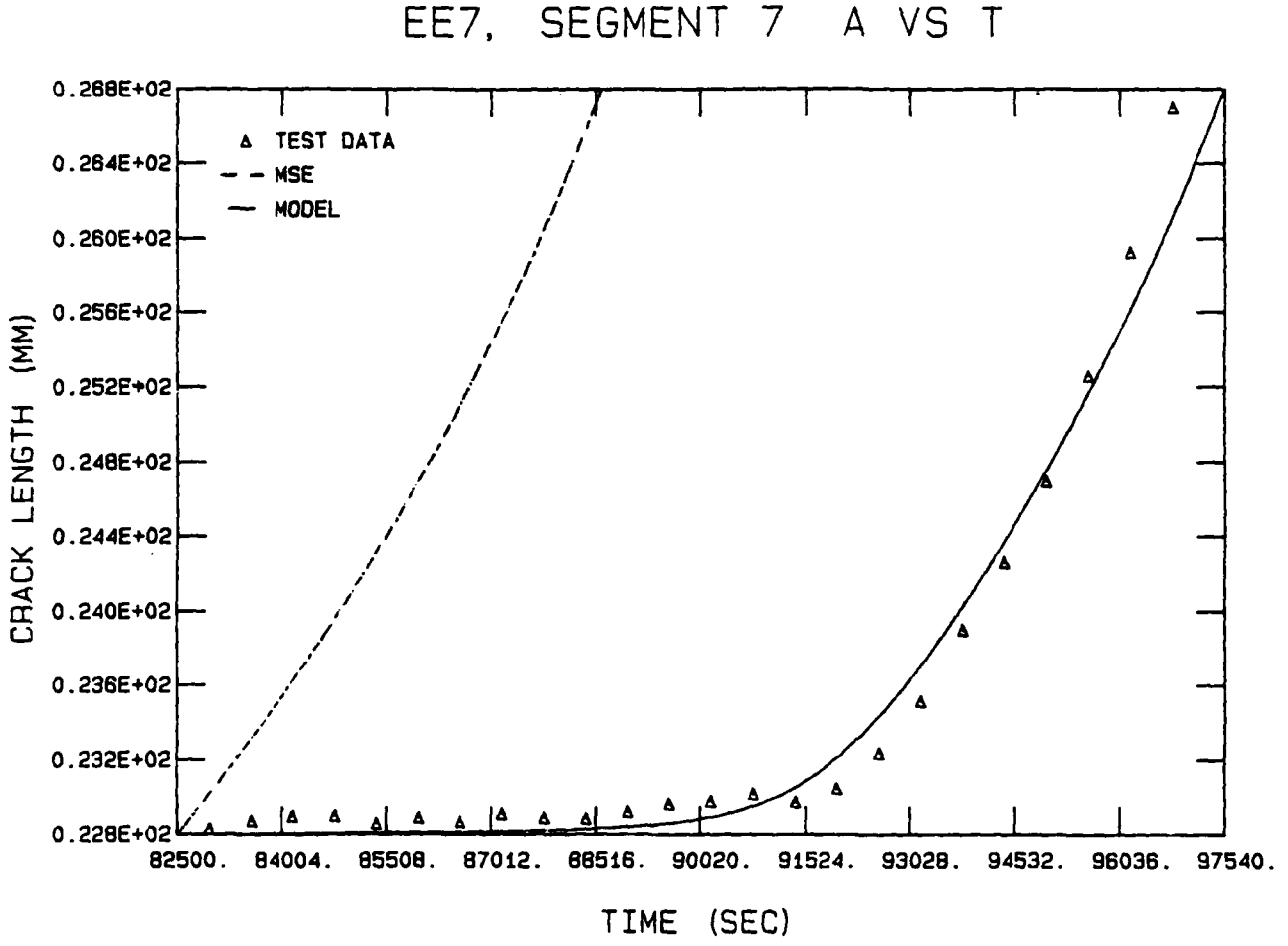
EE7, SEGMENT 7 A VS T
0.268E+02
0.264E+02
0.260E+02
0.256E+02
0.252E+02
0.248E+02
0.244E+02
0.240E+02
0.236E+02
0.232E+02
0.228E+02
CRACK LENGTH (MM)
TEST DATA
MSE
MODEL
82500.
84004.
85508.
87012.
88516.
90020.
91524.
93028.
94532.
96036.
97540.
TIME (SEC)

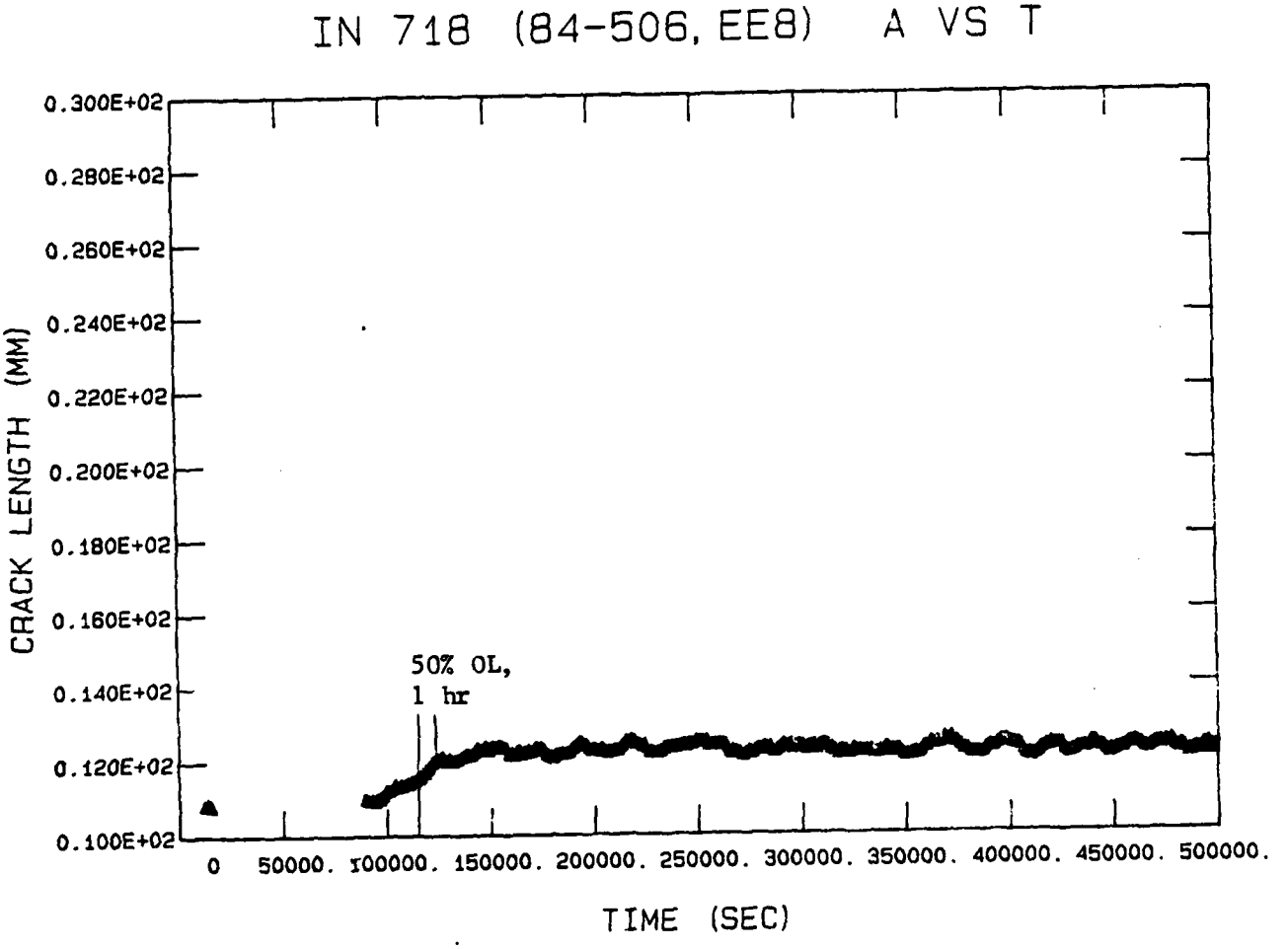
IN 718 (84-506, EE8) A VS T
0.300E+02
0.280E+02
0.260E+02
0.240E+02
0.220E+02
0.200E+02
0.180E+02
0.160E+02
0.140E+02
0.120E+02
0.100E+02
CRACK LENGTH (MM)
50% OL,
1 hr
0
50000.
100000.
150000.
200000.
250000.
300000.
350000.
400000.
450000.
500000.
TIME (SEC)

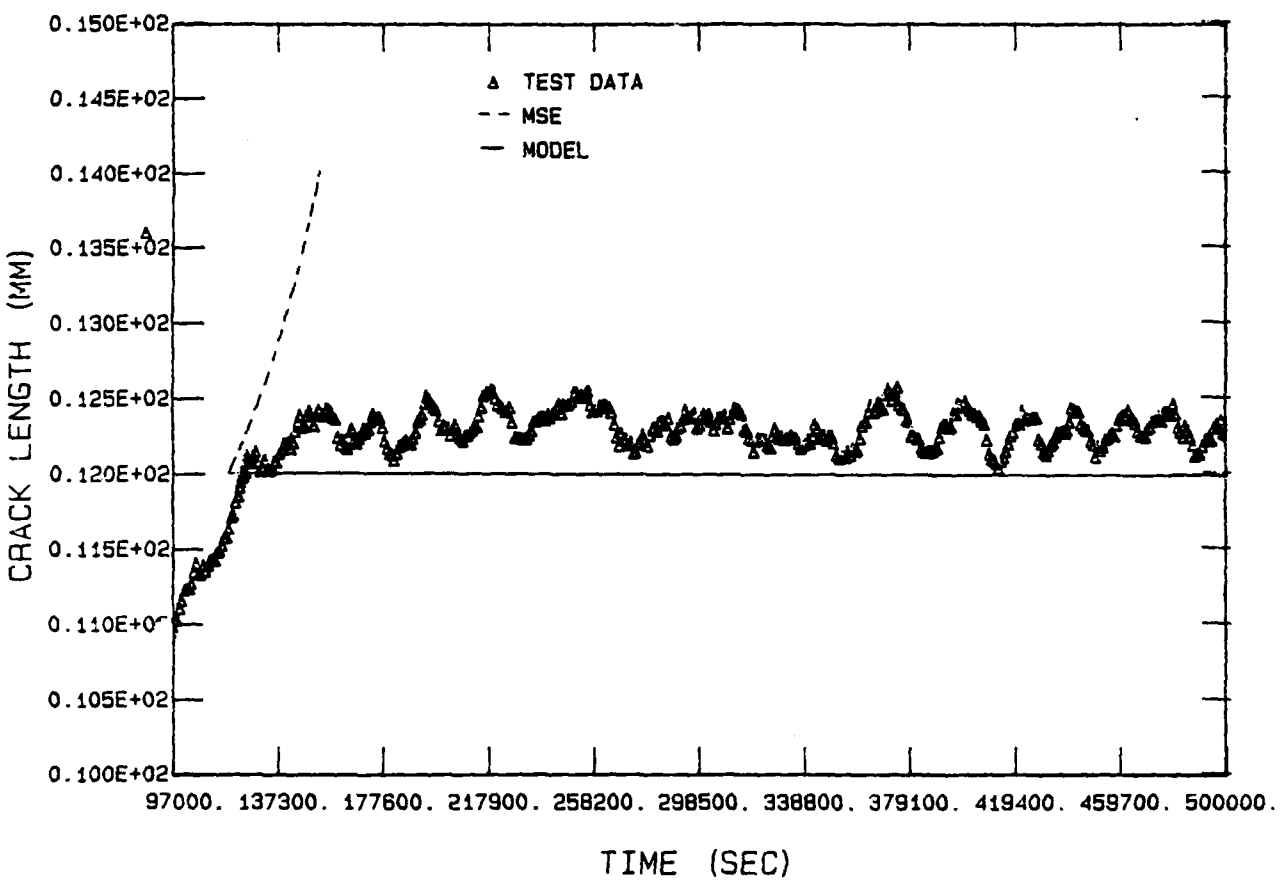
EE8, SEGMENT 2 A VS T
Δ TEST DATA
-- MSE
— MODEL
CRACK LENGTH (MM)
0.150E+02
0.145E+02
0.140E+02
0.135E+02
0.130E+02
0.125E+02
0.120E+02
0.115E+02
0.110E+02
0.105E+02
0.100E+02
97000. 137300. 177600. 217900. 258200. 298500. 338800. 379100. 419400. 459700. 500000.
TIME (SEC)

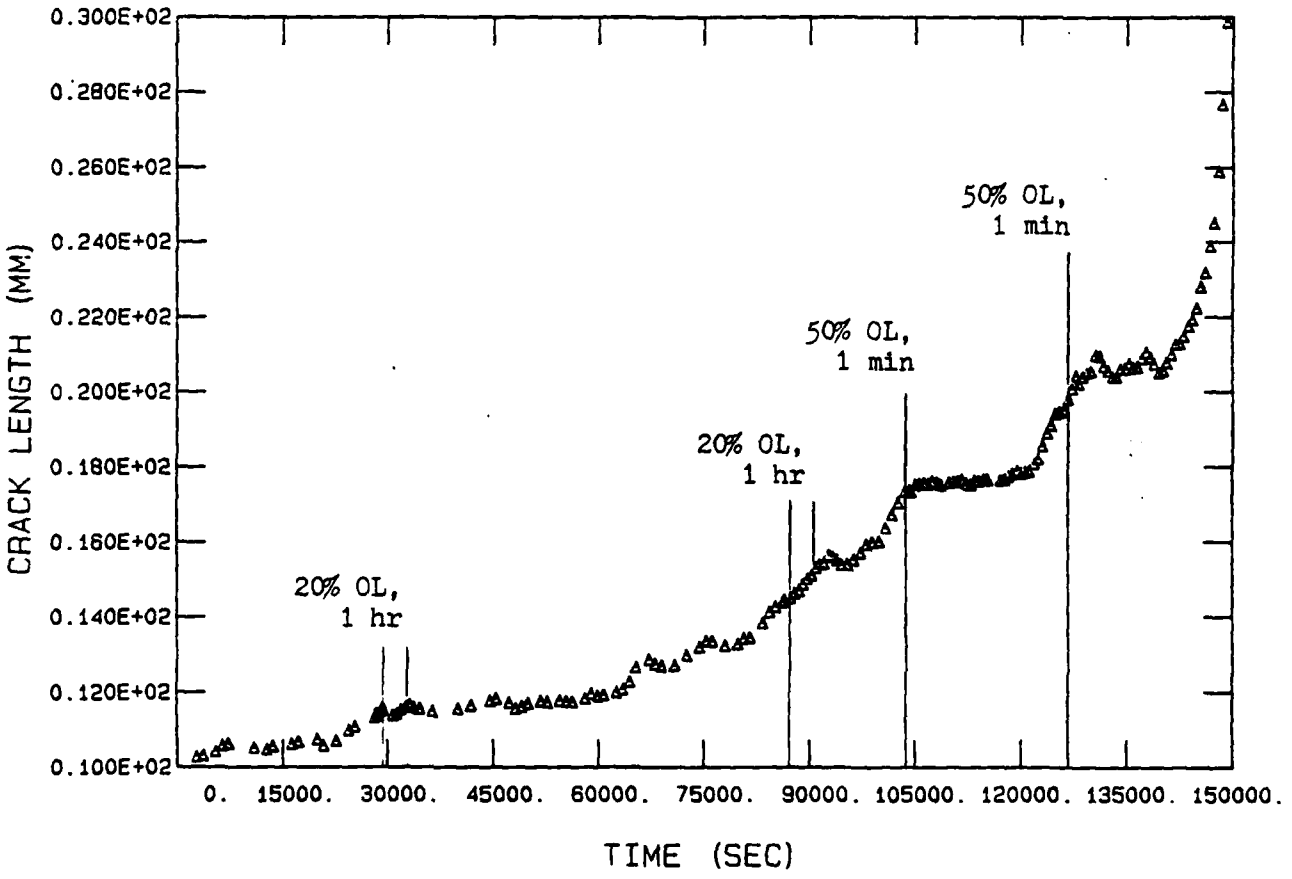
IN 718 (84-508, EE9) A VS T
CRACK LENGTH (MM)
0.300E+02
0.280E+02
0.260E+02
0.240E+02
0.220E+02
0.200E+02
0.180E+02
0.160E+02
0.140E+02
0.120E+02
0.100E+02
20% OL, 1 hr
20% OL, 1 hr
50% OL, 1 min
50% OL, 1 min
0.
15000.
30000.
45000.
60000.
75000.
90000.
105000.
120000.
135000.
150000.
TIME (SEC)

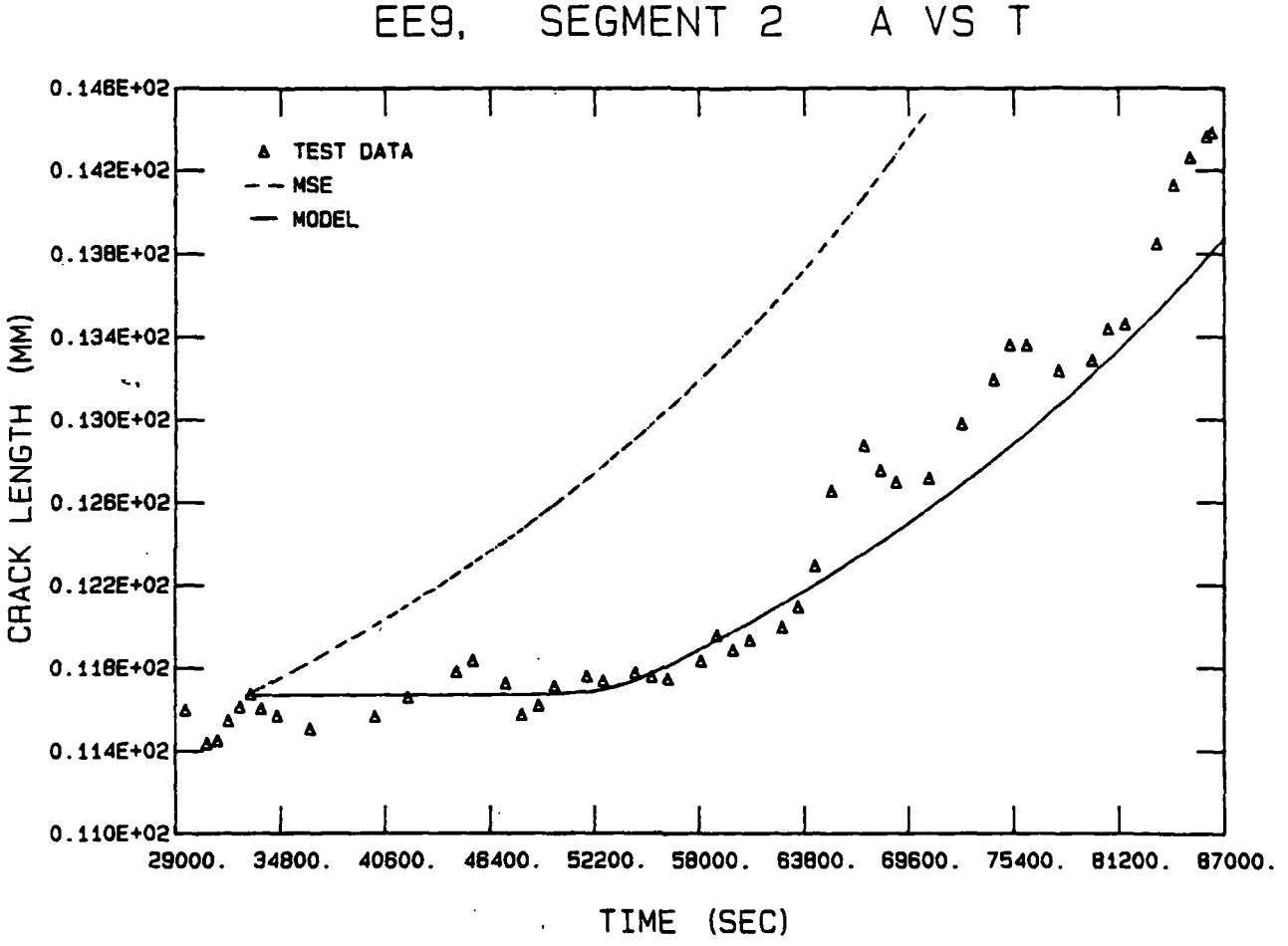
EE9, SEGMENT 2 A VS T
0.146E+02
0.142E+02
0.138E+02
0.134E+02
0.130E+02
0.126E+02
0.122E+02
0.118E+02
0.114E+02
0.110E+02
CRACK LENGTH (MM)
TEST DATA
MSE
MODEL
29000.
34800.
40600.
46400.
52200.
58000.
63800.
69600.
75400.
81200.
87000.
TIME (SEC)

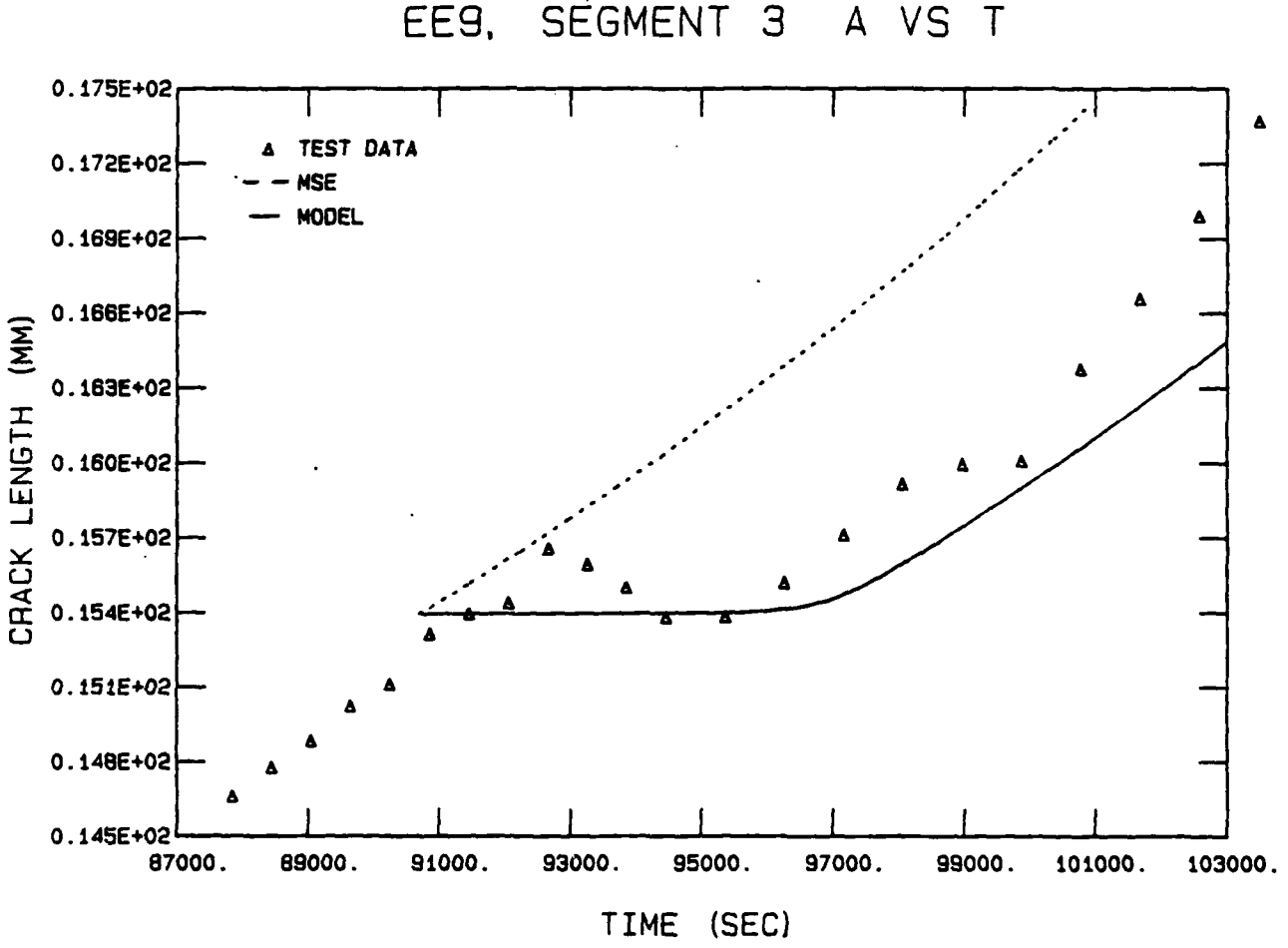
EE9, SEGMENT 3 A VS T
TEST DATA
MSE
MODEL
CRACK LENGTH (MM)
0.175E+02
0.172E+02
0.169E+02
0.166E+02
0.163E+02
0.160E+02
0.157E+02
0.154E+02
0.151E+02
0.148E+02
0.145E+02
87000.
89000.
91000.
93000.
95000.
97000.
99000.
101000.
103000.
TIME (SEC)

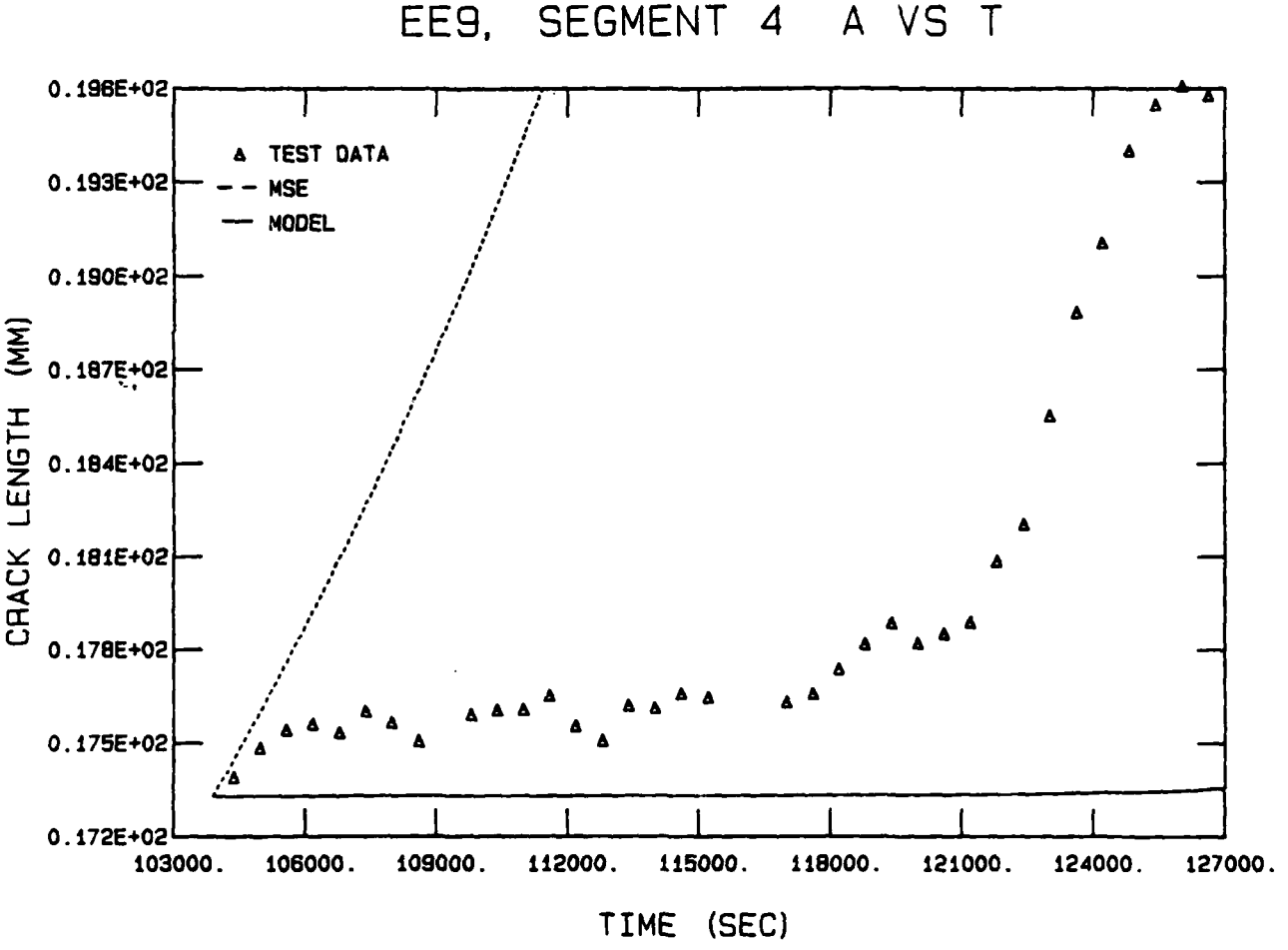
EE9, SEGMENT 4 A VS T
0.196E+02
0.193E+02
0.190E+02
0.187E+02
0.184E+02
0.181E+02
0.178E+02
0.175E+02
0.172E+02
CRACK LENGTH (MM)
TEST DATA
MSE
MODEL
103000.
106000.
109000.
112000.
115000.
118000.
121000.
124000.
127000.
TIME (SEC)

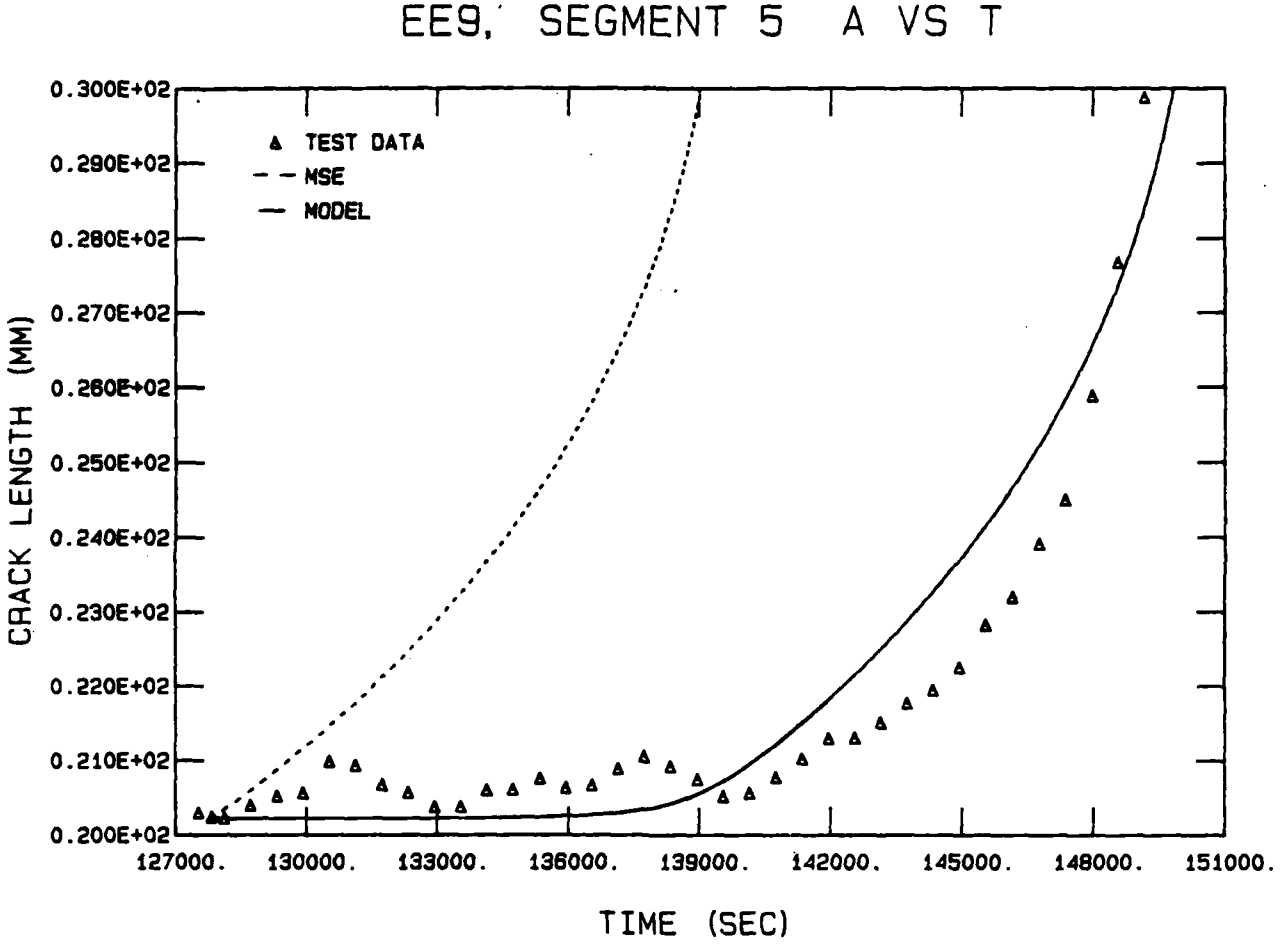
EE9, SEGMENT 5 A VS T
TEST DATA
MSE
MODEL
CRACK LENGTH (MM)
0.300E+02
0.290E+02
0.280E+02
0.270E+02
0.260E+02
0.250E+02
0.240E+02
0.230E+02
0.220E+02
0.210E+02
0.200E+02
127000.
130000.
133000.
136000.
139000.
142000.
145000.
148000.
151000.
TIME (SEC)

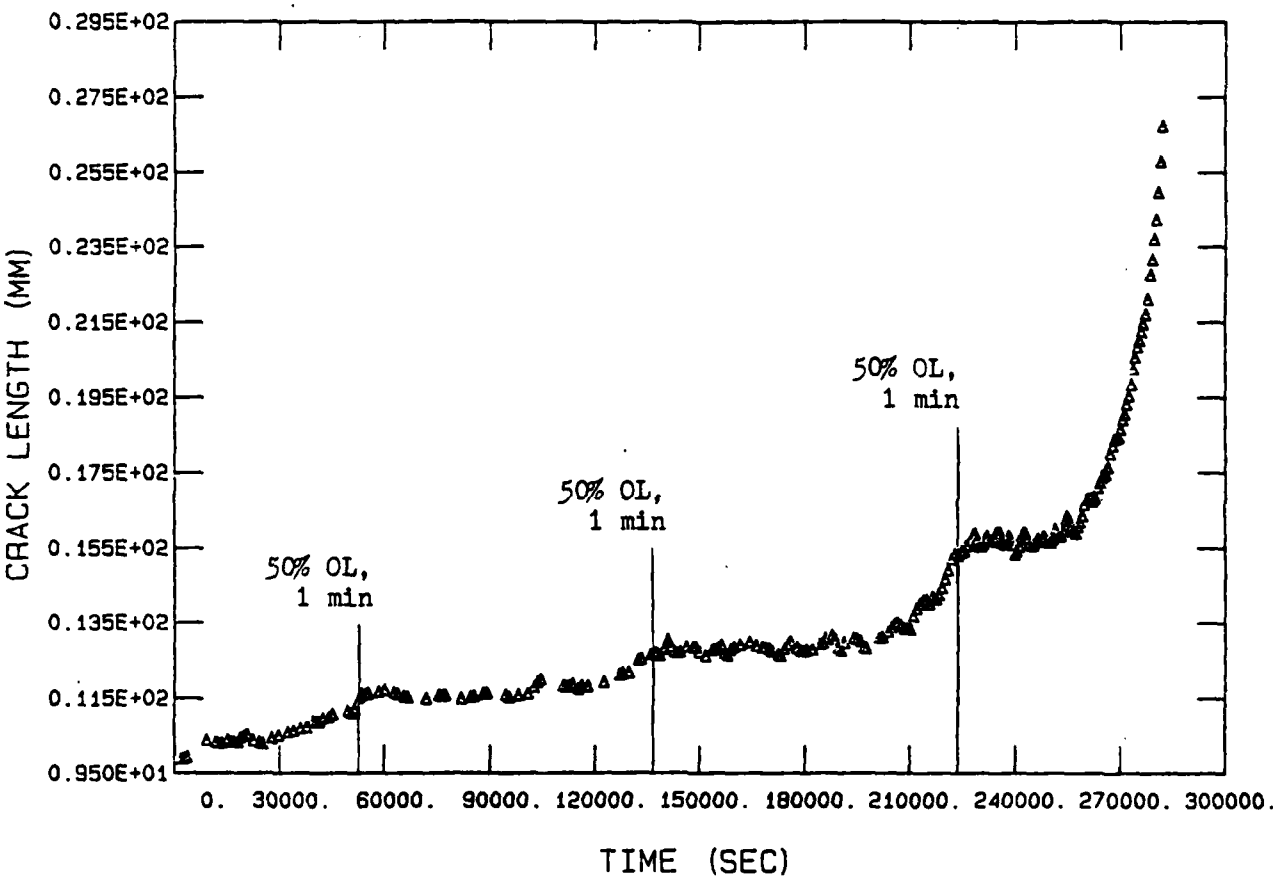
IN 718 (84-509, EE10) A VS T
CRACK LENGTH (MM)
0.295E+02
0.275E+02
0.255E+02
0.235E+02
0.215E+02
0.195E+02
0.175E+02
0.155E+02
0.135E+02
0.115E+02
0.950E+01
50% OL, 1 min
50% OL, 1 min
50% OL, 1 min
0. 30000. 60000. 90000. 120000. 150000. 180000. 210000. 240000. 270000. 300000.
TIME (SEC)

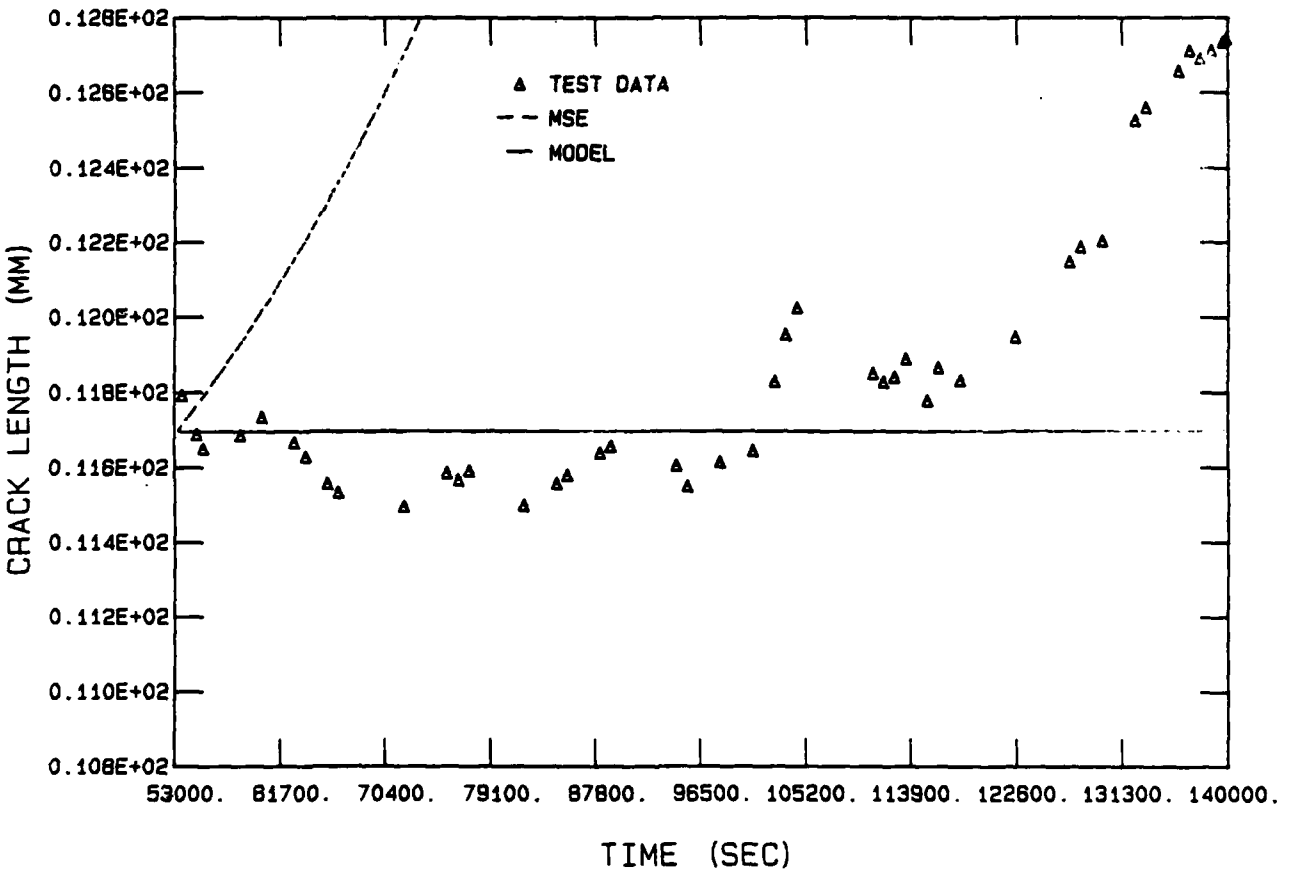
EE10, SEGMENT 2 A VS T
TEST DATA
MSE
MODEL
CRACK LENGTH (MM)
0.128E+02
0.126E+02
0.124E+02
0.122E+02
0.120E+02
0.118E+02
0.116E+02
0.114E+02
0.112E+02
0.110E+02
0.108E+02
53000.
61700.
70400.
79100.
87800.
96500.
105200.
113900.
122600.
131300.
140000.
TIME (SEC)

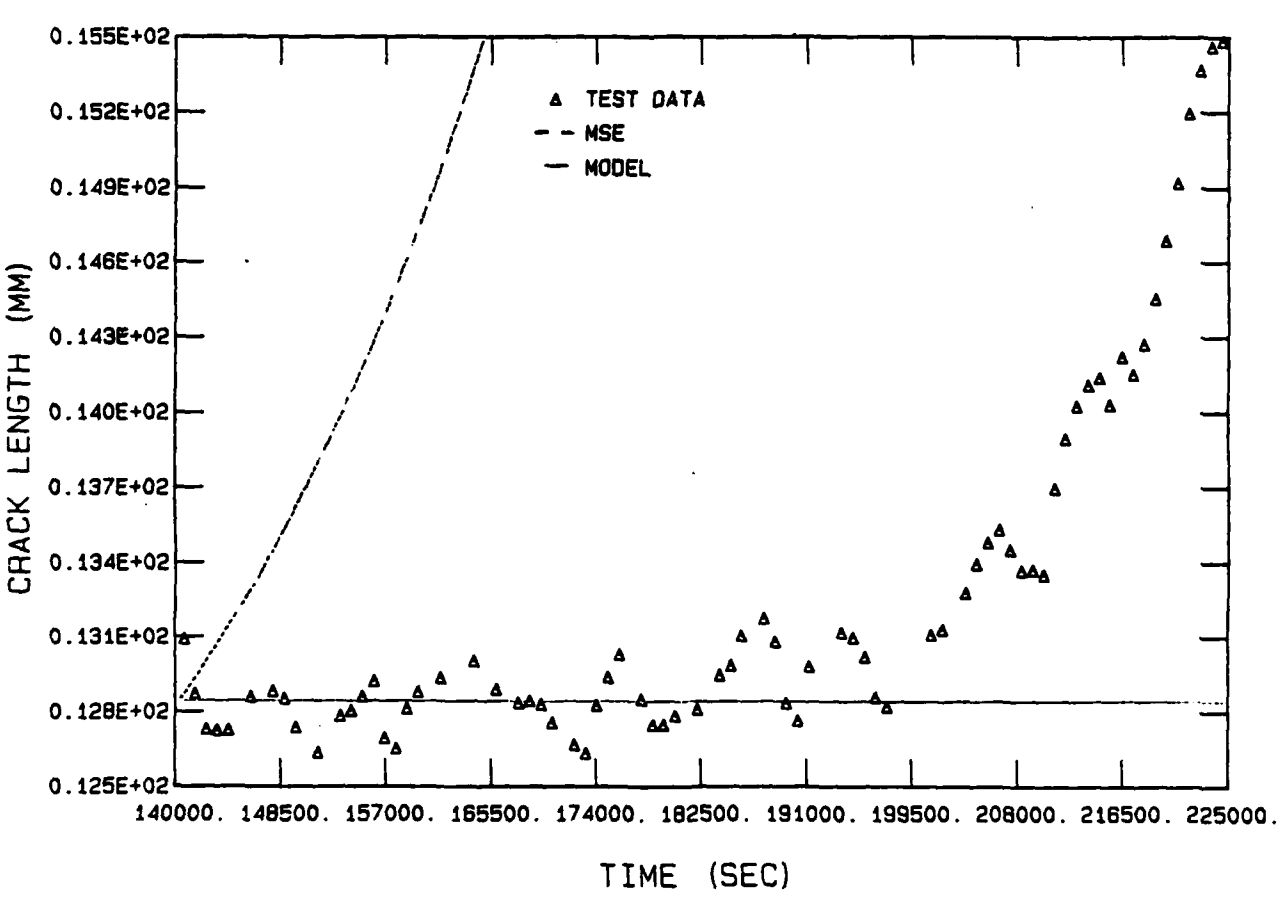
EE10, SEGMENT 3 A VS T
0.155E+02
0.152E+02
0.149E+02
0.146E+02
0.143E+02
0.140E+02
0.137E+02
0.134E+02
0.131E+02
0.128E+02
0.125E+02
CRACK LENGTH (MM)
TEST DATA
MSE
MODEL
140000. 148500. 157000. 165500. 174000. 182500. 191000. 199500. 208000. 216500. 225000.
TIME (SEC)

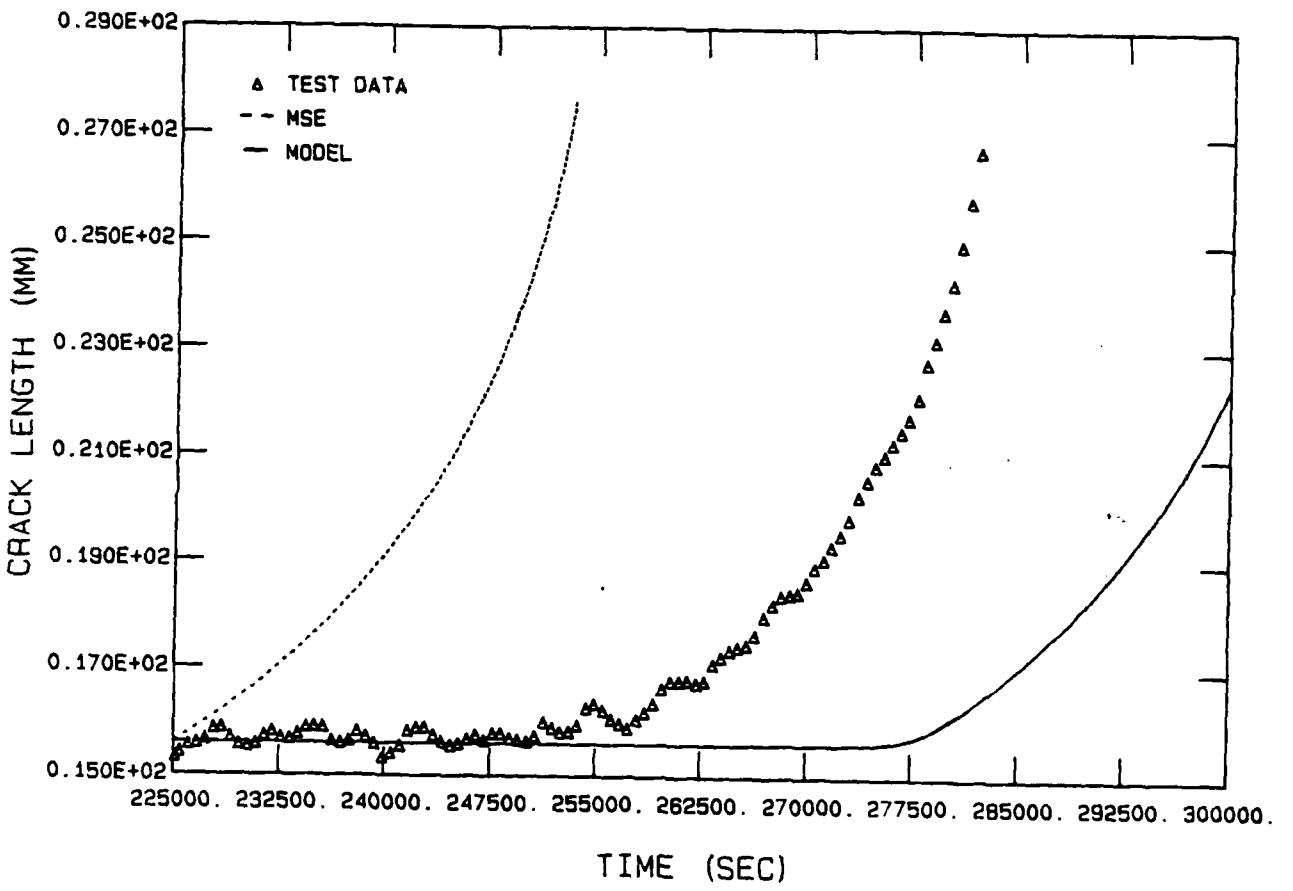
EE10, SEGMENT 4 A VS T
0.290E+02
0.270E+02
0.250E+02
0.230E+02
0.210E+02
0.190E+02
0.170E+02
0.150E+02
TEST DATA
MSE
MODEL
CRACK LENGTH (MM)
225000. 232500. 240000. 247500. 255000. 262500. 270000. 277500. 285000. 292500. 300000.
TIME (SEC)

Vita

Kevin Edward Harms was born on 20 January 1958 in Buffalo, New York. He graduated from high school in 1976 in Tonawanda, New York and attended the Pennsylvania State University. In, May 1980, he received a Bachelor of Science degree in Mechanical Engineering. Upon graduation, he received a commission in the USAF through the ROTC program. He was called to active duty in August 1980 and served as a Re-entry Vehicle Project Officer for the Peacekeeper Missile at the Ballistic Missile Office, Norton AFB, California. In June, 1983, Captain Harms entered the School of Engineering, Air Force Institute of Technology, to earn a Masters of Science degree in Aeronautical Engineering.

Permanent address: 127 Findlay Avenue
Tonawanda, New York 14150

UNCLASSIFIED

SECURITY CLASSIFICATION OF THIS PAGE

REPORT DOCUMENTATION PAGE

1a. REPORT SECURITY CLASSIFICATION UNCLASSIFIED	1b. RESTRICTIVE MARKINGS
2a. SECURITY CLASSIFICATION AUTHORITY	3. DISTRIBUTION/AVAILABILITY OF REPORT APPROVED FOR PUBLIC RELEASE: DISTRIBUTION UNLIMITED
2b. DECLASSIFICATION/DOWNGRADING SCHEDULE	
4. PERFORMING ORGANIZATION REPORT NUMBER(S) AFIT/GAE/AA/84D-8	5. MONITORING ORGANIZATION REPORT NUMBER(S)
6a. NAME OF PERFORMING ORGANIZATION SCHOOL OF ENGINEERING 6b. OFFICE SYMBOL (If applicable) AFIT/ENY	7a. NAME OF MONITORING ORGANIZATION
6c. ADDRESS (City, State and ZIP Code) AIR FORCE INSTITUTE OF TECHNOLOGY WRIGHT-PATTERSON AFB, OHIO 45433	7b. ADDRESS (City, State and ZIP Code)
8a. NAME OF FUNDING/SPONSORING ORGANIZATION 8b. OFFICE SYMBOL (If applicable)	9. PROCUREMENT INSTRUMENT IDENTIFICATION NUMBER
8c. ADDRESS (City, State and ZIP Code)	10. SOURCE OF FUNDING NOS. PROGRAM ELEMENT NO.: 61102F PROJECT NO.: 2302 TASK NO.: P1 WORK UNIT NO.: 01
11. TITLE (Include Security Classification) SEE BOX 19	
12. PERSONAL AUTHOR(S) KEVIN E. HARMS, B.S., CAPTAIN, USAF	
13a. TYPE OF REPORT MS THESIS 13b. TIME COVERED FROM _____ TO _____	14. DATE OF REPORT (Yr., Mo., Day) 1984 DECEMBER 15. PAGE COUNT 178
16. SUPPLEMENTARY NOTATION	Approved for public release: IAW AFR 190-17. LYNN E. WOLAVER 21 Feb 85 Dean for Research and Professional Development Air Force Institute of Technology (AIC) Wright-Patterson AFB OH 45433
17. COSATI CODES FIELD: 20 GROUP: 11 SUB. GR.	18. SUBJECT TERMS (Continue on reverse if necessary and identify by block number) SUSTAINED-LOAD CRACK GROWTH, CRACK GROWTH RETARDATION, ELEVATED TEMPERATURE, NICKEL-BASE SUPERALLOY, CRACK GROWTH MODEL, OVERLOADS Cole Reduction, Graphs.

19. ABSTRACT (Continue on reverse if necessary and identify by block number)

TITLE: OVERLOAD EFFECTS ON SUSTAINED LOAD CRACK GROWTH AT ELEVATED TEMPERATURE

THESIS CHAIRMAN: GEORGE K. HARITOS, MAJOR, USAF

THIS ~~STUDY~~ INVESTIGATES THE CRACK GROWTH BEHAVIOR OF INCONEL 718 EFFECTED BY OVER-LOADS AT ELEVATED TEMPERATURE. A CUMULATIVE DAMAGE MODEL WAS DEVELOPED TO PREDICT THE TOTAL TIME-TO-FAILURE. PREDICTIONS WERE NOTED TO IMPROVE AT HIGHER VALUES OF STRESS INTENSITIES.

ALL TESTS WERE CONDUCTED UNDER SUSTAINED LOADING WITH ISOTHERMAL CONDITIONS OF 650°C. PRECRACKED COMPACT TENSION SPECIMENS WERE USED TO ESTABLISH A DATA BASE FOR BASELINE AND OVERLOAD CONDITIONS. THE DELAY TIME ASSOCIATED WITH CRACK GROWTH RETARDATION WAS DETERMINED BY COMPARING THE BASELINE BEHAVIOR WITH THE RESULTS OF THE OVERLOAD SPECIMENS. THE EFFECTS OF 20-AND 50-PERCENT OVERLOADS OF 1 MINUTE OR 1 HOUR DURATION (SEE REVERSE)

20. DISTRIBUTION/AVAILABILITY OF ABSTRACT UNCLASSIFIED/UNLIMITED ☒ SAME AS RPT. ☐ DTIC USERS ☐	21. ABSTRACT SECURITY CLASSIFICATION UNCLASSIFIED
22a. NAME OF RESPONSIBLE INDIVIDUAL GEORGE K. HARITOS, ASSOCIATE PROFESSOR	22b. TELEPHONE NUMBER (Include Area Code) (513) 255-2998 22c. OFFICE SYMBOL AFIT/ENY

DD FORM 1473, 83 APR EDITION OF 1 JAN 73 IS OBSOLETE.

UNCLASSIFIED

SECURITY CLASSIFICATION OF THIS PAGE

19. CONTINUED

WERE INVESTIGATED. THE SHAPE OF THE CRACK TIP PLASTIC ZONE AND, HENCE, THE RETARDATION EFFECT WAS FOUND TO BE INDEPENDENT OF OVERLOAD DURATION.

THE RETARDATION DELAY TIME WAS FOUND TO BE DEPENDENT UPON THE OVERLOAD MAGNITUDE AND THE VALUE OF K AT WHICH THE OVERLOAD WAS REMOVED. IT WAS ALSO FOUND THAT A SUDDEN CRACK ADVANCEMENT OCCURRED WHEN THE OVERLOAD WAS APPLIED. THE ABOVE FACTORS WERE ACCOUNTED FOR IN THE MODEL DEVELOPMENT. THE MODEL WAS GENERALLY CAPABLE OF PREDICTING THE TIME-TO-FAILURE WITHIN ABOUT 10 PERCENT OF THE ACTUAL MATERIAL BEHAVIOR.

Note Supplemental Keywords continued > previous page

END

FILMED

5-85

DTIC